

DISSERTATION

INVESTIGATIONS OF NITROGEN OXIDE PLASMAS:  
FUNDAMENTAL CHEMISTRY AND SURFACE REACTIVITY  
AND

MONITORING STUDENT PERCEPTIONS IN A GENERAL CHEMISTRY RECITATION

Submitted by

Joshua M. Blechle

Department of Chemistry

In partial fulfillment of the requirements

For the Degree of Doctor of Philosophy

Colorado State University

Fort Collins, Colorado

Fall 2016

Doctoral Committee:

Advisor: Ellen R. Fisher

Nancy E. Levinger

Charles S. Henry

Christopher R. Weinberger

Copyright by Joshua M. Blechle 2016

All Rights Reserved

## ABSTRACT

# INVESTIGATIONS OF NITROGEN OXIDE PLASMAS: FUNDAMENTAL CHEMISTRY AND SURFACE REACTIVITY AND MONITORING STUDENT PERCEPTIONS IN A GENERAL CHEMISTRY RECITATION

Part I of this dissertation focuses on investigations of nitrogen oxide plasma systems. With increasing concerns over the environmental presence of  $N_xO_y$  species, there is growing interest in utilizing plasma-assisted conversion techniques. Advances, however, have been limited because of the lack of knowledge regarding the fundamental chemistry of these plasma systems. Understanding the kinetics and thermodynamics of processes in these systems is vital to realizing their potential in a range of applications. Unraveling the complex chemical nature of these systems, however, presents numerous challenges. As such, this work serves as a foundational step in the diagnostics and assessment of these  $N_xO_y$  plasmas.

The partitioning of energy within the plasma system is essential to unraveling these complications as it provides insight into both gas and surface reactivity. To obtain this information, techniques such as optical emission spectroscopy (OES), broadband absorption spectroscopy (BAS), and laser induced fluorescence (LIF) were utilized to determine species energetics (vibrational, rotational, translational temperatures). These temperature data provide mechanistic insight and establish the relationships between system parameters and energetic outcomes. Additionally, these data are also correlated to surface reactivity data collected with the Imaging of Radicals Interacting with Surfaces (IRIS) technique. IRIS data demonstrate the

relationship between internal temperatures of radicals and their observed surface scatter coefficients (S), the latter of which is directly related to surface reactivity (R) [ $R = 1-S$ ]. Furthermore, time-resolved (TR) spectroscopic techniques, specifically TR-OES, revealed kinetic trends in NO and N<sub>2</sub> formation from a range of precursors (NO, N<sub>2</sub>O, N<sub>2</sub>/O<sub>2</sub>). By examining the rate constants associated with the generation and destruction of various plasma species we can investigate possible mechanistic implications. All told, such data provides unparalleled insight into the chemistry of these plasma systems.

Part II of this work is focused on understanding the efficacy of a general chemistry recitation program. Such programs can be an valuable tool for improving students' problem-solving skills and understanding using methods that are difficult to implement in large lecture settings. Here, general chemistry students at Colorado State University participated in a variety of recitation activities throughout the first semester of a 2-semester general chemistry sequence, including peer-led exercises, games, and scaffolded worksheets. Through weekly surveys, students were asked to evaluate and assess recitation activities for both interest and effectiveness as part of their course homework. Also included in these survey assignments were content questions relevant to the weekly themes, providing a measure of student learning of recitation topics. Student opinions were correlated with content retention, and these data were compared against student responses to a pre-survey administered before the first recitation session. This analysis allows for monitoring students' expectations of recitation courses and how well those expectations are met through the various types of activities employed. Ultimately, this work has found that students have positive feeling with respect to individual assignments, but that perspectives on chemistry and the course in general decrease dramatically from the beginning to the end of the semester. Thus, this work can serve as a significant starting points for future

efforts to monitor and record student perceptions in the general chemistry recitation classroom, leading to further investigation into the source of changing attitudes and the role that week-to-week activities have on global course attitudes.

## ACKNOWLEDGMENTS

I lack the ability to succinctly thank all of those responsible for this academic journey, as the list is long and brevity is not my strength. Still, there are some that I would be remiss to not mention here. First, Joyce Brown, the woman who introduced me to chemistry and started me on this path: your classroom was a haven, a place of mystery and excitement unlike anything I had ever experienced. Those at Truman State University, especially Dr. Russell Baughman and Dr. Eric Patterson: you fostered a love of research and were constant mentors both in the classroom and outside of it. My advisor, Prof. Ellen R. Fisher: your patience and support has known no bounds throughout these years, even in times when it felt underserved. Your impact on me as a scientist and as a person is without measure, though there is no doubt that you have shown me how to be both confident and humble, and to fight for the things that matter while letting go of the things that don't. Other members of the Fisher Group: in you I have found kindred spirits and life-long friends. My parents, Ronald and Alice: you always believed in every crazy dream that I had and encouraged them whole-heartedly. There is no doubt that it is you are the ones that taught me the value of education and showed me that school was not a chore, but instead a great beast to be conquered simply for the love of learning. My brother, Alexander: you continually push me to reach higher and farther. More than a brother, you have been a friend, confidant, and inspiration each and every day. And finally, my wife, Lindsey: you are my best friend and my ultimate role-model. Your strength and passion drive me to achieve far beyond what I think I am capable of, and you were there to listen, coach, motivate, scold, comfort, and otherwise be everything I needed every step of the way.

Thank you all.

## DEDICATION

To my grandparents, for their guidance and love:

Frank and Theresa Schaefer, Robert and Margaret Blechle, George and Ruth Hafley

## TABLE OF CONTENTS

ABSTRACT.....	ii
ACKNOWLEDGMENTS .....	v
DEDICATION .....	vi
TABLE OF CONTENTS .....	vii
CHAPTER 1. Introduction to Plasma Chemistry.....	1
1.1 Plasma Chemistry .....	1
1.2 Motivation for Nitrogen Oxide Studies.....	6
1.3 Research Overview .....	9
1.4 References.....	12
CHAPTER 2. Experimental Details for the Investigation of Various Nitrogen Oxide Plasma Systems .....	15
2.1 Plasma Systems.....	15
2.2 Optical Spectroscopies.....	15
2.3 Mass Spectrometry.....	18
2.4 IRIS Technique .....	20
References.....	25
CHAPTER 3. The Design and Implementation of a Broadband Absorption Spectroscopy System for Ground State Temperature Measurements .....	26
3.1 Introduction.....	26
3.2 System Development .....	27
3.3 Results and Discussion.....	42
3.4 Summary .....	54
References.....	56
CHAPTER 4. Determination of Internal Temperatures within Nitric Oxide Inductively-Coupled Plasma Systems.....	58
4.1 Introduction.....	58



4.2 Results and Discussion.....	61
4.3 Summary .....	70
References.....	72
CHAPTER 5. The Effect of Ion Energies on the Surface Interactions of Nitric Oxide Formed in Nitrogen Oxide Plasma Systems .....	76
5.1 Introduction.....	76
5.2 Results and Discussion.....	79
5.3 Summary .....	104
References.....	106
CHAPTER 6. Time-Resolved Optical Emission Spectroscopy for the Investigation of Nitrogen Oxide Plasma Chemistry.....	109
6.1 Introduction.....	109
6.2 Results and Discussion.....	111
6.3 Summary .....	114
References.....	116
CHAPTER 7. Summary and Perspectives in Nitric Oxide Plasma Studies .....	118
7.1 Research Synopsis.....	118
7.2 Future Directions.....	120
References.....	124
CHAPTER 8. Student Perceptions with Respect to Recitation Techniques in General Chemistry.....	126
8.1 Introduction.....	126
8.2 CSU General Chemistry Recitation.....	128
8.3 Activity Development .....	134
8.4 Assessment Design.....	137
8.5 Early Expectations .....	141
8.6 Weekly Responses .....	144
8.7 Final Reflections from Students.....	150

8.8 Preliminary Qualitative Analysis of Survey Data.....	159
8.9 Summary and Future Directions.....	162
References.....	165
APPENDIX A. Independent Research Proposal .....	168
A.1 Abstract .....	168
A.2 Background and Significance.....	169
A.3 Specific Aims .....	171
A.4 Design and Methods .....	174
A.5 Summary .....	184
References.....	186
APPENDIX B. Supplemental Information for Recitation Studies.....	190
B.1 Week 1 Survey .....	191
B.2 Week 3 Survey .....	192
B.3 Week 16 Survey .....	194
B.4 The Mole Worksheet .....	196
B.5 Stoichiometry Worksheet .....	200

# CHAPTER 1

## INTRODUCTION TO PLASMA CHEMISTRY

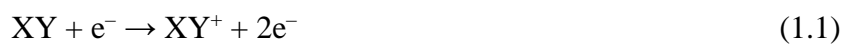
This chapter contains a brief introduction to plasma chemistry, specifically aspects relevant to inductively-coupled and nitrogen oxide control systems are presented. The discussion herein outlines the multi-faceted nature of these systems, as well as how these systems can be utilized to achieve a number of gas-phase outcomes. Many plasma systems are of particular interest to the scientific community due to their effectiveness as a method of semiconductor processing, atmospheric remediation, surface modification, medical sterilization, and in other applications. However, the ultimate utility of these systems is hindered by a lack of sufficient fundamental understanding. Indeed, the role of system parameters on energy partitioning, reactivity, gas-surface mechanisms, and kinetics are still areas in need of sufficient expansion. Successful elucidation of these complex problems, however, is necessary for optimal use and application of these systems.

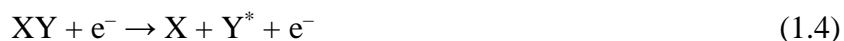
### 1.1 Plasma Chemistry

The term plasma is used to collectively describe partially-ionized discharges, which are known to contain a large number of chemical species such as ions, radicals, reactive atoms and molecules in excited and ground states, and electrons. This complex state of matter is believed to comprise well over 95% of the universe, although the only naturally occurring plasma on Earth is found within lightning arcs. In addition, these discharges can be created in laboratory conditions, allowing for unique and controllable chemical environments. These man-made plasmas fall into two broad categories: (1) thermal and (2) non-thermal. The distinction between

these two systems is made by comparing two of the characteristic parameters of the system, the ion temperature ( $T_i$ ) and the electron temperature ( $T_e$ ), both of which describe the energy distribution of the two species. Thermal plasmas are denoted by a  $T_e$  far greater (often 1-2 orders of magnitude) than that of  $T_i$ , whereas non-thermal plasmas have these two parameters in thermal equilibrium with one another.<sup>1</sup>

The work presented herein is based upon investigations of radio frequency (rf) inductively-coupled discharges, which fall into the category of non-thermal, or cold, plasmas. These systems are of particular interest in many applications, especially technological ones, as they provide a number of controllable parameters that significantly impact the overall chemistry of the resulting system. The variety of achievable reactions arising from this tunability is unique to plasma systems, allowing for relative ease of use in achieving a number of desirable outcomes.<sup>1</sup> One of the key parameters of interest is the applied plasma power ( $P$ ), which is ultimately responsible for the ignition of the plasma itself. Indeed,  $P$  is inductively-coupled to a volume of gas within the plasma reactor and, in an effort to counteract the applied electric field, there is stimulated Brownian motion among the free-electrons present within the system.<sup>2</sup> This motion leads to increased collisions with gas-phase precursor molecules, some of which ionize the gas and create the electron cascade needed to sustain the plasma discharge. Even at relatively low  $P$  ( $\sim 5$  W), the electrons can achieve enough energy via inelastic collisions to ionize nearly any atomic or molecular species. Electrons with less energy, however, can still lead to excitation or decomposition of the of gas-phase species.<sup>3</sup> A series of key electron-mediated reactions are shown below for the hypothetical diatomic precursor, XY.





Note, the choice of Y as an excitation species in Equation 1.4 and X as an ionization species in Equation 1.5 is purely arbitrary.

In addition to P, there is also the choice of the precursor gases used and the resulting system pressure, p, which influence the plasma discharge. The choice of precursor gas(es) provides the basis for all possible reactive species and is quite literally an infinite parameter space, as slight changes in percent composition of the gas feed can alter the chemistry of the plasma. Not only is the gas itself an important parameter, but the concentration(s) of the component gases is as well. As the concentration is increased, so is the pressure within the reactor, leading to increased collisions and further transfer of energy between plasma species.<sup>1,3</sup>

With this parameter set, the plasma achieves quasi-neutrality rapidly upon ignition, resulting from equilibration of the positive ions and electrons within the bulk of the plasma. Within the plasma bulk, there are several metrics by which to evaluate the species present. Beyond the aforementioned  $T_e$  and  $T_i$ , there are a number of other characteristic energies that can be monitored within plasmas.<sup>1</sup> Some of these are the translational, rotational and vibrational temperature ( $T_T$ ,  $T_R$  and  $T_V$ , respectively) of the non-ionized species.<sup>4-5</sup> Evaluating these characteristic temperatures provides insight into the complex energetic environment of the system and can be used to elucidate the mechanisms of species formation and evaluation of the system's non-equilibrium nature.<sup>6-8</sup>

Additionally, each of these measureable quantities can be sensitive to the parameter space (P, p, and precursor) and can be additionally influenced by the presence of a substrate within the

system, leading to a host of surface-mediation reactions. Indeed, the bulk of plasma applications involve etching, deposition, or surface modification, whereas some systems utilize gas-surface interactions to influence the downstream chemistry of resulting gas phase species.<sup>9-14</sup> Whether these species are involved in adsorption/desorption mechanisms, molecule-surface quenching, or a combination thereof, there is very little that is currently understood about the nature of these plasma-surface interactions. This in part arises from the three distinct regions of the plasma/surface composite, Fig. 1.1, each of which plays a significant role in the chemistry of the others. Indeed the choice of substrate can significantly alter the energy of the plasma itself whereas the choice of precursor(s) can significantly impact the chemistry of the surface, resulting in an interconnected system of plasma-surface reactions and mechanism.

In an effort to unravel this multi-layered system, many diagnostic methods (some of which will be discussed later in this chapter) exist to evaluate the inherent chemistry of plasma systems. These tools help to identify key species and determine energetic trends, which is of supreme interest to the plasma community.<sup>15-17</sup> Additionally, the plasma-surface interface itself can be directly investigated, providing in situ monitoring of the underlying chemistry occurring at a substrate.<sup>18</sup> Each of these independent systems are, in theory, tunable and controllable, though it requires significant fundamental knowledge of the role that the parameter space involved plays out the resulting systems. Thus, the impact of these tunable components must be catalogued and understood to link together the complex and interdependent web that exists within the system itself.<sup>19</sup> This work serves as one step towards understanding the role that plasma parameters play on the species and energetics of nitrogen oxide ( $N_xO_y$ ) plasma systems.

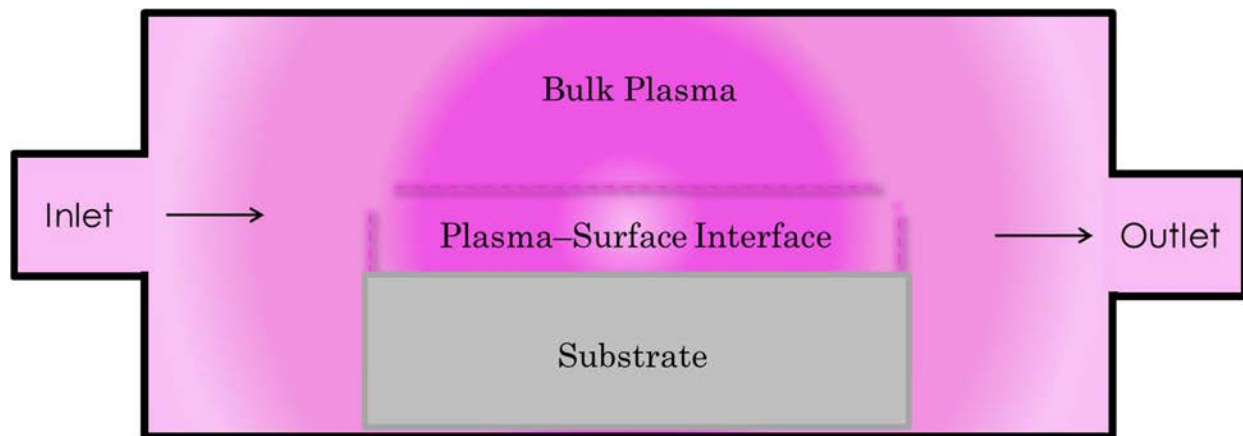


Figure 1.1 A pictorial representation of a plasma reactor cross-section, highlighting the three distinct regions of interest for this work: the plasma bulk, the substrate, and the region in which these two distinct systems interact with one another.

## 1.2 Motivation for Nitrogen Oxide Studies

The need for a fundamental understanding of  $N_xO_y$  plasmas arises from a distinct concern over increasing air and water pollution. Such pollution has led to organizations, such as the Environmental Protection Agency (EPA) to introduce legislation focused on decreasing the amount of pollution produced in the United States as well as reducing the levels of contaminants already present in the environment.<sup>20</sup> Notably, industrial and vehicular combustion are major sources of air pollution throughout the world, and the byproducts of such reactions are being closely monitored. These contaminants contain primarily hydrocarbons, carbon monoxide, and  $N_xO_y$  species.<sup>21</sup> Nitrogen oxides are of particular interest because of their contribution to acid rain and increasing levels of nitrates in water sources around the globe. This concern is markedly increased by the observation that nitrogen oxides and volatile organic compounds (VOCs) can react with sunlight to form photochemical smog.<sup>22</sup>

The most prominent method of  $N_xO_y$  control is the three-way catalytic converter (TWC). The descriptive name comes from the three separate catalytic reactions that take place between exhaust gas and the substrates found within TWCs, namely (1) reduction of  $NO_x$ , (2) oxidation of CO, and (3) oxidation of unburned hydrocarbons.<sup>23</sup> Since the implementation of TWCs in vehicles in 1981, the levels of nitrates measured in various water sources throughout the U.S. have fortunately decreased, but there are drawbacks to this method of control.<sup>24</sup> First, the substrates within TWCs only effectively reduce the  $NO_x$  species produced during combustion which leaves several other nitrogen oxides, such as  $N_2O$ , free to enter the environment. Secondly, the reduction of  $NO_x$  is only favorable under very precise exhaust (air to gasoline ratio) conditions.<sup>23</sup> It is not uncommon for TWCs to therefore be inefficient at reducing  $NO_x$  in older or poorly maintained engines. Another significant issue with current TWCs is that they



only work with unleaded gasoline, leading to significant pollution from diesel engines, which are widely used throughout the world. In addition to these flaws, TWCs are quite vulnerable to catalyst poisoning, specifically by sulfur compounds.<sup>25</sup> Unfortunately, because of the presence of sulfur dioxide in most exhaust systems, there is a significant likelihood of catalyst poisoning occurring within these catalytic converters. All of these factors contribute to an overall ineffective means of  $N_xO_y$  abatement, and as such, better methods need to be developed to more efficiently control this type of pollution.

Such efforts have been numerous and varied, including abatement of sulfur compounds responsible for catalytic poisoning, control of high-stability greenhouse gases, and improved smoke conversion in biodiesel based engines. One of the most promising, however, is plasma-assisted catalysis (PAC).<sup>26-29</sup> For years, techniques in PAC have focused on the ability to interface the plasma and catalytic systems in a variety of ways, the most popular of which are shown in Fig. 1.2. Additionally, several studies have examined plasma-enhanced pollution abatement, but these projects have primarily focused on creating model exhaust systems (by controlling gas composition) that create reducing environments to eliminate  $N_xO_y$  or on the catalytic surface, but these studies fail to consider the plasma system itself.<sup>26-28, 30-33</sup> Indeed, despite a number of successful attempts with PAC systems, one of the underlying issues is a lack of understanding of the fundamental chemistry of these plasma systems, limiting the potential effectiveness of plasmas as a reliable method of  $N_xO_y$  control. One of the driving forces in the plasma-abatement field, Bernadino Penetrante,<sup>31-32, 34</sup> who holds a patent for PAC system,<sup>35</sup> highlighted this need in a 1999 manuscript, stating:

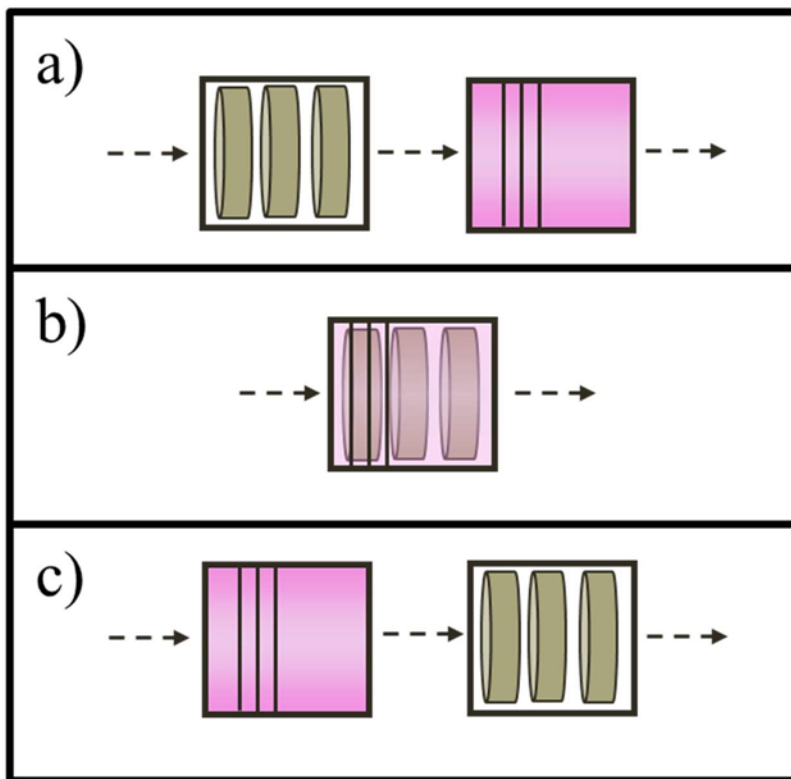


Figure 1.2 Representation of the three common methods for plasma-catalysis interfacing, which are (a) pre-plasma catalysis, (b) in-plasma catalysis, and (c) post-plasma catalysis. Each of these has been investigated to varying degrees within the PAC literature.

“This study illustrates the value of understanding the plasma chemistry in order to establish the feasibility of using low-temperature plasmas for treating emissions from internal-combustion vehicles... understanding of the plasma chemistry serves as an important design tool for minimizing the electrical energy consumption of the process and identifying the process products.”<sup>36</sup>

Indeed, the chemistry of 100% nitrogen oxide plasmas, as well as their direct interactions with surfaces is relatively unknown. Ultimately, if PACs are to be a viable method for pollution control, the role of the precursor gas mixture and surface on the chemistry of the plasma is needed for proper optimization, control, and deployment. Thus, to address these needs, this work serves as the beginnings of a foundational catalogue of plasma chemistry in  $N_xO_y$  systems.

### 1.3 Research Overview

The goal of this work is to utilize plasmas as a method of investigating the gas-phase and surface chemistry of  $N_xO_y$  plasmas. The approach is two-fold: (1) understand the fundamental chemistry of gas-phase nitrogen oxides produced in inductively-coupled plasmas (ICPs) by different precursor gas sources and the role that plasma parameters (power, pressure, etc.) have on gas-phase composition; and (2) investigate the inherent behavior of these species when in contact with substrates (especially catalytic ones), to establish trends in surface-mediated reactions and the means by which they occur. Efforts to complete this task utilize gas phase analysis using various diagnostic tools including optical emission spectroscopy (OES), broadband absorption spectroscopy (BAS), laser induced fluorescence (LIF), and mass spectrometry (MS). Data from these analyses can also be correlated to data from the LIF-based Imaging of Radicals Interacting with Surfaces (IRIS) technique to elucidate the gas-phase species surface reactivity during plasma processing, thereby providing unique and unparalleled

insight into the chemistry of  $N_xO_y$  systems. More specific information on these techniques can be found in Chapter 2.

More explicitly, the design and implementation of a new BAS reactor and instrument system is the focus of Chapter 3. The system allows for in situ investigation of ground state species, with numerous potential applications within the Fisher Research Group. Chapter 3 details all aspects of the instrument, from conception to early data analysis and pitfalls along the way. The hope is that it serves as something of a handbook to the implementation and design considerations within the system. Evaluation of absorbance data collected with this apparatus, specifically  $T_R$  and  $T_V$  of nitric oxide is the focus of Chapter 4. These data are compared to temperatures determined for the excited state via OES, as well as those calculated in the presence of a silicon substrate. Such work is integral to unraveling the delicate nature of energy partitioning within our ICP systems, and the distinct disparities found between individual species, depending on their formation mechanism.

Chapter 5 describes a combined IRIS and MS investigation of  $N_xO_y$  plasma systems. The MS portion of the chapter discusses the determination of nascent ion energies within several plasma systems, as impacted by both P and p. The IRIS component examines identical conditions, but investigates the probability of surface reactivity by determining the likelihood of a molecule scattering from the surface, denoted by a surface scatter coefficient, S. Additional IRIS work is done under ion-free conditions, allowing for a direct measure of the role of ions in surface reactions. Combined with the ion-energy data, this provides insight into the energies required for surface reactions to occur with these  $N_xO_y$  plasma systems.

In Chapter 6, data from time-resolved OES are presented. These efforts detail our ability to monitor the production of excited state species upon ignition of the plasma, providing kinetic

information about species production and lifetimes. Indeed, this serves to illustrate the brief timeframe upon ignition in which the plasma achieves its quasi-neutral equilibrium, resulting in a surge of excitation within the plasma. By monitoring the emission of these species across the first few seconds of the plasma lifetime, we can gain insight into the mechanisms that may lead to the overall bulk conditions of the plasma itself.

Ultimately, the overall intent of this work is to provide advances to our understanding of gas-phase nitrogen oxides and the impact of ions, neutrals, excited states, etc. on their surface interactions. It also works to help establish the viability of plasma processing as a tool for the breakdown of nitrogen oxides, and in turn, improved catalytic conversion. A summary of this progress, as well as future steps that are possible to further advance upon what has been done here is the focus of Chapter 7. The data that result from this dissertation could spawn additional research in which fundamental knowledge is applied to further develop plasma-processing, increase our understanding of how pollutants interact with substrates relevant to atmospheric chemistry, and interface the two methods to lead to overall improvement in the conversion of nitrogen oxide compounds.

## REFERENCES

1. Grill, A., Cold Plasma in Materials Fabrication. IEEE Press, New York: 1994; Vol. 151.
2. Iverson, G. J.; Williams, R. M., Brownian Motion of Electrons in Time-Dependent Magnetic Fields. *Journal of Physics A: Mathematical, Nuclear and General* 1973, 6 (1), 106.
3. Meichsner, J.; Schmidt, M.; Schneider, R.; Wagner, H.-E., Nonthermal Plasma Chemistry and Physics. CRC Press: 2012.
4. Fridman, A., Plasma Chemistry. Cambridge University Press: 2008.
5. Fridman, A.; Kennedy, L. A., Plasma Physics and Engineering. CRC Press: 2004.
6. Shimada, M.; Tynan, G. R.; Cattolica, R., Rotational and Translational Temperature Equilibrium in an Inductively Coupled Plasma. *Journal of Vacuum Science & Technology A* 2006, 24 (5), 1878-1883.
7. Zheng-De, K.; Yi-Kang, P., Molecular Nitrogen Vibrational Temperature in an Inductively Coupled Plasma. *Chinese Physics Letters* 2002, 19 (2), 211.
8. Porter, R. A.; Harshbarger, W. R., Gas Rotational Temperature in an RF Plasma. *Journal of the Electrochemical Society* 1979, 126 (3), 460-464.
9. Dave, H.; Ledwani, L.; Nema, S., Surface Modification by Atmospheric Pressure Air Plasma Treatment to Improve Dyeing with Natural Dyes: An Environment Friendly Approach for Leather Processing. *Plasma Chemistry and Plasma Processing* 2016, 36 (2), 599-613.
10. Hetemi, D.; Médard, J. r. m.; Kanoufi, F. d. r.; Combellas, C.; Pinson, J.; Podvorica, F. I., Surface Modification of Polymers by Reaction of Alkyl Radicals. *Langmuir* 2016, 32 (2), 512-518.
11. Liston, E. M.; Martinu, L.; Wertheimer, M. R., Plasma Surface Modification of Polymers for Improved Adhesion: A Critical Review. *Journal of Adhesion Science and Technology* 1993, 7 (10), 1091-1127.
12. Griesser, H. J.; Gengenbach, T. R.; Dai, L. M.; Li, S.; Chatelier, R. C. In *Plasma Surface Modifications for Structural and Biomedical Adhesion Applications, First International Congress on Adhesion Science and Technology-Invited Papers*, 1998; pp 307-328.
13. Martinu, L.; Poitras, D., Plasma Deposition of Optical Films and Coatings: A Review. *Journal of Vacuum Science & Technology A* 2000, 18 (6), 2619-2645.
14. Lee, Y. H.; Sung, Y. J.; Yeom, G. Y.; Lee, J. W.; Kim, T. I., Magnetized Inductively Coupled Plasma Etching of GaN in Cl<sub>2</sub>/BCl<sub>3</sub> Plasmas. *Journal of Vacuum Science & Technology A* 2000, 18 (4), 1390-1394.
15. Auciello, O.; Flamm, D. L., Plasma Diagnostics: Discharge Parameters and Chemistry. Academic Press: 2013; Vol. 1.
16. Lochte-Holtgreven, W., Plasma-Diagnostics. North-Holland Publication Co.: Amsterdam, 1968; Vol. 1.
17. Hutchinson, I. H., Principles of Plasma Diagnostics. Cambridge University Press: 1990; Vol. 1.
18. McCurdy, P. R.; Bogart, K. H. A.; Dalleska, N. F.; Fisher, E. R., A Modified Molecular Beam Instrument for the Imaging of Radicals Interacting with Surfaces During Plasma Processing. *Review of Scientific Instruments* 1997, 68 (4), 1684-1693.

19. Williams, K. L.; Martin, I. T.; Fisher, E. R., On the Importance of Ions and Ion-Molecule Reactions to Plasma-Surface Interface Reactions. *Journal of the American Society for Mass Spectrometry* 2002, 13 (5), 518-529.
20. Portney, P. R., *Public Policies for Environmental Protection*. Routledge: 2016.
21. Lucena, P.; Vadillo, J. M.; Laserna, J. J., Compositional Mapping of Poisoning Elements in Automobile Three-Way Catalytic Converters by Using Laser-Induced Breakdown Spectrometry. *Applied Spectroscopy* 2001, 55 (3), 267-272.
22. Devahasdin, S.; Fan, C.; Li, K.; Chen, D. H., TiO<sub>2</sub> Photocatalytic Oxidation of Nitric Oxide: Transient Behavior and Reaction Kinetics. *Journal of Photochemistry and Photobiology A: Chemistry* 2003, 156 (1), 161-170.
23. Brandt, E. P.; Wang, Y.; Grizzle, J. W., Dynamic Modeling of a Three-Way Catalyst for SI Engine Exhaust Emission Control. *IEEE Transactions on Control Systems Technology* 2000, 8 (5), 767-776.
24. Agency, U. E. P., *Our Nation's Air—Status and Trends Through 2010*. Office of Air Quality and Planning Standards: 2012.
25. Beck, D. D.; Sommers, J. W., Impact of Sulfur on the Performance of Vehicle-Aged Palladium Monoliths. *Applied Catalysis B: Environmental* 1995, 6 (2), 185-200.
26. Chen, H. L.; Lee, H. M.; Chen, S. H.; Chang, M. B.; Yu, S. J.; Li, S. N., Removal of Volatile Organic Compounds by Single-Stage and Two-Stage Plasma Catalysis Systems: A Review of the Performance Enhancement Mechanisms, Current Status, and Suitable Applications. *Environmental Science & Technology* 2009, 43 (7), 2216-2227.
27. Miessner, H.; Francke, K.-P.; Rudolph, R.; Hammer, T., NO<sub>x</sub> Removal in Excess Oxygen by Plasma-Enhanced Selective Catalytic Reduction. *Catalysis Today* 2002, 75 (1), 325-330.
28. Orlando, T. M.; Alexandrov, A.; Lebsack, A.; Herring, J.; Hoard, J. W., The Reactions of NO<sub>2</sub> and CH<sub>3</sub>CHO with Na-Y Zeolite and the Relevance to Plasma-Activated Lean NO<sub>x</sub> Catalysis. *Catalysis Today* 2004, 89 (1), 151-157.
29. Wang, P.; Cai, Y.-X.; Zhang, L.; Tolksdorf, C., Physical and Chemical Characteristics of Particulate Matter from Biodiesel Exhaust Emission Using Non-Thermal Plasma Technology. *Energy & Fuels* 2010, 24 (5), 3195-3198.
30. Fresnet, F.; Baravian, G.; Magne, L.; Pasquiers, S.; Postel, C.; Puech, V.; Rousseau, A., Kinetic of the NO Removal by Nonthermal Plasma in N<sub>2</sub>/NO/C<sub>2</sub>H<sub>4</sub> Mixtures. *Applied Physics Letters* 2000, 77, 4118.
31. Penetrante, B. M.; Hsiao, M. C.; Bardsley, J. N.; Merritt, B. T.; Vogtlin, G. E.; Kuthi, A.; Burkhart, C. P.; Bayless, J. R., Identification of Mechanisms for Decomposition of Air Pollutants by Non-Thermal Plasma Processing. *Plasma Sources Science and Technology* 1997, 6 (3), 251.
32. Penetrante, B. M.; Hsiao, M. C.; Merritt, B. T.; Vogtlin, G. E.; Wallman, P. H., Comparison of Electrical Discharge Techniques for Nonthermal Plasma Processing of NO in N<sub>2</sub>. *IEEE Transactions on Plasma Science* 1995, 23 (4), 679-687.
33. Ighigeanu, D.; Martin, D.; Zissulescu, E.; Macarie, R.; Oproiu, C.; Cirstea, E.; Iovu, H.; Calinescu, I.; Iacob, N., SO<sub>2</sub> and NO<sub>x</sub> Removal by Electron Beam and Electrical Discharge Induced Non-Thermal Plasmas. *Vacuum* 2005, 77 (4), 493-500.
34. Penetrante, B. M.; Bardsley, J. N.; Hsiao, M. C., Kinetic Analysis of Non-Thermal Plasmas Used for Pollution Control. *Japanese Journal of Applied Physics* 1997, 36 (7S), 5007.
35. Penetrante, B. M.; Vogtlin, G. E.; Merritt, B. T.; Brusasco, R. M. Plasma Regenerated Particulate Trap and NO<sub>x</sub> Reduction System. 2000.

36. Penetrante, B. M.; Brusasco, R. M.; Merritt, B. T.; Vogtlin, G. E., Environmental Applications of Low-Temperature Plasmas. *Pure and Applied Chemistry* 1999, 71 (10), 1829-1835.



## CHAPTER 2

### EXPERIMENTAL DETAILS FOR THE INVESTIGATION OF VARIOUS NITROGEN OXIDE PLASMA SYSTEMS

#### 2.1 Plasma Systems

Inductively-coupled plasmas (ICPs) formed in glass tubular reactors via the coupling of 13.56 MHz rf power through an eight-turn Ni-plated copper coil were used in these studies (see Fig. 2.1). Depending on the experiment, these reactors were interfaced to a mass spectrometer, an optical spectrometer, or the IRIS apparatus. Plasma precursor gases used were NO (either Matheson or American Gas Group, >95%), NO<sub>2</sub> (Matheson, >95%), N<sub>2</sub>O (either General Air or Airgas, >95%) and a 50/50 mixture (by partial pressure) of N<sub>2</sub> and O<sub>2</sub> (each Airgas, >95%). Applied rf power (P) ranged from 25 to 200 W, and system pressures (p) were primarily 50-200 mTorr above a base pressure, as measured by a Baratron capacitance manometer.

#### 2.2 Optical Spectroscopies

Optical spectra, both emission and absorption, were collected with an AvaSpec-2048L-USB2-RM multichannel spectrometer, Fig. 2.2. In conjunction with an Avantes DCL-UV/VIS-200 collimating lens, spectra were collected over a wavelength range of 197 – 1061 nm. The spectrometer houses six gratings, each synchronized for simultaneous data collection with 2048-pixel linear array charged couple device (CCD) detectors. In addition, a fiber optic probe was placed against a quartz window downstream from the coil, allowing for coaxial data collection along the length of the reactor to maximize signal intensity. Integration times and the number of averages collected depend on the specific experiment to maximize signal-to-noise ratios.

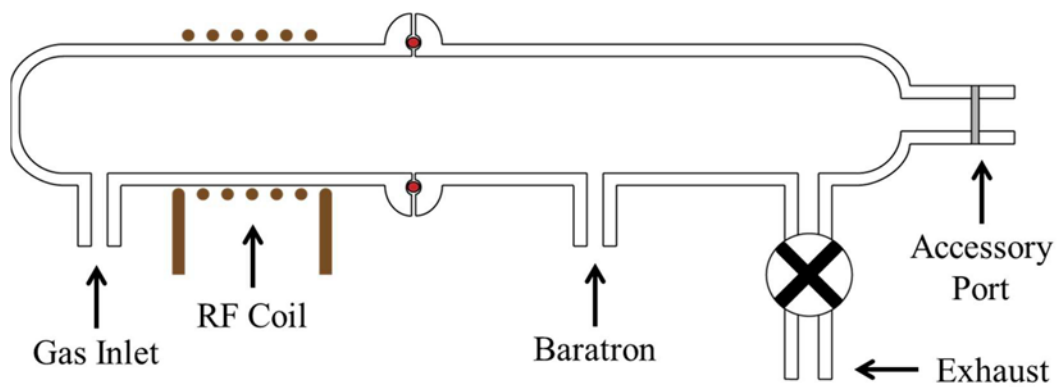


Figure 2.1 Schematic of a standard glass tubular ICP reactor used for plasma-based experiments.

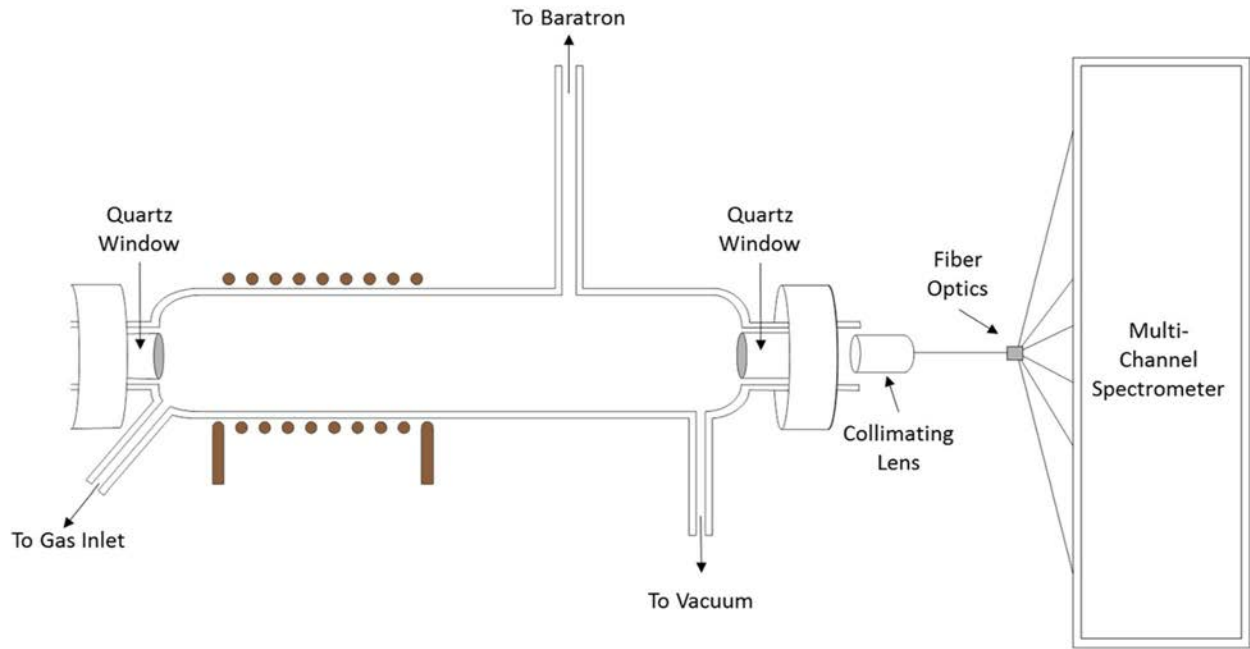


Figure 2.2 Generic schematic of ICP reactor interfaced to optical spectrometer.

For absorption studies (discussed in detail in Chapter 3), experiments were performed with an AvaLight-DHS deuterium-halogen light source. Data were collected using the AvaSoft 7.8 program, and spectra were fit using both Specair and LIFBASE spectral database programs.

Directly comparing OES spectra can be problematic because of inconsistencies in excitation and deexcitation pathways of different plasma species. Consequently, actinometry was used for all OES experiments.<sup>1-2</sup> In this technique, the addition of a noble gas (with well-known emission characteristics) allows for comparisons of the densities of excited state NO species. In this work, a 5% by partial pressure addition of argon was employed; thus all reported values for NO\* are relative to Ar\*, monitored at 750.4 nm.

### 2.3 Mass Spectrometry

A Hiden PSM003 mass spectrometer, described previously,<sup>3</sup> was used to identify nascent ions within the plasma. A cross-sectional diagram of the experimental apparatus is provided in Fig. 2.3. Energy scans of nascent ions were completed with the aid of a  $\pm 1000$  V Bessel box energy filter and a triple-filter quadrupole to provide ion energy distributions. The base pressure of the apparatus was maintained at  $\sim 10^{-8}$  Torr via a pump stack comprising a 60 l/s turbomolecular pump backed by a 400 l/min mechanical pump; the operating pressure was generally  $\sim 10^{-5}$  Torr. Plasma ions traveled 5 cm from the exit of the reactor and entered the mass spectrometer probe through a 600  $\mu\text{m}$  sampling orifice. IEDs were obtained for individual ions identified in the raw mass spectrum of each system by scanning a 300 eV energy range for selected mass-to-charge ratios. Mean ion energies for individual ions,  $\langle E_i \rangle$ , were determined by normalized integration of the IEDs over the appropriate energy range according to equation (2.1),<sup>4</sup>

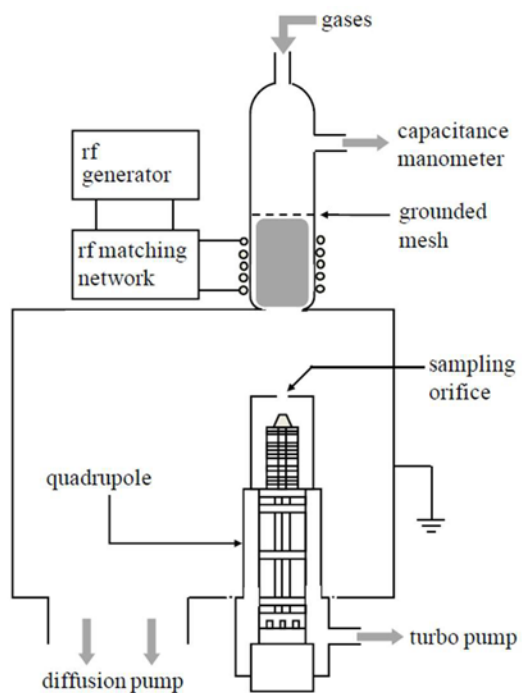


Figure 2.3 Schematic of the mass spectrometer system interfaced to an ICP reactor.

$$\langle E_i \rangle = \frac{\int f(E) E dE}{\int f(E) dE} \quad (2.1)$$

where  $E$  denotes ion energy. The total mean ion energy,  $\langle E_i \rangle_{\text{total}}$ , was determined by averaging the  $\langle E_i \rangle$  values for all ions (regardless of identity) in a particular plasma system at a given set of operating conditions.

Although the degree of ionization is minimal in ICPs, we have previously measured the ion density in our ICPs to be  $\sim 1-5 \times 10^{10} \text{ cm}^{-3}$  which is similar, albeit slightly higher, than the electron density, supporting the idea that ICPs such as those employed here are quasi-neutral.<sup>3</sup> We estimate using a modified Saha analytical approach that ionization fractions are roughly 3-10% of the neutral NO density in the systems discussed here.<sup>5</sup> Similarly, these non-thermal systems give rise to electron temperatures that are 2-3 orders of magnitude greater than the neutral gas temperatures.<sup>6</sup>

## 2.4 IRIS Technique

IRIS data were collected to determine scatter coefficients for NO species in all four precursor systems. The IRIS apparatus, described in detail previously,<sup>7</sup> and depicted in Fig. 2.4, utilizes laser-induced fluorescence (LIF) to image radicals in a plasma molecular beam. Species generated in the plasma source are collimated via differential pumping through a series of slits (0.78-1.07 mm) and enter a high-vacuum ( $< 5 \times 10^{-6}$  Torr) interaction region as an effusive molecular beam. Stimulated fluorescence for a species of interest was obtained by intersecting the molecular beam at a  $45^\circ$  angle with a tunable XeCl excimer-pumped (Lambda Physik LPX210i, 180 mJ/pulse, 25 Hz) dye laser. For these experiments, an excitation wavelength of 226.199 nm was used for on-resonance images, corresponding to the  $A^2\Sigma^+ \leftarrow X^2\Pi$  transition of

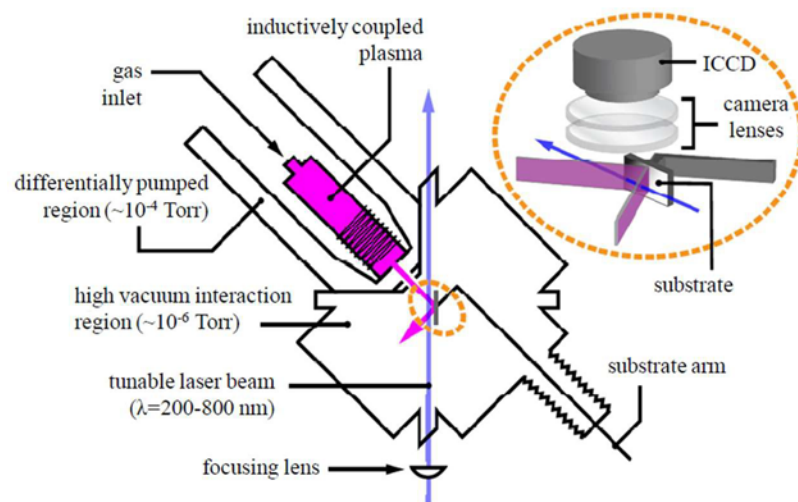


Figure 2.4 Schematic of the IRIS apparatus.

NO. Off-resonance background images taken at 226.500 nm were subtracted from on-resonance LIF images. The images were collected with the use of a gated intensified CCD (ICCD) located above and orthogonal to the interaction region. The ICCD images consisted of 512 x 512 pixels with 4 x 4 pixel binning. The ICCD gate width was 100 ns and the gate delay ranged from 1500-1550 ns for all experiments.

LIF images were also collected with a Si wafer in the path of the plasma molecular beam and parallel to the propagation of the laser. These images contain fluorescence from species both within the molecular beam as well as those scattered off of the surface. The initial image (without a substrate present) can be subtracted from images taken with the substrate in the path of the molecular beam to provide an image corresponding to only signal arising from scattered molecules. The scatter and incident beam images are pixel averaged for a 20-pixel wide cross-section along the laser axis. These cross-sections are then simulated to calculate the surface scatter coefficient (or surface scattering coefficient),  $S$ , as described elsewhere.<sup>8-9</sup> Specifically, the method used to determine  $S$  values is a model that calculates profiles for both the incident molecular beam and scattered signal, and is based on the experimental geometry (including laser-surface distance, laser-molecular beam angle (here 45°), defining slit widths, and distance from slits to laser beam). Further, the model assumes Gaussian broadening, an adsorption-desorption scattering mechanism (cosine distribution about the surface normal), and allows for inclusion of temperature effects (i.e. where internal/translational temperatures for both incident and scattered species are known; otherwise desorbing molecules are assumed to have a rotational temperature characterized by the substrate temperature, here 300 °C). The only truly adjustable parameter in the model is the amount of scatter off of the substrate for molecules in the specific state being probed. Thus, errors in  $S$  values are determined from error in fitting a particular data set



(determined by residual analysis) and also averaging fits to several data sets. Thus, the resulting error limits represent both the uncertainty within a particular data set as well as the set-to-set reproducibility of the measurement. Note that IRIS measurements can be made by probing a range of electronic states to evaluate if various rovibrational states are responding differently at a surface.  $S$  values are thus essentially a measure of the flux of radicals of a specific electronic state (i.e.  $\text{NO } X^2\Pi$ ) scattered from a substrate, relative to the incident flux of those same radicals from the plasma molecular beam.

Because the IRIS experiment monitors a selected electronic state for a specific radical of interest,  $S$  values can exceed unity as a result of contributions from processes such as surface quenching of excited electronic state radicals, surface-mediated dissociation or recombination reactions, surface-mediated ion neutralization, etc. In such scenarios, the scattered radicals are essentially generated at the surface. Thus,  $S$  generally provides an estimate of the proclivity for some type of radical (again,  $\text{NO } X^2\Pi$ , in a specific rovibrational state, for example) to scatter from, rather than react or be consumed at some surface (here, a Si wafer). It is important to remember that the  $S$  values measured here provide but one level of insight as to how NO reacts at a surface during plasma bombardment of the surface, not under well-controlled UHV conditions with a lone molecular state of NO hitting a pristine surface. Consequently, IRIS data provide a “real-world” glimpse into plasma-surface interactions, making it incredibly valuable in applications such as those investigated here.

Values for  $S(\text{NO})$  were determined for biased and unbiased substrates, and substrate biasing was accomplished by directly applying a +300 V<sub>dc</sub> bias to the Si wafer. This repels positive ions in the plasma molecular beam and allows for the determination of ion/scatter

relationships. In this ion-limited scenario, the measured scatter coefficients are denoted  $S_{\text{ion-limited}}$ ; the effect of removal of ions can be gauged by determining  $\Delta S$ , defined as  $S - S_{\text{ion-limited}}$ .<sup>10</sup>

## REFERENCES

1. Hancock, G.; Sucksmith, J. P.; Toogood, M. J., Plasma Kinetic Measurements Using Time-Resolved Actinometry: Comparisons with Laser-Induced Fluorescence. *Journal of Physical Chemistry* 1990, 94 (8), 3269-3272.
2. Kiss, L. D. B.; Nicolai, J. P.; Conner, W. T.; Sawin, H. H., CF and CF<sub>2</sub> Actinometry in a CF<sub>4</sub>/Ar Plasma. *Journal of Applied Physics* 1992, 71 (7), 3186-3192.
3. Zhou, J.; Martin, I. T.; Ayers, R.; Adams, E.; Liu, D.; Fisher, E. R., Investigation of Inductively Coupled Ar and CH<sub>4</sub>/Ar Plasmas and the Effect of Ion Energy on DLC Film Properties. *Plasma Sources Science and Technology* 2006, 15 (4), 714.
4. Edelberg, E. A.; Perry, A.; Benjamin, N.; Aydil, E. S., Energy Distribution of Ions Bombarding Biased Electrodes in High Density Plasma Reactors. *Journal of Vacuum Science & Technology A* 1999, 17 (2), 506-516.
5. Ray, S. S.; Chaudhuri, K. S.; Bera, R. K., Application of Modified Decomposition Method for the Analytical Solution of Space Fractional Diffusion Equation. *Applied Mathematics and Computation* 2008, 196 (1), 294-302.
6. Lieberman, M. A.; Lichtenberg, A. J., *Principles of Plasma Discharges and Materials Processing*. Wiley: New York, 1994.
7. McCurdy, P. R.; Bogart, K. H. A.; Dalleska, N. F.; Fisher, E. R., A Modified Molecular Beam Instrument for the Imaging of Radicals Interacting with Surfaces During Plasma Processing. *Review of Scientific Instruments* 1997, 68 (4), 1684-1693.
8. Bogart, K. H. A.; Cushing, J. P.; Fisher, E. R., Effects of Plasma Processing Parameters on the Surface Reactivity of OH (X<sup>2</sup>II) in Tetraethoxysilane/O<sub>2</sub> Plasmas During Deposition of SiO<sub>2</sub>. *The Journal of Physical Chemistry B* 1997, 101 (48), 10016-10023.
9. Ho, P.; Breiland, W. G.; Buss, R. J., Laser Studies of the Reactivity of SiH with the Surface of a Depositing Film. *The Journal of Chemical Physics* 1989, 91 (4), 2627-2634.
10. Cuddy, M. F.; Blechle, J. M.; Fisher, E. R., Ion Contributions to Gas-Surface Interactions in Inductively-Coupled Fluorocarbon Plasmas. *International Journal of Mass Spectrometry* 2012, 330, 46-57.

## CHAPTER 3

### THE DESIGN AND IMPLEMENTATION OF A BROADBAND SPECTROSCOPY SYSTEM FOR GROUND STATE TEMPERATURE MEASUREMENTS

This chapter contains work completed by Joshua M. Blechle, Angela R. Hanna, and Ellen R. Fisher. It focuses on the analysis and description of our home-built broadband absorption spectroscopy (BAS) system, as well as methods of data analysis. In addition, this chapter focuses on the design of the BAS instrument (including details of the construction process and methods of troubleshooting different aspects of apparatus design and implementation) and the data analysis process.

#### 3.1 Introduction

Plasma diagnostics provide the critical foundation for developing a fundamental understanding of species identification and energetics within inductively coupled plasmas (ICPs). Within ICPs, there are numerous key figures of merit, such as gas temperature, as well as rotational and vibrational temperatures for individual species. Gas temperatures have been shown to be both independent of and highly dependent on plasma parameters, conditional to the plasma system. These system and parameter differences leads to an increased desire to understand trends in energy partitioning in ICPs.<sup>1-7</sup>

Plasma species that are promoted to excited electronic states via electron impact and other collisions within the plasma are often studied using optical emission spectroscopy (OES). Monitoring these species decay back to their ground states via emission is widely used for determination of species concentration and temperature profiles of the excited state species.<sup>8-12</sup>

There are, however, inherent challenges in using excited-state data to evaluate ground state molecules, which are the majority of species in low temperature plasmas. Therefore, in situ investigations of ground state species are critical to understanding underlying mechanisms and reactions occurring within these systems. The most common method for probing ground state species is laser-induced fluorescence,<sup>12-14</sup> which is a powerful non-intrusive spectroscopic technique. Shortcomings of LIF, however, include its use being confined to species that possess a fluorescing excited state, requisite expensive instrumentation (e. g. a laser system), and being inherently limited because of non-radiative relaxation processes.<sup>15</sup> Recent studies have demonstrated the utility of an alternate technique, broadband absorption spectroscopy (BAS) within a variety of plasma systems.<sup>16-21</sup> There is, however, no widely-accepted methodology for the assessment of BAS spectra from plasmas or the subsequent determination of energies from the data. It is with this in mind that we aimed to compare multiple analyses and simulation techniques for data acquired with our new BAS system.

## 3.2 System Development

### A. Reactor Design

In the early development of this instrumentation, the goal was to create a method by which to incorporate an absorbance measurement with our standard glass plasma reactors. Ultimately, this would allow for a direct comparison to existing spectroscopic data within our ICP systems, including identical path lengths and reactor volume. Early reactor sketches and designs, Fig. 3.1, demonstrate the evolution of our design considerations. The reactor systems used within the Fisher Group are generally 2-piece designs, and as we already had half-reactor systems designed to interface to the detector, we planned to create a new upstream reactor

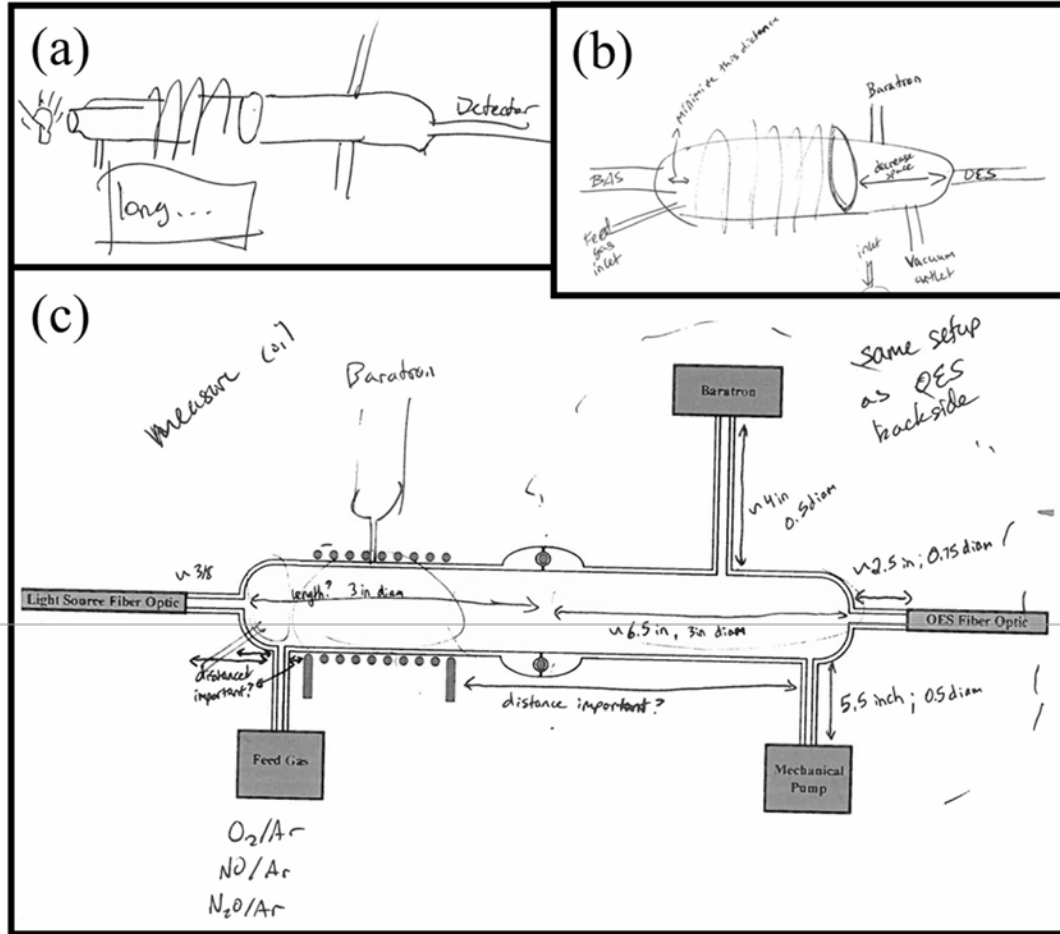


Figure 3.1 Collection of original design ideas for the BAS system, including trouble shooting notes. Panels (a) and (b) both show initial designs and spatial considerations. Panel (c) is the schematic given to the glassblower for implementation.

section to incorporate the light source. We were, however, interested in utilizing a broadband light source from ~200-800 nm to encompass the absorbance of many common species (NO, N<sub>2</sub>, O<sub>2</sub>, Ar, CH, etc) within a variety of plasma systems utilized by the entire Fisher Research Group. The problem with this design was the broadening of the source across the desired path length, which was feared to lead to low absorbance signals at the detector. Thus, adding a series of collimating lenses at each end of the reactor was deemed ideal. The diameters of the available lenses (~10 cm) were, however, much greater than the quartz windows commonly used within the research group (~1.25 cm). This presented an issue as the common method used to interface quartz windows to our reactor systems employed Swagelok Ultra-Torr<sup>®</sup> fittings, and it was not possible to acquire these fittings at the appropriate diameter. Ultimately, this resulted in a need to incorporate much larger quartz windows into each end of the reactor, which was achieved via the use of RODAVISS<sup>®</sup> joints.

To minimize cost and maintain equivalent reactor lengths/volumes, a completely new design was created that eliminated the central o-ring joint in favor of a continuous reactor design. We knew the diameter of the RODAVISS<sup>®</sup> joints would be large enough to allow for introduction of substrate samples into the reactor (which is the primary rationale for 2-piece reactor systems), although the disassembly may be a bit more time consuming. It is still possible to create a 2-piece reactor for this experiment if desired (e.g. to allow for easy introduction of substrates), but in the early design phases we opted to minimize the sources for potential vacuum leaks. The result of these repeated iterations was a final reactor design, based on input from both Mike Olson (university glassblower) and representatives from Avantes Inc. (manufacturer of the spectrometer), utilizing a modified glass tubular, ICP reactor specifically designed to perform BAS experiments, Fig. 3.2. Our BAS experimental apparatus consists of an AvaLight-DHS

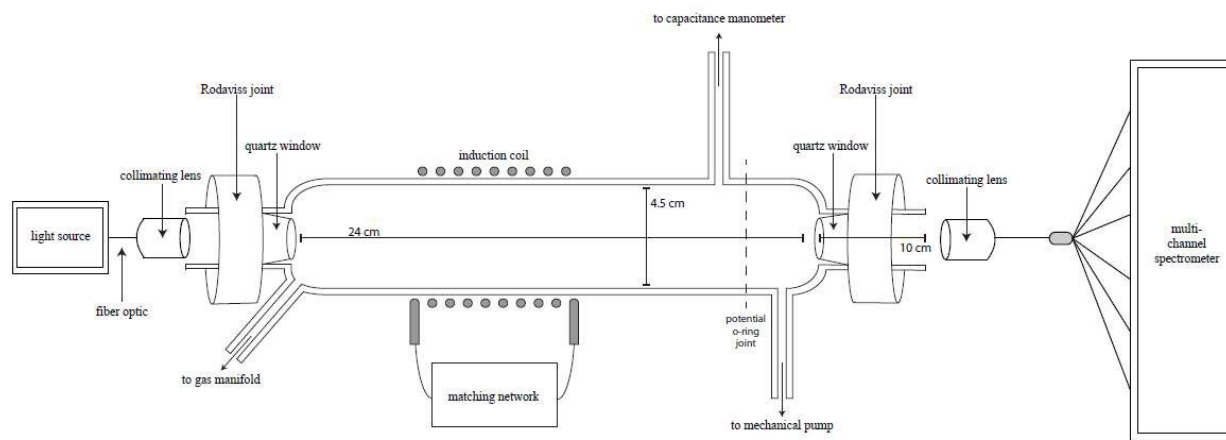


Figure 3.2. Schematic representation of final BAS apparatus for low-temperature ICP systems.



deuterium-halogen light source interfaced to the ICP reactor via a fiber optic cable and collimating lens (Avantes DCL-UV/VIS-200). Emission from the light source and the plasma is collected by the spectrometer in a similar manner on the opposite end of the reactor. Quartz windows are secured to the reactor using RODAVISS® joints, enabling maximal signal intensities via the coaxial collection of plasma emission. An AvaSpec-2048L-USB2-RM multichannel optic spectrometer was employed to collect spectra over a wavelength range of 197 – 1061 nm. The spectrometer houses six gratings, each synchronized for simultaneous data collection with 2048-pixel linear array charged couple device detectors. Integration times and the number of averages collected depend on the specific experiment to maximize signal-to-noise ratios.

Operationally, this design seemed quite effective, provided the collimating lenses were appropriately aligned. To achieve proper system alignment, the lenses were originally mounted in optics holders and affixed to a breadboard below the reactor. The reactor itself was attached to a monkey bar system, in keeping with the standard reactor mounting systems used in the Fisher group. This arrangement, however, required alignment in 3-dimensions. Specifically, the height of the clamp at each end of the reactor, the height of the lenses, the depth of each clamp relative to the monkey bars, and the overall angle of the clamps could all be modified and were subject to random drifts as a result of laboratory conditions. To minimize the number of optimizable parameters, the reactor clamps were ultimately placed in optics mounts aligned with the collimating lens mounts so that the heights of each mount was the sole variable. A photograph of the final reactor mounts and comparisons of signal intensities based on alignment, are shown in Fig. 3.3.

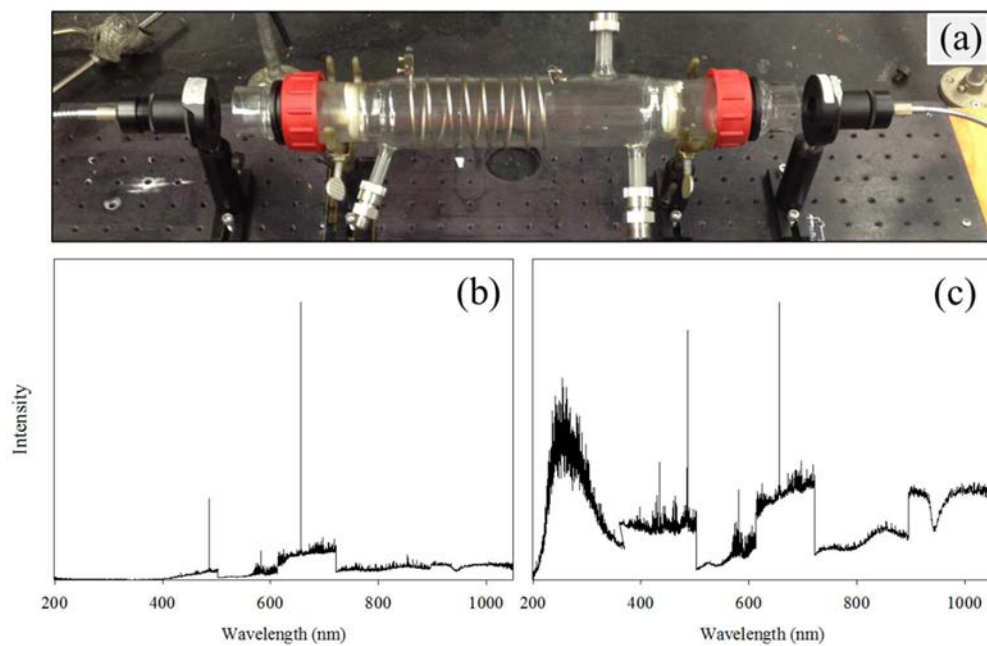


Figure 3.3 Panel (a) photograph of the optics employed to align the light source and the detector along with the reactor. Panels (b) and (c) show source emission when the system is misaligned and properly aligned, respectively.

For the remainder of the experiments delineated in this chapter, the above described system design was used in conjunction with the following plasma precursors: NO (American Gas Group, >99.5%), N<sub>2</sub>O (Airgas, >99%), as well as a combination of N<sub>2</sub> and O<sub>2</sub> (both Airgas, >99.99%). Precursor flow rates were monitored with MKS flow controllers, yielding flow rates that ranged from 3–5 sccm. The base pressure of the system was maintained at approximately 10<sup>-3</sup> Torr via a 400 l/min mechanical pump, where system gas pressures (p) were measured by a Baratron capacitance manometer. The mixed gas (N<sub>2</sub>, O<sub>2</sub>) system was a 50/50 mixture, measured via partial pressures. Radio frequency (rf) at 13.56 MHz power was applied through a matching network; applied rf power (P) ranged from 50 to 200 W.

#### B. Determination of Absorbance

The ability of the designed system to generate an absorption spectrum was verified using NO<sub>(g)</sub> (sans plasma), as shown in Fig. 3.4. Using the absorbance function of AvaSoft 7.8, light source emission was used as a reference to determine the absorbance of a 250 mTorr NO gas system. Spectral absorbance data were fit in LIFBASE<sup>22</sup> as described below. As the gas phase system is thermalized at room temperature, a simulation was generated at 297 K corresponding to the measured laboratory temperature. The resolution was then adjusted to maximize peak correlation, ultimately resulting in a 99% correlation. Thus, an experimentally determined resolution of 6.21 nm was used in all subsequent data analyses.

One of the difficulties of these plasma absorbance measurements is the dual-reference nature of the system (both the light source and the plasma are emitting). There is also the assumption that the ignition of the plasma will not impact the emission of the light source, as any interaction between the two would cause an incorrectly measured absorbance. Early attempts to verify system function were performed using a total absorbance measurement (described below).

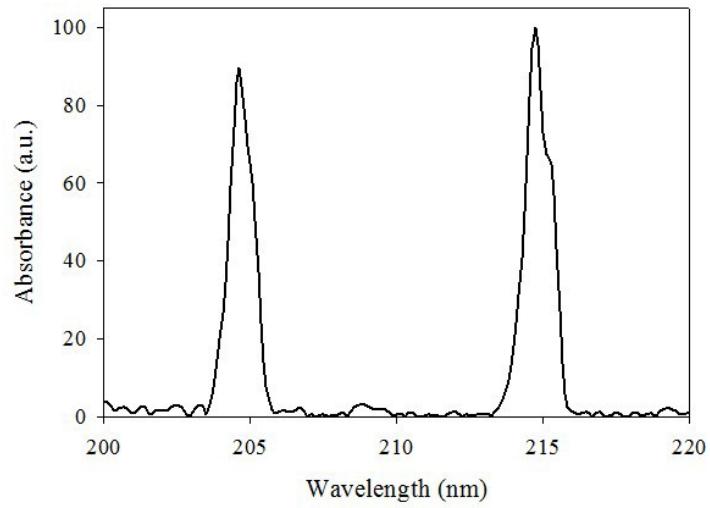


Figure 3.4 Absorbance spectrum for NO gas (sans plasma) at p=250 mTorr. Peaks correspond to X  $\rightarrow$  A transition.

These attempts yielded elevated baselines, and in many cases, the features of the absorbance spectra were almost entirely lost to the baseline (Fig. 3.5a). To investigate whether an interaction of plasma and source was the cause of these issues, various spectral comparisons were performed. Specifically, three independent irradiance-calibrated emission spectra were collected for the plasma ( $I_p$ ), the light source ( $I_s$ ), and for trials in which both the plasma and light source were emitting ( $I_{ps}$ ). Specifically, by comparing the two equivalent spectra of ( $I_p$ ) and ( $I_{ps} - I_s$ ), the cause of the baseline shift was believed to be a deviation in source emission with respect to plasma ignition, Fig. 3.5b. This resulted in multiple attempts to isolate the source from the plasma system. Ultimately, a Faraday cage was built to house the source, which led to successful isolation of the reactor system and well-resolved absorbance spectra, Fig. 3.5c. Once the system was isolated, all spectra were background corrected within the AvaSoft 7.8 program and efforts were made to quantify absorbance. The most basic method to evaluate absorbance is by simply finding the difference of the dual source emission relative to the sample, demonstrated by the individual emission spectra in Fig. 3.6. This total absorbance ( $A_T$ ) spectrum fully represents all rovibrational absorption, determined via Equation 3.1:

$$= - \quad - ( \quad + \quad ) \quad (3.1)$$

Following Bruggeman and coworkers,<sup>16</sup> we also generated a fractional absorbance ( $A_F$ ) spectrum, determined via Equation 3.2:

$$= - \frac{(\quad)}{\quad} \quad (3.2)$$

The immediate benefit of this approach is that it is directly applicable to a Beer-Lambert Law analysis; it accounts for the emission of the light source and more accurately represents the magnitude of absorbance from each vibrational state.

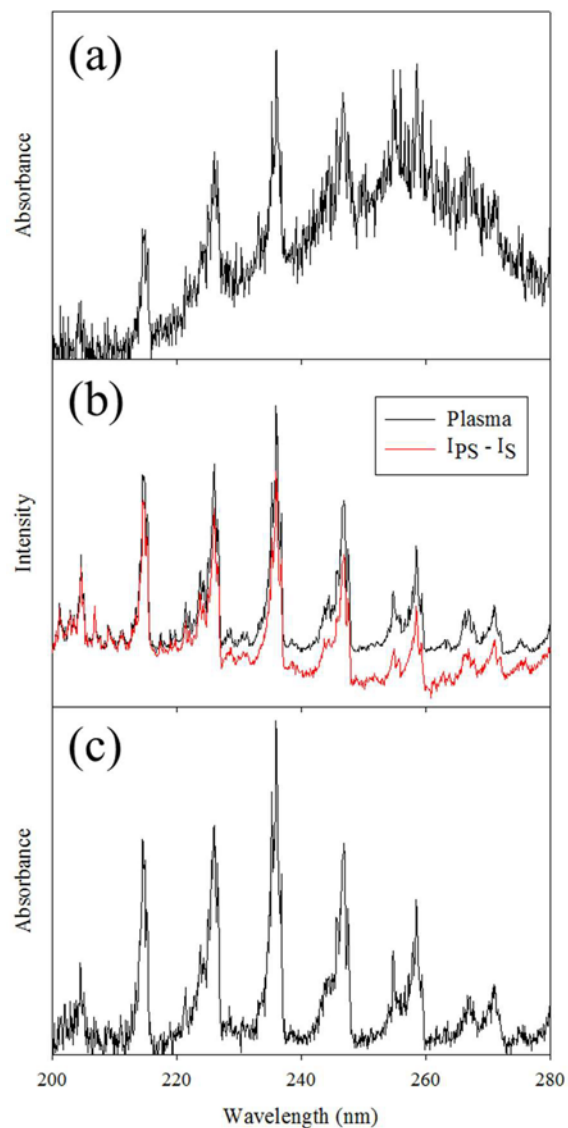


Figure 3.5 Panel (a) contains a representative absorbance spectrum from early measurements which included an elevated baseline. By comparing the plasma emission system to an equivalent spectrum in the plasma/source system (b) it is clear the addition of the light source directly impacts the baseline signal arising from the plasma. Panel (c) contains an absorbance spectrum collected after the addition of the Faraday cage structure surrounding the light source, demonstrating reduced electric field coupling to the apparatus.

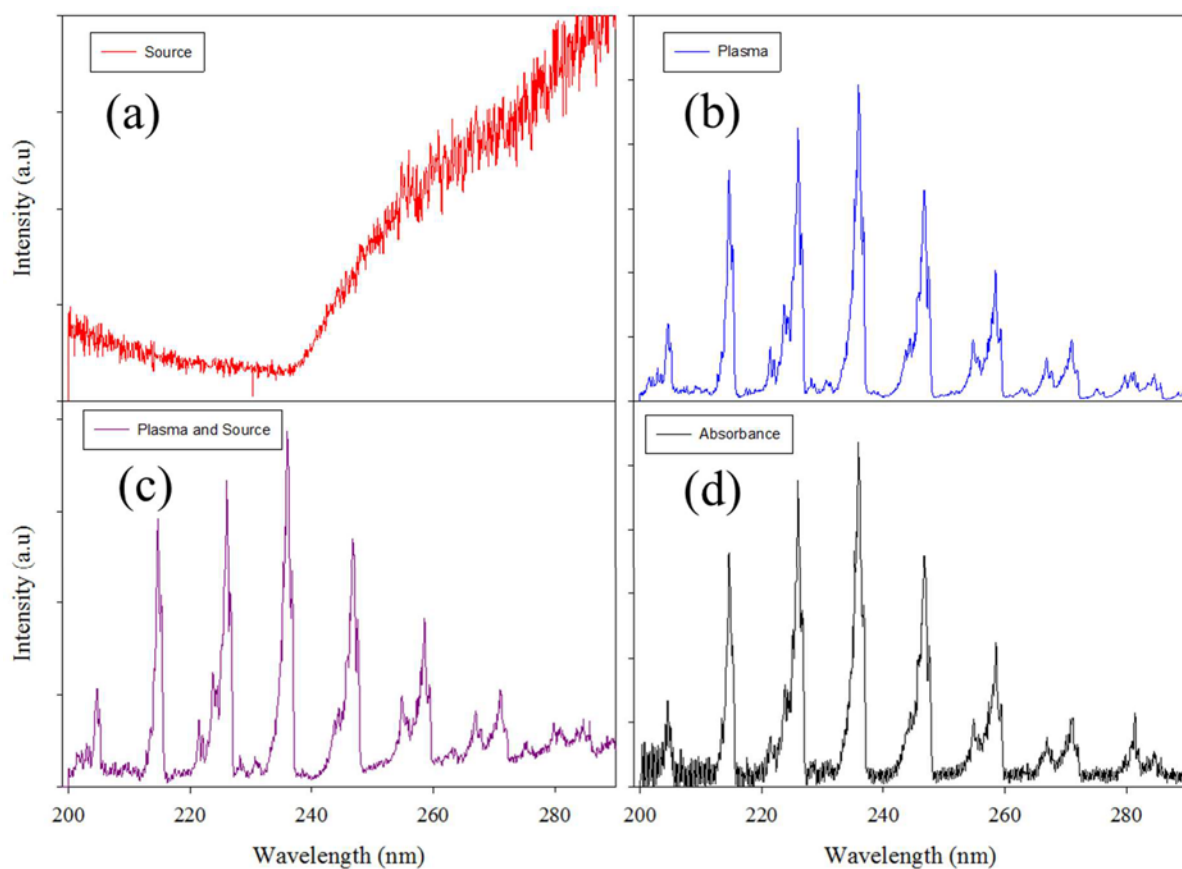


Figure 3.6 Individual spectra collected for a 50 mTorr, 100 W NO plasma absorbance experiment. (a) Source emission in the region of interest; (b) plasma emission; (c) emission from the combined plasma and source system; and (d) absorbance calculated by subtracting spectra shown in (a) and (b) from spectrum shown in (c).

It is also common in gas-phase spectroscopy to determine a percent transmittance and convert this value to absorbance. When such a method is applied to a plasma system, absorbance can be calculated using Equation 3.3:

$$= -\frac{I}{I_0} \quad (3.3)$$

These three absorption calculation methods have been utilized for the purpose of comparative analysis, with example absorbance spectra shown in Fig. 3.7. The impact of each method on the determination of vibrational ( $T_V$ ) and rotational ( $T_R$ ) temperatures for non-equilibrium plasma systems was evaluated for the purpose of determining the most appropriate method for analyses of future BAS studies.

### C. Evaluation of Absorbance Spectra

Total absorbance spectra were analyzed using different simulation programs, depending on the molecule of interest. In one method, fitting was completed through LIFBASE 2.1.1 simulations. After importing experimental spectra and specifying the parameter space (Table 3.1), the simulated vibrational histogram was manually manipulated to best represent experimental peak heights, yielding non-equilibrium distributions. Using these vibrational state populations, we determined  $T_V$  via Equation 3.4,

$$= \frac{\sum_i I_i (\hbar \omega)^{v+1/2}}{n} \quad (3.4)$$

where  $n$  represents the fractional population of an individual vibrational state,  $\omega$  is the angular frequency,  $v$  is the numeric vibrational state, and  $k_B$  is Boltzmann's constant.

To streamline the calculation of  $T_V$ , a spreadsheet calculator was designed. With this program, populations can be taken from the LIFBASE histogram and entered into the spreadsheet. An example histogram and  $T_R$  calculation are shown in Table 3.2. Determination of  $T_R$  was achieved by adjusting the rotational temperature within LIFBASE to match peak



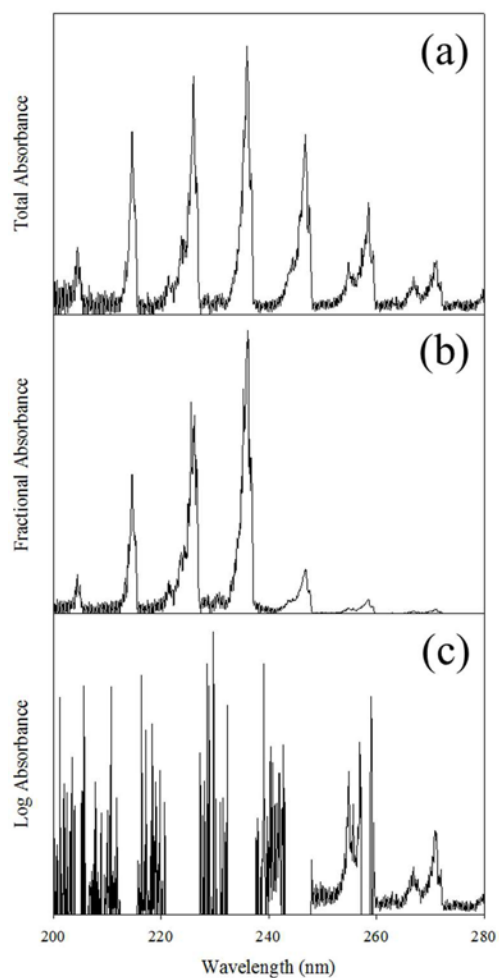


Figure 3.7 Spectra from a 50 mTorr, 100 W NO plasma were evaluated via three different common absorbance calculation techniques as discussed in the text: (a) total absorbance; (b) fractional absorbance; and (c) log absorbance.

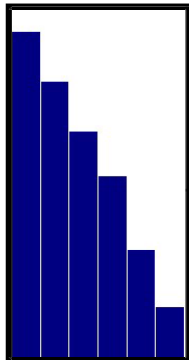
Table 3.1 Representative user-defined values needed in both fitting programs to achieve appropriate simulations to experimental spectra.

<b>LIFBASE</b>				
<b>Parameter</b>	<b>Description</b>	<b>Value</b>		<b>Units</b>
$\lambda$ start	Start wavelength	230		nm
$\lambda$ end	End wavelength	280		nm
Broadening	Doppler broadening	0.00628		-
	Predissociation broadening	on: default		-
Resolution	Experimentally determined resolution	6.21		Å
L	Simulated lineshape	Lorentzian		-

<b>SPECAIR</b>				
<b>Parameter</b>	<b>Description</b>	<b>Value</b>		<b>Units</b>
$\lambda$ start	Starting wavelength	NO: 230	N <sub>2</sub> : 290	nm
$\lambda$ end	End wavelength	NO: 280	N <sub>2</sub> : 450	nm
Slab width	Width of plasma along line of spectrometer	19		cm
Self-absorption	Self-absorption of radiation along length of plasma	on		-
Room air absorbers	Includes effects of room air absorption (H <sub>2</sub> O, CO <sub>2</sub> , and O <sub>2</sub> )	on: default		-
Room air absorbers length	Optical path length for absorption by default molecules	13		cm

Table 3.2 Tool designed to use vibrational state populations (from LIFBASE simulation histogram at left) and calculate corresponding energies. These energies are then used to determine  $T_v$  using the harmonic oscillator model.



Vibrational State	Population	$\hbar$ (J/s)	$\omega$ (s)	Energy (J)	$E_{\text{Total}}$ (J)	$k$ (J/K)	$\Theta_v$ (K)
0	0.280609	1.05E-34	3.54E+14	5.22907E-21	8.10615E-20	1.3806E-23	5871.5
1	0.235340			1.31565E-20			
2	0.192551			1.79407E-20			
3	0.155110			2.0233E-20			
4	0.092710			1.55486E-20			
5	0.043680			8.95361E-21			

FWHM, assuming a thermalized distribution. A second database used for data simulation was Specair,<sup>23</sup> a commercial program specializing in non-thermal equilibrium spectra. Primary fitting parameters used are shown in Table 3.1. A trapezoidal slit function, which takes into account the broadening of spectral lines by the instrument, was generated with a FWHM of 6.21 nm to match the experimentally-determined resolution. Upon selecting the radiative transition of interest, the “Temperature Loop” function of the program was used. Using the initial temperatures suggested by Specair’s “Find Transition” function, the translational, rotational, and vibrational temperatures were held constant while electronic temperatures were looped to match peak intensity. After determination of electronic temperature,  $T_R$  and  $T_V$  were fit in an alternating fashion until both of them remain roughly constant between each round of temperature adjustments and a simulated fit was generated to adequately represent the experimental spectrum.

The spectral lines of the second positive system of  $N_2$  ( $B^3\Pi \rightarrow C^3\Pi$ ) ( $2^+$ ) were used to determine both  $T_R$  and  $T_V$  within a 100%  $N_2$  plasma system, a 100%  $N_2O$  plasma, and a 50/50 mixed gas plasma containing  $N_2$  and  $O_2$ . The radiative transition of NO gamma ( $X^2\Pi \rightarrow A^2\Sigma^+$ ) was used to determine  $T_R$  and  $T_V$  of NO within a 100% NO plasma system, 100%  $N_2O$  plasma system, and the  $NO_{(g)}$  formed from a 50/50 mixed gas system described above.

### 3.3 Results and Discussion

#### A. Results

To verify the functionality of our BAS reactor, it was employed to acquire energy partitioning data from a range of plasma systems. For example, two different absorption calculation methods were employed ( $A_T$  and  $A_F$ ) to analyze spectra for NO formed in a 50 mTorr,

100 W NO plasma (Fig. 3.8). The simulations in Fig. 3.8a and 3.8b were generated in LIFBASE, giving rise to  $T_V = 4100$  K,  $T_R = 600$  K when the fractional absorption method (Equation 3.2) was used and  $T_V = 6300$  K,  $T_R = 700$  when the total absorption method was used (Equation 3.1). Utilizing  $A_T$  enabled us to explicitly identify higher order vibrational states populated in the ICP, which in turn improved our ability to fit these peaks. The increased contributions of these states represented in the simulation, however, leads to a larger calculated value for  $T_V$  in the  $A_T$  spectrum. Alternatively, the  $A_F$  method more accurately accounts for the non-uniform emission from the light source. Because of the profile of our light source in the wavelength range of interest (i.e. 230-280 nm), Fig. 3.3b, the overall peak height for higher order states is significantly reduced, leading to a reduced  $T_V$ .

In addition to comparing calculation methods, there is an interest in comparing the efficacy of and consistency between the results generated by different spectral simulation programs. The use of multiple simulation programs enables us to study a larger library of molecules and radiative transitions. It is not clear, however, if the different simulation programs provide comparable or consistent results. To this end, one spectrum from a 50 mTorr, 100 W NO absorbance experiment was simulated with the two programs used in this work. Figure 3.8a shows the simulation of experimental data using LIFBASE, in which  $T_R = 700$  K and  $T_V = 6300$  K, and Figure 3.8c contains the same experimental spectrum, fit using Specair, yielding  $T_R = 650$  K and  $T_V = 6100$  K. Both simulations fit the NO gamma radiative transition. Note that these values may not represent an absolute determination of the internal temperatures for the ground state species within an NO plasma; however, strong agreement between two different spectral analyses lends itself to validity in elucidating energy partitioning trends. In addition, the agreement between the results of the two calculations suggests validity of our calculation of  $T_V$  in

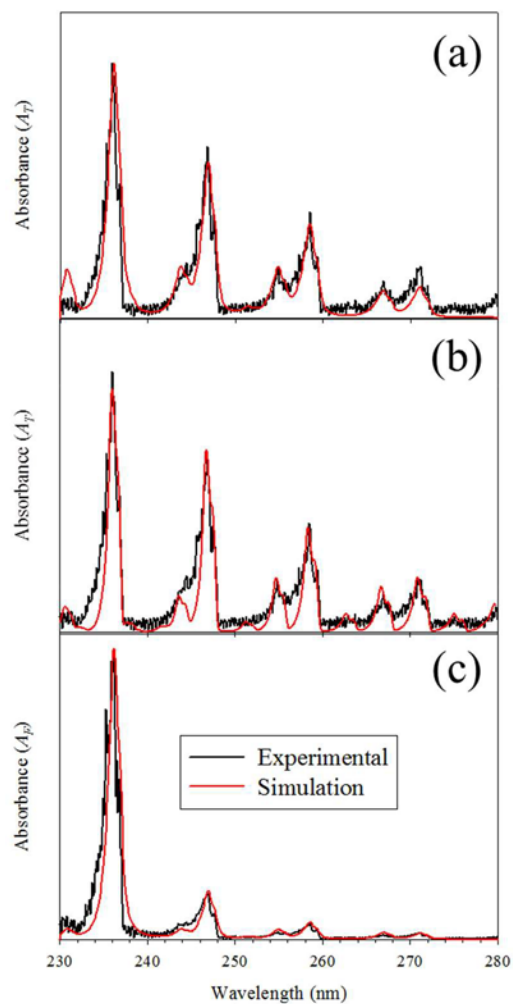


Figure 3.8 Absorbance spectrum from a 50 mTorr, 100 W NO plasma was evaluated via different simulation programs: (a) total absorbance fit using LIFBASE; (b) total absorbance fit using Specair; and (c) fractional absorbance via LIFBASE.

the LIFBASE simulations, and allows us to confidently compare temperature values calculated via each program. This is of vital importance as each simulation library contains a different set of species for which simulations can be performed. One species not available within LIFBASE, but accessible via Specair is  $N_2As$  depicted in Fig. 3.9,  $N_2$  is clearly one of the absorbing species present in NO plasmas, along with the expected absorbance from NO. Utilizing Specair, the radiative transitions of the NO gamma and the  $N_2$  second positive bands were simulated. Figure 3.9a contains the total absorbance ( $A_T$ ) spectrum, wherein  $N_2$  absorbance peaks (290 – 450 nm) clearly dominate the spectrum. Analysis of this spectrum using Specair gives rise to the internal temperatures reported in the inset table. Figure 3.9b shows the fractional absorbance spectrum for the same spectrum.

The above results demonstrate the efficacy of our BAS apparatus for collecting data to determine vibrational and rotational temperatures of molecules within single gas systems. Abrar and coworkers, however, have observed that temperatures of  $N_2$  increase as the percentage of gas additive increases.<sup>24</sup> Thus, we have also employed this apparatus and spectral programs to calculate species temperature data for an  $N_2$  mixed gas system. Specifically, we generated a 50/50 (by partial pressure) mixture of  $N_2$  and  $O_2$  with a total system pressure of 100 mTorr and  $P = 100$  W. As shown in Fig. 3.10, the NO gamma band and the  $N_2$  (second positive) band appear in the resulting absorbance spectrum. Vibrational and rotational temperatures were determined for both molecules using Specair, resulting in  $T_R(N_2) = 300$  K,  $T_V(N_2) = 4800$  K and  $T_R(NO) = 600$  K,  $T_V(NO) = 6600$  K. As evidenced by the peak broadening in the experimental spectrum, NO is a highly rotationally excitable molecule that ultimately yields a higher rotational temperature in comparison to  $N_2$ .

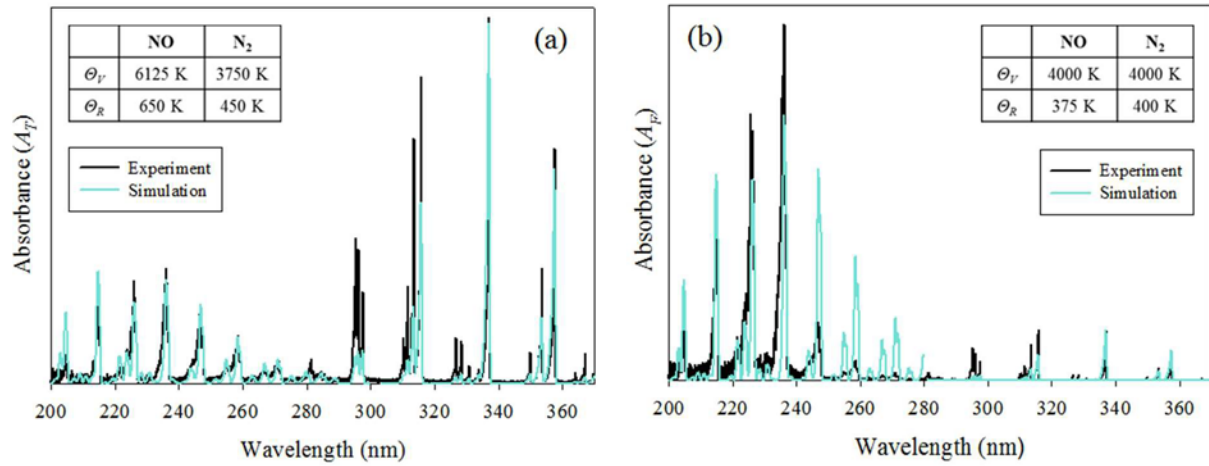


Figure 3.9 Absorbance spectra for an NO plasma system at  $p=50$  mTorr and  $P=100$  W with both NO and N<sub>2</sub> bands fit using Specair for (a) total ( $A_T$ ) and (b) fractional absorbance ( $A_F$ ) giving rise to  $\Theta_R$  and  $\Theta_V$  values.



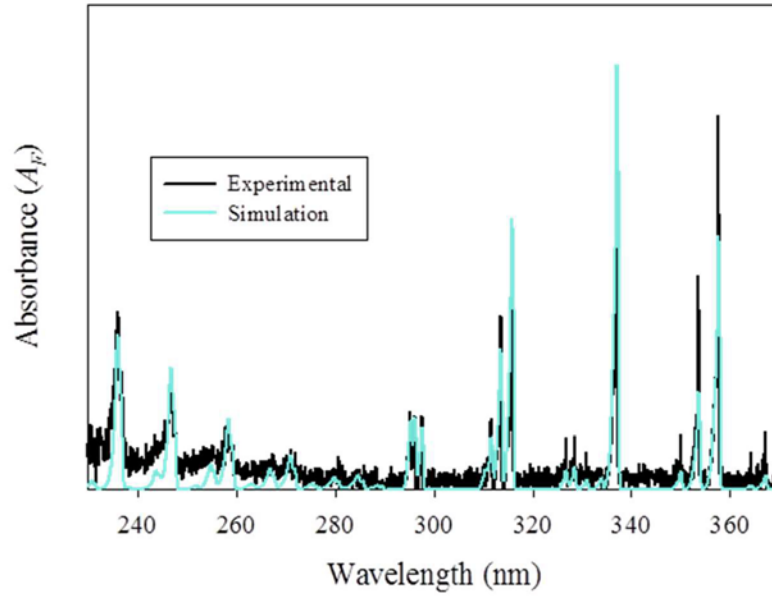


Figure 3.10 Representative fractional absorbance spectrum for a plasma formed from a 50/50 mixture of  $N_2$  and  $O_2$  at  $p=100$  mTorr and  $P=100$  W. The simulation represents  $\Theta_R=350$  K,  $\Theta_V=5500$  K for  $N_2$  and  $\Theta_R=900$  K,  $\Theta_V=3700$  K for  $NO$ .

## B. Discussion

As noted in Section 3.1, determination of rotational and vibrational temperatures of ground state species within plasma systems is essential to gaining a more complete molecular-level understanding of plasma chemistry. The goal of this work was to demonstrate the utility of a new BAS apparatus in our laboratory and to evaluate and compare the ability of two spectral simulation programs to evaluation our spectra. This is done in the hopes of maintaining consistency and reproducibility of our data and with our reported internal temperatures.

Currently, data transformation techniques used to generate an absorption spectrum for plasmas do not adhere to a single, set protocol or “best practice”. Although recent efforts have addressed such concerns, disparity still exists within the literature.<sup>25-26</sup> One approach, often utilized for gas-phase measurements, is to determine a percent transmittance and convert this value to absorbance. With plasmas, however, this raises the question of how appropriate it is to attempt to measure the amount of light traveling through a given sample medium when the sample itself (the plasma) is also emitting. Indeed, as a result of the dual-reference nature of the system, there are additional difficulties with this approach. Namely, even small inconsistencies within the plasma emission can lead to the determination of negative values that are undefined for the logarithmic function (Equation 3.3). For example, if no absorbance is occurring, we would expect that  $\ln\left(\frac{I_{\text{plasma}}}{I_{\text{plasma}}}\right) = 0$ , but fluctuations in intensity could result in a negative result. As such, the absorption value may be indeterminable for values at or near 100% transmittance.

To avoid these potential issues and derive a direct measure of absorbance, we must independently consider the two reference spectra utilized in this system, specifically the emission of the plasma and the emission of the light source. Assuming the ignition of the plasma does not directly impact the emission of the light source, these two references can be directly compared to

the combined system emission. Therefore, the most concise absorbance expression is  $A_T$  (Equation 3.1), where absorbance is calculated by simply subtracting the two reference spectra from the sample. This is especially valuable for species and state identification because of the increased signal arising from this calculation representing the total amount of light absorbed by the system. This method does not, however, take into account the total amount of light available to be absorbed at a particular wavelength. In the case of systems in which multiple species are being investigated across a range on the order of 10-100 nm, such distinctions are of utmost importance. Specifically, this is because many light sources have variance in emission across a broad wavelength range and increased absorbance may be the result of increased available light. As such, the intensity of absorbance as calculated via  $A_T$  can be used for species (and rovibrational transition) identification.

To address the light source, another data transform used in the literature is  $A_F$ , described here in Equation 3.2. This determination of absorbance is also derived from the Beer-Lambert Law, but avoids the potential complications of logarithmic conversion while still accounting for the (potentially variable) light source emission. Indeed,  $A_F$  is similar to  $A_T$ , except for the division of the light source spectra across the wavelength range. This metric, therefore, will generate an identical spectrum (with respect to relative peak heights and shapes) to  $A_T$  if the source emission is a constant. Additionally,  $A_F$  more accurately represents vibrational and rotational state populations necessary for temperature calculations. This is because using the source emission as a divisor ensures there is not an over- or under-representation of the magnitude of the absorbance of the species.

One of the benefits to a broadband absorption experiment is the large wavelength range accessible for analysis, which allows a huge variety of species to be investigated. Given the

complexity of many plasma systems, often containing dozens of different neutral species, simultaneous determination of internal temperatures for multiple species would be ideal. These simulations, however, could require a wavelength range spanning hundreds of nanometers and are subject to oversimplification, such as having the most intense absorbance peaks dwarf the higher order vibrational states that are much less populated. This could lead to complete omission of a particular vibrational state from the simulation, which would therefore misrepresent  $T_v$ . One example of this behavior is shown in Fig. 3.8, in which we compare simulations of NO absorbance using both  $A_F$  and  $A_T$  methods. The total absorbance spectrum clearly reveals that higher order states of NO (such as  $v = 4$  and  $v = 5$ ) are populated within this plasma system. The associated populations determined through an  $A_T$  calculation are higher than one might expect for such systems (10-20%). Alternatively, although  $A_F$  calculations across the same spectral range still show these states are populated, the weak absorbance of these higher order states makes it potentially difficult to adequately simulate vibrational state populations across this 50 nm range.

Within our system, temperature results from spectra that are analyzed using the total absorbance calculation represented by  $A_T$  can be thought of as an upper bound to the internal temperatures of a molecule, as the  $A_T$  analysis over-emphasizes the populations of these higher order states. This is particular to our system as our light source intensity increases across the wavelength range of interest. One example of why this upper bound may be a valuable benchmark arises from the data in Table 3.3. When calculating  $T_v$  (NO) for NO,  $N_2O$ , and the  $N_2/O_2$  mixed system via a single (multi-state) simulation,  $A_F$  analysis shows no change in the temperatures. Thus, the conclusion would be that the vibrational state population distribution is equal in all three systems. When examining the results of simulated  $A_T$  spectra, however, we see

Table 3.3 Comparison of internal temperatures determined from Specair for the NO plasma system at P=100 W and p=50 mTorr via both simulation programs.

<b>Internal Temperature Comparison</b>				
<b>Plasma Feed Gas</b>	<b>Fractional (<math>A_F</math>)</b>		<b>Total (<math>A_T</math>)</b>	
	$\Theta_V(\text{NO})$	$\Theta_R(\text{NO})$	$\Theta_V(\text{NO})$	$\Theta_R(\text{NO})$
100% NO	4100 K	600 K	6300 K	700 K

that this may not be an accurate supposition. Within the NO plasma system, there is a significantly higher population in the  $v = 4$  and  $v = 5$  vibrational states of NO as rf power increases. Therefore, when the entire vibrational band within the  $A_F$  spectrum is simulated simultaneously, the higher order states are difficult to discern above the baseline. Admittedly, a more accurate measure of vibrational state populations could potentially be made by simulating each vibrational state transition of NO independently using the  $A_F$  calculation. Still the overall efficiency of simulating multiple rovibrational states simultaneously makes such efforts valuable, as it is possible that these concurrent simulations may misrepresent the experimental data unless  $A_T$  measurements are also taken into account.

Simultaneously simulating multiple species within a single plasma environment demonstrates the benefit of both calculations. Even though the measured populations lead to temperatures that are higher than the actual vibrational temperatures, the temperature data reported for  $A_T$  is unique when the simulation spans large wavelength ranges. As noted above, these values are exclusive to our light source and are probably best used in direct comparison to each other; nevertheless, the observed trends are applicable to other systems and configurations. Despite this restriction, these values can still be utilized to establish internal temperature trends within our system. Ultimately, the exact emission of the light source across the wavelength range of interest, has a significant impact on the determination of absorption spectra for plasmas. This profile helps to further explain the difference between the  $A_F$  and  $A_T$  spectra for the NO band. We have also generated  $A_F$  and  $A_T$  spectra for the  $N_2$  second positive band, where the emission of the deuterium/halogen light source is fairly constant. Using Specair, simulations of  $A_T$  and  $A_F$  spectra yielded  $T_V(A_F) = T_V(A_T)$ , within experimental error, as a result of to the relatively constant nature of the light source over this wavelength range.

To overall corroborate the results achieved with our simulations with respect to “expected” temperature values for species formed in plasmas, we compare here our preliminary results for N<sub>2</sub> and NO with values reported in the literature. For example, Zhang and coworkers reported T<sub>V</sub>(N<sub>2</sub>) ranging from 3000-5000 K and T<sub>R</sub>(N<sub>2</sub>) from 350-700 K in a constricted atmospheric pressure N<sub>2</sub> plasma jet across power densities of 7-85 W/cm.<sup>3,27</sup> This corresponds well to results from our plasmas, as we have determined T<sub>V</sub>(N<sub>2</sub>) from 3550-5000 K and T<sub>R</sub>(N<sub>2</sub>) ranging from 350-475 K at 50 mTorr with P = 100-200 W (Fig. 3.9). In an unrelated system, Liu et al. determined T<sub>R</sub> for CF and CF<sub>2</sub> spans ~400-700 K in a CF<sub>4</sub>/Ar dual-frequency capacitively-coupled plasma system.<sup>18</sup> Their work had high-frequency powers of 50-250 W with p=10-110 mTorr. Notably, NO is isoelectronic with CF, so this comparison lends some validity to our measured NO values, Table 3.3. Furthermore, Foucher and coworkers determined T<sub>R</sub> for O<sub>2</sub> on the order of 400-900 K in an ICP system with P ranging from 100-500 W and p from 10-80 mTorr.<sup>13, 17</sup> These temperatures, albeit measured in different systems and for different molecular species, are all clearly in rough agreement of the values we have extracted from our simulations of N<sub>2</sub> and NO. Similar to what we have measured within our ICPs, these groups all report T<sub>V</sub> >> T<sub>R</sub>. Notably, the temperatures reported in the works described above were determined using several different spectral fitting programs.

Here, we explicitly explored the effects of using two different spectral fitting programs by fitting the same experimental spectrum with two different programs. One program (Specair) models 37 molecular transitions and the other (LIFBASE) models 11 molecular transitions, with the NO gamma band being included within both databases. As shown in Fig. 3.8, there was excellent agreement between the two spectral fits of this transition, yielding a combined T<sub>R</sub> = 675 ± 25 K and T<sub>V</sub> = 6200 ± 100 K. By using two spectral programs we increase our overall spectral

library, and the consistency between the two programs allows us to compare energy partitioning trends with those reported in other studies. In this work, we have shown that our innovative BAS reactor setup and design can be employed to obtain versatile absorbance spectra, which in turn can be analyzed with different calculations and spectral programs to determine vibrational and rotational temperatures within multiple gas systems. By studying the internal temperatures of ground state neutral plasma species, we can further our fundamental understanding of energy partitioning within these complex systems.

### 3.4 Summary

An in situ broadband absorption spectroscopy system was built and utilized to examine energy partitioning within inductively coupled plasmas, focusing on neutral species energetics. Our designed experimental set-up included a deuterium-halogen light source interfaced to an ICP reactor, in which multiple emission spectra can be collected for the determination of absorbance spectra. This BAS system allows for simultaneous measurement and investigation of complex plasma chemistries by employing a >800 nm wavelength range.

We have demonstrated the ability of this experimental apparatus to generate an absorption spectrum, as well as addressing the difficulties of plasma absorbance measurements, which arise from the dual-reference nature of the system. Rather than utilizing the typical determination of absorbance via percent transmittance, we compared alternative ways to calculate absorbance and presented a means of analyzing absorbance spectra with two simulation programs (LIFBASE 2.1.1 and Specair), depending on the molecule of interest. Both were employed to simulate experimental spectra and determine vibrational and rotational temperatures. These temperatures can be used to examine energy partitioning within vibrational



and rotational states and determine trends based on applied rf power, system pressure, and feed gas composition. Data shown here illustrate the utility of our BAS system for the determination of temperature for both single-gas component systems (NO and N<sub>2</sub>) at differing powers and a mixed gas system (N<sub>2</sub>/O<sub>2</sub>) as well. This apparatus can be extended to study gas systems over a large parameter space to elucidate information regarding energy partitioning within plasma systems.

## REFERENCES

1. Bai, B.; Sawin, H. H.; Cruden, B. A., Neutral Gas Temperature Measurements of High-Power-Density Fluorocarbon Plasmas by Fitting Swan Bands of C<sub>2</sub> Molecules. *Journal of Applied Physics* 2006, 99 (1).
2. Bibinov, N. K.; Fateev, A. A.; Wiesemann, K., Variations of the Gas Temperature in He/N<sub>2</sub> Barrier Discharges. *Plasma Sources Science & Technology* 2001, 10 (4), 579-588.
3. Bol'shakov, A. A.; Cruden, B. A.; Sharma, S. P., Determination of Gas Temperature and Thermometric Species in Inductively Coupled Plasmas by Emission and Diode Laser Absorption. *Plasma Sources Science & Technology* 2004, 13 (4), 691-700.
4. Chen, C.-J.; Li, S.-Z., Spectroscopic Measurement of Plasma Gas Temperature of the Atmospheric-Pressure Microwave Induced Nitrogen Plasma Torch. *Plasma Sources Science & Technology* 2015, 24 (3).
5. Cruden, B. A.; Rao, M.; Sharma, S. P.; Meyyappan, M., Neutral Gas Temperature Estimate in CF<sub>4</sub>/O<sub>2</sub>/Ar Inductively Coupled Plasmas. *Applied Physics Letters* 2002, 81 (6), 990-992.
6. Silva, T.; Britun, N.; Godfroid, T.; Snyders, R., Simple Method for Gas Temperature Determination in CO<sub>2</sub>-Containing Discharges. *Optics Letters* 2014, 39 (21), 6146-6149.
7. Raud, J.; Laan, M.; Jogi, I., Rotational Temperatures of N<sub>2</sub>(C,0) and OH(A,0) as Gas Temperature Estimates in the Middle Pressure Ar/O<sub>2</sub> Discharge. *Journal of Physics D: Applied Physics* 2011, 44 (34).
8. Belostotskiy, S. G.; Ouk, T.; Donnelly, V. M.; Economou, D. J.; Sadeghi, N., Gas Temperature and Electron Density Profiles in an Argon DC Microdischarge Measured by Optical Emission Spectroscopy. *Journal of Applied Physics* 2010, 107 (5).
9. Cruden, B. A.; Rao, M.; Sharma, S. P.; Meyyappan, M., Neutral Gas Temperature Estimates in an Inductively Coupled CF<sub>4</sub> Plasma by Fitting Diatomic Emission Spectra. *Journal of Applied Physics* 2002, 91 (11), 8955-8964.
10. Luque, J.; Kraus, M.; Wokaun, A.; Haffner, K.; Kogelschatz, U.; Eliasson, B., Gas Temperature Measurement in CH<sub>4</sub>/CO<sub>2</sub> Dielectric-Barrier Discharges by Optical Emission Spectroscopy. *Journal of Applied Physics* 2003, 93 (8), 4432-4438.
11. van der Horst, R. M.; Verreycken, T.; van Veldhuizen, E. M.; Bruggeman, P. J., Time-Resolved Optical Emission Spectroscopy of Nanosecond Pulsed Discharges in Atmospheric-Pressure N<sub>2</sub> and N<sub>2</sub>/H<sub>2</sub>O Mixtures. *Journal of Physics D: Applied Physics* 2012, 45 (34).
12. van Gessel, A. F. H.; Hrycak, B.; Jasinski, M.; Mizeraczyk, J.; van der Mullen, J. J. A. M.; Bruggeman, P. J., Temperature and NO Density Measurements by LIF and OES on an Atmospheric Pressure Plasma Jet. *Journal of Physics D: Applied Physics* 2013, 46 (9).
13. Davis, G. P.; Gottscho, R. A., Measurement of Spatially Resolved Gas-Phase Plasma Temperatures by Optical-Emission and Laser-Induced Fluorescence Spectroscopy. *Journal of Applied Physics* 1983, 54 (6), 3080-3086.
14. Huwel, L.; Guyer, D. R.; Lin, G. H.; Leone, S. R., Laser-Induced Fluorescence Measurement of Nascent Vibrational and Rotational Product State Distributions in the Charge Transfer of Ar<sup>+</sup>+N<sub>2</sub>→Ar+N<sub>2</sub><sup>+</sup> (v=0,1) at 0.2 eV. *Journal of Chemical Physics* 1984, 81 (8), 3520-3535.

15. Stillahn, J. A.; Trevino, K. J.; Fisher, E. R., Plasma Diagnostics for Unraveling Process Chemistry. *Annual Review of Analytical Chemistry* 2008, 1, 261-291.
16. Bruggeman, P.; Cunge, G.; Sadeghi, N., Absolute OH Density Measurements by Broadband UV Absorption in Diffuse Atmospheric-Pressure He–H<sub>2</sub>O. *Plasma Sources Science and Technology* 2012, 21 (3), 035019.
17. Foucher, M.; Marinov, D.; Carbone, E.; Chabert, P.; Booth, J.-P., Highly Vibrationally Excited O<sub>2</sub> Molecules in Low-Pressure Inductively-Coupled Plasmas Detected by High Sensitivity Ultra-Broad-band Optical Absorption Spectroscopy. *Plasma Sources Science & Technology* 2015, 24 (4).
18. Liu, W.-Y.; Xu, Y.; Liu, Y.-X.; Peng, F.; Gong, F.-P.; Li, X.-S.; Zhu, A.-M.; Wang, Y.-N., Absolute CF<sub>2</sub> Density and Gas Temperature Measurements by Absorption Spectroscopy in Dual-Frequency Capacitively Coupled CF<sub>4</sub>/Ar Plasmas. *Physics of Plasmas* 2014, 21 (10).
19. Luque, J.; Hudson, E. A.; Booth, J. P., CF A<sup>2</sup>Σ<sup>+</sup>→X<sup>2</sup>Π and B<sup>2</sup>Δ→X<sup>2</sup>Π Study by Broadband Absorption Spectroscopy in a Plasma Etch Reactor: Determination of Transition Probabilities, CF X<sup>2</sup>Π Concentrations and Gas Temperatures. *Journal of Chemical Physics* 2003, 118 (2), 622-632.
20. Neuilly, F.; Booth, J.-P.; Vallier, L., Chlorine Dissociation Fraction in an Inductively Coupled Plasma Measured by Ultraviolet Absorption Spectroscopy. *Journal of Vacuum Science & Technology A* 2002, 20 (1), 225-229.
21. Ramos, R.; Cunge, G.; Touzeau, M.; Sadeghi, N., Absorption Spectroscopy in BCl<sub>3</sub> Inductively Coupled Plasmas: Determination of Density, Rotational, Translational and Vibrational Temperatures of BCl Molecule. *Journal of Physics D: Applied Physics* 2008, 41 (11), 115205.
22. Luque, J.; Crosley, D. R. LIFBASE: Database and Spectral Simulation Program (Version 1.5); 1999.
23. Laux, C. O. In *Radiation and Nonequilibrium Collisional-Radiative Models*, von Karman Institute Lecture Series (2002-07), Rhode-Saint-Genèse, Belgium, Fletcher, D., Ed. Rhode-Saint-Genèse, Belgium, 2002.
24. Abrar, M.; Qayyum, A.; Gilani, A. R.; Khan, A. W.; Saeed, A.; Naseer, S.; Zakaullah, M., Effect of Helium Mixing on Excitation Temperature and Nitrogen Dissociation in Inductively Coupled Plasma. *Current Applied Physics* 2013, 13 (6), 969-974.
25. Bruggeman, P.; Sadeghi, N.; Schram, D. C.; Linss, V., Gas Temperature Determination from Rotational Lines in Non-Equilibrium Plasmas: A Review. *Plasma Sources Science & Technology* 2014, 23 (2), 023001.
26. Ishii, I.; Montaser, A., A Tutorial Discussion on Measurements of Rotational Temperature in Inductively Coupled Plasmas. *Spectrochimica Acta Part B: Atomic Spectroscopy* 1991, 46 (8), 1197-1206.
27. Zhang, Q. Y.; Shi, D. Q.; Xu, W.; Miao, C. Y.; Ma, C. Y.; Ren, C. S.; Zhang, C.; Yi, Z., Determination of Vibrational and Rotational Temperatures in Highly Constricted Nitrogen Plasmas by Fitting the Second Positive System of N<sub>2</sub> Molecules. *AIP Advances* 2015, 5 (5).

## CHAPTER 4

### DETERMINATION OF INTERNAL TEMPERATURES WITHIN NITRIC OXIDE INDUCTIVELY-COUPLED PLASMAS

This chapter contains data to be published as a full paper by Joshua M. Blechle, Angela R. Hanna, and Ellen R. Fisher. These studies investigate the determination of characteristic temperatures within inductively-coupled plasmas, which is the key to understanding the reactions that drive the chemistry of these systems. To investigate such interactions, a dual in situ broadband absorption and optical emission spectroscopy system has been designed and constructed. This system provides insight into neutral and excited state species energetics, specifically rotational and vibrational temperatures, across a broad spectral range (200 – 1000 nm) allowing for the potential to simultaneously investigate multiple plasma species.

#### 4.1 Introduction

Plasma diagnostics provide the critical foundation for developing a fundamental understanding of species identification and energetics of inductively coupled plasmas (ICPs). Within ICPs, there are several critical figures of merit including what is termed “gas temperature”, which can be used to describe the overall translational energy of the gas, as well as rotational ( $T_R$ ) and vibrational ( $T_V$ ) temperatures for individual species.<sup>1</sup> Plasma species that are promoted to excited electronic states via electron impact and other collisions within the plasma are often studied using optical emission spectroscopy (OES). Observing relaxation via photon emission allows for determination of species concentration and temperature profiles of excited state species.<sup>2-6</sup>

Non-thermal low temperature plasmas (LTPs), utilized for the work presented herein, generally comprise molecules that follow a classical relationship wherein  $T_V$  is nominally greater than  $T_R$  and translational temperature ( $T_T$ ), yet each temperature remains significantly lower than the electron temperature ( $T_e$ ).<sup>7-8</sup> Additionally, gas temperature ( $T_g$ ) is highly dependent on plasma parameters, leading to an increased desire to understand the trends in energy partitioning.<sup>9-15</sup> Nevertheless,  $T_R$  values have long been employed as a measure of the neutral  $T_g$ ,<sup>16-19</sup> with the assumption that rotational and collective translational temperatures of the gas equilibrate within the plasma.<sup>20</sup> Although this estimate may be useful for approximating  $T_g$  in the absence of a full complement of temperature data, several studies have demonstrated there are significant differences between  $T_R$  and  $T_V$  and likewise between these properties and  $T_T$ .<sup>7, 21-23</sup> Indeed, Bruggeman, et al. showed  $T_R$  equilibrates with  $T_T$  only when rotational energy transfer is relatively fast or when the nascent rotational distribution is a thermalized distribution.<sup>23</sup> Nevertheless, ground and excited state species can have substantially different characteristic  $T_R$  under the same conditions, distributions can strongly deviate from Boltzmann, and different radicals in the same LTP can exhibit distinct internal temperatures.<sup>24-25</sup> One additional consideration is that a single plasma species can be produced via different mechanisms (e.g. direct precursor decomposition vs. bimolecular recombination reactions), which may ultimately result in very different energy partitioning for that species. As many studies focused primarily on  $N_2$ ,<sup>7, 26-28</sup> with few examining other diatomic molecules,<sup>22, 29-32</sup> a vast data gap persists for the majority of species found in technologically-relevant plasmas, severely limiting the application of such systems and computational methods which attempt to model them.

Moreover, despite the fact that the complexity of LTPs can constrain the utility of theoretical methods, a range of numerical simulations [e.g. molecular dynamics (MD)

calculations] have been used to model LTP processes.<sup>33-35</sup> Likewise, electronic structure calculations have used to investigate gas adsorption properties<sup>36</sup> as well as the role of coupled nuclear and electronic dynamics<sup>37</sup> on molecule formation mechanisms. Ultimately, although the inclusion of electronic structure analyses, such as multi-reference configuration interaction (MR-CI) and time-dependent density functional theory (TD-DFT), can provide a more thorough understanding of the role formation mechanisms and relevant energy barriers have on energy partitioning, these systems are limited by a lack of underlying experimental data.<sup>38</sup>

There are, however, inherent challenges in elucidating temperature trends experimentally. This is especially problematic when information about excited-states is used to infer behavior of the ground state (which constitutes the majority of electronic-state populations in low temperature plasmas), because of issues including non-radiative decay and varying vibrational-translational relaxation pathways. Therefore, in situ investigations of ground state species are critical for a complete evaluation of gas phase mechanisms. The most common method for probing ground state species is laser-induced fluorescence (LIF),<sup>39-41</sup> which is a powerful non-intrusive spectroscopic technique. Shortcomings of LIF, however, include its use being confined to species that possess a fluorescing excited state, requisite expensive instrumentation (laser system), and being inherently limited because of non-radiative relaxation processes.<sup>42</sup> Recent studies have demonstrated the utility of an alternate technique, broadband absorption spectroscopy (BAS) within a variety of plasma systems.<sup>32, 43-48</sup> Here we detail a newly constructed combination OES/BAS system with which to conduct nearly concurrent investigations of ground and excited state species within the plasma (as described in Chapter 3). In addition to the plasma chemistry itself, the direct interaction of nitric oxide plasmas with a

surface is largely unknown, therefore we sought to study the impact of a substrate on the energy portioning of the plasma system.

## 4.2 Results and Discussion

As stated in Section 4.1, our new OES/BAS system allows for monitoring of plasma temperatures in both the ground and excited states, where we have specifically focused on rotational and vibrational temperatures. Raw emission and absorbance spectra for a 150 mTorr and 150 W NO plasma are shown in Fig. 4.1, along with simulated fits for the NO molecule's  $X^2\Pi \leftrightarrow A^2\Sigma^+$  transition. Both simulations were generated in LIFBASE, giving rise to  $T_V = 3100$  K,  $T_R = 610$  K for OES measurements and  $T_V = 5800$  K,  $T_R = 800$  K for BAS measurements (error is assumed to be ~10% based on peak correlation). Note that, under these conditions, both  $T_R$  and  $T_V$  are higher for the ground electronic state than for the first excited electronic state. To fully investigate the impact of the system parameters on ground and excited state molecules, a range of pressure and power conditions were studied. Note that for all of the following data, error is determined from a standard deviation of  $n = 3$  trials, except under conditions in which the signal to noise ratio made fitting individual trials difficult. In these latter cases, multiple spectra were averaged together to reduce random noise and the resulting (i.e., averaged) spectrum was fit in LIFBASE. As a result, error in these instances is representative of the reported peak correlation within LIFBASE (~10%), as noted above.

Figure 4.2a shows  $T_R$  determined via OES for the first excited state ( $A^2\Sigma^+$ ) NO as a function of power, whereas Fig. 4.2b shows  $T_R$  for those in the ground state ( $X^2\Pi$ ) via BAS. Dashed lines represent linear regressions of power trends for individual pressure conditions.

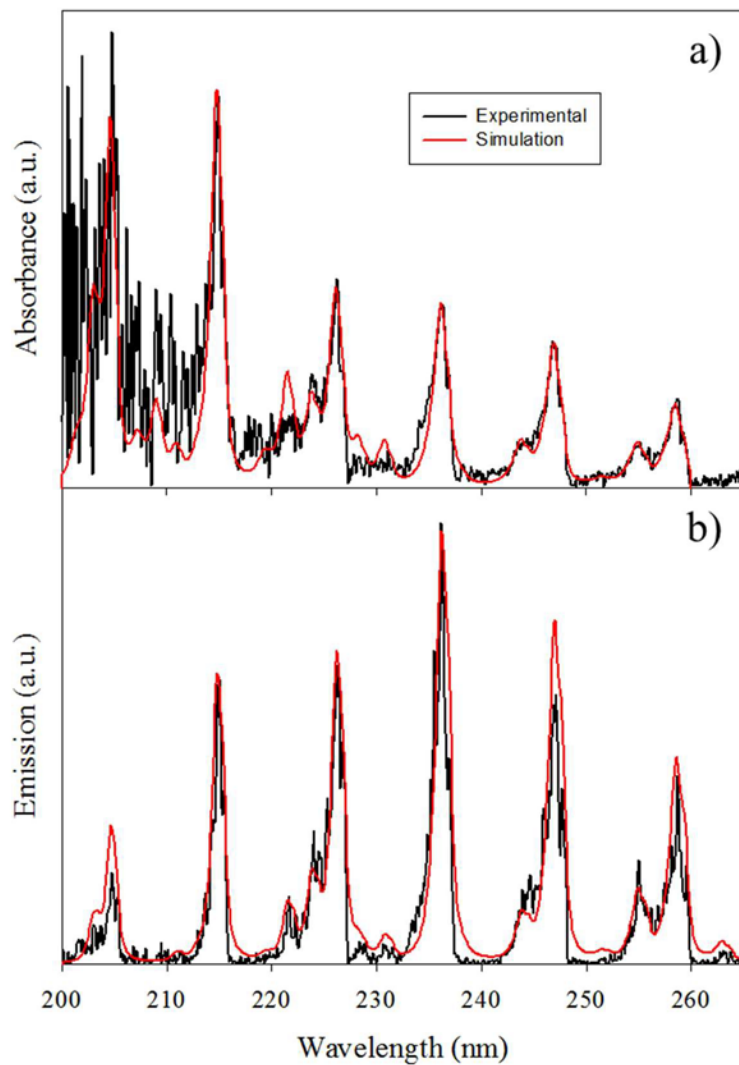


Figure 4.1 Simulated fit of raw NO absorbance (a) and emission (b) spectra from an NO plasma at  $p = 150$  mTorr and  $P = 150$  W. Peak correlations were  $>90\%$  in both cases.



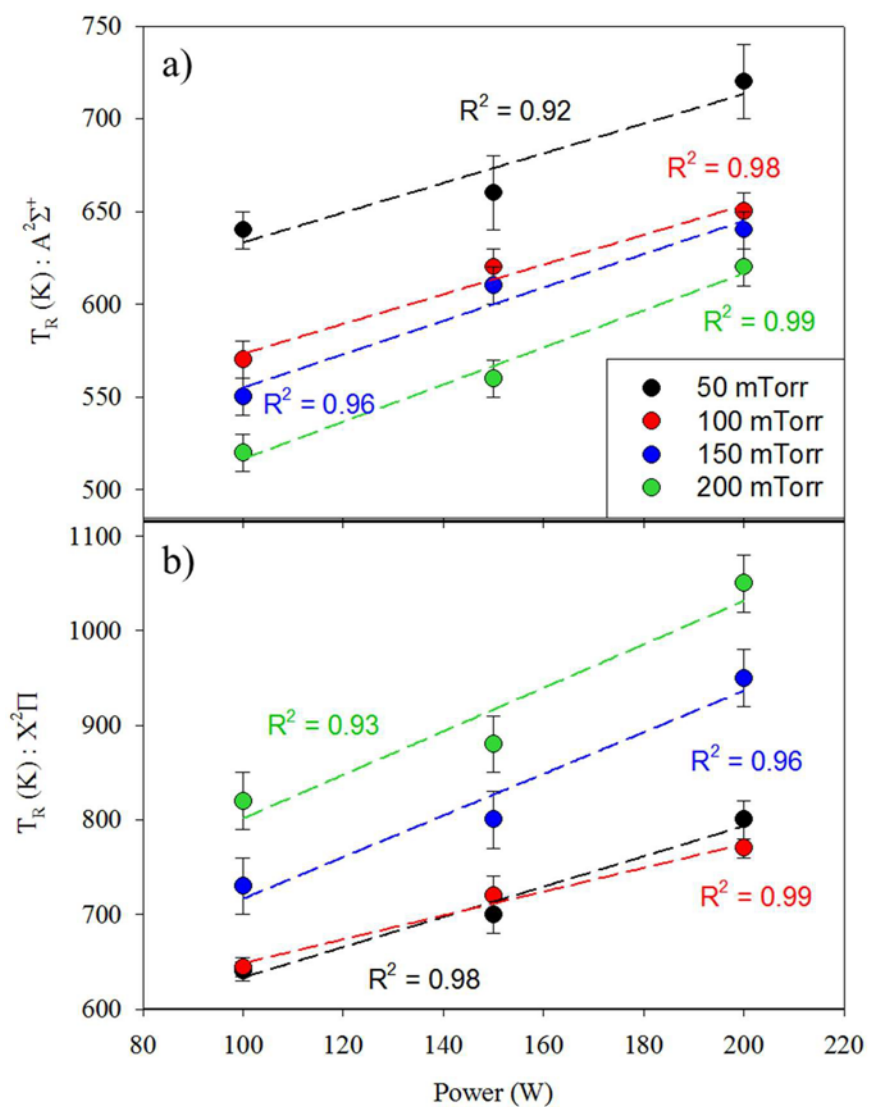


Figure 4.2 Nitric oxide rotational temperatures as a function of applied rf power over a range of pressures for both the (a) excited state and (b) ground state. Dashes represent a line of best fit for each data set.

Here, we see that as power increases,  $T_R$  increases for both ground and excited state species. This has been observed previously and is attributed to neutral-electron collisions for which there is an increase in  $T_e$  with power.<sup>41, 49</sup> Temperatures associated with ground state molecules, however, are almost exclusively higher than those found in the excited state, which suggests energy transfer in the excited state is fast enough to achieve thermalization. In addition, we observe that increasing pressure causes an increase in  $T_R$  for the ground state, whereas the opposite trend is observed in the excited state. As pressure is increased in the system, the number of collisions occurring in the discharge also increase, causing an increased amount of collisional quenching in the system. The pressure dependence in the ground state can be also attributed to increased neutral-electron collisions as the density of NO precursor is increased with pressure. Additionally, rotational relaxation is a relatively fast process, typically requiring fewer than ten collisions to reach equilibrium.<sup>50</sup> Hence, rotational temperatures in the excited state decrease as the number of collisions within the system increases. Linear regressions for all eight power/pressure combinations evaluated here show a high degree of linearity in each circumstance (e.g.,  $R^2 > 0.92$ ). This linear behavior has also been documented within  $N_2$ ,  $N_2O$ , and a mixture of  $N_2$  and  $O_2$  radio frequency ICPs, including work completed within the Fisher group.<sup>51</sup>

Interestingly,  $T_R$  trends observed in the present work are also at odds with other previously determined temperatures within the Fisher Research Group, specifically with respect to NO.<sup>52</sup> Indeed, Morgan et al. report  $T_R \sim 340$  K (determined via LIF under a similar parameter space), with no discernable trend as a function of pressure or power. The system used in this previous work, however, relies on induced fluorescence within a nominally collision-free molecular beam that is formed downstream from the ignition of the plasma. In contrast, the in-

line coaxial collection set-up used in this work probes the entire plasma bulk including the coil region of the reactor. As a result, it is likely that the BAS/OES system is more sensitive to the greater number of ground state species that dominate in the electron-mediated coil region. This sensitivity may also suggest that a significant amount of rotational cooling takes place as species migrate out of the coil region, generating equilibrated temperatures downstream.

An identical parameter space is studied with respect to measured  $T_V$  values, as Fig. 4.3a and b contain temperatures determined from OES data and BAS data, respectively. Once again, we see that increasing rf power leads to increased temperatures for both species. In general,  $T_V$  values are much greater than  $T_R$  under identical conditions, and  $T_V$  for ground state molecules is much higher than that for excited state molecules. This relationship between rotational and vibrational temperatures has been observed in a variety of plasma systems with a range of precursors.<sup>39, 45, 48, 53-54</sup>

An additional observation from Fig. 4.3, is that pressure trends for  $T_V$  are different than those observed for  $T_R$ , Fig. 4.2. In the ground state, power trends observed in both the 100 mTorr and 150 mTorr systems are nearly identical. The 50 mTorr temperature values, however, increase with power at a much smaller rate than those at 200 mTorr. Excited state species in the 100 mTorr and 150 mTorr are also similar to one another, although the overall trend is a decrease in  $T_V$  with increasing pressure. Altogether, values for  $T_R$  and  $T_V$  maintain similar trends and orders of magnitude observed for molecules found in other plasma systems, including  $N_2$  and the isoelectronic CF molecule in fluorocarbon systems.<sup>45, 54-55</sup> This data can also be compared to previous work by Morgan et al., where  $T_V$  is reported for excited state species via OES analysis,<sup>52</sup> which employed very similar reactors and collection methods (without BAS capabilities). A positive correlation between power and  $T_V$  is observed in the

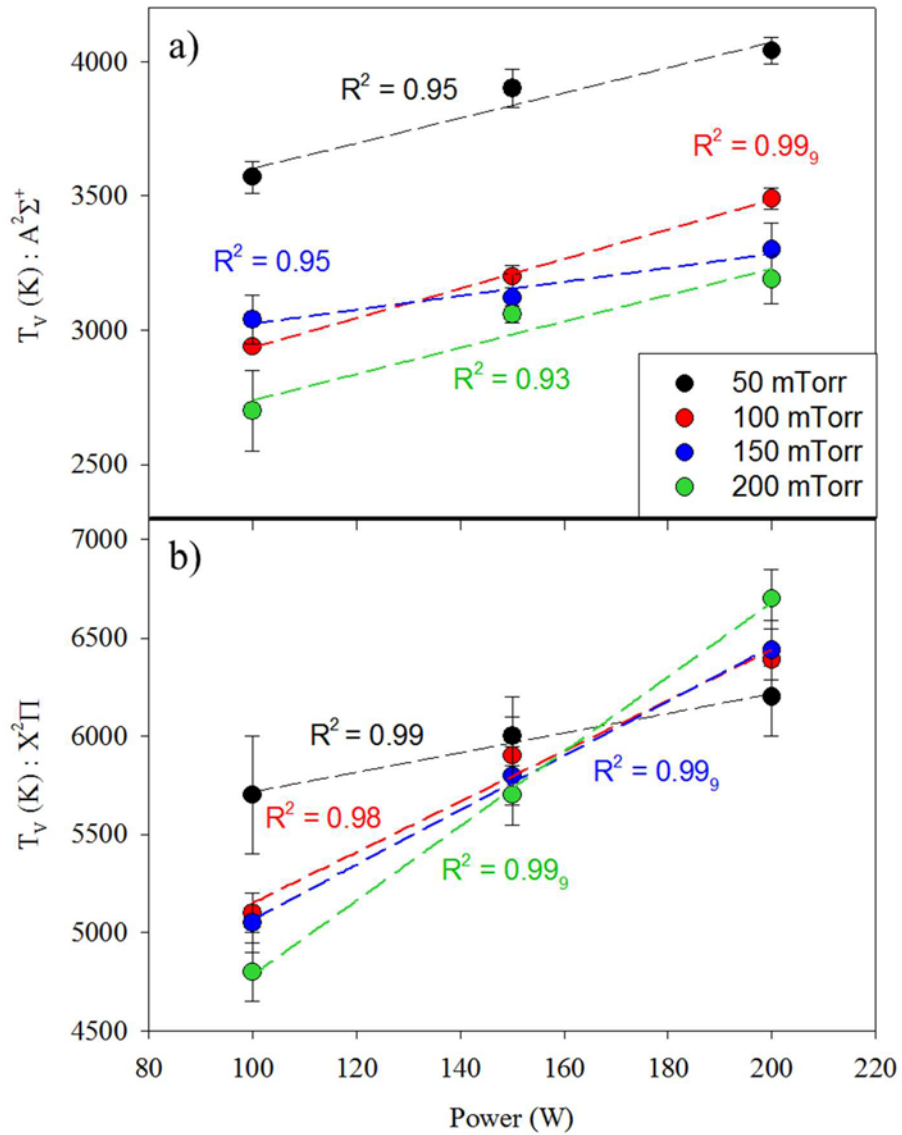


Figure 4.3 Nitric oxide vibrational temperatures versus power over a range of pressures for both the (a) excited state and (b) ground state. Dashes represent a line of best fit for each data set.

previous experiments as well as the ones presented herein, however, previous values are reported to range from ~1400-1800 K (as opposed to ~2500-4000 K) for ICP systems under similar power and pressure conditions. Note, however, that in the previous work by Morgan et al., efforts were made to monitor NO concentration within these systems using an Ar actinometer. Thus, all reported values are for NO plasmas that include 5-7% Ar by pressure. As such, the reduction in  $T_V$  is likely the result of increased quenching via collisions with the much larger Ar atoms.

Lastly, a primary challenge to understanding LTP chemistry lies in deciphering plasma-surface interactions.<sup>56</sup> One key piece of this challenge includes separating effects arising from different types of species bombarding the surface; synergistic or coupled reactions at the surface (e.g., ion bombardment assisting chemical etching<sup>28, 57</sup>); and energy partitioning in a particular molecule as different types of energy (e.g., vibrational vs. translational). Each of these factors can impact how a molecule behaves when interacting with a surface. Indeed, the rates of many surface reactions are likely controlled by the vibrational and electronic states of plasma species.<sup>58</sup> As such, the effect of inclusion of a silicon substrate on NO internal temperatures was investigated for a 50 mTorr NO plasma. The substrate, a ~2x2 cm Si wafer, was placed in the center of the coil region of the reactor. Figure 4.4 contains  $T_R$  and  $T_V$  values as a function of P for both OES and BAS measurements in the presence of the Si substrate. With a substrate present,  $T_V$  is once again higher for the ground state than the excited state. This trend does not hold for  $T_R$ , however, as the excited state species have a higher temperature than the ground, suggesting that the substrate has an impact on the thermalization of the rotational states of the gas-phase NO molecules.

When compared to the temperatures found in a substrate-free reactor under identical conditions, Fig. 4.2, we observe that  $T_R$  for ground state species is largely unaffected by the

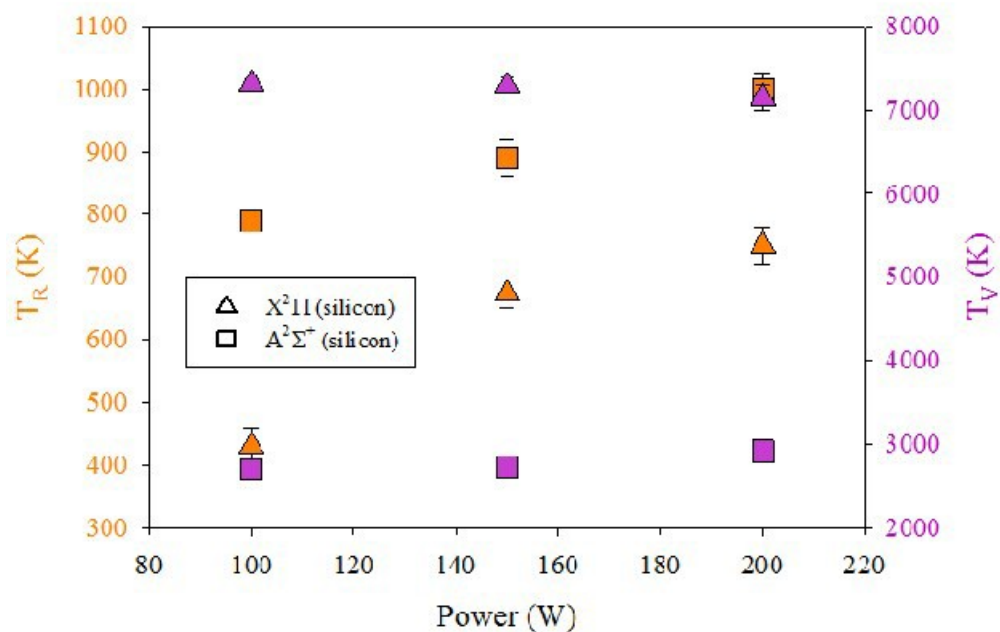


Figure 4.4 Rotational (orange) and vibrational (purple) temperatures calculated from spectra of NO in an NO plasma at  $p = 50$  mTorr with a silicon substrate placed in the coil region are shown on the left and right axes, respectively. Triangles represent ground state BAS data, whereas squares are for excited state OES data.

presence of the Si substrate (one notable exception comes with data collected at 100 W, where  $T_R$  is greatly reduced by approximately 250 K). In contrast,  $T_V$  is significantly increased under all conditions, by approximately 1000 K. The excited state, on the other hand, experiences an increase in  $T_R$  (by a factor of  $\sim 1.3$ ) and a similar reduction in  $T_V$  with the silicon substrate in the plasma. Therefore, the addition of the substrate causes a simultaneous decrease in ground state  $T_R$  and increase in excited state  $T_R$ , along with an increase in ground state  $T_V$  and a decrease in excited state  $T_V$ . Such a response illustrates the interconnected nature of energy partitioning in these plasma systems and the inherent importance of exploring plasma chemistry, as well as the energetic implications of interfacing plasmas and substrates. Note that energetic trends may be influenced, at least in part, by the surface area of the silicon substrate. By collecting data coaxially along the reactor's length, the instrument is exposed to the entirety of the plasma species. Thus, a sufficiently large substrate is required to generate a noticeable impact on the high density of the NO, both in the ground and excited states. This is further supported by the result that an initial test of a much smaller ( $\sim 0.5 \times 0.5$  cm) Si substrate did not significantly alter the measured temperatures. The exact nature of the role surface area plays in energy partitioning is not known, but it seems reasonable that a sufficient amount of NO must interact with the substrate to induce a measurable surface-mediated response using plasma diagnostic strategies employed in the present work.

This substrate investigation can be further compared to the work of Morgan et al., as the previous measurements of  $T_V$  were made using OES in the presence of a variety of substrates, including Si.<sup>52,59</sup> The authors report that the inclusion of a surface did not impact  $T_V$ , regardless of the substrate identity. This provides another interesting difference to the work reported herein. Previous experiments, however, were conducted using substrates positioned 5 and 12 cm

downstream from the end of the coil, as opposed to the center of the coil region. Such a difference provides further support to the idea that the gas phase in the electron-mediated coil region has vastly different chemistry than that of the downstream region, and further suggesting that equilibration of these internal temperatures occurs across a small translational space. Considering that a significant excited state population is established after plasma ignition, and thus exists primarily downstream, we can assume that intermolecular collision processes dominate the gas-phase chemistry of the system. As such, it is likely that the OES signal is more directly impacted by the dominant excited state population downstream of plasma ignition, where continued collisions have generated a cooler energetic environment and thus, lower measured temperatures. Signal from the BAS, however, is more directly impacted by the dominant ground state population that exists within the hotter region of plasma ignition. Such an explanation provides context for significantly higher ground state  $T_R$  values when measured via BAS as compared to LIF, as well as significant impact that a substrate placed within the coil region has on the energy partitioning of these ICP systems when compared to similar systems with downstream substrate placement.

#### 4.3 Summary

An in situ optical emission and broadband absorption spectroscopy system was built and utilized to examine energy partitioning within inductively coupled plasmas. An understanding of how energy is dispersed into rotational and vibrational modes for NO molecules yields critical insight into the overall character of the plasma. Our newly designed and constructed experimental apparatus included a deuterium-halogen light source interfaced to an ICP reactor in which multiple emission spectra can be collected for the determination of absorbance spectra,



overcoming the inherent difficulties associated with plasma absorbance measurements. This OES/BAS system allows for simultaneous measurement and investigation of complex plasma chemistries by employing a greater than 800 nm wavelength range. We have demonstrated the utility of our OES/ BAS system for the determination of temperatures for a model gas system under a variety of pressure and power conditions with and without a substrate for both excited and ground state species. Evidence suggests two distinct energetic regions of these systems, and speaks to the complex synergisms that exist within these systems. In the future, this apparatus can be used to study more complex precursor gas systems over a large parameter space to elucidate information regarding energy partitioning within a variety of plasma systems, as well the role of spatial resolution on measured temperatures.

## REFERENCES

1. Grill, A., Cold Plasma Materials Fabrications. IEEE Press: Piscataway, NJ, 1994.
2. Belostotskiy, S. G.; Ouk, T.; Donnelly, V. M.; Economou, D. J.; Sadeghi, N., Gas Temperature and Electron Density Profiles in an Argon DC Microdischarge Measured by Optical Emission Spectroscopy. *Journal of Applied Physics* 2010, 107 (5).
3. Cruden, B. A.; Rao, M.; Sharma, S. P.; Meyyappan, M., Neutral Gas Temperature Estimates in an Inductively Coupled CF<sub>4</sub> Plasma by Fitting Diatomic Emission Spectra. *Journal of Applied Physics* 2002, 91 (11), 8955-8964.
4. Luque, J.; Kraus, M.; Wokaun, A.; Haffner, K.; Kogelschatz, U.; Eliasson, B., Gas Temperature Measurement in CH<sub>4</sub>/CO<sub>2</sub> Dielectric-Barrier Discharges by Optical Emission Spectroscopy. *Journal of Applied Physics* 2003, 93 (8), 4432-4438.
5. van der Horst, R. M.; Verreycken, T.; van Veldhuizen, E. M.; Bruggeman, P. J., Time-Resolved Optical Emission Spectroscopy of Nanosecond Pulsed Discharges in Atmospheric-Pressure N<sub>2</sub> and N<sub>2</sub>/H<sub>2</sub>O Mixtures. *Journal of Physics D: Applied Physics* 2012, 45 (34).
6. van Gessel, A. F. H.; Hrycak, B.; Jasinski, M.; Mizeraczyk, J.; van der Mullen, J. J. A. M.; Bruggeman, P. J., Temperature and NO density measurements by LIF and OES on an atmospheric pressure plasma jet. *Journal of Physics D-Applied Physics* 2013, 46 (9).
7. Britun, N.; Gaillard, M.; Ricard, A.; Kim, Y. M.; Kim, K. S.; Han, J. G., Determination of the Vibrational, Rotational, and Electron Temperatures in N<sub>2</sub> and N<sub>2</sub>/Ar rf Discharge. *J. Phys. D: Appl. Phys.* 2007, 40, 1022.
8. Fridman, A., Plasma Chemistry. Cambridge University Press: New York, 2008.
9. Bai, B.; Sawin, H. H.; Cruden, B. A., Neutral Gas Temperature Measurements of High-Power-Density Fluorocarbon Plasmas by Fitting Swan Bands of C<sub>2</sub> Molecules. *Journal of Applied Physics* 2006, 99 (1).
10. Bibinov, N. K.; Fateev, A. A.; Wiesemann, K., Variations of the Gas Temperature in He/N<sub>2</sub> Barrier Discharges. *Plasma Sources Science & Technology* 2001, 10 (4), 579-588.
11. Bol'shakov, A. A.; Cruden, B. A.; Sharma, S. P., Determination of Gas Temperature and Thermometric Species in Inductively Coupled Plasmas by Emission and Diode Laser Absorption. *Plasma Sources Science & Technology* 2004, 13 (4), 691-700.
12. Chen, C.-J.; Li, S.-Z., Spectroscopic Measurement of Plasma Gas Temperature of the Atmospheric-Pressure Microwave Induced Nitrogen Plasma Torch. *Plasma Sources Science & Technology* 2015, 24 (3).
13. Cruden, B. A.; Rao, M.; Sharma, S. P.; Meyyappan, M., Neutral Gas Temperature Estimate in CF<sub>4</sub>/O<sub>2</sub>/Ar Inductively Coupled Plasmas. *Applied Physics Letters* 2002, 81 (6), 990-992.
14. Silva, T.; Britun, N.; Godfroid, T.; Snyders, R., Simple Method for Gas Temperature Determination in CO<sub>2</sub>-Containing Discharges. *Optics Letters* 2014, 39 (21), 6146-6149.
15. Raud, J.; Laan, M.; Jogi, I., Rotational temperatures of N<sub>2</sub>(C,0) and OH(A,0) as Gas Temperature Estimates in the Middle Pressure Ar/O<sub>2</sub> Discharge. *Journal of Physics D: Applied Physics* 2011, T44 (34).
16. Davis, S. J.; Hadley, S. G., Measurement of the Radiative Lifetime of the A<sup>2</sup>Σ<sup>+</sup>(v'=0) State of SiF. *Physical Review A* 1976, 14 (3), 1146-1150.

17. Golubovskii, Y. B.; Telezhko, V. M., Measurement of Gas Temperature from the Unresolved Rotational Structure of the First Positive Band System of Nitrogen. *Journal of Applied Spectroscopy* 1983, 39 (3), 999-1003.
18. Porter, R. A.; Harshbarger, W. R., Gas Rotational Temperature in an RF Plasma. *Journal of the Electrochemical Society* 1979, 126 (3), 460-464.
19. Schabel, M. J.; Donnelly, V. M.; Kornblit, A.; Tai, W. W., Determination of Electron Temperature, Atomic Fluorine Concentration, and Gas Temperature in Inductively Coupled Fluorocarbon/Rare Gas Plasmas Using Optical Emission Spectroscopy. *Journal of Vacuum Science & Technology A* 2002, 20 (2), 555-563.
20. Shimada, M.; Tynan, G. R.; Cattolica, R., Rotational and Translational Temperature Equilibrium in an Inductively Coupled Plasma. *Journal of Vacuum Science & Technology A* 2006, 24 (5), 1878-1883.
21. Hollmann, E. M.; Pigarov, A. Y.; Taylor, K., Measurement and Modeling of H<sub>2</sub> Vibrational and Rotational Temperatures in Weakly Ionized Hydrogen discharges. *Journal of Nuclear Materials* 2005, 337, 451-455.
22. Zhao, T.-L.; Xu, Y.; Song, Y.-H.; Li, X.-S.; Liu, J.-L.; Liu, J.-B.; Zhu, A.-M., Determination of Vibrational and Rotational Temperatures in a Gliding Arc Discharge by Using Overlapped Molecular Emission Spectra. *Journal of Physics D* 2013, 46, 345201.
23. Bruggeman, P.; Sadeghi, N.; Schram, D. C.; Linss, V., Gas Temperature Determination from Rotational Lines in Non-Equilibrium Plasmas: A Review. *Plasma Sources Science & Technology* 2014, 23, 023001.
24. Williams, K. L.; Fisher, E. R., Substrate Temperature Effects on Surface Reactivity of SiF<sub>x</sub> (x=1,2) Radicals in Fluorosilane Plasmas. *Journal of Vacuum Science & Technology A* 2003, 21 (4), 1024-1032.
25. Zhang, J.; Williams, K. L.; Fisher, E. R., Velocity Distributions of SiF and SiF<sub>2</sub> in an SiF<sub>4</sub> Plasma Molecular Beam. *Journal of Physical Chemistry A* 2003, 107 (5), 593-597.
26. Shakhatov, V. A.; Mavlyudov, N. B.; Lebedev, Y. A., Studies of the Distribution Functions of Molecular Nitrogen and Its Ion over the Vibrational and Rotational Levels in the DC Glow Discharge and the Microwave Discharge in a Nitrogen-Hydrogen Mixture by the Emission Spectroscopy Technique. *High Temp.* 2013, 51 (4), 551-565.
27. Ambrico, P. F.; Bektursunova, R.; Dilecce, G.; De Benedictis, S., Nitrogen Vibrational Excitation in a N<sub>2</sub>/He Pulsed Planar-ICP RF Discharge. *Plasma Sources Science & Technology* 2005, 14, 676-685.
28. Van Laer, K.; Tinck, S.; Samara, V.; de Marneffe, J. F.; Bogaerts, A., Etching of Low-k Materials for Microelectronics Applications by Means of a N<sub>2</sub>/H<sub>2</sub> Plasma: Modeling and Experimental Investigation. *Plasma Sources Science & Technology* 2013, 22, 025011.
29. Niu, J.; Peng, B.; Yang, Q.; Cong, Y.; Liu, D.; Fan, H., Spectroscopic Diagnostics of Plasma-Assisted Catalytic Systems for NO Removal from NO/N<sub>2</sub>/O<sub>2</sub>/C<sub>2</sub>H<sub>4</sub> Mixtures. *Catalysis Today* 2013, 211, 58-65.
30. Bruggeman, P.; Cunge, G.; Sadeghi, N., Absolute OH Density Measurements by Broadband UV Absorption in Diffuse Atmospheric Pressure He-H<sub>2</sub>O RF Glow Discharges. *Plasma Sources Science & Technology* 2012, 21, 035019.
31. Miotk, R.; Jasinski, M.; Mizeraczyk, J., Optical Emission Spectroscopy of Microwave (915 MHz) Plasma in Atmospheric Pressure Nitrogen with Addition of Ethanol Vapour. *Acta Physica Polonica A* 2014, 125 (6), 1329-1331.

32. Luque, J.; Hudson, E. A.; Booth, J. P., CF  $A^2\Sigma^+ \rightarrow X^2\Pi$  and  $B^2\Delta \rightarrow X^2\Pi$  Study by Broadband Absorption Spectroscopy in a Plasma Etch Reactor: Determination of Transition Probabilities, CF  $X^2\Pi$  Concentrations and Gas Temperatures. *Journal of Chemical Physics* 2003, 118 (2), 622-632.
33. Graves, D. B.; Brault, P., Molecular Dynamics for Low Temperature Plasma-Surface Interaction Studies. *J. Phys. D: Appl. Phys.* 2009, 42, 194011 (27 pp).
34. Jimenez-Redondo, M.; Carrasco, E.; Herrero, V. J.; Tanarro, I., Chemistry in Glow Discharges of  $H_2/O_2$  Mixtures: Diagnostics and Modeling. *Plasma Sources Science & Technology* 2015, 24, 015029 (12 pp).
35. Capitelli, M.; Celiberto, R.; Esposito, F.; Laricchiuta, A., Molecular Dynamics for State-to-State Kinetics of Non-Equilibrium Molecular Plasmas: State of Art and Perspectives. *Plasma Process. Polym.* 2009, 6, 279-294.
36. Chandiramouli, R.; Srivastava, A.; Nagarajan, V., NO Adsorption Studies on Silicene Nanosheet: DFT Investigation. *Applied Surface Science* 2015, 351, 662-672.
37. Trabs, P.; Buchner, F.; Ghotbi, M.; Lubcke, A.; Ritze, H.-H.; Vrakking, M. J. J.; Rouzee, A., Time-, Angle- and Kinetic-Energy-Resolved Photoelectron Spectroscopy of Highly Excited States of NO. *Journal of Physics B* 2014, 47, 124016 (14 pp).
38. Neyts, E. C.; Bogaerts, A., Understanding Plasma Catalysis Through Modelling and Simulations - A Review *Journal of Physics D* 2014, 47, 224010.
39. Davis, G. P.; Gottscho, R. A., Measurement of Spatially Resolved Gas-Phase Plasma Temperatures by Optical Emission and Laser-Induced Fluorescence Spectroscopy. *Journal of Applied Physics* 1983, 54 (6), 3080-3086.
40. Huwel, L.; Guyer, D. R.; Lin, G. H.; Leone, S. R., Laser-Induced Fluorescence Measurement of Nascent Vibrational and Rotational Product State Distributions in the Charge Transfer of  $Ar+N_2 \rightarrow Ar+N_2^+$  ( $v=0,1$ ) at 0.2 eV. *Journal of Chemical Physics* 1984, 81 (8), 3520-3535.
41. van Gessel, A. F. H.; Hrycak, B.; Jasinski, M.; Mizeraczyk, J.; van der Mullen, J. J. A. M.; Bruggeman, P. J., Temperature and NO Density Measurements by LIF and OES on an Atmospheric Pressure Plasma Jet. *Journal of Physics D: Applied Physics* 2013, 46 (9).
42. Stillahn, J. A.; Trevino, K. J.; Fisher, E. R., Plasma Diagnostics for Unraveling Process Chemistry. *Annual Review of Analytical Chemistry* 2008, 1, 261-291.
43. Bruggeman, P.; Cunge, G.; Sadeghi, N., Absolute OH Density Measurements by Broadband UV Absorption in Diffuse Atmospheric-Pressure He- $H_2O$ . *Plasma Sources Science and Technology* 2012, 21 (3), 035019.
44. Foucher, M.; Marinov, D.; Carbone, E.; Chabert, P.; Booth, J.-P., Highly vibrationally excited O-2 molecules in low-pressure inductively-coupled plasmas detected by high sensitivity ultra-broad-band optical absorption spectroscopy. *Plasma Sources Science & Technology* 2015, 24 (4).
45. Liu, W.-Y.; Xu, Y.; Liu, Y.-X.; Peng, F.; Gong, F.-P.; Li, X.-S.; Zhu, A.-M.; Wang, Y.-N., Absolute  $CF_2$  Density and Gas Temperature Measurements by Absorption Spectroscopy in Dual-Frequency Capacitively Coupled  $CF_4/Ar$  Plasmas. *Physics of Plasmas* 2014, 21 (10).
46. Neuilly, F.; Booth, J.-P.; Vallier, L., Chlorine Dissociation Fraction in an Inductively Coupled Plasma Measured by Ultraviolet Absorption Spectroscopy. *Journal of Vacuum Science & Technology A* 2002, 20 (1), 225-229.
47. Ramos, R.; Cunge, G.; Touzeau, M.; Sadeghi, N., Absorption Spectroscopy in  $BCl_3$  Inductively Coupled Plasmas: Determination of Density, Rotational, Translational and

- Vibrational Temperatures of BCl Molecule. *Journal of Physics D: Applied Physics* 2008, 41 (11), 115205.
48. Foucher, M.; Marinov, D.; Carbone, E.; Chabert, P.; Booth, J.-P., Highly vibrationally excited O<sub>2</sub> molecules in low-pressure inductively-coupled plasmas detected by high sensitivity ultra-broad-band optical absorption spectroscopy. *Plasma Sources Science & Technology* 2015, 24 (4).
  49. Ramos, R.; Cunge, G.; Touzeau, M.; Sadeghi, N., Absorption spectroscopy in BCl 3 inductively coupled plasmas: determination of density, rotational, translational and vibrational temperatures of BCl molecule. *Journal of Physics D: Applied Physics* 2008, 41 (11), 115205.
  50. Blechle, J. M.; Cuddy, M. F.; Fisher, E. R., Effect of ion energies on the surface interactions of NO formed in nitrogen oxide plasma systems. *The Journal of Physical Chemistry A* 2013, 117 (6), 1204-1215.
  51. Hanna, A. R.; Blechle, J. M.; Fisher, E. R., Manuscript in Preparation 2016.
  52. Morgan, M. M.; Cuddy, M. F.; Fisher, E. R., Gas-phase chemistry in inductively coupled plasmas for NO removal from mixed gas systems. *Journal of Physical Chemistry A* 2010, 114 (4), 1722-1733.
  53. Tonniss, E. J.; Graves, D. B., Neutral gas temperatures measured within a high-density, inductively coupled plasma abatement device. *Journal of Vacuum Science & Technology A* 2002, 20 (5), 1787-1795.
  54. Zhang, Q. Y.; Shi, D. Q.; Xu, W.; Miao, C. Y.; Ma, C. Y.; Ren, C. S.; Zhang, C.; Yi, Z., Determination of vibrational and rotational temperatures in highly constricted nitrogen plasmas by fitting the second positive system of N<sub>2</sub> molecules. *AIP Advances* 2015, 5 (5).
  55. Iza, F.; Hopwood, J. A., Rotational, vibrational, and excitation temperatures of a microwave-frequency microplasma. *IEEE Transactions on Plasma Science* 2004, 32 (2), 498-504.
  56. Low Temperature Plasma Science: Not Only the Fourth State of Matter but All of Them; Report of the Department of Energy Office of Fusion Energy Sciences, Workshop on Low Temperature Plasmas: 2008.
  57. Lee, C. G. N.; Kanarik, K. J.; Gottscho, R. A., The grand challenges of plasma etching: a manufacturing perspective. *Journal of Physics D* 2014, 47, 273001.
  58. Meichsner, J.; Schmidt, M.; Schneider, R.; Wagner, H.-E., *Nonthermal Plasma Chemistry and Physics*. CRC Press, Taylor & Francis Group: Boca Raton, FL, 2013.
  59. Morgan, M. M.; Cuddy, M. F.; Fisher, E. R., Gas-phase chemistry in inductively coupled plasmas for NO removal from mixed gas systems. *The Journal of Physical Chemistry A* 2010, 114 (4), 1722-1733.

## CHAPTER 5

### THE EFFECT OF ION ENERGIES ON THE SURFACE INTERACTIONS OF NITRIC OXIDE FORMED IN NITROGEN OXIDE PLASMA SYSTEMS

This chapter is reproduced with permission from an article published in *The Journal of Physical Chemistry A* by Joshua M. Blechle, Michael F. Cuddy, and Ellen R. Fisher [117 (6), pp 1204-1215, Copyright 2013 American Chemical Society]. This work was an expansion of previously published work by the same authors, albeit with M.F. Cuddy as the lead author. These studies examine the influence of ion energies on surface scatter coefficients. The previous work focused on fluorocarbon plasma systems, whereas the information in this Chapter details the similar relationships found within nitrogen oxide plasmas. The dependence of these relationships on different plasma parameters such as pressure, applied RF power, and precursor composition was explored. Ion energies were determined via mass spectrometry and surface scatter coefficients were calculated using the IRIS technique under ion-rich and ion-free environments.

#### 5.1 Introduction

Nitric oxide is a relatively simple molecule with surprisingly interesting and complex chemistry, eliciting a vast array of studies spanning a range of areas both fundamental and technologically relevant. NO has long been implicated as a pollutant arising from automobile and industrial exhaust, and its atmospheric remediation, generally via the use of a metal or metal oxide catalyst, has become one of the most studied environmental problems.<sup>1-2</sup> In addition, NO is an important participant in many biological processes, including blood pressure regulation,

vasodilation, and increased biocompatibility for various medical implant devices,<sup>3-4</sup> many of which could ideally be monitored via NO-bioimaging.<sup>5</sup> In both atmospheric chemistry and in the context of biological processes, understanding the mechanisms and kinetics of NO reactions with both metal ions and at a range of surfaces is key to improving process performance.<sup>6-10</sup> Ions, in particular, are critical contributors to the exacerbation of environmentally detrimental NO effects. For example, NO<sup>+</sup> may be produced in the atmosphere by reactions between nitrogen ions and oxygen as in reaction (5.1). The relatively low rate constant for this reaction,



$2.5 \times 10^{-10} \text{ cm}^3\text{s}^{-1}$ ,<sup>9</sup> facilitates ample production of atmospheric NO<sup>+</sup> species. Karasek and Denney have demonstrated that the nitric oxide ion is readily hydrated in the atmosphere and that the (H<sub>2</sub>O)NO<sup>+</sup> complex is highly mobile.<sup>11</sup> Thus, gas-phase ion processes are of paramount interest in determining remediation pathways for nitric oxide contamination.

Armentrout and coworkers have explored a number of gas-phase ion-molecule reactions of relevance to NO<sub>x</sub> chemistry with the overall goal to determine the kinetic energy dependence of reactions of relevance to fundamental organometallic chemistry as well as atmospheric reactions.<sup>12-18</sup> Systems such as M<sup>+</sup> + NO, NO<sub>2</sub> or N<sub>2</sub>O (where M<sup>+</sup> = metal ion), or, alternatively, systems that explored the reactions of O<sup>+</sup>, O<sub>2</sub><sup>+</sup>, N<sub>2</sub><sup>+</sup>, and N<sub>4</sub><sup>+</sup> with reaction partners such as N<sub>2</sub> or O<sub>2</sub> provided fundamental thermochemistry and kinetics as well as an evaluation of reaction dynamics. One significant result from the Armentrout laboratory demonstrated the formation of NO<sup>+</sup> species by the reaction of O<sup>+</sup> + N<sub>2</sub> through N<sub>2</sub>O<sup>+</sup> intermediates.<sup>12</sup> The efficacy of NO<sup>+</sup> formation is dictated by the O<sup>+</sup> energy in flowing afterglow and flow/drift tube experiments. Their results also suggest that variations in ion energy distributions are chief contributors to discrepancies in measurements of NO<sup>+</sup> by different methods. A second significant area of

research explored by the Armentrout group focused on the potential catalytic activity of Cu ions for decomposition of NO<sub>x</sub> pollutants.<sup>16</sup> This work demonstrated that sequential bond dissociation energies exist for Cu(NO)<sub>2</sub><sup>+</sup> complexes, suggesting that a fundamental understanding of surface-specific interactions of nitric oxide species (e.g. on Cu-containing zeolite substrates) is necessary for NO<sub>x</sub> abatement.

In catalytic processes, several approaches have been explored to improve NO decomposition and removal of NO<sub>x</sub> species, including investigation of a range of different catalyst materials, photocatalytic decomposition, use of various reductants, and more recently, employing plasmas to excite NO<sub>x</sub> for more efficient removal or to modify catalyst surfaces to increase the efficiency of the catalytic process.<sup>19-20</sup> Understanding the contributions of various gas-phase species in surface reactions is thus extremely valuable for the assessment of catalytic performance and ultimately for improving catalytic substrates for enhanced control of vehicular emissions. Many investigations of plasma-based methods for NO<sub>x</sub> remediation are conspicuously devoid of discussions of the fundamental chemistry involved in plasma processes. Previous work in our laboratory explored much of the neutral gas-phase chemistry in N<sub>x</sub>O<sub>y</sub> plasmas through optical emission spectroscopy (OES) and laser-induced fluorescence.<sup>21</sup> One chief aspect to consider for plasma modifications, however, is the role of ions in both the gas-phase and in reactions at plasma-surface interfaces. Interestingly, not all ions participate in surface-mediated processes. For example, NO<sup>+</sup> ions in nitric oxide afterglows exhibit relatively high diffusivities ( $\sim 85 \text{ cm}^2 \text{ Torr s}^{-1}$ )<sup>22</sup> and tend to not dissociate at catalytic surfaces under ambient conditions.<sup>23</sup>

Here, we have attempted to gauge the influence of ions in N<sub>x</sub>O<sub>y</sub> plasmas on surface reactivity via the imaging of radicals interacting with surfaces (IRIS) technique. To date, only a



limited number of IRIS experiments have been expressly devoted to examining the surface reactivity of NO radicals; rather, such IRIS work in our laboratory has focused on the contributions of vibrational energies to surface reactivity.<sup>24</sup> We have previously demonstrated, however, that ions are largely responsible for the apparent surface production of CF<sub>x</sub> species from fluorocarbon-passivated surfaces associated with C<sub>x</sub>F<sub>y</sub> plasma processing.<sup>25-28</sup> Increased surface scatter for CF<sub>x</sub> radicals in these systems is commensurate with increasing ion energies for nascent plasma species. As such, we have extended these investigations to NO-producing systems, including 100% NO, NO<sub>2</sub>, N<sub>2</sub>O, and mixed precursor (N<sub>2</sub> + O<sub>2</sub>) plasmas. Energy analyses of nascent ions are accomplished via mass spectrometric techniques to determine ion energy distributions (IEDs) for plasma constituents. From these IEDs, total mean ion energies,  $\langle E_i \rangle_{\text{total}}$ , are determined. Ions may be repelled from a surface in the IRIS experiment through substrate biasing at an appropriate potential to prevent plasma ions of some  $\langle E_i \rangle_{\text{total}}$  from reaching the substrate. Ion contributions to the surface reactivity of NO radicals can be determined by comparing this ion-limited case to the scatter coefficients determined when there is no applied substrate bias. Eventually, the extension of these investigations could contribute to improved methodologies for NO<sub>x</sub> removal and allow for tailored surfaces that control the reduction of nitrogen oxide (N<sub>x</sub>O<sub>y</sub>) species through the utilization of inductively coupled plasmas.

## 5.2 Results and Discussion

Raw mass spectra allow for the identification of nascent ions formed within the various nitrogen oxide plasma systems studied. For example, Figure 5.1 shows those ions formed in a 50 mTorr, 200 W N<sub>2</sub>O plasma. This system, as with the others, displays a prominent NO<sup>+</sup> peak

as well as signal from  $\text{N}^+$ ,  $\text{O}^+$ , and the parent ion,  $\text{N}_2\text{O}^+$ . Similar mass spectra were obtained for all precursor systems, with the only major difference between the spectra being the intensity of the signals for each ion and the presence of different parent ions. In all cases,  $\text{NO}^+$  signal dominated the mass spectra. Ion energy distributions were collected for all primary ions in each plasma system by scanning energies for specific mass-to-charge ratios.

IEDs for  $\text{NO}^+$  ( $m/z = 30$ ) formed in each of the four plasma systems are shown in Fig. 5.2a. It is important to note that these IEDs are plotted on different ordinate scales to focus primarily on the shape of the distributions, rather than the ion intensities. The  $\text{NO}^+$  energy distributions in the  $\text{NO}$ ,  $\text{NO}_2$  and  $\text{N}_2\text{O}$  plasmas are all relatively narrow, and consist of one primary peak, with the  $\text{NO}$  plasma generating the most energetic ions (IED main peak centered at  $\sim 250$  eV). In the  $\text{NO}_2$  and  $\text{N}_2\text{O}$  system, there is a low energy tail on the distribution, whereas in the  $\text{NO}$  system, a fairly substantial lower energy shoulder is present, centered at  $\sim 225$  eV. Interestingly, in the  $\text{N}_2 + \text{O}_2$  system, the distribution is bimodal, with nearly equivalent peaks centered at  $\sim 90$  eV and  $\sim 160$  eV. As a final note on ion intensities in these systems, the most intense  $\text{NO}^+$  signal arises in the  $\text{NO}$  plasma, as expected given the relatively low ionization energy of  $\text{NO}$  ( $9.26436 \pm 0.00006$  eV).<sup>29</sup> Formation of  $\text{NO}^+$  from the other precursors requires  $\sim 2$ - $5$  eV more energy.

Figure 5.2b displays the individual IEDs for each ion formed in a  $\text{N}_2\text{O}$  plasma using the same conditions as were employed to collect the mass spectrum. Note that these distributions are plotted on the same y-axis scale to demonstrate the relative densities of each ion formed within the plasma system. With all four ions, it is noticed that the individual energy distributions are centered at approximately the same energy ( $\sim 160$  eV) regardless of the particular distribution. It is noted that the lower mass ions,  $\text{O}^+$  and  $\text{N}^+$ , have substantially broader energy distributions,

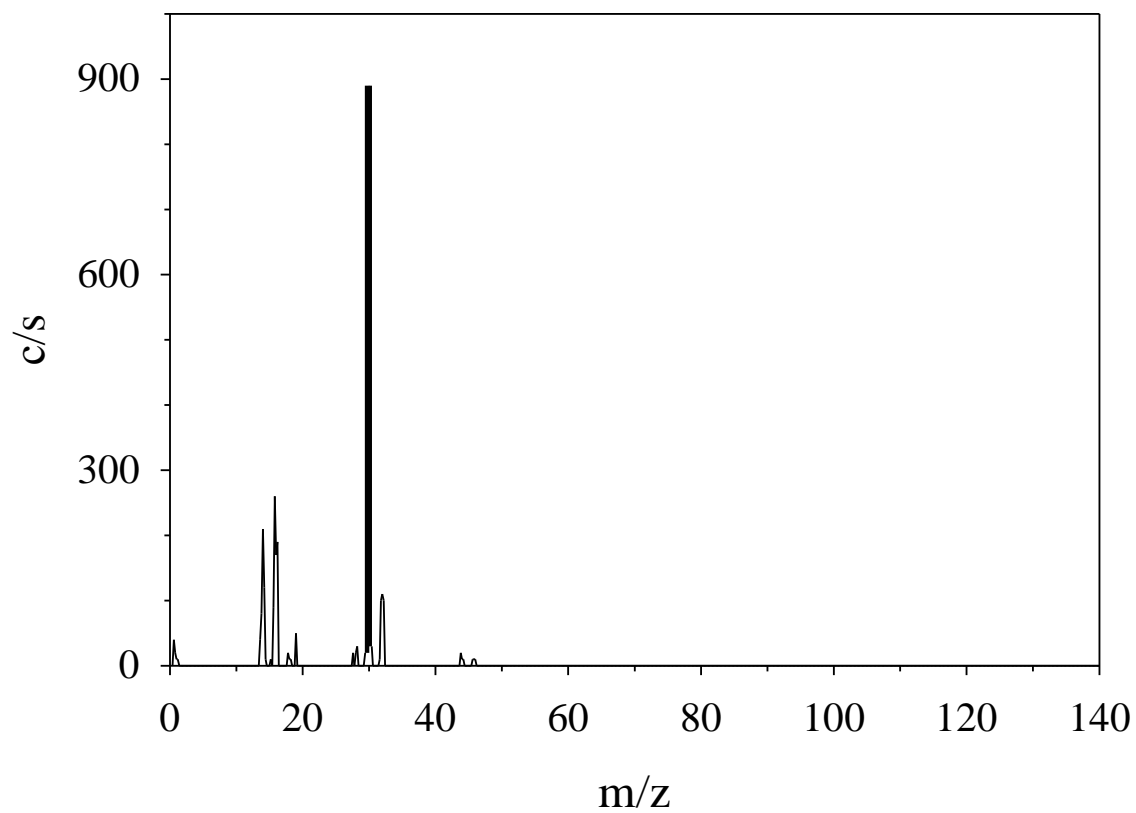


Figure 5.1 Representative mass spectrum of nascent ions formed in an  $\text{N}_2\text{O}$  plasma at  $P = 200$  W and  $p = 50$  mTorr.

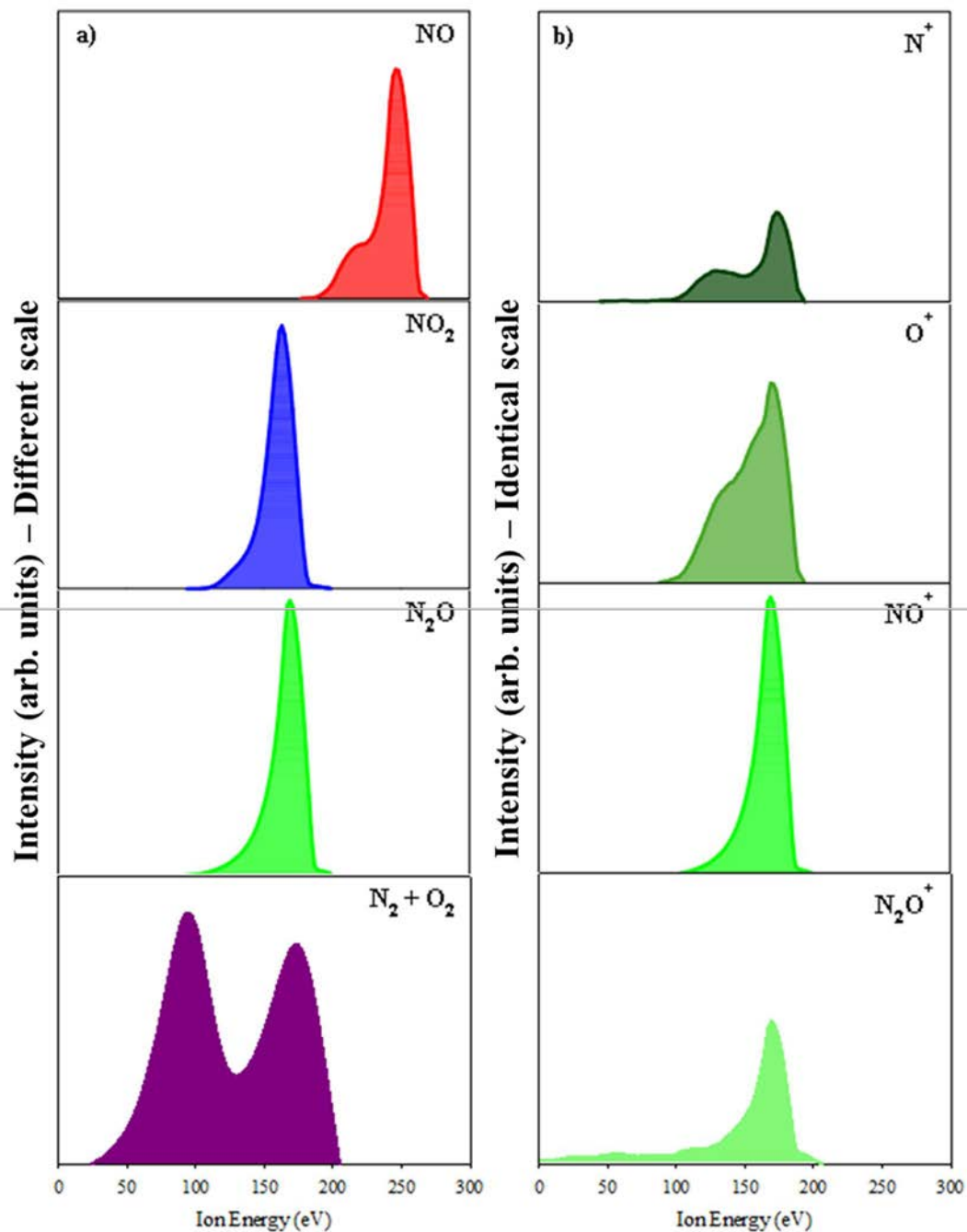


Figure 5.2 Ion energy distributions of a) (left column) nascent  $\text{NO}^+$  ions formed in all four precursor plasmas ( $P = 200$  W and  $p = 50$  mTorr), and b) (right column) all nascent ions formed in an  $\text{N}_2\text{O}$  plasma at  $P = 200$  W and  $p = 50$  mTorr.

with multiple features, whereas both  $\text{NO}^+$  and  $\text{N}_2\text{O}^+$  have one peak, with substantive low energy tails. However, the observation that all of the ions found in a plasma system have similar mean energies is further verified in Fig. 5.3a, where  $\langle E_i \rangle$  for all ions formed in a NO plasma is plotted as a function of  $p$ . Clearly, the average value does not change appreciably with ion identity under a given set of conditions (regardless of distribution), suggesting that ions of all types have thermalized within the plasma. Given that the ion energy distributions vary (i.e. bimodal or multimodal) between ions for some systems, this may be a simplification, the impact of which is addressed below. The benefit of this assumption, however, is that it allows for the evaluation and comparison of data from various plasma systems and many different types of ions. Moreover, this same behavior (i.e. average ion energies for all individual ions in a particular system are the same) is observed in all four plasma systems, which allows us to average  $\langle E_i \rangle$  values for all ions formed in a given plasma, yielding  $\langle E_i \rangle_{\text{total}}$ . This total mean ion energy effectively describes the energy of all ions in a system under a given set of conditions, regardless of the identity of the ion. Notably, the presence of high energy tails in some of the IEDs can affect the interpretation of surface scatter data, as discussed further below. Trends in  $\langle E_i \rangle_{\text{total}}$  for all four precursors as a function of  $P$  can be seen in Fig. 5.3b. Examining Figs. 5.3a and 5.3b together reveals that  $\langle E_i \rangle_{\text{total}}$  for each system is negatively correlated with system pressure and positively correlated with applied rf power. This indicates that low pressure/high power combinations will determine the upper-bound for ion energies in a particular plasma system. For this reason, data for  $\langle E_i \rangle_{\text{total}}$  has been determined only at  $P = 200$  W for system pressures exceeding 50 mTorr. The trends in rf power dependence at 50 mTorr can be applied to higher pressures to predict what ion energies may exist at  $P < 200$  W. All calculated  $\langle E_i \rangle_{\text{total}}$  values are tabulated in Table 5.1.

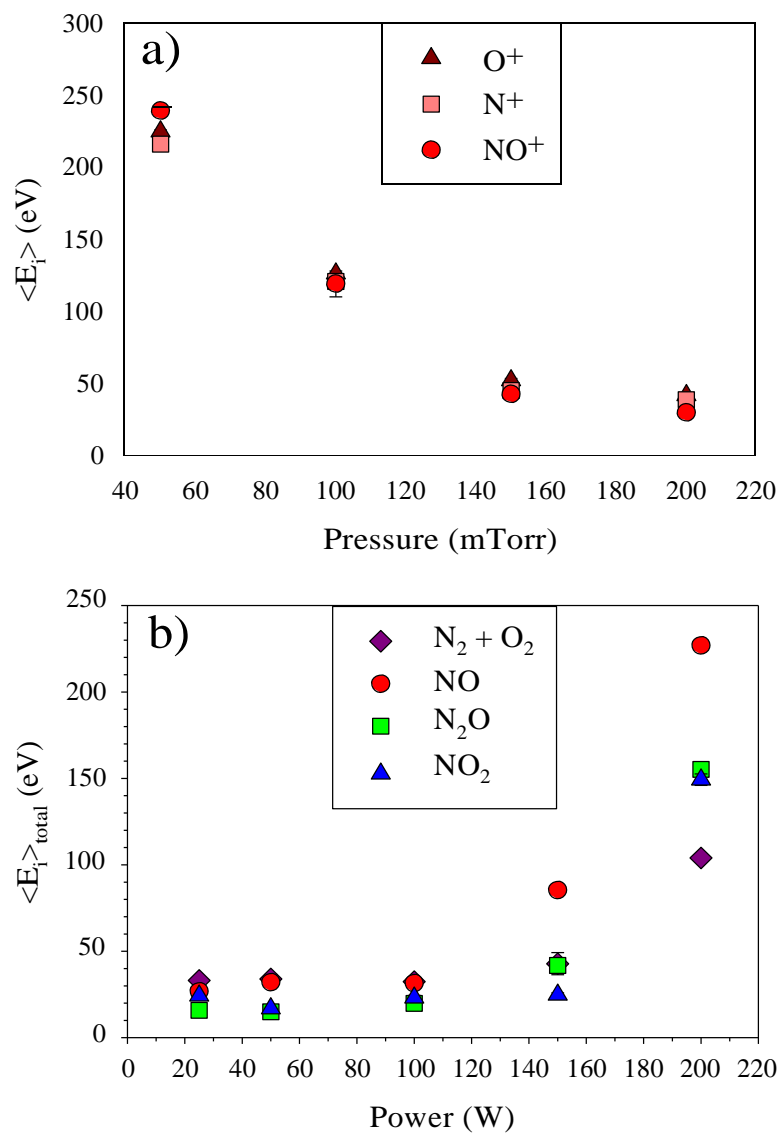


Figure 5.3 Average ion energies a) for individual ions plotted as a function of feed gas pressure for all nascent ions formed in 100% NO plasmas with  $P = 200$  W. b) Total average ion energies plotted as a function of applied rf power for plasmas formed from four precursors all with  $p = 50$  mTorr.

IRIS data were collected for NO radicals to determine surface scatter in the nitrogen oxide plasma systems as a function of plasma parameters. Representative IRIS images acquired using a 50 mTorr, 200 W N<sub>2</sub>O plasma molecular beam are shown in Fig. 5.4. The image in Fig. 5.4a contains signal from both NO in the molecular beam and NO scattered off of a Si substrate. Likewise, the image in Fig. 5.4b includes signal from NO in the molecular beam and scattered off of a +300 V dc biased Si substrate. The image in Fig. 5.4c was acquired without a substrate in the path of the molecular beam, and so contains LIF signal arising solely from NO in the plasma molecular beam. Subtraction of the beam image in Fig. 5.4c from the images in Figs. 5.4a and 5.4b, individually, results in images that contain only signal from molecules scattered from the Si substrate with and without bias, Figs. 5.4d and 5.4e, respectively. Cross-sections of these images are compared to simulated data to determine S(NO) in both the non-biased and biased systems, Figs. 5.4f and 5.4g, respectively. For the images shown in Fig. 5.4, this process yields  $S(\text{NO}) = 0.70$  and  $S(\text{NO})_{\text{ion limited}} = 0.46$ . Thus,  $\Delta S(\text{NO}) = 0.24$  for a 50 mTorr, 200 W N<sub>2</sub>O plasma. All S(NO) and  $\Delta S(\text{NO})$  values measured are listed in Table 5.2.

The effects of system pressure and applied rf power on S(NO) for 100% NO plasmas are shown in Fig. 5.5. In general, S(NO) increases with increasing system pressure, although at  $P < 100$  W, the values in the 100 mTorr and 50 mTorr plasmas are the same within experimental error. Notably, the S(NO) values measured at  $P \approx 150$  W and  $p \approx 100$  mTorr are all less than unity. This indicates some fraction of the NO molecules is lost upon surface interaction. Indeed, we have previously defined IRIS surface reactivity, R, as  $R = 1 - S$ , where R then represents the fraction that either reacts (e.g. dissociates) or “sticks” to the surface. Again, we note that IRIS measurements do not track individual molecules, and therefore cannot distinguish between loss (or production) mechanisms at the surface. Thus, at low rf powers and pressures, it appears that

Table 5.1 Calculated values for  $\langle E_i \rangle_{\text{total}}$  in all four precursor systems. Error given in parentheses is one standard deviation of the mean of  $\langle E_i \rangle$  for all ions.

Conditions		NO Plasmas	N <sub>2</sub> O Plasmas	N <sub>2</sub> + O <sub>2</sub> Plasmas	NO <sub>2</sub> Plasmas
p (mTorr)	P (W)	$\langle E_i \rangle_{\text{total}}$ (eV)	$\langle E_i \rangle_{\text{total}}$ (eV)	$\langle E_i \rangle_{\text{total}}$ (eV)	$\langle E_i \rangle_{\text{total}}$ (eV)
50	25	26.8 (1.1)	15.9 (0.4)	33.1 (1.6)	24.3 (0.5)
50	50	32.1 (2.6)	15.0 (0.1)	34.0(2.6)	16.9 (0.3)
50	100	31.5 (2.3)	19.8 (0.6)	32.4 (1.3)	23.1 (1.3)
50	150	85.4 (1.8)	41.7 (1.3)	42.8 (6.4)	24.8 (1.1)
50	200	226.9 (1.6)	155.2 (1.5)	104 (2.4)	149.3 (3.3)
100	200	122.1 (10.2)			
150	200	46.6 (2.9)			
200	200	36.7 (0.4)			



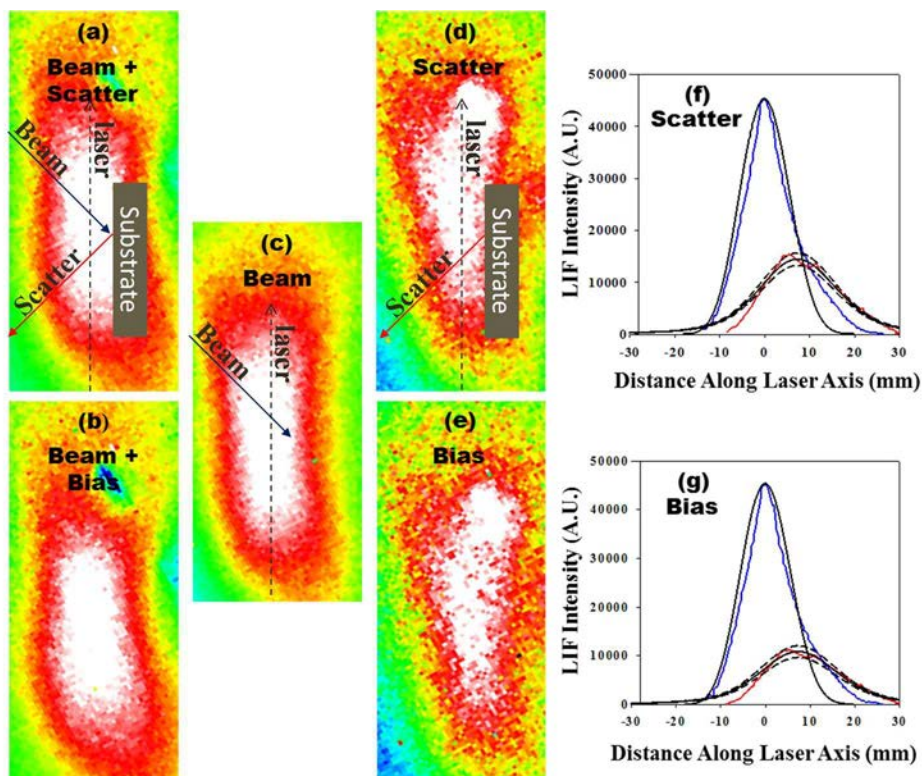


Figure 5.4 LIF images for NO species generated in an  $\text{N}_2\text{O}$  plasma with  $P = 200$  W and  $p = 50$  mTorr: a) NO radicals both incident and scattered from a Si substrate; b) NO radicals both incident and scattered from a +300 V dc biased Si substrate; c) NO radicals in the plasma molecular beam only. Subtraction of image c) from a) yields d), an NO scatter image for the unbiased substrate; subtraction of image c) from b) results in e), an NO scatter image for the biased substrate. Lines added to images in a), c), and d) indicate the propagation of the laser beam, the plasma molecular beam, and species scattered from a substrate (assuming specular scattering). IRIS cross-sections taken along the laser propagation axes of the beam (blue) and scatter (red) images along with fits (black) to these data yield f)  $S(\text{NO}) = 0.70$  in the case of no substrate biasing; and g)  $S(\text{NO}) = 0.46$  in the case of +300 V biased Si. Thus,  $\Delta S(\text{NO}) = 0.24$  under these experimental conditions.

~80% of the NO in the plasma molecular beam is lost at the surface, with only ~20% scattering. For the 50 mTorr systems,  $S(\text{NO})$  remains essentially constant as a function of  $P$ , whereas in the 100 mTorr systems,  $S(\text{NO})$  increases nearly linearly with  $P$ , reaching a maximum of ~1.45 at  $P = 200 \text{ W}$ . At the highest pressure examined ( $p = 200 \text{ mTorr}$ ),  $S(\text{NO}) > 1$  at all  $P$ , rising from  $1.20 \pm 0.25$  at 25 W to a maximum of  $2.30 \pm 0.30$  at 100 W. Notably, at  $P \geq 50 \text{ W}$ , the measured  $S(\text{NO})$  values are the same within experimental error, indicating no tangible dependence on  $P$  in the system. Overall, the data in Figure 5.5 suggest that  $p$  is much more influential than  $P$  in determining  $S(\text{NO})$ . An important consideration in rationalizing the IRIS results for NO is the knowledge of the rotational and vibrational temperatures of the radical. These internal energy values are important for understanding properties including rotational/vibrational state populations, propensity for the radical to undergo surface interactions, and the potential for inelastic scattering of the radical resulting in apparent surface loss. Previous experiments in our laboratory have measured the rotational and vibrational temperatures of the NO molecules in 100% NO plasma molecular beams.<sup>24</sup> In that work, we found the rotational temperature of NO was essentially room temperature (~320-340 K) for 50-150 W plasmas. Given that the substrates used here are all at room temperature, assuming in the model that no changes in rotational populations occur as a result of surface interactions is likely valid. The vibrational temperature of the  $X^2\Sigma^+$  ground state was measured to be slightly higher, with values ranging from  $410 \pm 40 \text{ K}$  to  $530 \pm 40 \text{ K}$  (with  $P = 50\text{-}200 \text{ W}$ ). Notably, the vibrational temperature of the  $A^2\Sigma^+$  excited state was considerably higher,  $1450 \pm 20 \text{ K}$  to  $1740 \pm 40 \text{ K}$ , and the impact of these values is discussed in detail elsewhere.<sup>24</sup> Moreover, current work in our laboratory is focused on measuring the translational temperature of NO via velocity measurements as described previously for other molecules.<sup>30-32</sup> Results from these varied studies, specifically for  $\text{NH}_2$

Table 5.2 Surface scatter coefficients for NO in all four precursor systems. Error given in parentheses is one standard deviation of the mean

Conditions		NO plasmas			N <sub>2</sub> O Plasmas			N <sub>2</sub> + O <sub>2</sub> Plasmas			NO <sub>2</sub> plasmas
<i>p</i> (m Torr)	<i>P</i> (W)	<i>S</i> (NO)	<i>S</i> (NO) <sub>ion</sub> limited	Δ <i>S</i> (NO)	<i>S</i> (NO)	<i>S</i> (NO) <sub>ion</sub> limited	Δ <i>S</i> (NO)	<i>S</i> (NO)	<i>S</i> (NO) <sub>ion</sub> limited	Δ <i>S</i> (NO)	<i>S</i> (NO)
50	25	0.22(0.05)	0.20(0.03)	<b>0.02(0.04)</b>	0.73(0.15)	0.95(0.30)	<b>-0.22(0.23)</b>				
	50	0.24(0.08)	0.25(0.03)	<b>-0.01(0.05)</b>	0.60(0.15)	0.50(0.20)	<b>0.10(0.17)</b>	1.90(0.40)	1.90(0.40)	<b>0.00(0.40)</b>	
	100	0.43(0.05)	0.37(0.05)	<b>0.06(0.05)</b>	0.50(0.15)	0.40(0.15)	<b>0.10(0.15)</b>	1.20(0.20)	1.30(0.40)	<b>-0.10(0.30)</b>	
	150	0.42(0.07)	0.27(0.05)	<b>0.15(0.06)</b>	0.65(0.15)	0.50(0.12)	<b>0.15(0.13)</b>	1.30(0.40)	0.70(0.10)	<b>0.40(0.25)</b>	
	200	0.42(0.08)	0.23(0.04)	<b>0.19(0.06)</b>	0.70(0.15)	0.46(0.10)	<b>0.24(0.12)</b>	1.10(0.30)	0.65(0.15)	<b>0.45(0.22)</b>	
100	25	0.23(0.03)	0.21(0.04)	<b>0.02(0.04)</b>							
	50	0.26(0.03)	0.19(0.07)	<b>0.07(0.05)</b>							
	100	0.55(0.10)	0.62(0.03)	<b>-0.07(0.07)</b>							
	150	0.91(0.10)	0.95(0.10)	<b>-0.04(0.10)</b>							
	200	1.45(0.10)	1.25(0.10)	<b>0.20(0.10)</b>							
200	25	1.20(0.25)			1.60(0.30)						0.82(0.16)
	50	2.15(0.35)			0.90(0.20)						0.54(0.09)
	100	2.30(0.30)			0.80(0.20)						0.43(0.09)
	150	2.10(0.25)			0.65(0.15)						0.41(0.08)
	200	2.00(0.50)			0.70(0.15)						0.26(0.08)

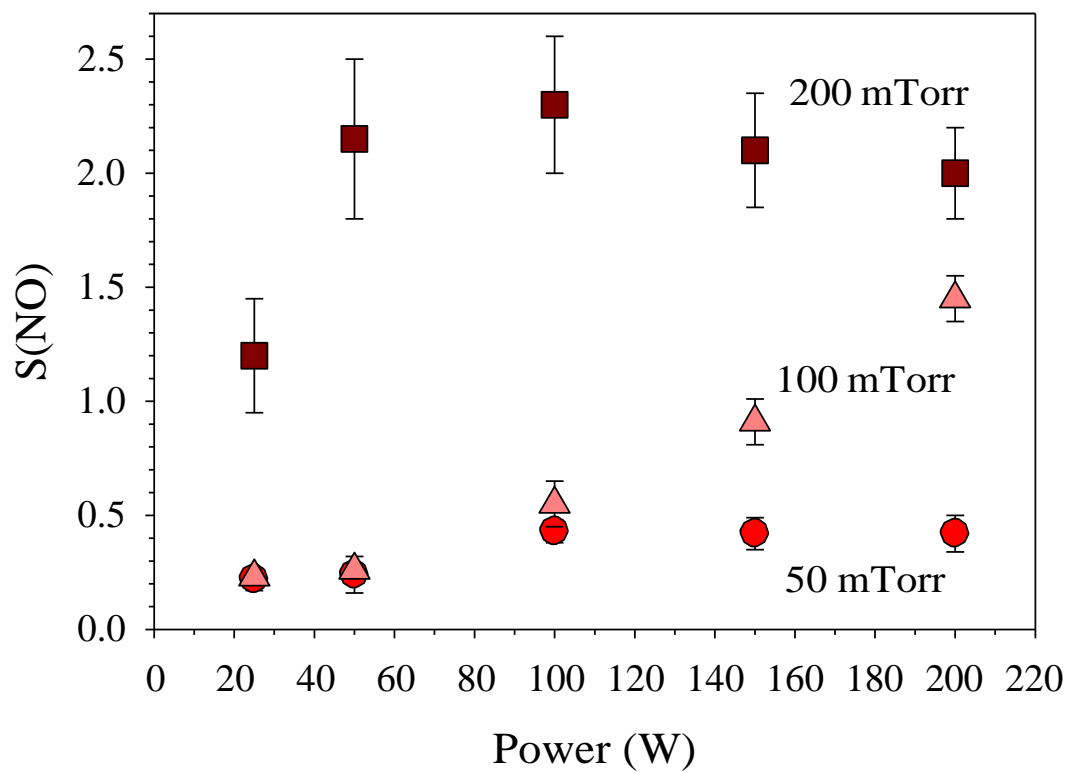


Figure 5.5 NO scatter coefficients as a function of applied rf power for 100% NO plasmas at system pressures ranging from  $p = 50\text{-}200$  mTorr.

formed from  $\text{NH}_3$  plasmas,<sup>31-32</sup> would suggest the translational temperatures we could anticipate measuring for NO are likely to depend on plasma conditions. More specifically, this indicates a ~30% increase in translational temperature from 25-150 W as well as a positive correlation with pressure. Preliminary work shows that the kinetic energies (i.e. translational temperatures) for NO molecules in 100% NO plasmas operating at  $P = 100$  W and  $p = 100$  mTorr are  $1350 \pm 350$  K. Thus, the translational temperatures we would expect for this system are ~1100-1450 K at 100 mTorr, which coincides with the vibrational temperatures. However, we expect translational temperatures at 50 mTorr (where most of these experiments were completed) to be lower than these values.

The effect of precursor choice on surface scatter is demonstrated in Fig. 5.6. At  $p = 50$  mTorr, Fig. 5.6a, the NO scatter values are relatively constant within combined experimental error for a particular precursor gas, especially at  $P \geq 100$  W. Notably,  $S(\text{NO})$  values measured in the  $\text{N}_2 + \text{O}_2$  system are significantly higher than those measured in the  $\text{N}_2\text{O}$  and NO systems, especially at the lowest  $P$ . Note that signal from NO radicals is not strong enough in  $\text{N}_2 + \text{O}_2$  plasmas at  $P < 50$  W to adequately determine scatter. At  $p = 200$  mTorr, Fig. 5.6b, the precursors show significantly different trends as a function of  $P$ . Here,  $S(\text{NO})$  is significantly higher in the NO systems at  $P \geq 50$  W, and, as noted above, stay relatively constant with  $P$ . In contrast,  $S(\text{NO})$  measured in the other precursor systems decreases monotonically with increasing  $P$ , dropping from ~1.6 to ~0.25 in the  $\text{N}_2\text{O}$  system and from ~0.75 to ~0.25 in the  $\text{NO}_2$  system between  $P = 25$ -200 W. This is discussed further below.

As reactor pressure and applied rf power appear to have some influence on  $S(\text{NO})$ , it is possible that ions are contributing to the observed scatter coefficients (especially  $S(\text{NO}) > 1$ ), as ion density is known to increase with rf power in ICPs.<sup>33</sup> As a function of increasing pressure

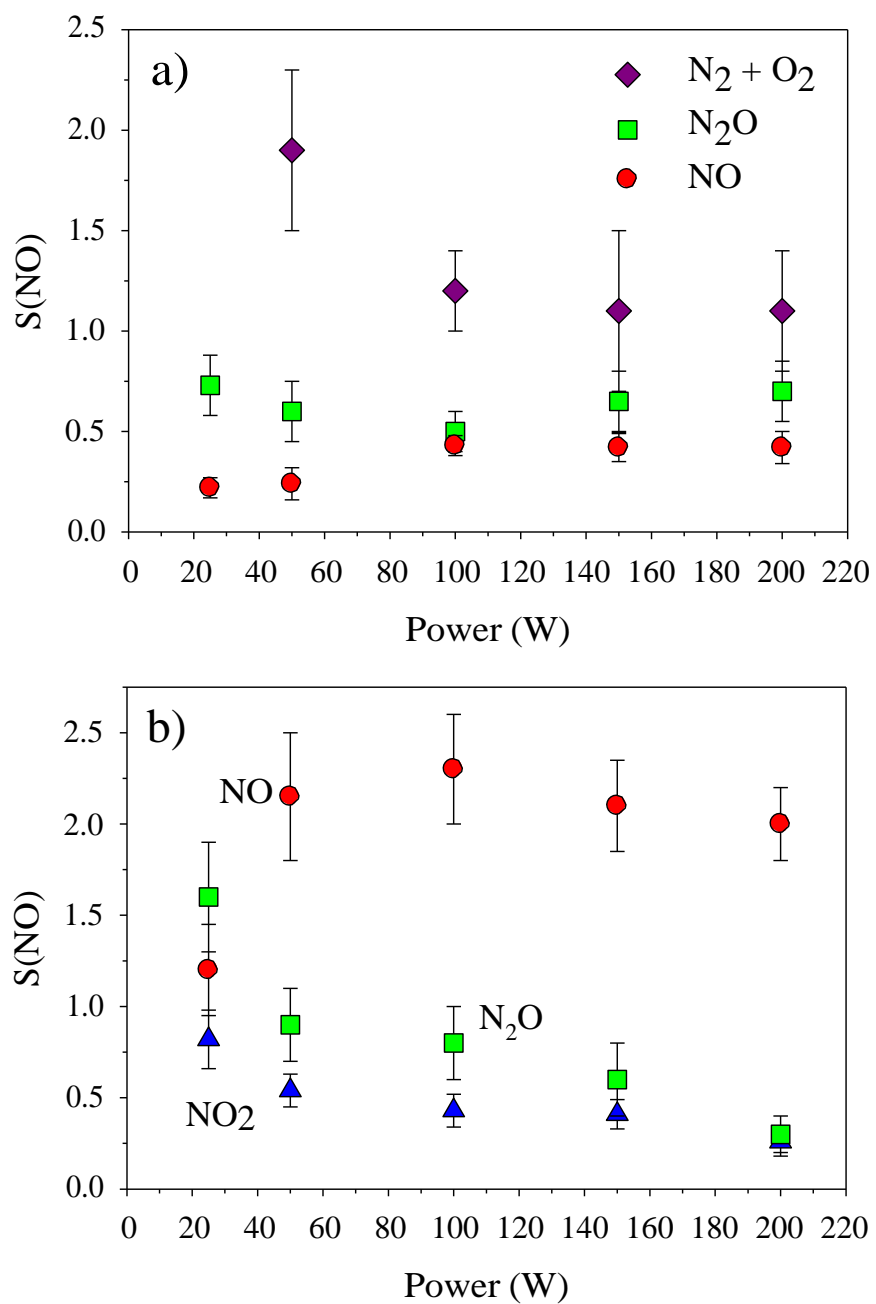


Figure 5.6 NO scatter coefficient values plotted as a function of applied rf power for discrete precursors in a)  $p = 50$  mTorr and b)  $p = 200$  mTorr plasmas.

for  $P = 200$  W, the intensity of  $\text{NO}^+$  signal in a pure NO plasma decreased by more than 83% over the range  $p = 50\text{-}100$  mTorr, with less profound decreases occurring for  $p > 100$  mTorr. Thus,  $\Delta S(\text{NO})$  was determined in NO plasmas for two different system pressures (50 and 100 mTorr) and as a function of  $P$ , Fig. 5.7. Surprisingly, the change in scatter is essentially zero within experimental error for systems at  $P \leq 100$  W, with non-zero values only occurring at  $P \geq 150$  W. For the 100 mTorr system,  $\Delta S(\text{NO})$  is only significantly higher than zero at  $P = 200$  W. As noted above, both applied rf power and system pressure have significant impact on  $\langle E_i \rangle_{\text{total}}$ , with the highest energies arising in low pressure and high power plasmas, similar to where the highest  $\Delta S(\text{NO})$  values occur. Thus,  $\Delta S(\text{NO})$  was directly compared to ion energy, Fig. 5.8, to explore the correlation between these two parameters. Notably, the Fig. 5.8 data demonstrate that ions affect NO scatter only when their energy is  $\sim 50$  eV or higher.

A comprehensive understanding of any plasma system necessitates the recognition of the roles of ions. Indeed, ions perform critical functions in many plasma processes, and are related to surface modification via both deposition and removal of materials. Surface-specific interactions of ions may include, but are not limited to, neutralization and desorption at a surface or surface-mediated dissociation facilitating subsequent surface recombination reactions. In general, ions play a key role in surface scatter regardless of ion energy; one archetypal example is the fluorocarbon plasma.<sup>26</sup> In this depositing system, ions take on dual roles as initiators of film growth (the so-called activated growth model)<sup>34</sup> and as etchants for ablation of deposited material.

Specifically, high energy ions create active sites by cleaving chemical bonds during surface bombardment, and these active sites provide a starting point for fluorocarbon film growth and propagation. Low energy ions can lead to the formation of oligomeric film precursors.

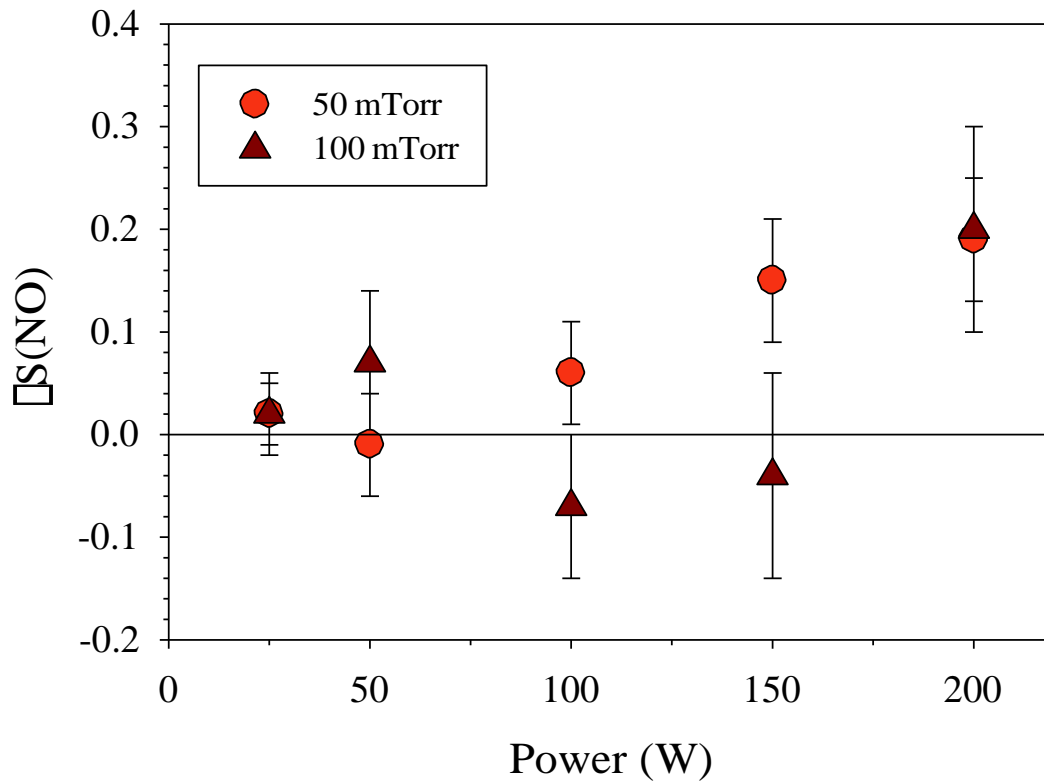


Figure 5.7  $\Delta S(\text{NO})$  values as a function of applied rf power for 100% NO plasmas at system pressures of 50 and 100 mTorr.



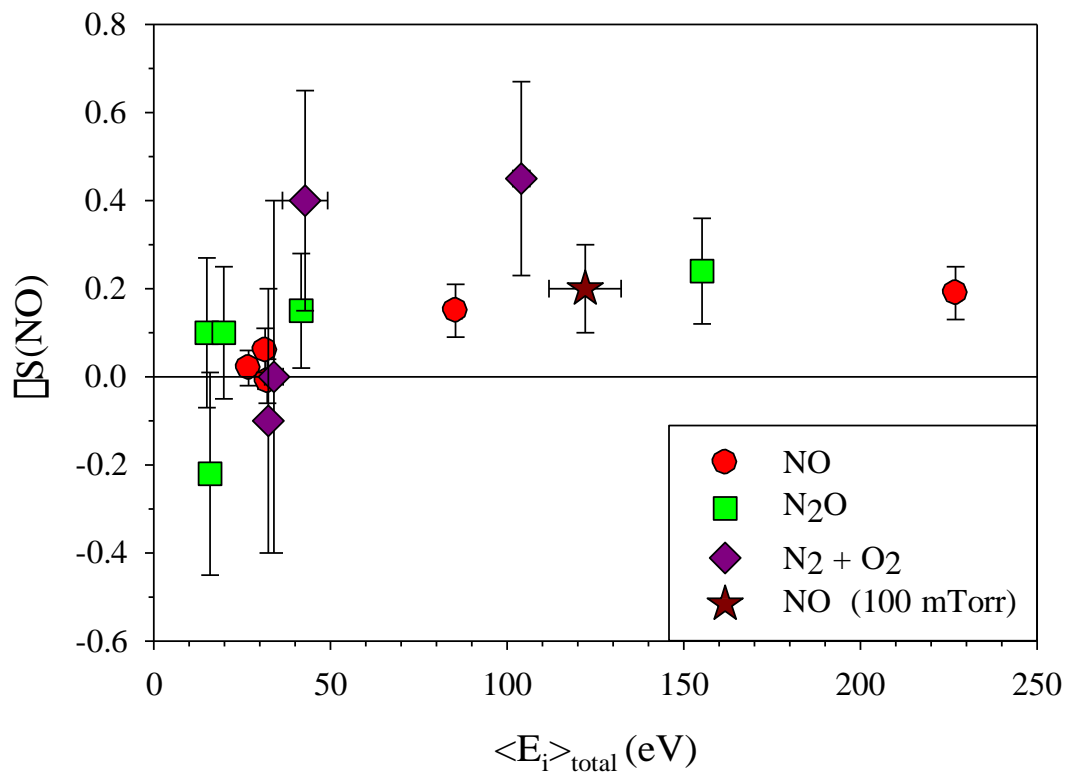


Figure 5.8  $\Delta S(\text{NO})$  as a function of total average ion energy for  $\text{N}_x\text{O}_y$  precursor plasma systems. All values were acquired with  $p = 50$  mTorr except for the  $p = 100$  mTorr,  $P = 200$  W (NO plasma) value indicated by a star.

Simultaneously, the growing fluorocarbon film inevitably loses material through ion-mediated ablation of the film.<sup>35</sup> Because of this, ions play a significant role in surface scatter under all plasma conditions and for values of  $\langle E_i \rangle_{\text{total}}$ . Indeed, we have demonstrated that  $\Delta S(\text{CF}_x) > 0$  under essentially all experimental conditions.<sup>26</sup> We have not, however, extended these investigations to non-depositing systems. Thus, we examine here the contributions of plasma ions to the observed scatter for NO radicals in the non-depositing  $\text{N}_x\text{O}_y$  plasma systems, along with possible explanations for the  $S(\text{NO})$  values measured here under a range of conditions.

As noted above, it is valuable to discuss the primary assumption made in the calculation of ion energies. Specifically, IEDs were used to calculate  $\langle E_i \rangle$  for each ion in a system and then (due to nearly identical values) these values were averaged to produce  $\langle E_i \rangle_{\text{total}}$ , which serves as an indication of ion energy for all ions present in a plasma system under a given set of conditions. This method, however, does not directly account for the shapes of the distributions (e.g. bimodal, multimodal, etc.), which may introduce slight deviations in correlating  $\langle E_i \rangle$  and  $\Delta S(\text{NO})$ . This correlation ultimately lead us to predict a threshold of  $\sim 50$  eV, for ion energies to affect NO surface scatter. Thus, to help understand these nuances, each precursor gas system will first be evaluated under conditions in which  $\langle E_i \rangle_{\text{total}}$  is calculated to be below 50 eV, but the distributions include energies of 50 eV. IEDS that do not contain a significant population of ions at 50 eV or higher, will not appreciably impact the determination of the threshold, and any potential error in the  $\langle E_i \rangle_{\text{total}}$  value becomes moot.

Examining each individual system, we see the NO precursor system eclipses the threshold value at 50 mTorr with both 50 and 100 W systems. At 50 W, the distributions for  $\text{N}^+$ ,  $\text{O}^+$ , and  $\text{NO}^+$  are all bimodal with a small node centered at 50 eV and energies extending up to  $\sim 65$  eV, whereas at 100 W, the  $\text{N}^+$  and  $\text{O}^+$  exhibit bimodal distributions with the trough centered

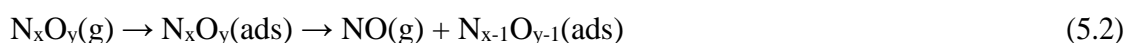
near 50 eV. In contrast, the  $\text{NO}^+$  distribution is trimodal with the smallest, high energy mode centered at  $\sim 50$  eV. All three distributions tail off at  $\sim 75$  eV. For the  $\text{N}_2\text{O}$  precursor at 50 mTorr and 150 W, the  $\text{N}^+$  IED is bimodal with the high energy mode centered at 40 eV and extending to  $\sim 65$  eV. The distributions for  $\text{O}^+$  and  $\text{NO}^+$  are unimodal, but broad, centered at 40 eV and extending to  $\sim 65$  and  $\sim 60$  eV, respectively. The  $\text{N}_2\text{O}^+$  IED in this system is also broad and unimodal but centered at 45 eV and extends to  $\sim 75$  eV. Similarly, the  $\text{NO}_2$  precursor at 50 mTorr and 150 W contains nearly identical, bimodal IEDs for  $\text{N}^+$  and  $\text{O}^+$ , the smaller of the modes is centered at 55 eV and extends to 70 eV. The  $\text{NO}^+$  distribution in this system is trimodal with a small peak centered at 60 eV and extending to 65 eV. The parent ion,  $\text{NO}_2^+$ , has a bimodal IED in which the higher energy mode is centered at 50 eV and extends to  $\sim 60$  eV. For the mixed gas precursor system,  $\text{N}_2+\text{O}_2$ , two sets of conditions are worthy of attention, 100 and 150 W and a pressure of 50 mTorr. At 100 W, the IEDs for  $\text{N}^+$  and  $\text{O}_2^+$  are similarly bimodal, with the trough at 50 eV and the high energy mode extending to  $\sim 75$  eV. The  $\text{O}^+$ ,  $\text{N}_2^+$  and  $\text{NO}^+$  IEDs are all broad and unimodal, with the peak centered at  $\sim 35$  eV and extending to  $\sim 70$  eV. At 150 W, all IEDs extend to  $\sim 100$  eV, but have primary peaks centered at low energies. The  $\text{N}^+$ ,  $\text{O}^+$ , and  $\text{O}_2^+$  distributions are quite broad, but are centered near 25 eV. The  $\text{N}_2^+$  distribution is also quite broad but centered at 15 eV. Finally, the  $\text{NO}^+$  IED is bimodal with a very small high energy mode centered at 70 eV. Ultimately, the result of this IED analysis, indicates that all values for  $\langle E_i \rangle_{\text{total}}$  are below 50 eV, but still contain ions (though generally only a small fraction) with higher energies. Thus, it can be assumed that the proposed threshold for ions impacting NO surface scatter of  $\sim 50$  eV is a lower limit. The observation that the system employing NO as the precursor at 50 mTorr and 150 W ( $\langle E_i \rangle_{\text{total}}=85.4$ ) contains IEDs that include significant portions of the distributions at energies as low as  $\sim 60$  eV, provides some credence to the original analysis

of the ion energy threshold, thereby supporting our use of the  $\langle E_i \rangle_{\text{total}}$  value. As noted in the Results section, under many conditions  $S(\text{NO}) < 1$ , indicating that NO is vanishing from the gas-phase upon interaction with the Si substrate. This is consistent with experimental and theoretical studies that have examined the adsorption of NO on various Si substrates (e.g. Si(100), Si(100)  $2 \times 1$ , Si(001)  $7 \times 7$ ).<sup>36-41</sup> In general, these studies find the sticking probability (equivalent to our surface reactivity, R) of NO to be quite high ( $\geq 0.8$ ), regardless of the crystal face of the Si, which is attributed to the high reactivity associated with the unpaired electron on NO. Although there is some disagreement on this, adsorption on many Si surfaces appears to occur via dissociative chemisorption of NO, rather than molecular chemisorption, largely because dissociation barriers are quite low at Si dimer sites (recently calculated to be  $< 0.07$  eV, depending on geometry).<sup>36</sup> One exception to this is the work of Sasse and Sifhout who determined via both theory and experiment that NO largely adsorbs as a molecule onto the Si(100)  $2 \times 1$  surface, although some dissociation was observed. The presence of missing-dimer effects was invoked as a possible explanation,<sup>39</sup> which was also supported by their calculations that revealed NO dissociation was energetically unfavorable. Interestingly, Namiki et al. examined both the adsorption and scattering of NO on bare as well as alkali metal saturated Si surfaces using a NO molecular beam.<sup>37</sup> They found there was nearly a perfect inverse correlation between sticking and scattering as a function of NO dose. This result was rationalized as NO sticking to active surface sites, which then became inert to NO after the surface was saturated with N and O atoms (from NO dissociation). Arguably, it is difficult to directly compare the results of pure NO (with no excitation, ions, or other species) impinging on a specific crystal face of a Si wafer under UHV conditions to our work with very complex

plasma molecular beams impinging on a relatively non-pristine Si substrate, we attempt below to discuss further the impact of this observation on our IRIS results.

Surface scatter coefficients for NO radicals generally increase with both pressure and applied plasma power for 100% NO plasmas, Fig. 5.5. These trends have been attributed in part to quenching of vibrationally hot NO ( $^2\Sigma^+$ ) and subsequent desorption of NO ( $^2\Pi$ ) molecules upon surface interaction of the plasma molecular beam.<sup>24</sup> S(NO) values do appear to depend upon the choice of feed gas, as well, Fig. 5.6. In particular, scatter coefficients for NO radicals produced as a dissociation or recombination product (i.e. from N<sub>2</sub>O, NO<sub>2</sub>, or N<sub>2</sub> + O<sub>2</sub> feed gases) either decrease or remain essentially constant with increasing P, regardless of pressure, Fig. 5.6. In contrast, S(NO) for the 100% NO precursor increases with P for both system pressures depicted in Fig. 5.6. This discrepancy between S(NO) for 100% NO plasmas and other N<sub>x</sub>O<sub>y</sub> systems indicates that NO surface reactivities are at least partially dependent upon the source of the radical (i.e. the formation mechanism).

Alternatively, at low P (independent of pressure), high scatter coefficients may arise from surface-mediated decomposition of the plasma precursor, as in reaction (5.2)



where  $x$  or  $y > 1$ . We observe through OES analyses that NO formed from plasma-stimulated decomposition of the N<sub>x</sub>O<sub>y</sub> precursor increases in concentration with increased P. Thus, at low P, there is relatively little NO in the incident plasma molecular beam employed in the IRIS experiment. Reactions of the type shown in reaction (5.2) could yield a significant amount of scattered NO, resulting in the high S values observed under some conditions. As P increases, the amount of NO in the plasma molecular beam concomitantly increases (due to breakdown of the N<sub>x</sub>O<sub>y</sub>(g) precursor) and the contributions of the type shown in reaction (5.2) become less

important in determining  $S(\text{NO})$ ; thus, we observe a marked decline in surface scatter coefficients. Although the preceding may explain the trends observed with respect to plasma parameters, there are other complicating factors, such as ion bombardment of the surface, that also warrant consideration for contributions to the absolute values of  $S$ .

Plasma ions attain high energies through sheath effects within the plasma. Briefly, an electric double layer is formed around surfaces (i.e. reactor walls) upon ignition of the plasma, and this sheath accelerates proximal (positive) ions based upon the potential drop from within the plasma bulk, ostensibly to the Bohm velocity.<sup>42</sup> Those ions that traverse the sheath may experience energy modulations by collisions within the sheath before exiting the confined plasma. As such, a broad range of ion energies may be observed under a given set of plasma conditions. We have discussed the phenomena associated with increased ion energy as a function of increasing  $P$  previously.<sup>26</sup> Here, we note that feed gas pressure also significantly influences  $\langle E_i \rangle_{\text{total}}$ , Fig. 5.3a. The decrease in ion energy with increasing  $p$  results from an increase in the number of collisions the ions experience in the bulk of the plasma, as the mean free path of a given species decreases dramatically with increasing  $p$ . Moreover, increases in  $p$  generally result in an increase in electron density;<sup>34</sup> the higher density of species ultimately results in a decrease in electron temperature,  $T_e$ , which, in turn, leads to a decrease in  $V_p$ , the plasma potential.<sup>43</sup> Consequently, ions do not experience as sharp a gradient between  $V_p$  and the sheath potential,  $\Phi$ , and thus ion energies tend to decrease. Ultimately, these factors result in a narrowing, or thermalization, of ion energy distributions and reduction of  $\langle E_i \rangle_{\text{total}}$ .

The effect of energetic ions on NO scatter, as gauged by trends in  $\Delta S(\text{NO})$ , deviate significantly from those trends observed previously for  $\text{CF}_x$  species in fluorocarbon systems. We suspect that because these  $\text{N}_x\text{O}_y$  systems are non-depositing, there is an entirely different

mechanism than described for the fluorocarbon plasmas, which gives rise to the observed behavior in  $\Delta S(\text{NO})$ . Ions in this case do not ablate material to produce NO, and as such, other ion-surface processes must be considered. In a review from Grill and coworkers,<sup>8</sup> the authors outline several key surface interactions specific to ion bombardment. These include (1) simple elastic scattering of the incident ion, (2) chemical sputtering, (3) neutralization of the ion with or without adsorption and (4) surface-induced dissociation. Process (1) is likely applicable only to the low energy ions in our system. Thus, it is possible that at  $\langle E_i \rangle_{\text{total}} < \sim 50$  eV, incident ions simply rebound from the surface without neutralizing [i.e.  $\text{NO}^+(\text{g}) + \text{surf.} \rightarrow \text{NO}^+(\text{g})$ ] or that the incident low energy  $\text{NO}^+$  undergoes dissociative neutralization at the surface. Because the nitric oxide ion is transparent to the LIF scheme employed here, such scattering events are not observed nor accounted for in the IRIS experiment and dissociation would also not be measurable in our system. Thus, removal of ions should have little effect on scatter for systems with low  $\langle E_i \rangle_{\text{total}}$  (i.e.  $\Delta S(\text{NO}) = 0$ ). Indeed,  $\Delta S(\text{NO})$  values of essentially zero are generally observed for low total mean ion energies, Fig. 5.8. However, as energies of nascent plasma ions increase, ion contributions to scatter become significant, as evidenced by the increased  $\Delta S(\text{NO})$ .

Grill et al.'s process (2) can be excluded from this discussion on the basis of the  $\text{N}_x\text{O}_y$  systems being non-depositing; there exist no surface moieties or films comprising  $\text{N}_x\text{O}_y(\text{s})$  for which chemical sputtering would be relevant. To explicitly evaluate the effects of  $\text{N}_x\text{O}_y$  plasmas on our substrates, high resolution  $\text{O}_{1s}$ ,  $\text{Si}_{2p}$ , and  $\text{N}_{1s}$  x-ray photoelectron spectroscopy (XPS) was employed to analyze Si wafers before and after  $\text{N}_x\text{O}_y$  plasma treatments. Prior to plasma exposure, the substrates contained a thin native oxide layer with  $< 1\%$  N. Upon 60 min exposure in an  $\text{N}_x\text{O}_y$  plasma system, the surface oxide layer grew by  $\sim 10\text{-}20$  nm and no significant additional nitrogen incorporation was observed. For example, the only observable difference

between Si wafers before and after treatment with a 200 mTorr, 200 W N<sub>2</sub>O plasma was an increase in the O/Si ratio from ~1.1 to ~2.4. Thus, the surface exposed to the plasma molecular beam likely does not contain a wealth of nitrogen available for abstraction (and production of NO) during plasma processing events. It should be noted that removal of the native oxide layer prior to plasma exposure likewise does not affect surface scatter. Indeed, Si wafers treated in HF solution gave rise to similar S values in the IRIS experiment as those wafers that experienced only minimal cleaning (i.e. MeOH wash). We therefore infer that high NO scatter coefficients (especially where  $S \gg 1$ ) do not preferentially arise due to substrate composition effects. Other surface-mediated interactions consequently must contribute to the observed scatter of NO radicals.

As noted above, several scenarios exist that could lead to NO production from a surface and influence the observed S. For example, one can imagine the neutralization, process (3) from Grill et al., of nitric oxide ions (transparent to the LIF scheme) at some surface to produce NO, reaction (5.3). It should be noted that neutralization events, as in



reaction (5.4), appear to be applicable to ion energy regimes that surpass 50 eV. As mentioned above, the  $\Delta S(\text{NO})$  values for  $\langle E_i \rangle_{\text{total}} < 50$  eV are essentially zero, Fig. 5.8, suggesting that ions contribute minimally to NO surface scatter under such conditions. The activation energy for neutral NO(ads) desorption from a Si surface is only 11.6 kcal/mol,<sup>40</sup> or ~0.5 eV per molecule. It is estimated that as much as 70% of the translational energy associated with the incident ion is transferred to the surface upon impact, with the remaining 30% allocated to internal energies (i.e. vibration).<sup>8</sup> Nonetheless, this energy should be more than sufficient to overcome the desorption barrier from a surface such as Si for incident ions with energies > 50 eV. Previous reports from



the literature suggest that  $\text{NO}^+$  efficiently and readily neutralizes through charge-exchange mechanisms when the ion is within very close proximity ( $\sim 5 \text{ \AA}$ ) to metal surfaces.<sup>44</sup>

Interestingly, this same study showed that the propensity for collision-induced dissociation of the incident ion increased with increasing ion energy up to 500 eV. Thus, for high energy ions, reaction (5.3) may be reimagined as in reaction (5.4) where either of the dissociation products may retain the positive charge.



These surface nitrogen and oxygen atoms can readily react with other incident species (i.e. gaseous nitrogen or oxygen atoms) and desorb (the energy of the original  $\text{NO}^+$  reactant is transferred to its dissociation products<sup>44</sup>) as NO in the fashion of either a Langmuir-Hinshelwood or Eley-Rideal recombination. Indeed, the literature suggests that NO recombination products form with comparable efficiency to  $\text{N}_2$  and  $\text{O}_2$  products on quartz.<sup>45</sup> A similar dissociative adsorption and recombination process could also be envisioned for excited NO ( $\text{NO}^*$ ) in the case of the 100% NO molecular beam, where  $S(\text{NO})$  values exceed 2.0 at nearly all P. Because  $\langle E_i \rangle_{\text{total}}$  generally increases with increased P, Fig. 5.3b, and this change is commensurate with increased  $S(\text{NO})$ , Fig. 5.5, we believe the combined scenarios outlined in reactions (4) and (5) most plausibly explain the high surface scatter coefficients. As such,  $S(\text{NO})$  values at these conditions (i.e. high P, high  $\langle E_i \rangle_{\text{total}}$ ) should be most susceptible to limited ion flux to the surface. Indeed,  $\Delta S(\text{NO})$  only exceeds non-zero values when total mean ion energies surpass  $\sim 50 \text{ eV}$ , Fig. 5.8.

The data shown here clearly demonstrate that  $\Delta S(\text{NO})$  is only affected by  $>50 \text{ eV}$  ions, which suggests that reaction 4 only occurs for high energy  $\text{NO}^+$ . Notably, when  $\langle E_i \rangle_{\text{total}}$  is sufficient to affect the observed  $S(\text{NO})$ ,  $\Delta S(\text{NO}) \sim 0.2$  (within experimental error), regardless of

$\langle E_i \rangle_{\text{total}}$ . The only system for which  $\Delta S(\text{NO})$  is significantly higher, albeit with significantly higher experimental error, is the  $\text{N}_2 + \text{O}_2$  precursor, Fig. 5.8. This difference likely arises from the appreciable disparity in ion energies distributed about the mean, as evidenced by the bimodal distribution, discussed elsewhere,<sup>26, 46</sup> of  $E_i$  for NO in the  $\text{N}_2 + \text{O}_2$  system, Fig. 5.2a. In all other systems, with comparatively narrow IEDs, and it is likely that the higher error in both  $\langle E_i \rangle_{\text{total}}$  and  $\Delta S(\text{NO})$  is the result of the larger spread in ion energies. This observation may explain the inconsistencies between the  $\text{N}_2 + \text{O}_2$  system and the other  $\text{N}_x\text{O}_y$  systems, and reaffirms the influence of high energy ions within these complex plasma systems. Ultimately, understanding the effect of ions on surface scatter coefficients for NO radicals provides a contribution to molecule-surface interactions crucial for advancement of fundamental investigations of  $\text{N}_x\text{O}_y$  remediation. This general reactivity profile elucidates the inherent surface chemistry of NO formed in these ICP systems, and it details the intricate dependence of scatter on varying plasma parameters.

### 5.3 Summary

The experiments described here have sought to improve understanding of the role of ions at the plasma-surface interface for  $\text{N}_x\text{O}_y$  plasmas. Specifically, using both mass spectrometry and IRIS experiments, we have elucidated the effect of ion energies on the surface scatter of NO. Significantly, only high energy ions (i.e. those with  $\langle E_i \rangle > \sim 50$  eV) affect the  $S(\text{NO})$  values from the IRIS experiment; such ion energies are achieved in  $\text{N}_x\text{O}_y$  systems of low pressure and high applied rf power. Interestingly, although the choice of precursor gas does affect  $\langle E_i \rangle_{\text{total}}$ , it does not play a significant part in determining  $\Delta S(\text{NO})$ . Indeed, values for  $\Delta S(\text{NO})$  are always near 0.2 when  $\langle E_i \rangle_{\text{total}} \geq \sim 50$  eV, regardless of plasma conditions.

Ultimately, this research validates a complex surface reactivity model for NO-containing plasmas in which the ion-scatter relationship is unlike any previously observed in IRIS studies. As a result of using non-catalytic silicon substrates, this work demonstrates the inherent behavior of NO when in contact with a surface. The significance lies not only in the knowledge of NO-silicon interactions, but potentially for applicability to other systems, as well. Indeed, a fundamental understanding of non-catalytic behavior can be extended to glean insights into catalytic surface behavior, and this work may well lead to improved studies in the abatement of nitrogen oxides. Future IRIS studies in our laboratories will employ catalytic substrates such as Pt, Ru, Ni, and Rh to determine if catalytic activity significantly alters NO-surface interactions.

## REFERENCES

1. Roy, S.; Hegde, M. S.; Madras, G., Catalysis for NO<sub>x</sub> Abatement. *Applied Energy* 2009, 86, 2283-2297.
2. Parvulescu, V. I.; Grange, P.; Delmon, B., Catalytic Removal of NO. *Catalysis Today* 1998, 46, 233-316.
3. Ford, P. C.; Lorkovic, I. M., Mechanistic Aspects of the Reactions of Nitric Oxide with Transition-Metal Complexes. *Chemical Reviews* 2002, 102 (4), 993-1017.
4. Joslin, J. M.; Reynolds, M. M., Kinetics of S-Nitrosation Processes in Aqueous Polymer Solution for Controlled Nitric Oxide Loading: Toward Tunable Biomaterials. *ACS Applied Materials & Interfaces* 2012, 4, 1126-1133.
5. Miao, R.; Mu, L.; Zhang, H.; Xu, H.; She, G.; Wang, P.; Shi, W., Modified Silicon Nanowires: A Fluorescent Nitric Oxide Biosensor with Enhanced Selectivity and Stability. *Journal of Materials Research* 2012, 22, 3348-3353.
6. Cruz-Cabeza, A. J.; Esquivel, D.; Jimenez-Sanchidrian, C.; Romero-Salguero, F. J., Metal-Exchanged Beta Zeolites as Catalysts for the Conversion of Acetone to Hydrocarbons. *Materials* 2012, 5 (1), 121-134.
7. Fabris, S.; Stepanow, S.; Lin, N.; Gambardella, P.; Dmitriev, A.; Honolka, J.; Baroni, S.; Kern, K., Oxygen Dissociation by Concerted Action of Di-Iron Centers in Metal-Organic Coordination Networks at Surfaces: Modeling Non-Heme Iron Enzymes. *Nano Letters* 2011, 11 (12), 5414-5420.
8. Grill, V.; Shen, J.; Evans, C.; Cooks, R. G., Collisions of Ions with Surfaces at Chemically Relevant Energies: Instrumentation and Phenomena. *Review of Scientific Instruments* 2001, 72 (8), 3149-3179.
9. Ferguson, E. E.; Fehsenfeld, F. C.; Goldan, P. D.; Schmeltekopf, A. L., Positive Ion-Neutral Reactions in the Ionosphere. *Journal of Geophysical Research* 1965, 70 (17), 4323-4329.
10. Blagojevic, V.; Flaim, E.; Jarvis, M. J. Y.; Koyanagi, G. K.; Bohme, D. K., Nitric Oxide as an Electron Donor, an Atom Donor, an Atom Acceptor, and a Ligand in Reactions with Atomic Transition-Metal and Main-Group Cations in the Gas Phase. *Journal of Physical Chemistry A* 2005, 109, 11224-11235.
11. Karasek, F. W.; Denney, D. W., Role of Nitric Oxide in Positive Reactant Ions in Plasma Chromatography. *Analytical Chemistry* 1974, 46 (6), 633-637.
12. Burley, J. D.; Ervin, K. M.; Armentrout, P. B., Translational Energy Dependence of O<sup>+</sup>(<sup>4</sup>S)+N<sub>2</sub> → NO<sup>+</sup>+N from Thermal Energies to 30 eV c.m. *Journal of Chemical Physics* 1987, 86 (4), 1944-1953.
13. Clemmer, D. E.; Armentrout, P. B., Direct Determination of the Adiabatic Ionization Energy of NO<sub>2</sub> as Measured by Guided Ion-Beam Mass Spectrometry. *Journal of Chemical Physics* 1992, 97 (4), 2451-2458.
14. Clemmer, D. E.; Weber, M. E.; Armentrout, P. B., Reactions of Al<sup>+</sup>(<sup>1</sup>S) with NO<sub>2</sub>, N<sub>2</sub>O, and CO<sub>2</sub>: Thermochemistry of AlO and AlO<sup>+</sup>. *Journal of Physical Chemistry* 1992, 96, 10888-10893.
15. Khan, F. A.; Steele, D. L.; Armentrout, P. B., Ligand Effects in Organometallic Thermochemistry: The Sequential Bond Energies of Ni(CO)<sub>x</sub><sup>+</sup> and Ni(N<sub>2</sub>)<sub>x</sub><sup>+</sup> (x=1-4) and Ni(NO)<sub>x</sub> (x=1-3). *Journal Physical Chemistry* 1995, 99, 7819-7828.

16. Koszinowski, K.; Schroder, D.; Schwarz, H.; Holthausen, M. C.; Sauer, J.; Koizumi, H.; Armentrout, P. B., Bond Dissociation Energies and Structures of  $\text{CuNO}^+$  and  $\text{Cu}(\text{NO})_2^+$ . *Inorganic Chemistry* 2002, 41 (22), 5882-5890.
17. Rodgers, M. T.; Walker, B.; Armentrout, P. B., Reactions of  $\text{Cu}^+(^1\text{S}$  and  $^3\text{D})$  with  $\text{O}_2$ ,  $\text{CO}$ ,  $\text{CO}_2$ ,  $\text{N}_2$ ,  $\text{NO}$ ,  $\text{N}_2\text{O}$ , and  $\text{NO}_2$  Studied by Guided Ion Beam Mass Spectrometry. *International Journal of Mass Spectrometry* 1999, 182/183, 99-120.
18. Schultz, R. H.; Armentrout, P. B., Reactions of  $\text{N}_2^+$  and  $\text{N}_4^+$  with  $\text{O}_2$  from Thermal to 20 eV Center of Mass. *Journal of Chemical Physics* 1991, 95 (1), 121-129.
19. Fresnet, F.; Baravian, G.; Magne, L.; Pasquiers, S.; Postel, C.; Puech, V.; Rousseau, A., Kinetic of the NO Removal by Nonthermal Plasma in  $\text{N}_2/\text{NO}/\text{C}_2\text{H}_4$  Mixtures. *Applied Physics Letters* 2000, 77 (25), 4118-4120.
20. Orlando, T. M.; Alexandrov, A.; Lebsack, A.; Herring, J.; Hoard, J. W., The Reactions of  $\text{NO}_2$  and  $\text{CH}_3\text{CHO}$  with Na-Y Zeolite and the Relevance to Plasma-Activated Lean  $\text{NO}_x$  Catalysis. *Catalysis Today* 2004, 89 (1-2), 151-157.
21. Morgan, M. M.; Cuddy, M. F.; Fisher, E. R., Gas-Phase Chemistry in Inductively Coupled Plasmas for NO Removal from Mixed Gas Systems. *Journal of Physical Chemistry A* 2010, 114 (4), 1722-1733.
22. Lineberger, W. C.; Puckett, L. J., Positive Ions in Nitric Oxide Afterglows. *Physical Review* 1969, 186 (1), 116-127.
23. Solymosi, F.; Bansagi, T.; Suli Zakar, T., Surface Interaction and Reaction of  $\text{NO} + \text{CO}$  on a Supported Au Catalyst. *Physical Chemistry Chemical Physics* 2003, 5 (20), 4724-4730.
24. Cuddy, M. F.; Fisher, E. R., Energy Partitioning in Diatomic Radicals and its Influence on Surface Scatter Coefficients for NO, SiF and CF in Inductively Coupled Plasmas. *Journal of Physical Chemistry A* 2012, submitted for publication.
25. Capps, N. E.; Mackie, N. M.; Fisher, E. R., Surface Interactions of  $\text{CF}_2$  Radicals During Deposition of Amorphous Fluorocarbon Films from  $\text{CHF}_3$  Plasmas. *Journal of Applied Physics* 1998, 84 (9), 4736-4743.
26. Cuddy, M. F.; Blechle, J. M.; Fisher, E. R., Ion Contributions to Gas-Surface Interactions in Inductively-Coupled Fluorocarbon Plasmas. *International Journal of Mass Spectrometry* 2012, 330, 46-57.
27. Butoi, C. I.; Mackie, N. M.; Williams, K. L.; Capps, N. E.; Fisher, E. R., Ion and Substrate Effects on Surface Reactions of  $\text{CF}_2$  using  $\text{C}_2\text{F}_6$ ,  $\text{C}_2\text{F}_6/\text{H}_2$ , and Hexafluoropropylene Oxide Plasmas. *J. Vac. Sci. Technol. A-Vac. Surf. Films* 2000, 18 (6), 2685-2698.
28. Liu, D. P.; Cuddy, M. F.; Fisher, E. R., Comparison of CH,  $\text{C}_3$ , CHF, and  $\text{CF}_2$  Surface Reactivities during Plasma-Enhanced Chemical Vapor Deposition of Fluorocarbon Films. *ACS Applied Materials & Interfaces* 2009, 1 (4), 934-943.
29. Lias, S. G.; Bartmess, J. E.; Liebman, J. F.; Holmes, J. L.; Levin, R. D.; Mallard, W. G., Gas-Phase Ion and Neutral Thermochemistry. *Journal of Physical and Chemical Reference Data* 1988, 17, Supplement 1.
30. Kessels, W. M. M.; McCurdy, P. R.; Williams, K. L.; Barker, G. R.; Ventura, V. A.; Fisher, E. R., Surface Reactivity and Plasma Energetics of SiH Radicals During Plasma Deposition of Silicon-Based Materials. *Journal of Physical Chemistry B* 2002, 106 (10), 2680-2689.
31. McCurdy, P. R.; Butoi, C. I.; Williams, K. L.; Fisher, E. R., Surface Interactions of  $\text{NH}_2$  Radicals in  $\text{NH}_3$  Plasmas. *Journal of Physical Chemistry B* 1999, 103 (33), 6919-6929.

32. McCurdy, P. R.; Venturo, V. A.; Fisher, E. R., Velocity Distributions of  $\text{NH}_2$  Radicals in an  $\text{NH}_3$  Plasma Molecular Beam. *Chemical Physics Letters* 1997, 274, 120-126.
33. Hopwood, J., Review of Inductively Coupled Plasmas for Plasma Processing. *Plasma Sources Science and Technology* 1992, 1 (2), 109-116.
34. d'Agostino, R.; Cramarossa, F.; Fracassi, F.; Illuzzi, F., Plasma Polymerization of Fluorocarbons. Academic Press, Inc. : San Diego, CA, 1990.
35. Cuddy, M. F.; Fisher, E. R., Investigation of the Roles of Gas-Phase  $\text{CF}_2$  Molecules and F Atoms During Fluorocarbon Plasma Processing of Si and  $\text{ZrO}_2$  Substrates. *Journal of Applied Physics* 2010, 108 (3), 033303-9.
36. Jeong, S., Dissociation of NO on Si(001) and Incorporation of N into the Subsurface. *Journal of the Korean Physical Society* 2007, 51 (6), 1962-1967.
37. Namiki, A.; Suzuki, S.; Kato, H.; Babasaki, Y.; Tanaka, M.; Nakamura, T.; Suzuki, T., A Molecular Beam Study of Alkali Promotion of NO Sticking on Si(100): Local Promotion in a Single Collision Regime. *Journal of Chemical Physics* 1992, 97 (5), 3781-3792.
38. Riehl-Chudoba, M.; Surnev, L.; Soukiassian, P., Nitric Oxide Adsorption on the Si(111)7x7 Surface: Effect of Potassium Overlayers. *Surface Science* 1994, 306, 313-326.
39. Sasse, A. G. B. M.; van Silfhout, A., Adsorption of Nitric Oxide on the Si(100)2x1 Surface: A Theoretical and Experimental Approach. *Physical Reviews B* 1989, 40 (3), 1773-1782.
40. Ying, Z.; Ho, W., Adsorption and Reactions of Nitric Oxide on Si(111)7x7. *J. Vac. Sci. Technol. A-Vac. Surf. Films* 1989, 7 (3), 2099-2103.
41. Carbone, M.; Bobrov, K.; Comtet, G.; Dujardin, G.; Hellner, L., Initial Stage of NO Adsorption on Si(100)-(2x1) Studied by Synchrotron Radiation Photoemission and Photodesorption. *Surface Science* 2000, 467, 49-57.
42. Panagopoulos, T.; Economou, D. J., Plasma Sheath Model and Ion Energy Distribution for all Radio Frequencies. *Journal of Applied Physics* 1999, 85 (7), 3435-3443.
43. Woodworth, J. R.; Riley, M. E.; Miller, P. A.; Nichols, C. A.; Hamilton, T. W., Ion Distribution Functions in Inductively Coupled Radio Frequency Discharges in Argon-Chlorine Mixtures. *J. Vac. Sci. Technol. A-Vac. Surf. Films* 1997, 15 (6), 3015-3023.
44. Taylor, J. A.; Lancaster, G. M.; Rabalais, J. W., Interactions of nitrogen  $\text{N}_2^+$  and nitrosyl  $\text{NO}^+$  Ions with Surfaces of Graphite, Diamond, Teflon, and Graphite Monofluoride. *Journal of the American Chemical Society* 1978, 100 (14), 4441-4447.
45. Pejakovic, D. A.; Marschall, J.; Duan, L.; Martin, M. P., Nitric Oxide Production from Surface Recombination of Oxygen and Nitrogen Atoms. *Journal of Thermophysics and Heat Transfer* 2008, 22 (2), 178-186.
46. Edelberg, E. A.; Perry, A.; Benjamin, N.; Aydil, E. S., Energy Distribution of Ions Bombarding Biased Electrodes in High Density Plasma Reactors. *Journal Vacuum Science & Technology A* 1999, 17 (2), 506-516.

## CHAPTER 6

### TIME-RESOLVED OPTICAL EMISSION SPECTROSCOPY FOR THE INVESTIGATION OF NITROGEN OXIDE PLASMA KINETICS

This chapter contains data to be submitted as a full paper, written by Joshua M. Blechle and Ellen R. Fisher. These studies examine the influence of plasma parameters (such as pressure, power, and precursor) on the formation and destruction of species within nitrogen oxide plasmas. Rate constants for reactions involving  $N_2$  and  $NO$  are explored and related to broader nitrogen oxide chemistries.

#### 6.1 Introduction

Nitric oxide has long been the focus of numerous research investigations, from fundamental characterization to technologically relevant advancements.<sup>1-3</sup> With surprisingly complex chemistry, despite being a simple heteronuclear diatom,  $NO$  continues to be an area of significant scientific inquiry. Of special interest is atmospheric  $NO$ , generated from industrial and automotive exhaust, which is often the focus of pollution remediation studies.<sup>4-6</sup>  $NO$  is also an important participant in many biological processes, including blood pressure regulation, coagulation, and fighting infection.<sup>7-9</sup> In both atmospheric chemistry and in the context of biological processes, understanding the mechanisms and kinetics of  $NO$  reactions is integral to improved methodologies. Indeed, the diversity of  $NO$ -containing environments requires development of in situ investigations to more adequately explore unique  $NO$  chemistries.

An additional field of study with respect to  $NO$  chemistry is catalytic reduction, a promising field for  $NO_x$  control and mediation. In these catalytic processes, several approaches

have been explored to improve NO decomposition and removal of NO<sub>x</sub> species.<sup>10</sup> These efforts include the investigation of a range of catalyst materials, photocatalytic decomposition, use of various reductants, and more recently, employing plasmas either to excite NO<sub>x</sub> for more efficient removal or to modify catalyst surfaces to increase the efficiency of the catalytic process. As discussed in Chapter 1, plasma-assisted catalysis is a valuable tool for more effective gas phase conversions.<sup>11</sup> Furthermore, plasma diagnostics can be used to develop understanding of the contributions of various gas-phase species to surface-mediated reactions. Such a development is indispensable for the assessment of catalytic performance and ultimately for improving catalytic substrates for enhanced control of vehicular emissions.

Many investigations of plasma-based methods for NO<sub>x</sub> remediation are conspicuously devoid of discussions regarding the fundamental chemistry involved in plasma processes. Efforts to elucidate the complex interconnected nature of species kinetics, however, is an ongoing effort in the plasma and chemical physics community, albeit not necessarily with a focus on N<sub>x</sub>O<sub>y</sub> species.<sup>12</sup> Because of significant shifts from equilibrium conditions, as well as complex energetic deviations among species (as discussed in Chapter 4), the kinetic profiles found in plasmas can significantly differ from gas-phase analogues. Ultimately, a thorough understanding of the kinetic nature of these systems will rely on a multi-disciplinary approach, utilizing experimental as well as computational investigations. In an effort to contribute to this expanding field, the Fisher Research Group is able to use their expertise in plasma diagnostics to probe the fundamental chemistry of these systems. Indeed, previous work in our laboratory explored much of the neutral gas-phase chemistry in N<sub>x</sub>O<sub>y</sub> plasmas through optical emission spectroscopy (OES) and laser-induced fluorescence (LIF).<sup>13</sup> In general, however, our instruments have required long (on the order of several minutes) collection times to achieve



sufficient data signal, which has prohibited the use of adequate temporal resolution to allow for detailed kinetic studies within our systems.

Efforts to expand into this area of study have been significantly improved by the acquisition of a new spectrometer with enhanced temporal resolution for kinetic studies. As such, we have utilized time-resolved OES (TR-OES) to investigate changes in plasma species density over time to provide insight into the possible mechanisms of species formation within ICPs. More specifically, the data presented herein focuses on NO and N<sub>2</sub> formed from NO, N<sub>2</sub>O, and mixed N<sub>2</sub>/O<sub>2</sub> gas precursors. Eventually, extensions of these investigations could contribute to improved methodologies for NO<sub>x</sub> waste-gas removal and further investigations into surfaces that control the reduction of nitrogen oxide (N<sub>x</sub>O<sub>y</sub>) species through the utilization of inductively coupled plasmas.

## 6.2 Results and Discussion

Nitrogen oxide plasmas, such as those relevant to gas remediation studies, contain a multitude of excited state species that could be evaluated via TR-OES. Paramount of these are NO and N<sub>2</sub>, as they are the primary pollutant and the desired by-product in remediation systems, respectively. Formation and destruction of these key excited state species in N<sub>x</sub>O<sub>y</sub> plasmas were investigated to provide foundational information and mechanistic insight. Emission intensity as a function of time for each species was collected and compared to that of an actinometer (Ar, 5% by pressure in the plasma feedgas).<sup>14-16</sup> Notably, the actinometric method operates under the assumption that the resulting emission intensity ratio [i.e.  $I_x/I_{Ar}$ ] is proportional to species concentration.<sup>17-18</sup> Thus, we can indirectly monitor [X] over time, where X is either NO\* or N<sub>2</sub>\* for work presented in this chapter. An example is illustrated in Fig. 6.1 for N<sub>2</sub>\* generated in an

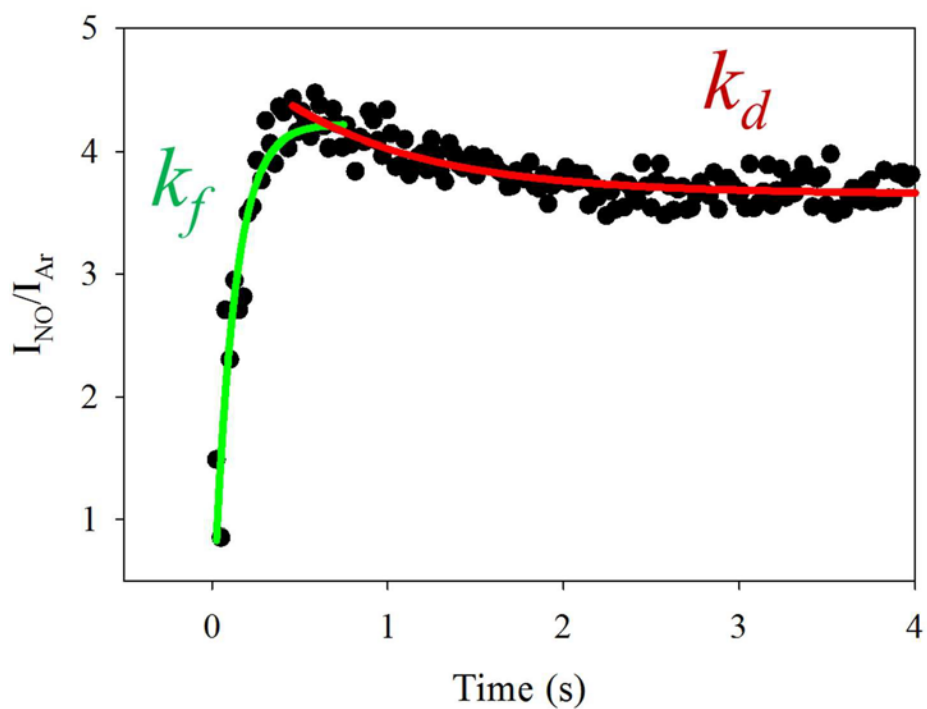


Figure 6.1 Representative TR-OES profile, monitoring the relative intensity of  $N_2$  emission relative to an Ar actinometer in a 100 mTorr, 100 W NO plasma system. The rise and decay are fit with exponentials to determine first order rate constants,  $k_f$  and  $k_d$ .

NO plasma, in which it takes ~4 seconds to reach steady-state concentrations of  $N_2^*$  within the plasma bulk. Once again, these individual data points are determined by taking a ratio of  $N_2^*$  emission relative to the  $Ar^*$  actinometer, which serves as a proportional value to  $[N_2^*]$ . Thus, the observed rise and decay in intensity ratio as a function of time corresponds to the formation and destruction of the excited state species, which can be analyzed via peak simulation to determine rate constants,  $k_{\text{formation}}$  and  $k_{\text{destruction}}$ . For consistent analysis and comparison, TR-OES data collection begins before ignition of the plasma and lasts for ~10 s after ignition. The first non-zero data point is, for convenience, set as time = 0.0 s and time points of all subsequent data points are set accordingly. The point(s) of highest intensity is identified, marking the end of the rise and beginning of the fall, thereby providing two separate data subsets that can be used to identify rate constants. In some cases, a rise and/or fall in the data profile is not observed; either the first data point detected is a maximum, followed by decay; the rise is seen, but after reaching the maximum the intensity holds constant; or the intensity remains constant throughout the entirety of the experiment.

Assuming both the excitation and de-excitation are direct processes, the formation and relaxation of these species is first order with respect to the molecule (NO is included as an example in Equations 6.1 and 6.2). Thus, simulation of the intensity profiles is performed with both exponential rise and decay of the form  $e^{-kt}$ , corresponding to a first-order process.



Because of the relatively small number of data points collected in the early stages of plasma ignition, the influence of noise on the collected peak profiles can be rather substantial.

Comparing multiple emission lines from a single transition band of a species, however, reveals that the calculated values for the rate constants are nearly identical, Fig. 6.2. Thus, to combat issues with noise and reproducibility, these lines are averaged together before regression is performed. This process helps to minimize the impact of random noise and improve the success of the exponential fitting.

Any deviations from the profile presented in Fig. 6.1 can provide further insight into the chemistry within nitrogen oxide plasma systems. For example, excited state species must be formed within the plasma, as they are not present natively in the gas-phase precursor; therefore, a formation profile must exist in some capacity. As a result, an inability to discern changes in emission intensity after plasma ignition indicates the formation process is faster than 25.5 ms, the time resolution of the instrument. With the NO precursor, formation profiles are observed for  $N_2^*$  but not  $NO^*$ . This is not particularly surprising, as the direct electron-impact excitation of NO is relatively straightforward in systems in which it is the native precursor species. Further support is provided when considering that the approximate mean-free path for NO within these systems is 2.5 mm, meaning there are far fewer NO-NO collisions than NO-electron collisions. Additionally, molecular nitrogen must be formed through decomposition and subsequent reaction (or vice versa) before excitation can occur. Thus, the formation of  $N_2^*$  is delayed from the ignition point in NO plasma systems and can be monitored directly within the plasma.

It is important to note that these data do not necessarily provide exclusive evidence for a single mechanism, as there are limitations to our ability to discern competing processes. For example, if we consider the formation of  $N_2^*$  in the NO plasma system, there are many possible scenarios. To begin,  $N_2$  could be formed from decomposition of NO in which the products recombine, Equation 6.3.

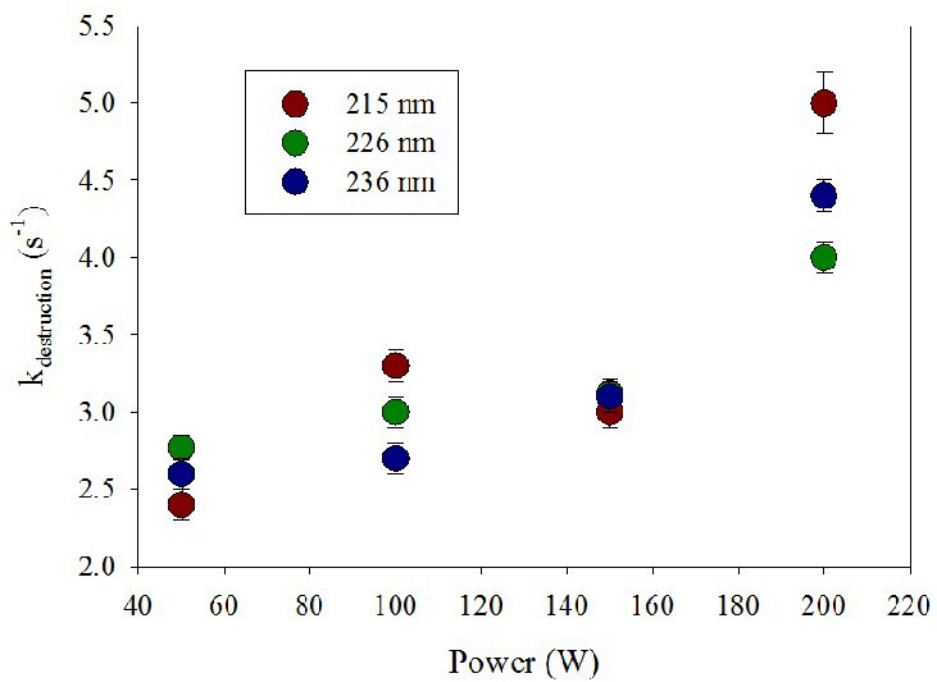
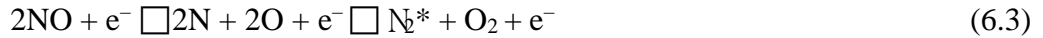
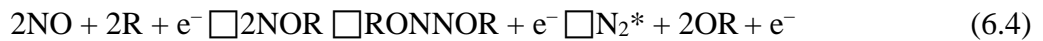


Figure 6.2 Comparison of  $k_d$  as a function of applied rf power for three NO emission lines. To combat signal-to-noise issues, all three emission lines were averaged to generate the reported rate constants.



Additionally, NO could react with some other species (R) that has been formed previously within the plasma to form NOR. This reaction could generate a larger intermediate that decomposes into N<sub>2</sub>, Equation 6.4.



Additionally, in both of these cases, N<sub>2</sub>\* is shown to be formed directly, but excitation could take place as a separate step after the formation of ground state N<sub>2</sub>. Regardless of the excitation step, however, it is likely that the NOR mechanism (Equation 6.4) would take considerably longer than the more direct process shown in Equation 6.3, because the formation of the NOR species would also be a time-consuming and less energetically favorable process. As such, this possible mechanism would likely be lost within the steady-state concentration of the plasma, essentially concealed by the more prevalent competing pathways. Thus, our data support a multi-step formation mechanism for N<sub>2</sub>\*, as opposed to a direct formation mechanism, but provide nothing about the exact process occurring.

Interestingly, the N<sub>2</sub>O precursor behaves identically to the NO precursor, in that NO\* formation is not observed, Table 6.1. This suggests that the excited state is formed directly upon electron impact (Equation 6.5) or at the very least, that it is the predominant mechanism.



When compared to the observed trends in the NO system, the observed N<sub>2</sub>\* formation in N<sub>2</sub>O (Table 6.2) suggests this process is indirect and involves some decomposition and reaction prior to excitation, Equation 6.6.

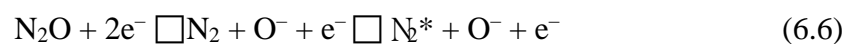


Table 6.1 Calculated values for  $k_{\text{formation}}$  and  $k_{\text{destruction}}$  for NO in all three precursor systems, as a function of pressure and power.

NO Kinetic Comparison*												
100 mTorr												
50 W			100 W			150 W			200 W			
NO	N2O	N2/O2	NO	N2O	N2/O2	NO	N2O	N2/O2	NO	N2O	N2/O2	
K Formation	---	---	XX	---	---	XX	---	---	$3 \pm 2$	---	---	$1.7 \pm 0.5$
K Destruction	$4.8 \pm 0.2$	$2.9 \pm 0.2$	XX	$6.4 \pm 0.2$	$4.3 \pm 0.3$	XX	$4.3 \pm 0.2$	$3.3 \pm 0.2$	---	$4.7 \pm 0.2$	$4.8 \pm 0.2$	---
150 mTorr												
50 W			100 W			150 W			200 W			
NO	N2O	N2/O2	NO	N2O	N2/O2	NO	N2O	N2/O2	NO	N2O	N2/O2	
K Formation	---	---	XX	---	---	$1.6 \pm 0.8$	---	---	$3 \pm 2$	---	$11 \pm 8$	$15 \pm 8$
K Destruction	$2.6 \pm 0.1$	$3.4 \pm 0.2$	XX	$3.7 \pm 0.1$	$5.0 \pm 0.3$	---	$4.1 \pm 0.1$	$7.0 \pm 0.3$	---	$4.2 \pm 0.2$	$6.9 \pm 0.4$	$8 \pm 3$
200 mTorr												
50 W			100 W			150 W			200 W			
NO	N2O	N2/O2	NO	N2O	N2/O2	NO	N2O	N2/O2	NO	N2O	N2/O2	
K Formation	---	---	XX	---	---	$12 \pm 4$	---	---	$11 \pm 3$	---	---	$26 \pm 8$
K Destruction	$2.42 \pm 0.05$	$5 \pm 2$	XX	$3.05 \pm 0.04$	$3.3 \pm 0.1$	---	$3.11 \pm 0.06$	$3.5 \pm 0.1$	---	$4.57 \pm 0.08$	$2.7 \pm 0.2$	---

\*Cells with “---” represent conditions in which non-zero concentrations are seen, but the particular rate constant cannot be determined, due to insufficient time resolution. Cells with “XX” represent conditions in which NO is not formed.

Table 6.2 Calculated values for  $k_{\text{formation}}$  and  $k_{\text{destruction}}$  of  $\text{N}_2$  in all three precursor systems, as a function of pressure and power.

<b><math>\text{N}_2</math> Kinetic Comparison*</b>												
100 mTorr												
50 W			100 W			150 W			200 W			
	NO	N2O	N2/O2	NO	N2O	N2/O2	NO	N2O	N2/O2	NO	N2O	N2/O2
K Formation	$17 \pm 4$	---	---	$16 \pm 2$	$5 \pm 2$	---	$15 \pm 2$	$15 \pm 5$	---	$7.3 \pm 0.7$	$20 \pm 4$	---
K Destruction	$1.3 \pm 0.5$	$1.6 \pm 0.5$	$2.5 \pm 0.9$	$1.2 \pm 0.2$	$2.0 \pm 0.3$	$1.4 \pm 0.1$	$0.67 \pm 0.02$	$2.2 \pm 0.2$	$1.7 \pm 0.2$	$0.68 \pm 0.08$	$2.0 \pm 0.2$	$1.08 \pm 0.03$
150 mTorr												
50 W			100 W			150 W			200 W			
	NO	N2O	N2/O2	NO	N2O	N2/O2	NO	N2O	N2/O2	NO	N2O	N2/O2
K Formation	$4.4 \pm 0.5$	---	---	$5.9 \pm 0.6$	$9 \pm 4$	---	$5.4 \pm 0.7$	$10 \pm 8$	---	$4.6 \pm 0.5$	$6 \pm 1$	---
K Destruction	$0.006 \pm 0.001$	$4.0 \pm 0.6$	$1.3 \pm 0.5$	$0.9 \pm 0.2$	$2.3 \pm 0.3$	$1.4 \pm 0.2$	$1.2 \pm 0.2$	$1.6 \pm 0.1$	$2.1 \pm 0.2$	$1.0 \pm 0.1$	$1.8 \pm 0.1$	$1.9 \pm 0.2$
200 mTorr												
50 W			100 W			150 W			200 W			
	NO	N2O	N2/O2	NO	N2O	N2/O2	NO	N2O	N2/O2	NO	N2O	N2/O2
K Formation	$3.2 \pm 0.5$	---	---	$3.3 \pm 0.5$	---	---	$7 \pm 1$	$11 \pm 8$	---	$7.7 \pm 0.6$	$10 \pm 3$	---
K Destruction	$6 \pm 1$	$4 \pm 2$	---	$1.1 \pm 0.3$	$3.7 \pm 0.5$	$1.4 \pm 0.7$	$1.3 \pm 0.2$	$2.9 \pm 0.5$	$1.3 \pm 0.3$	$1.1 \pm 0.1$	$3.3 \pm 0.4$	$1.3 \pm 0.1$

\*Cells with “---” represent conditions in which non-zero concentrations are seen, but the particular rate constant cannot be determined, due to insufficient time resolution.



Indeed, this interpretation is further validated by observations made within the  $N_2+O_2$  precursor system. Here, the onset of formation of  $N_2^*$  is not observed whereas it can be determined for  $NO^*$  (i.e., opposite behavior to  $N_2O$  systems). This observation again suggests that  $N_2$  as a parent molecule in the feed gas undergoes a direct excitation that cannot be detected within the time resolution of our apparatus, whereas  $NO^*$  formation is evidence of further decomposition reactions necessary for generation of  $NO$  in this system. The observed intensity profile indicates, however, that the rate-limiting step is still 1<sup>st</sup> order as the data still follow the same  $e^{-kt}$  behavior. Additionally, we can make a few assumptions about conditions under which destruction constants cannot be determined (while formation rate constants can). First, under such conditions, it is likely that quenching of the excited state is occurring at the same rate as steady-state production of the excited state. Second, under these conditions there is likely no alternative pathways for the quenching of the excited state. Notably, this behavior is only observed for  $NO^*$  in the  $N_2+O_2$  precursor.

Comparing the destruction of  $NO^*$ , as well as the formation of  $N_2^*$  within the  $NO$  precursor system as a function of pressure and power allows us to elucidate trends within these systems. Noticeably, in Fig. 6.3 we see that, for the 150 and 200 mTorr systems,  $k_{\text{destruction}}$  of  $NO^*$  increases as  $P$  increases. The 100 mTorr system, however, differs from the 150 and 200 mTorr systems. Specifically, this system has a much higher rate constant at low powers but a mode change in the 100-150 W range that causes a significant decrease in  $k_{\text{destruction}}$  at higher powers. This suggests that pressure plays less of a role in quenching of the excited state than power does, and thus, the rate of  $NO^*$  deexcitation is not dominated by collisional quenching. Similarly, parameter dependence of  $N_2^*$  formation within the  $NO$  precursor, Fig. 6.4, indicates

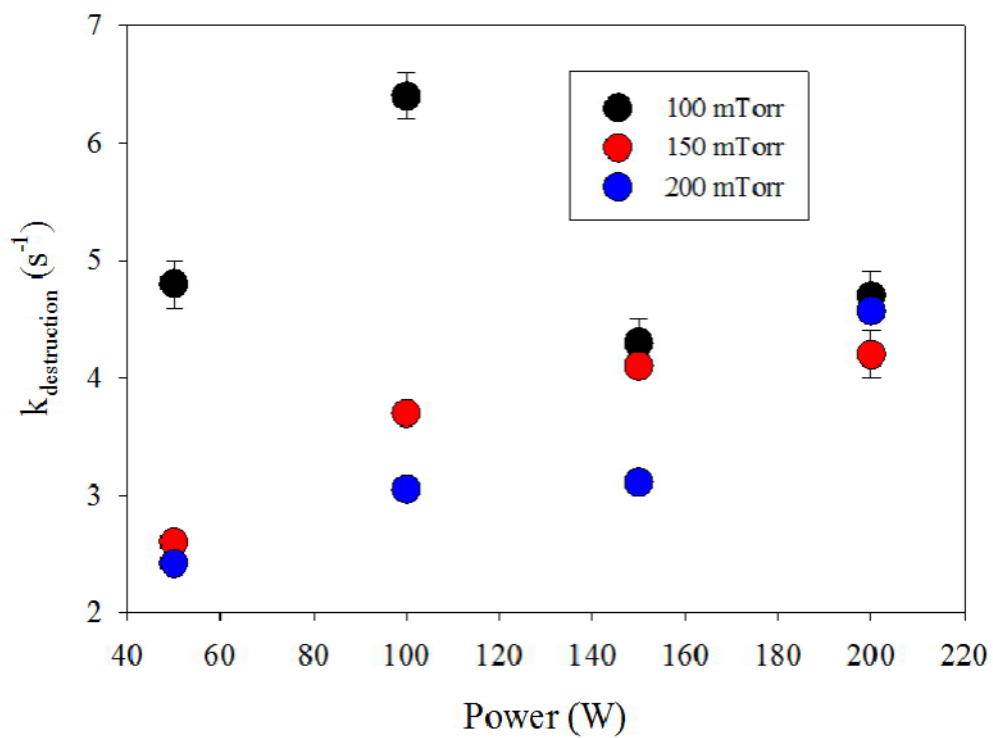


Figure 6.3 Destruction rate constants for  $\text{NO}^*$  species formed in a  $\text{NO}$  plasma as a function of power for three different system pressures.

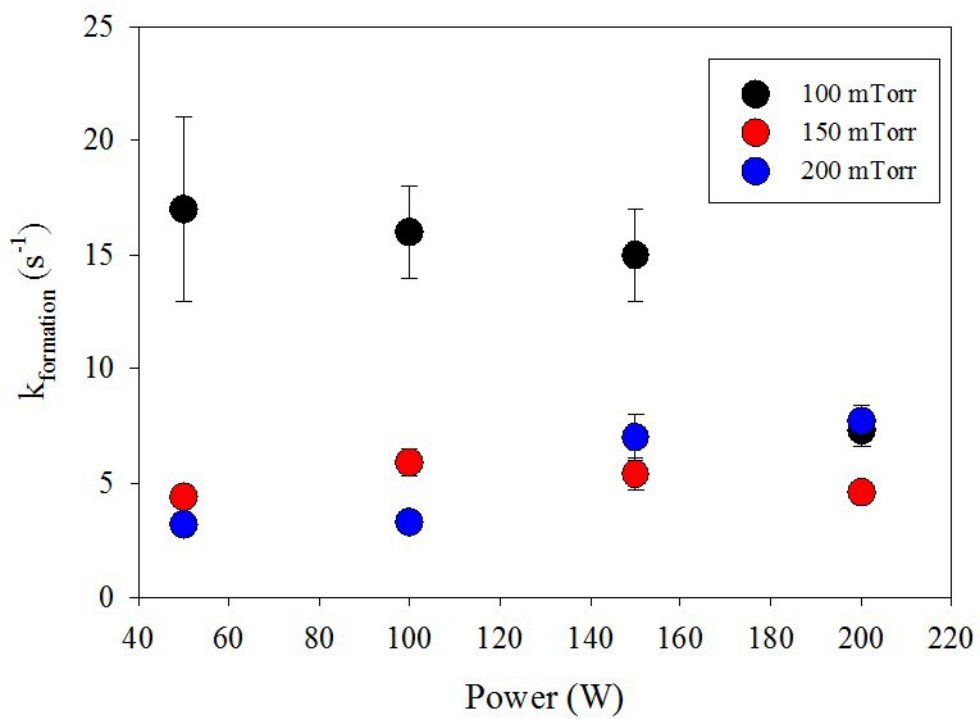


Figure 6.4 Formation rate constants for  $\text{N}_2^*$  species formed in NO plasmas as a function of power for three different system pressures.

the 100 mTorr system behaves differently than the higher pressure systems, with greater  $k_{\text{formation}}$  values at nearly all  $P$ . This observation suggests the mechanism of  $\text{N}_2$  formation in NO plasmas has a clear dependence on pressure but the trends with respect to applied power are much less clear. One hypothesis is that these pressure dependencies could be attributed to changes in the dominant formation mechanism, as the collision partners available can vary significantly with changing mean free path. A more complete description of the trends in rate constants for  $\text{N}_2^*$  can be seen in Table 6.2.

Although analysis of NO precursor systems represents the simplest  $\text{N}_x\text{O}_y$  plasma system, it does not provide insight into the more complex parent molecules commonly found in exhaust gas systems. Thus, in Fig. 6.5(a),  $\text{N}_2^*$  destruction rate constants are compared across all three precursors, under 100 mTorr conditions as a function of power. Within a given precursor system,  $k_{\text{destruction}}$  is unchanged with increasing  $P$ , within experimental error. Interestingly, the largest rate constants in the  $\text{N}_2\text{O}$  system, suggesting a collisional quenching mechanism, as  $\text{N}_2\text{O}$  is the largest parent molecule and would likely yield a greater number of gas phase collisions. For  $\text{NO}^*$  under identical conditions, Fig. 6.5(b), there are noticeably higher values for  $k_{\text{destruction}}$ . The trend for  $k_{\text{destruction}}$  with respect to power for NO and  $\text{N}_2\text{O}$  is, however, nearly identical. This suggests a similar mechanism for the quenching of the NO excited state in plasmas formed from the two unique precursors, regardless of identity, with the larger  $k_{\text{destruction}}$  values measured in the NO precursor system. This observation can be attributed to the higher  $[\text{NO}]$  in the NO precursor system when compared to the  $\text{N}_2\text{O}$  precursor system, providing additional evidence of the similarities in the mechanisms of  $\text{NO}^*$  reactions for both precursor systems.

As the actinometric intensity ratio is simply proportional to concentration, so too are reported values for both  $k_{\text{formation}}$  and  $k_{\text{destruction}}$ . The comparison of these

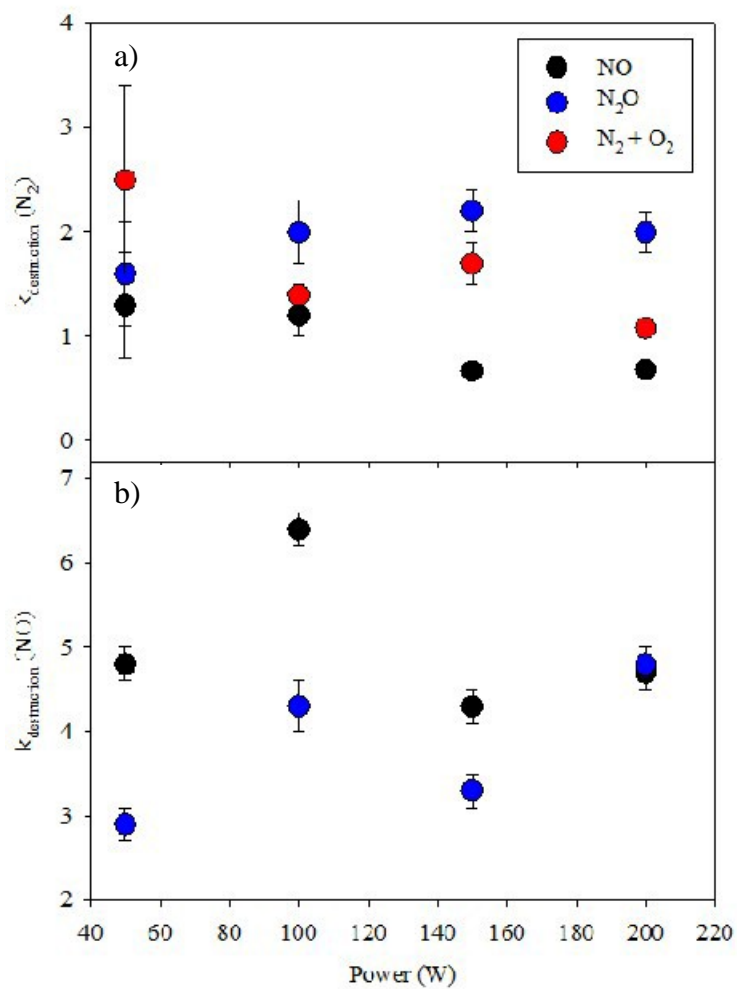


Figure 6.5 Comparison of  $k_d$  for the (a)  $\text{N}_2$  and (b)  $\text{NO}$  molecule as a function of applied rf power for all three precursor systems at 100 mTorr. Note, the  $\text{N}_2 + \text{O}_2$  precursor is not shown for  $k_d(\text{NO})$  as no measurable change in density is observed after the formation of the species.

values, however, across the varied parameter space chosen in these studies provides insight into probable reaction mechanisms within the first few seconds of plasma ignition. Because precursor gas flow is continuous, the system achieves a steady-state concentration of these various species. This results in constant  $[N_2^*]$  and  $[NO^*]$  throughout the life of the plasma, as equilibrium with respect to  $k_{\text{formation}}$  and  $k_{\text{destruction}}$  is achieved. The first moments after ignition, however, are shown to be dynamic with respect to the reactivity of these molecules.

### 6.3 Summary

The research presented here highlights the utility of TR-OES in elucidating the web of complex kinetic parameters that exist within even relatively simple precursor plasma systems. Rate constants of excited state species appear to depend on both applied rf power and system pressure. There is also evidence to support direct excitation of NO in both NO and  $N_2O$  plasma system, whereas direct excitation of  $N_2$  is likely only observed in the  $N_2+O_2$  system. Such observations are key to furthering the utility of these complex systems for plasma assisted catalysis processes. Additionally, by studying the first few seconds of the plasma lifetime, we gain insight into the mechanisms of species formation within individual plasma precursor systems. Such efforts have significant implications in pulsed and/or short-term discharges.

The work presented herein focuses heavily on the early stages of plasma generation, as after  $\sim 4-10$  s, the bulk of the plasma has achieved a macroscopic steady state. Thus, minute changes in species concentration are becoming lost in the signal of the plasma itself. By unlocking the primary sources of species generation, however, we take a significant step in achieving a more tunable and controllable set of operating conditions that lend themselves to a desired outcome. Thus, investigations using TR-OES can be beneficial in elucidating the

complex nature of plasma kinetics, especially in the first few seconds of the plasma ignition. Insight into the mechanisms of excited state species' reactions is critical to a deeper understanding of these nitrogen oxide systems, and this work demonstrates a level of control with respect to species production in these systems. Further efforts to characterize and understand the balance of species formation and destruction within these systems are paramount to the assessment and utilization of nitrogen oxide plasma systems in a variety of applications.

## REFERENCES

1. Änggård, E., Nitric Oxide: Mediator, Murderer, and Medicine. *The Lancet* 1994, 343 (8907), 1199-1206.
2. Cech, T. R.; Bennett, D.; Jasny, B.; Kelner, K. L.; Miller, L. J.; Szuromi, P. D.; Voss, D. F.; Kiberstis, P. A.; Parks, S.; Ray, L. B., The Molecule of the Year. *Science* 1992, 258, 1861.
3. Domingos, P.; Prado, A. M.; Wong, A.; Gehring, C.; Feijo, J. A., Nitric Oxide: A Multitasked Signaling Gas in Plants. *Molecular Plant* 2015, 8 (4), 506-520.
4. Crutzen, P. J., The Influence of Nitrogen Oxides on the Atmospheric Ozone Content. *Quarterly Journal of the Royal Meteorological Society* 1970, 96 (408), 320-325.
5. Roy, S.; Madras, G., Photocatalytic NO<sub>x</sub> Abatement: A Short Review. *Current Organic Chemistry* 2015, 19 (21), 2122-2131.
6. Brandt, E. P.; Yanying, W.; Grizzle, J. W., Dynamic Modeling of a Three-Way Catalyst for SI Engine Exhaust Emission Control. *IEEE Transactions on Control Systems Technology* 2000, 8 (5), 767-776.
7. Carpenter, A. W.; Schoenfish, M. H., Nitric Oxide Release: Part II. Therapeutic Applications. *Chemical Society Reviews* 2012, 41 (10), 3742-3752.
8. Fang, F. C., Perspectives Series: Host/Pathogen Interactions. Mechanisms of Nitric Oxide-Related Antimicrobial Activity. *Journal of Clinical Investigation* 1997, 99 (12), 2818.
9. Radomski, M. W.; Moncada, S., The Biological and Pharmacological Role of Nitric Oxide in Platelet Function. In *Mechanisms of Platelet Activation and Control*, Springer: 1993; pp 251-264.
10. Sun, Y.; Zwolińska, E.; Chmielewski, A. G., Abatement Technologies for High Concentrations of NO<sub>x</sub> and SO<sub>2</sub> Removal from Exhaust Gases: A Review. *Critical Reviews in Environmental Science and Technology* 2016, 46 (2), 119-142.
11. Kim, H.-H.; Teramoto, Y.; Negishi, N.; Ogata, A., A Multidisciplinary Approach to Understand the Interactions of Nonthermal Plasma and Catalyst: A Review. *Catalysis Today* 2015, 256, 13-22.
12. Capitelli, M.; Celiberto, R.; Colonna, G.; Esposito, F.; Gorse, C.; Hassouni, K.; Laricchiuta, A.; Longo, S., *Fundamental Aspects of Plasma Chemical Physics: Kinetics*. Springer Science & Business Media: 2015; Vol. 85.
13. Morgan, M. M.; Cuddy, M. F.; Fisher, E. R., Chemistry in Inductively-Coupled Plasmas for NO Removal from Mixed Gas Systems. *Journal of Physical Chemistry A* 2010, 114, 1722-1733.
14. Stillahn, J. M.; Trevino, K. J.; Fisher, E. R., Plasma Diagnostics for Unraveling Process Chemistry. *Annual Review of Analytical Chemistry* 2008, 1, 261-291.
15. Tompkins, B. D.; Dennison, J. M.; Fisher, E. R., H<sub>2</sub>O plasma Modification of Track-Etched Polymer Membranes for Increased Wettability and Improved Performance. *Journal of Membrane Science* 2013, 428, 576-588.
16. Trevino, K. J.; Fisher, E. R., Detection Limits and Decomposition Mechanisms for Organic Contaminants in Water Using Optical Emission Spectroscopy. *Plasma Processes and Polymers* 2009, 6 (3), 180-189.
17. Coburn, J. W.; Chen, M., Optical Emission Spectroscopy of Reactive Plasmas: A Method for Correlating Emission Intensities to Reactive Particle Density. *Journal of Applied Physics* 1980, 51 (6), 3134-3136.



18. d'Agostino, R.; Colaprico, V.; Cramarossa, F., The Use of "Actinometer" Gases in Optical Diagnostics of Plasma Etching Mixtures: SF<sub>6</sub>-O<sub>2</sub>. Plasma Chemistry and Plasma Processing 1981, 1 (4), 365-375.

## CHAPTER 7

### SUMMARY AND PERSPECTIVES WITH RESPECT TO INVESTIGATIONS OF NITROGEN OXIDE PLASMA CHEMISTRY

This chapter serves to broadly encapsulate the significance of the work presented in this dissertation. Additionally, it highlights possible improvements and advancements that can be made to further expand this area of research, with the aim of generating additional successful and sophisticated measures for plasma-assisted catalytic control.

#### 7.1 Research Synopsis

Despite being a relatively simple molecule, nitric oxide has a complex chemistry that is not yet fully understood.<sup>1</sup> The ability to tune plasma systems for complete control of reactivity and energy of all nitrogen oxides is key to fully understanding and utilizing plasmas as a method of atmospheric remediation. It is important to acknowledge the limitations of currently available atmospheric remediation systems, especially with respect to  $N_xO_y$  species.<sup>2-6</sup> Comprehensive utilization of inductively-coupled plasmas as a method of pollution control will depend heavily on the evaluation of their versatility and adaptability. Evaluating such requirements will require a multidisciplinary approach to system design and diagnostics. Indeed, a more complete understanding of current systems would play a key role in diagnosing problems and designing better control methods. Paramount to this advancement is the need for strong foundational knowledge of the chemistry of these plasma systems, especially with respect to the adjustable parameters within any ICP system. Only by investigating the underlying reactivity of these

systems can we begin to understand how best to tailor a system and its parameters for specific purposes or applications.

This work drives at such goals by identifying and investigating the great number of species present within  $N_xO_y$  plasma systems. A wide range of species, including N, O, NO,  $N_2$ ,  $O_2$ ,  $N_2O$ , and  $NO_2$  exist in their ground, excited, and ionic states within these plasmas. This observation clearly demonstrates the significant complexity of these systems, even with arguably the most simplistic of the possible  $N_xO_y$  feed gases, NO. Furthermore, specific aspects of each of these species are impacted by the parameter space selected, namely pressure and power. Our new broadband absorption spectroscopy apparatus allows investigation of the energy and concentrations of ground state species in a manner previously unavailable to us. This work has clearly demonstrated differences in energy partitioning between  $N_2$  and NO under identical system conditions, demonstrating different mechanisms for species generation. Additionally, our data indicate our ICPs generate vibrationally hot species, with  $T_v$  generally an order of magnitude larger than  $T_R$ , for both ground and excited state species, as established by BAS and OES, respectively. Further development of time-resolved spectroscopic techniques for our ICP systems have allowed us to investigate the rate of excited state species formation and destruction within the plasma, suggesting  $NO^*$  is formed through direct decomposition of an  $N_2O$  precursor, whereas  $N_2^*$  is not.

The role that surfaces play on the reactivity of  $N_xO_y$  species has also been explored. Even with a relatively inert substrate such as a Si wafer, a noteworthy change in the chemistry of the gas-phase portion of the system is observed. Using OES/BAS methods, we measured a decrease in species energies in the presence of a surface, suggesting collisional cooling of the molecules studied. Using the IRIS technique, we measured NO scatter probabilities significantly

greater than 1.0 under some conditions, indicating surface-mediated production of NO during plasma processing. Moreover, this work demonstrated ions play little role in the surface reactivity of NO unless the ion energies exceed ~50 eV. Such energies are only achieved in our systems via a combination of low pressures and high applied rf powers, implying that we can tailor systems to promote ion-mediated surface reactions if desired.

By utilizing several diagnostic techniques in a variety of model systems, this work has successfully expanded upon the existing understanding of nitrogen oxide plasma chemistry. Independently, these efforts provide unique insight into the nature of these systems and our ability to influence and control the resulting outcomes. Altogether, this document serves as the foundation for future efforts, by providing unique insight into the chemistry and reactivity of these foundational systems. Indeed, the challenge ahead will require the incorporation of more accurate, real-world conditions. Progress toward a more reliable plasma-assisted pollution control method will, however, require a knowledge of underlying system performance, serving as a benchmark by which to explore the impact of a host of other potential system variables.

## 7.2 Future Directions

The work presented herein establishes a basis for fundamental  $N_xO_y$  plasma chemistry. As such, future efforts in this area should focus on three overarching aims: (1) furthering our understanding of plasma-catalytic  $N_xO_y$  surface chemistry; (2) investigating fundamental energetics of increasingly complex model precursor systems; and (3) utilizing computational tools to elucidate mechanistic information. Collectively, this would encourage substantial improvement in our understanding of these systems, allowing for a solid foundational grasp of the behavior of nitrogen oxides in plasma systems.

The first aim can be approached in a number of ways. In general, however, plasma-assisted catalysis is studied in conjunction with actual exhaust systems. By utilizing simple gas-phase precursors, along with data from non-catalytic surfaces (Si), we can attempt to more adequately explore the role of the catalyst itself within these systems. In many respects, measuring  $S(\text{NO})$ ,  $T_R$ ,  $T_V$ , and  $\langle E_i \rangle$  in the presence of a catalyst may prove quite insightful, especially given the similar work with respect to Si as discussed in Chapters 4 and 5. The number of potential catalysts is vast, however, with numerous reports of success found in the literature.<sup>7-12</sup> By comparing the amount of NO produced at a surface, as well as the energy partitioning in the presence of that surface, we can begin to build up mechanistic information that is unique to a particular catalyst. Such catalysts include (but are not limited to) platinum, palladium, manganese, zeolites, and a host of other metal oxides.<sup>7, 9-10, 13-15</sup>

There have also been reports of successful modification of catalytic surfaces for the purpose of improved catalytic conversion.<sup>11-12, 16</sup> The Fisher Research Group stands uniquely poised to enter into this area of research, with significant contributions to plasma-enhanced surface modification techniques. It would be a valuable exercise to explore the role of various surface functionalities (such as OH and  $\text{NH}_x$ ) on NO production, adding another layer of insight into the role substrates play in catalytic conversion processes. Indeed, the work shown Chapters 4-6 highlight methodologies for assessing the role of the surface in these nitrogen oxide systems, suggesting a path for investigating a host of new and/or unique substrates.

The second major area of future work, increasingly complex precursor systems, is tremendously valuable to the ultimate assessment of plasma-assisted catalytic systems. Indeed, the work presented in this dissertation demonstrates the striking intricacy of systems composed entirely of nitrogen and oxygen, but real world exhaust systems comprise a vast array of gas-

phase species. From hydrocarbons to water vapor, even sulfur contaminants, these secondary molecules play a major role in the successful conversion of  $N_xO_y$  species by introducing a myriad of possible side reactions. Therefore, a more thorough understanding of how to tailor PAC systems for successful remediation will hinge upon explicit investigation of such secondary reactions. Numerous attempts have to been made to assess plasma-assisted conversion of actual exhaust systems, but success and/or failure does not inherently provide a reason for this outcome. Indeed, the amount of variability within vehicular and industrial exhaust poses a great number of scientific challenges and a set of conditions that show successful conversion of one sample may not exhibit this behavior in a second. Thus, it is critical that we investigate the role that each of these component species plays in the overall chemistry, energy, and reactivity of  $N_xO_y$  species.

With these challenges in mind, it is important to slowly introduce extra components into these systems and monitor the resulting outcomes. It is nearly impossible to extract or interpret mechanistic information from data collected in a true exhaust gas sample. By investigating the impact of individual components (and simplified model molecules), however, we can elucidate individual contributions. For example, mixtures of NO and  $CH_4$  may provide initial insight into the role of large hydrocarbon molecules found in exhaust streams. By slowly increasing the complexity of the gas feed, we can build a library of common reactions and energetic implications thereof. Ultimately, this would allow for the determination of conditions that most often yield successful conversion, which may make it possible to tune individual plasma-assisted catalysis reactors to specific conditions as to optimize success.

Finally, the use of computational methods shows great promise in improving our molecular-level understanding of these systems. From establishing appropriate methods to model the unique chemistry of plasma systems to generating methods to address relevant gas-

surface reactions, there is a tremendous opportunity for growth in this area. Especially intriguing is the potential for Atom-Centered Density Matrix Propagation (ADMP) to help yield reaction coordinate probabilities, when given a starting transition state. Further discussion of this method in particular, and possible avenues for study, can be found in Appendix A.

Ultimately, the future success of plasma-assisted catalysis as a method of exhaust remediation depends largely on efforts to understand the fundamental chemistry of these unique systems. Limited progress can be made through the process of trial and error, by testing a variety of conditions and catalysts, but true advancement will come through purposeful and knowledgeable investigations. If we can understand the role of each component: species, plasma parameter (pressure, power, precursor), catalyst, etc., we can take an important step toward a more viable and long-term method of atmospheric protection. Without this foundational work, however, we are unlikely to truly understand the cause of any given plasma-assisted outcome.

## REFERENCES

1. Cech, T. R.; Bennett, D.; Jasny, B.; Kelner, K. L.; Miller, L. J.; Szuromi, P. D.; Voss, D. F.; Kiberstis, P. A.; Parks, S.; Ray, L. B., The Molecule of the Year. **Science** 1992, 258, 1861.
2. Ighigeanu, D.; Martin, D.; Zissulescu, E.; Macarie, R.; Oproiu, C.; Cirstea, E.; Iovu, H.; Calinescu, I.; Iacob, N., SO<sub>2</sub> and NO<sub>x</sub> Removal by Electron Beam and Electrical Discharge Induced Non-Thermal Plasmas. **Vacuum** 2005, 77 (4), 493-500.
3. Chen, H. L.; Lee, H. M.; Chen, S. H.; Chang, M. B.; Yu, S. J.; Li, S. N., Removal of Volatile Organic Compounds by Single-Stage and Two-Stage Plasma Catalysis Systems: A Review of the Performance Enhancement Mechanisms, Surrent Status, and Suitable Applications. **Environmental Science & Technology** 2009, 43 (7), 2216-2227.
4. Penetrante, B. M.; Brusasco, R. M.; Merritt, B. T.; Vogtlin, G. E., Environmental Applications of Low-Temperature Plasmas. **Pure and Applied Chemistry** 1999, 71 (10), 1829-1835.
5. Penetrante, B. M.; Hsiao, M. C.; Bardsley, J. N.; Merritt, B. T.; Vogtlin, G. E.; Kuthi, A.; Burkhardt, C. P.; Bayless, J. R., Identification of Mechanisms for Decomposition of Air Pollutants by Non-Thermal Plasma Processing. **Plasma Sources Science & Technology** 1997, 6 (3), 251.
6. Penetrante, B. M.; Bardsley, J. N.; Hsiao, M. C., Kinetic Analysis of Non-Thermal Plasmas Used for Pollution Control. **Japanese Journal of Applied Physics** 1997, 36 (7S), 5007.
7. Brandenberger, S.; Kröcher, O.; Tissler, A.; Althoff, R., The State of the Art in Selective Catalytic Reduction of NO<sub>x</sub> by Ammonia Using Metal-Exchanged Zeolite Catalysts. **Catalysis Reviews** 2008, 50 (4), 492-531.
8. Brandt, E. P.; Yanying, W.; Grizzle, J. W., Dynamic Modeling of a Three-Way Catalyst for SI Engine Exhaust Emission Control. **IEEE Transactions on Control Systems Technology** 2000, 8 (5), 767-776.
9. Miyoshi, N.; Matsumoto, S. i.; Katoh, K.; Tanaka, T.; Harada, J.; Takahashi, N.; Yokota, K.; Sugiura, M.; Kasahara, K. **Development of New Concept Three-Way Catalyst for Automotive Lean-Burn Engines**; 0148-7191; SAE Technical Paper: 1995.
10. Qi, G.; Yang, R. T.; Chang, R., Low-Temperature SCR of NO with NH<sub>3</sub> over USY-Supported Manganese Oxide-Based Catalysts. **Catalysis Letters** 2003, 87 (1-2), 67-71.
11. Sharma, R.; Rimmer, R. D.; Gunamgari, J.; Shekhawat, R. S.; Davis, B. J.; Mazumder, M. K.; Lindquist, D. A., Plasma-Assisted Activation of Supported Au and Pd Catalysts for CO Oxidation. **IEEE Transactions on Industry Applications** 2005, 41 (5), 1373-1376.
12. Tang, X.; Li, K.; Yi, H.; Ning, P.; Xiang, Y.; Wang, J.; Wang, C., MnO<sub>x</sub> Catalysts Modified by Nonthermal Plasma for NO Catalytic Oxidation. **The Journal of Physical Chemistry C** 2012, 116 (18), 10017-10028.
13. Beck, D. D.; Sommers, J. W., Impact of Sulfur on the Performance of Vehicle-Aged Palladium Monoliths. **Applied Catalysis B: Environmental** 1995, 6 (2), 185-200.
14. Miessner, H.; Francke, K.-P.; Rudolph, R.; Hammer, T., NO<sub>x</sub> Removal in Excess Oxygen by Plasma-Enhanced Selective Catalytic Reduction. **Catalysis Today** 2002, 75 (1), 325-330.
15. Iwamoto, M.; Mizuno, N., NO<sub>x</sub> Emission Control in Oxygen-Rich Exhaust Through Selective Catalytic Reduction by Hydrocarbon. **Proceedings of the Institution of Mechanical Engineers, Part D: Journal of Automobile Engineering** 1993, 207 (1), 23-33.



16. Huang, X.; Huang, B.; Zhang, C.; Ye, D.; Luo, C., Plasma Modification of V-ACF for NO SCR at Low Temperatures. **Chemical Industry and Engineering Progress** 2010, 11, 035.

## CHAPTER 8

### ASSESSMENT OF GENERAL CHEMISTRY RECITATION ACTIVITIES AND ASSOCIATED STUDENT ATTITUDES

This chapter contains information about a chemistry education research project conducted through the recitation component of the General Chemistry I (CHEM 111) course at Colorado State University during the 2014-2015 academic year. The work herein was completed by Joshua M. Blechle under the guidance of Nancy E. Levinger and Ellen R. Fisher. Additional acknowledgments go out to acknowledge Dr. Heather Novak of the Institution Research, Planning and Effectiveness Office at Colorado State University for her help in compiling student grades and demographic information, as well as the general chemistry instructors that allowed this work to take place in their classrooms, specifically Dr. Ingrid Laughman, Dr. Randy Booth, and Dr. Harmony Tucker.

In this work, efforts were made to generate more effective and instructor-friendly content and to assess the efficacy of the recitation content in enhancing the overall course performance. In addition, student opinions on the activities and their perceived success was collected and analyzed, ultimately providing insight into student attitudes with regards to the recitation classroom.

#### 8.1 Introduction

In many academic institutions, recitation is a classroom program that serves to supplement standard lecture instruction.<sup>1-2</sup> Utilized in a variety of courses including chemistry, biology, mathematics, physics, engineering, languages, fine arts, among others, recitation is

commonly used to expand upon or clarify certain points within a subject matter that were either poorly understood or not sufficiently addressed.<sup>3-8</sup> It can also be used as a designated time for students to work on homework and study under the supervision of an instructor or teaching assistant. Given the wide array of potential goals for student learning, recitation sections can be designed in a number of ways, encouraging students to engage with the material using activities, discussions, self-guided inquiry, derivations, problems solving sessions, and/or cooperative group work.<sup>6-12</sup>

Due to their widespread application in a variety of different courses, as well as the multitude of approaches that can be used within them, evaluating the efficacy of a particular recitation course or activity can be difficult to ascertain. Despite these challenges, numerous efforts have been made to investigate the success of recitation sections.<sup>1-18</sup> Many investigations encouraged group collaboration among students, especially in undergraduate chemistry courses, which is shown to improve classroom efficacy in several ways.<sup>6</sup> Johnson and Johnson have reported on the value of cooperative learning, where learning goals are shared among peers to improve motivation and classroom engagement.<sup>19-22</sup> These studies show improved student achievement when compared to classrooms focused on competitive or individualistic learning goals. Cooperative learning has also been shown to improve content retention and student attitudes across a diverse student population. Bowen reports similar results in cooperative-based learning scenarios, specifically among high school and college chemistry students.<sup>23</sup> These investigations also report an increase in discussions among students, increased feelings of responsibility and ownership towards learning, and improved critical thinking skills.<sup>22-24</sup>

In addition to positive learning outcomes, group work has been shown to improve student perceptions and increase motivation to perform well in class.<sup>25</sup> Cooperative learning, however,

is not the only key element in these desirable shifts. Indeed, a number of studies<sup>25-34</sup> have examined a variety of other environmental factors which positively impact student interest and attitudes, in a range of courses and scenarios. The role of student expectations and interest has only been studied with relation to its impact on classroom efficacy.<sup>35</sup> Despite the array of potential motivators, identifying student expectations and monitoring shifts in student opinions can be valuable in gaining insight into evaluating the success of a particular topic or educational approach.

The work presented in this chapter discusses the structure of the General Chemistry I (CHEM 111) recitation at Colorado State University (CSU), the design of new recitation activities, and the investigation of student opinions and concept retention within the 2014-2015 academic year. A detailed outline of the research approach, the data collected and analyzed, and future directions for the optimization of the recitation for future semesters are presented. The primary focus of the work lies squarely in collecting and analyzing student opinions and insights into the various types of activities employed.

## 8.2 CSU General Chemistry Recitation

At CSU, all students enrolled in CHEM 111 are required to attend a weekly recitation course, with multiple sections of ~40 students offered to the >1200 students enrolled. These 50 minute sections are led by graduate teaching assistants (GTAs) and are focused on topics that the course instructors find to be troublesome/challenging for students or that require extra practice. In the two semesters in which these studies were completed, students received a weekly grade in recitation which contributed 25% to their overall CHEM 111 course grade (effectively making

recitation equate to 1 credit of the 4 credit class). The grades received in recitation were based on class attendance, participation, and the completion of online homework.

An outline of a typical week for CHEM 111 students can be seen in Fig 8.1. Lectures are held on Monday, Wednesday, and Friday. Students also have an assigned recitation on either Tuesday or Thursday (they do not attend both days), making the development of recitation activities especially challenging, as Thursday students have had one extra day of lecture. Recitation homework for the week is typically released to students on Wednesday evenings with a due date of the following Monday at 11:59 PM. As for the recitation itself, each section begins with a 3-5 minute electronic polling (iClicker) question on the topic with which the students will engage that day. This provides the GTAs information about how prepared students may be for the day's activity. Similarly, each class period ends with 6-10 minutes spent on two iClicker questions. One is identical to the first question of the day, to gauge student progress and the second is a more difficult question/problem designed to see if students have moved toward mastery of the topic. The majority of the class period (~35-40 minutes) is spent working in groups of 3 to 4 students on a topic-focused activity. In this study, we grouped these activities into five categories: traditional worksheet, scaffold worksheet, thematic worksheet, game, or computer simulation.

The traditional worksheet consists largely of independent problems, often forcing students to practice a certain type of problem in a variety of ways. Although the content is similar, each of the individual questions on a traditional worksheet can generally stand alone as an independent problem and do not necessarily provide any guidance to the student on how the problem should be solved. Scaffold worksheets, on the other hand, are designed to guide students to the solution of a problem. This can be done by providing them with step-by-step

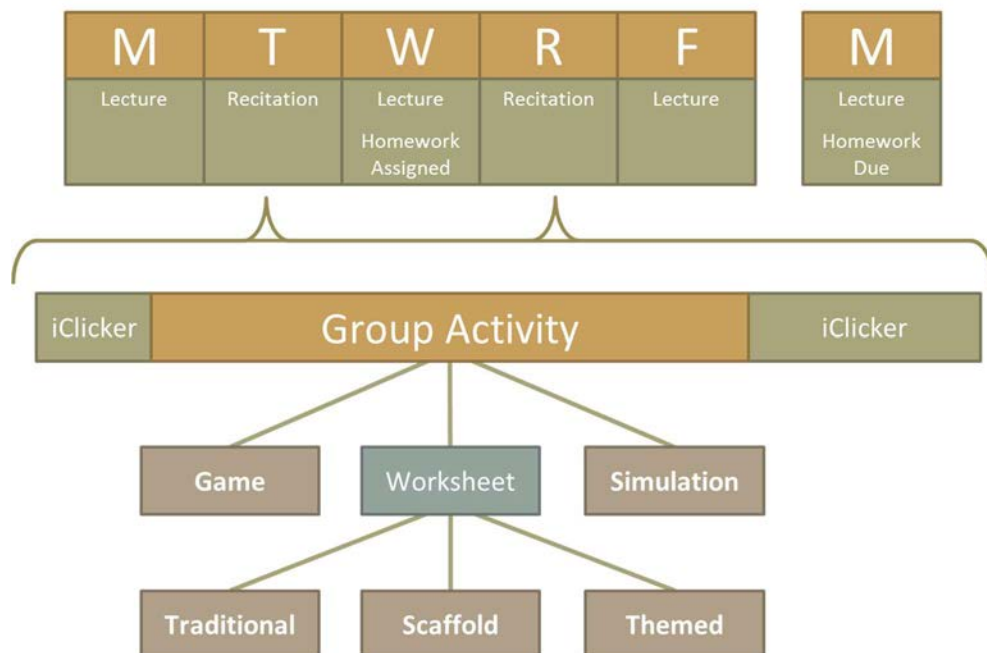


Figure 8.1 Breakdown of weekly recitation schedule in CHEM 111, as well as a timeline for each recitation activity and possible activities utilized.

problem-solving instructions on how to complete the initial question(s) and then offering less and less assistance on subsequent problems. The students must complete the final problem(s) of the activity on their own, thereby guiding them through the thought process and approach needed to understand a particular concept.

A second type of scaffold worksheet activity is one in which step-by-step instructions are provided for each problem of the activity, but some of the built-in guidance can be removed by the instructor. This provides an individual instructor the opportunity to remove specific directions, therefore requiring more of the work to be completed by the student, where they deem appropriate. Such control can help educators tailor activities to a specific section/semester of students, which can be necessary due to variations in student ability or the depth to which a skill or problem is addressed in the lecture portion of the course.

Yet another worksheet approach is the thematic activities. Although this approach can also be utilized in scaffold worksheets, thematic activities do not provide the ability to be readily tailored nor do they provide guided instruction. These long, text-based problems, were designed to place chemistry problems into a larger context. Such worksheets are often intended to help draw connections to real-world applications of chemistry and the curriculum. They engage students with the material by providing data and information they need to use to find a particular outcome. For example, a themed activity used in this study provided students with data from a “CSU crime scene” in which they worked to try and determine facts about the case from the data provided. In contrast, so-called “game” activities can be quite diverse, but ultimately focus on competitive group work. One game activity used in this study was a chalkboard relay race on molecular geometry and polarity. Each group was given a series of questions, and one student had to provide a piece of information before passing the chalk on to another teammate.

Finally, computer simulation activities are designed to expose students to a computational method of visualizing complex concepts. This provides students with a unique method of interacting with the course material, unlike anything else generally seen in other coursework components. For the activities used in these studies, students were asked to answer a series of questions that were paired with PhET simulations created at the University of Colorado – Boulder.<sup>36</sup> These interactive programs allow students to alter and explore certain parameters and observe both molecular and macroscopic impacts.<sup>36-38</sup>

Table 8.1 provides a full breakdown of each week's activity and material for each semester of CHEM 111. Ultimately, the activities discussed above accounted for 10 weeks of the 16-week semester. Four unit exams were administered in CHEM 111; an optional recitation was held on each of the exam weeks. Because these unit exams were administered on Wednesday evenings, students could attend any of the optional Tuesday sections to participate in GTA led review sessions. Thursday sections provided students an opportunity to meet with GTAs and discuss problematic exam questions they may have struggled with during the exam itself. These review weeks did not contain a recitation homework assignment. The remaining two weeks of the semester were the first and last of the semester, Weeks 1 and 16. Recitation attendance was required in Week 1, and recitation sections were used to administer the American Chemical Society Toledo Chemistry Placement Examination (TCPE), to provide both instructors and students with preparedness information for the coming semester. In Week 16, the final exam was administered and no recitation sessions (review or otherwise) were held. It is important to note, however, that both of these weeks did have accompanying online recitation homework, in which students were asked to provide their initial and final perceptions of the recitation course (the results of which are discussed further below).



Table 8.1 Weekly recitation schedule in CHEM 111 for the 2014-2015 academic year

<b>Week</b>	<b>Recitation Topic</b>	<b>Activity</b>
1	Pre-Test (TCPE)	Initial Perceptions
2	Dimensional Analysis	Traditional
3	The Mole	Scaffold
4	<i>Exam 1</i>	<i>TA Review Session</i>
5	Electron Configurations	Traditional
6	Periodic Trends	Traditional
7	<i>Exam 2</i>	<i>TA Review Session</i>
8	Molecular Polarity	Game
9	Intermolecular Forces	Game
10	<i>Exam 3</i>	<i>TA Review Session</i>
11	Stoichiometry	Scaffold
12	Limiting Reagents	Thematic
13	<i>Exam 4</i>	<i>TA Review Session</i>
14	Enthalpy	Thematic
15	Gas Properties	Simulations
16	Final Exam	Final Perceptions

### 8.3 Activity Development

One goal of this work was to design new recitation activities and to assess the efficacy of other various types of activities. In that effort, the scaffold activities used in Weeks 3 and 11 (found in Appendix B) were created to provide instructors with an increased amount of control over the activity presented to students. Both activities provide students with a scenario in which they work as a chemist for a fictional company named ChemLight. In each activity, their supervisor approaches them with a problem that can ultimately be addressed using the data provided and the student's knowledge of general chemistry. In this way, these scaffolded worksheets also had an element of the thematic activities in that there was a direct tie to "real-world" applications of chemistry.

The designed activities, however, focused on utilizing the concept of scaffolding within an individual assignment. Scaffolding is an educational technique in which instruction is designed with detailed building blocks that demonstrate a particular technique or skill.<sup>39</sup> Those details are then slowly removed (and can be re-added if necessary) to help foster independent mastery of a given skill. This can be accomplished by demonstrating the problem solving process, as well as approaches that can be successful for a given problem/concept. This helps students develop strategies for problem solving, as opposed to memorizing a particular strategy or formulaic approach to a question. Additionally, scaffolding can be employed in many ways at a multitude of levels, from deployment within a single assignment (as exemplified by this work) to the overall structure of a course's curriculum.<sup>39-44</sup>

The two activities designed and used in this work covered the concepts of (a) the mole (Week 3) and (b) stoichiometry (Week 11). At the onset of this project, an initial outline for the Week 3 activity was developed to integrate the scaffolding approach within a very finite

recitation time period. The particular content was chosen as the mole is a particularly challenging concept for students, due in large part to students' heavy reliance on numerical and algorithmically driven methods, without having a clear, conceptual understanding of the underlying chemistry.<sup>45-47</sup> As such, it is a prime candidate for a scaffold approach, where students are directed through the problem solving process as opposed to being shown a purely algebraic formulation. The activity itself presents students with a blank table of information that needs to be completed for their supervisor at ChemLight, who is hoping to investigate why a neon sign (filled with argon) is not functioning properly. The table requires students to provide the mass, number of moles, amount of each isotope, as well as the differences in protons, neutrons, and electrons of those isotopes. Such calculations can easily become formulaic, without taking time to consider the meaning behind the arithmetic being completed. Such an approach makes it difficult for students to assess the quality of their final answer (i.e., Does this answer make sense?) and to find alternative methods for solving the problem.

Throughout the worksheet, students are guided not only through the process of the calculations but also through the thought process one might use to achieve the desired results. Additionally, students are asked to compare values, predicting larger or smaller values, in an effort to have them consider the expected result from a purely conceptual standpoint. Furthermore, when given calculations to complete, students are guided through an example before being asked to complete problems on their own. Each subsequent attempt provides them with less information, requiring them to provide (or generate) more of the necessary information on their own. In the final version of the document, which was used in these studies, the basic outline of each calculation is provided, asking students to fill in the missing information. This level of scaffolding was used throughout the academic year, but could be tailored in the future by

removing some of the more guided calculations, asking students to generate the necessary calculations without the aid of the outlined set-up.

The Week 11 assignment, on stoichiometry, was designed to meet the requested needs of the course instructors. They felt that this particular area was one of weakness for students and one that could benefit from a scaffolded approach. This particular worksheet presents students with the problem of trying to design and develop a glow stick for the ChemLight company. It begins by providing some background information on the chemistry of glow sticks before leading them through the process of working with the information to determine how much of each reactant will be needed for the glow stick prototype. Once again, a fully scaffolded worksheet was generated, meaning each step was given in complete detail. However, much of this scaffolding was removed in the final version given to the students (Appendix B). This was a choice made by the instructors, as the concept of stoichiometry had been covered significantly prior to administering this activity. For example, Problem 3(a) describes the needed calculation at a similar level to the previous worksheet (the Week 3 exercise), but 3(b) gives much less guidance and Problem 4 gives none whatsoever. Despite being very similar calculations, students are still expected to take larger leaps without the aid of the information contained within the assignment itself. This demonstrates the ability to tailor an individual assignment to the needs of students, while still being able to add layers of scaffolding back into the worksheet in future semesters, if so desired. Additionally, this activity ends with a series of reflection questions, asking students to go beyond calculations and consider the underlying chemistry. For example, they are asked to consider how changing the amount of starting materials might impact the final product, trying to help build connections between the results of their calculations to real-world results.

## 8.4 Assessment Design

The research presented herein was aimed at providing data to help with potentially restructuring the CHEM 111 recitation program to maximize its effectiveness for students, faculty, and GTAs. By collecting satisfaction surveys and content assessments from the student population, we hoped to gauge student interest and effectiveness. This project tested each of the different recitation methods described in Section 8.2. The resulting survey data can be used to identify particular methods to implement in future semesters and will serve as a baseline for more thorough future research endeavors. This work was approved by the CSU Internal Review Board (IRB protocol ID: 120-15H). The goal of the work proposed within the IRB protocol was to address three specific research questions: 1) How effective is recitation in improving student learning? 2) What are student attitudes toward recitation? and 3) What role does the activity play in both student attitudes and learning? Although all of these questions can be addressed to various extents within the context of the research program implemented, the bulk of the data presented in the following sections focuses on the second research question. Initial results for the other research questions, as well as improved methods for addressing them, are also provided below.

To collect information about student attitudes and content retention, surveys were administered to students as part of their weekly recitation homework (noted above). During the first day of lecture, students were given a short presentation on the survey and the goals of the research and a more detailed letter was provided via the course management software, assuring informed consent from the students. Survey and homework questions were paired together in an online format using SurveyMonkey®. An example survey is provided in Fig. 8.2, reformatted to fit on a single page. Each Wednesday, students received two unique website URLs, with each

Welcome to the CHEM 111 recitation homework for CSU students

Welcome to the recitation homework for CHEM 111 at Colorado State University. You will be asked for your CSU ID number on the final page. You must complete each question to enter your ID, and you must enter your ID to receive credit for this assignment.

Next

Powered by  
SurveyMonkey  
See how easy it is to create a survey

\* 1. In what ways did this week's activity meet (or fail to meet) your expectations for recitation?

\* 2. What was your favorite aspect of this week's activity?

\* 3. What was your least favorite aspect of this week's activity?

Prev Next

\* 4. How effective was this week's activity at engaging your interest in the material?  
 Very Effective  
 Somewhat Effective  
 Not Very Effective  
 Not At All Effective

\* 5. How successful was this week's activity in improving your understanding of the material?  
 Very Successful  
 Somewhat Successful  
 Not Very Successful  
 Not At All Successful

\* 6. How reliant were you on the help of your TA to complete this week's activity?  
 Very Reliant  
 Somewhat Reliant  
 Not Very Reliant  
 Not At All Reliant

\* 7. Overall, how satisfied were you with this week's activity?  
 Very Satisfied  
 Somewhat Satisfied  
 Not Very Satisfied  
 Not At All Satisfied

\* 8. How interested would you be in participating in a similarly structured activity in the future?  
 Very Interested  
 Somewhat Interested  
 Not Very Interested  
 Not At All Interested

Prev Next

Practice Problems

\* 9. How many significant figures are justified in a measurement of a length that is between 9 and 10 centimeters if the measuring device (ruler) has smallest divisions of 0.1 cm?  
 One  
 Two  
 Three  
 Four

\* 10. A chemist wants to determine the density of an object. He places the object on a balance and measures the mass to be 2.9372 grams. He then takes a graduated cylinder containing 25.45 mL of water and adds the object to the graduated cylinder. The final volume is 26.32 mL. To how many significant figures should the density be reported?  
 1  
 2  
 3  
 4

\* 11. If urine has an average density of 1.08 g/mL, what would be the mass of a 125 mL urine sample?  
 135 g  
 0.00864 g  
 116 g  
 125 g


\* 12. Do the following calculation. How many significant figures are justified for the answer?  
 $6.02 + 5.119 + 0.04218$   
 Three  
 Four  
 Five  
 Seven

\* 13. A hiker began a hike with a pint canteen full of water. At the end of the hike, 7.0 fluid ounces of water remained. What percent of the water was used during the hike? (1 pint = 16 fluid ounces)  
 78%  
 44%  
 56%  
 13%

Prev Next

CSU ID#

Your CSU ID number is found on the bottom of your RamCard (shown below as 888888888 for Cam).



\* 14. What is your CSU ID number?

Prev Done

Powered by  
SurveyMonkey  
See how easy it is to create a survey

Figure 8.2 Condensed example survey from Week 2 in Spring 2015. All questions except for practice problems (#9-13) remained identical throughout the semester. Each “next” button would normally represent a new page in the survey.

one leading to an identical assignment. The difference between them being that one web address was for students who chose to consent and the other was for those who did not wish to participate in the research project. In this way, each student could receive credit for completing their homework assignment after compiling results from both survey code requests, but were not obligated to participate. This also allowed students an easy avenue for opting out of the research project at any point in time during the semester, and for participating on a week-to-week basis. Only results from consenting students are presented herein. As a result of the open nature of the consent process, numbers of participating students would change from week to week. Total student enrollment was 1,165 in Fall 2014 and 731 in Spring 2015; Fig. 8.3 shows the number of consenting students in each week. These numbers indicate that, on average, 555 and 449 students consented across the two respective semesters, amounting to ~53% of the enrolled population for the academic year.

In the first semester of this study (Fall 2014), students were asked to generate their own six-digit alpha numeric code to preserve anonymity. Each survey would ask students to provide this code, which was collected by the researchers. The codes for both consenting and non-consenting students were compiled and sent on to the instructors so that credit for completing the homework could be given. In this way, only the instructors had the ability to link names and codes, but did not know if the students chose to consent to be part of the research project. As a result of recurring issues with students not remembering or mistyping codes, a slight modification was made to the IRB protocol in Spring 2015 to allow students to use their CSU identification number instead of a user-generated code.

Initially, surveys were formatted such that each one began by requesting the student survey code, and was primarily focused on investigating student interest and satisfaction with the

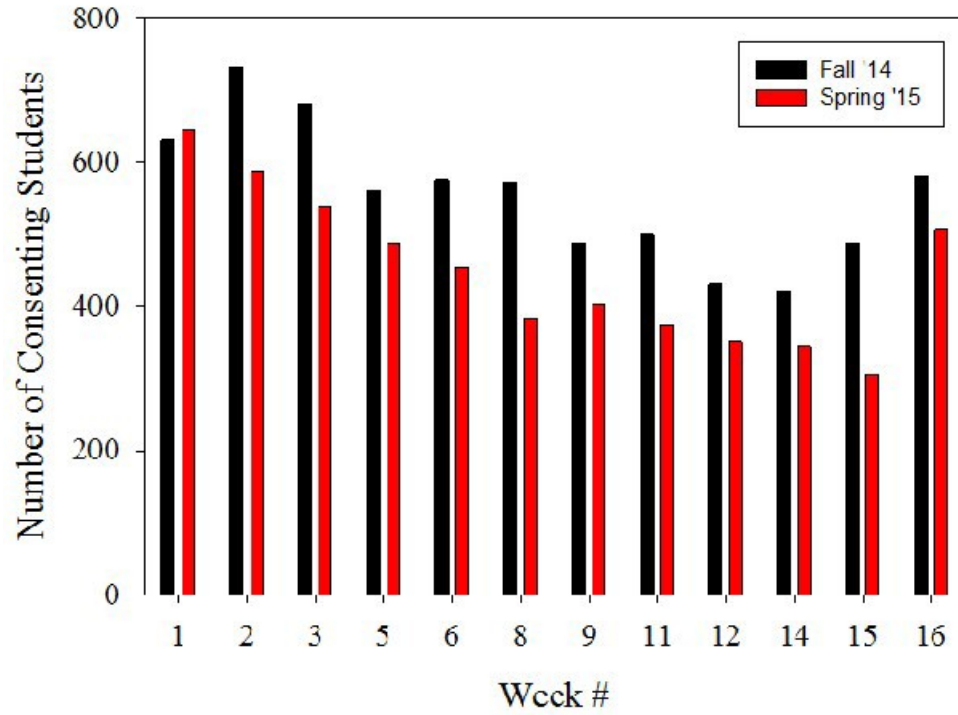


Figure 8.3 Number of students who agreed to participate in the research study for each semester based upon week.



week's activity. It also attempted to gauge how the activity fits with their expectations of the recitation course as well as how they feel it aided in their understanding of the particular topic on which the activity is focused. Each week also included several questions regarding the content of the previous week's activity to gauge student retention of previous material and to investigate how a particular activity may aid in content retention. The bulk of this format remained the same over both semesters. One major change between the first and second semesters, however, was that student code/ID requests were moved to the end of the survey. This change was made to address one issue that was identified during the first semester, namely that a number of students began to simply enter the code/ID on the first question of the survey and then closed the browser window. As such, their code was entered and recorded to receive credit even though they did not actually complete the assignment. Moving the student code/ID question to the end of the survey largely fixed this problem as completion of the entire assignment was required for a student to receive credit (the SurveyMonkey® activity was designed to require an answer to each question before moving forward).

## 8.5 Early Expectations

At the beginning of the semester, before attending a designed recitation activity, students were asked to complete an initial survey of 11 questions. The questions on the survey spanned a range of topics; some were short answer and others Likert-scale in style, designed to evaluate student interest with respect to general chemistry and recitation. Data compiled across both fall and spring semesters allowed for evaluation of student expectations and perceptions, and provided a baseline by which to compare student interest.

Likert-scale questions contained four general answer categories: strongly positive, moderately positive, moderately negative, and strongly negative. This was done purposefully to ensure that students' responses leaned toward a positive or negative response, thus avoiding an abundance of neutral opinions. In many cases, these options were written as "very \_", "somewhat\_\_\_\_", "not very\_\_\_\_", and "not at all\_\_\_\_". The blank space reflects the particular topic addressed within a question. For example, if a question read "how interested are you in recitation activities?", the answer choices would be "very interested", "somewhat interested", "not very interested", and "not at all interested". Three key questions from the initial questionnaire were:

- A. How interested are you in chemistry and the CHEM 111 course?
- B. How important do you think recitation will be to your understanding of the course material?
- C. How important do you think CHEM 111 material is to your desired career/major?

Responses to these three questions, Fig. 8.4, show that students at CSU are entering the general chemistry classroom with a predominantly positive outlook on the course and its overall importance to their educational program. Indeed, both semesters show positive responses for the majority (>80%) of students in all cases. These data are representative of the overall opinions presented by participating students at the outset of the semester, seemingly illustrating the overall expectations for the coming semester.

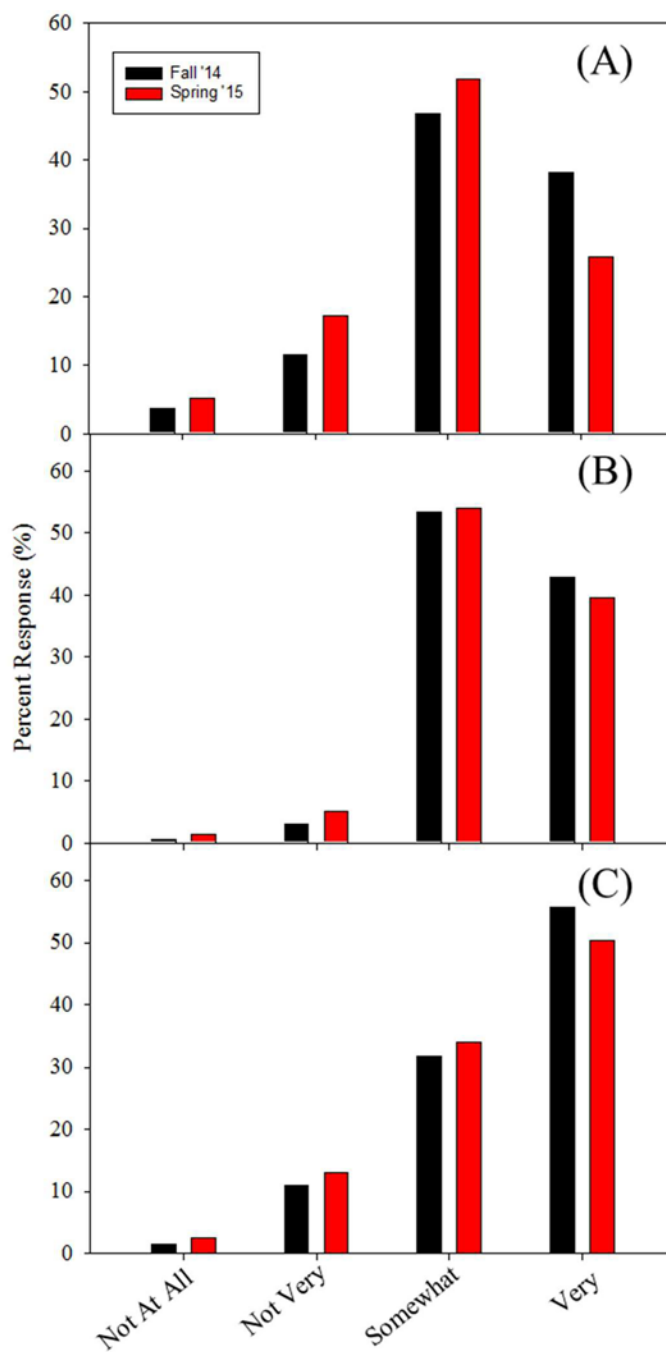


Figure 8.4 Percent of student responses to each of the four available answer categories for three different questions posed at the beginning of the each of two semesters: (A) How interested are you in chemistry and the CHEM 111 course? (B) How important do you think recitation will be to your understanding of the course material? (C) How important do you think CHEM 111 material is to your desired career/major?

## 8.6 Weekly Responses

During the ten weeks in which recitation activities were completed, student homework surveys consisted of 14 questions. There were 8 attitude and perception questions (five Likert, three free response), 5 content questions, and 1 identification question (discussed in Section 8.4). The attitude and perception questions remained identical throughout each week during both semesters, but the content questions were unique to the topic covered in that week's activity. Notably, the content questions given in Fall 2014 were all designed by the researchers, but in Spring 2015, at the request of the course instructors, one of the five content questions was changed to match an exam question from the previous semester.

Whereas the free response questions provided anecdotal information regarding student perceptions of the activity, the Likert-scale questions allowed for a more systematic assessment of student opinions. Four of the questions asked of students each week were:

1. How effective was this week's activity at engaging your interest in the material?
2. How successful was this week's activity in improving your understanding of the material?
3. Overall, how satisfied were you with this week's activity?
4. How interested would you be in participating in a similarly structured activity in the future?

The available answer choices for each of these questions were identical to those provided in the initial survey. They were written as "very\_\_\_\_", "somewhat\_\_\_\_", "not very\_\_\_\_", and "not at all \_\_\_\_" with the blank space reflecting the particular opinion addressed within a question. Again, this design prevented students from simply choosing a neutral option, but instead required them to report either more positively or more negatively.

To characterize the overall attitude of the students in a given week, a measurement referred to as the Positivity Index (PI) was developed. The PI of each week as calculated via Equation 8.1 using the four questions presented above.

$$= \frac{\sum(\% \quad \% \quad \% \quad \%)}{4} \quad (8.1)$$

The PI is, therefore, the average percentage of positive responses for all four questions in a given week, thus characterizing the overall positivity of students in a single value. Figure 8.5 shows weekly PI results for both semesters. These data clearly show that the majority of students respond positively over the entirety of the semester, with the lowest overall PI being  $57 \pm 5\%$  in Week 12. Another observation of note is that, within error, each week's PI is the same regardless of semester (i.e., Week X has the same PI for both fall and spring semesters). Ultimately, this indicates not only a level of consistency across the academic year, but also that it is possible to distinguish a particular positivity index for the individual activity itself.

In addition to PI values, student performance on the five content questions was evaluated. The percentage of students that answered each question correctly was averaged to generate a percentage value that reflects the overall homework performance each week, Fig. 8.6. Here, homework performance varied significantly between the two semesters, with lower overall scores reported for the Spring 2015 semester in 7 of the 10 weeks. One explanation for this difference could be the alteration of questions between semesters, as noted above. However, even with the differing questions removed, the Fall 2014 semester continually scored better than Spring 2015 (with Week 5 being the only exception).

Given that the content questions were not identical across semesters, a potentially more informative interpretation could arise from the mirrored trends between the semesters. If the relative performance of the individual semesters on a week-by-week basis is compared,

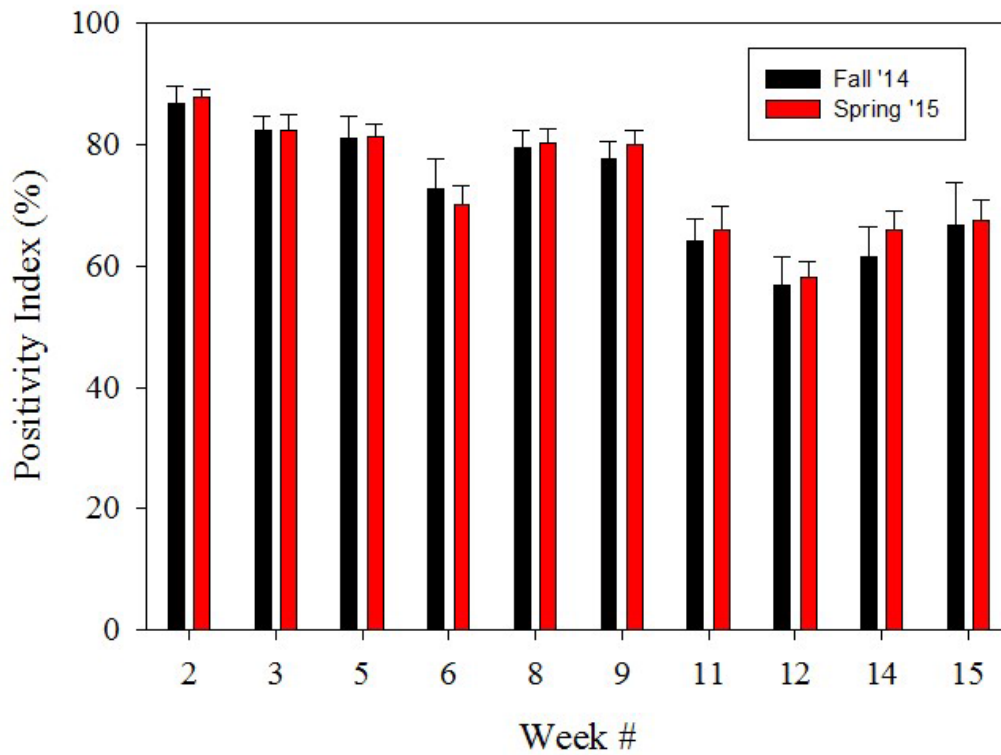


Figure 8.5 Positivity Index as a function of week for both fall and spring semesters. Error bars represent one standard deviation from the mean.

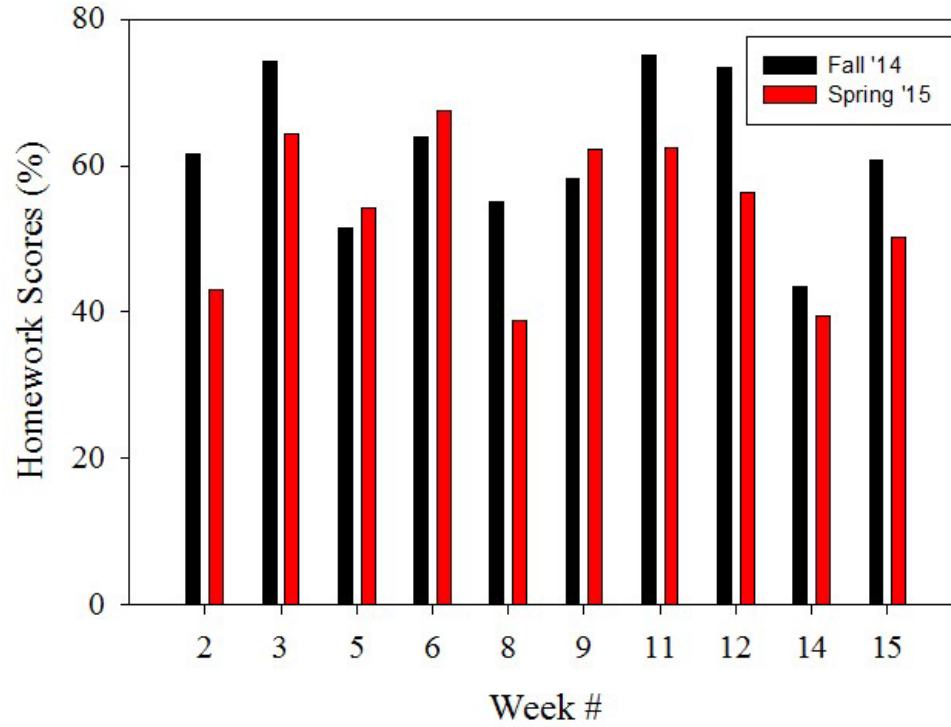


Figure 8.6 Average performance for the five content questions during each weekly activity over both semesters.

similarities between the semesters are easily identifiable. Specifically, performance increased between Weeks 2 and 3, decreased from 3 to 5, increased between 5 and 6, decreased from 6 to 8, increased between 8 and 9, decreased from 11 to 12 as well as 12 to 14, and finally performance increased again between Weeks 14 and 15. The only consecutive weeks in which performance trends are not mirrored is Weeks 9 and 11, as there was a 17% increase in performance in Fall 2014 and no changes (within error) in Spring 2015. Overall, this speaks to the potential impact of one activity compared to another. It is, however, important to note that these trends may be affected by the simple progression of the semester. For example, scores always decreased in the week immediately following that of an exam.

Finding a causal relationship for the trends in homework performance can be complicated, and would likely require continued investigations and additional data (see Section 8.8). Nevertheless, we decided to explore possible correlations between student performance and the opinions they expressed within the weekly surveys. Figure 8.7(A) shows content performance as a function of PI on an absolute scale for both semesters. Here, all of the assignments lie clustered in the upper-right quadrant, suggesting a positive correlation between performance and positivity. We were also curious if the type of activity played a role in this correlation. Figure 8.7(B) examines more closely the homework-positivity cluster by color-coding each data point as a function of type of activity. Additionally, the week in which that activity was presented is given inside the data point. In analyzing Fig. 8.7(B), some trends in the activity types become apparent. For example, both scaffold activities place among the highest content scores, but there is a large separation in positivity between the two activities. In contrast, the thematic activities place among the lowest scores in terms of positivity but varied significantly in content performance. Simulations are positioned in the middle of the correlation



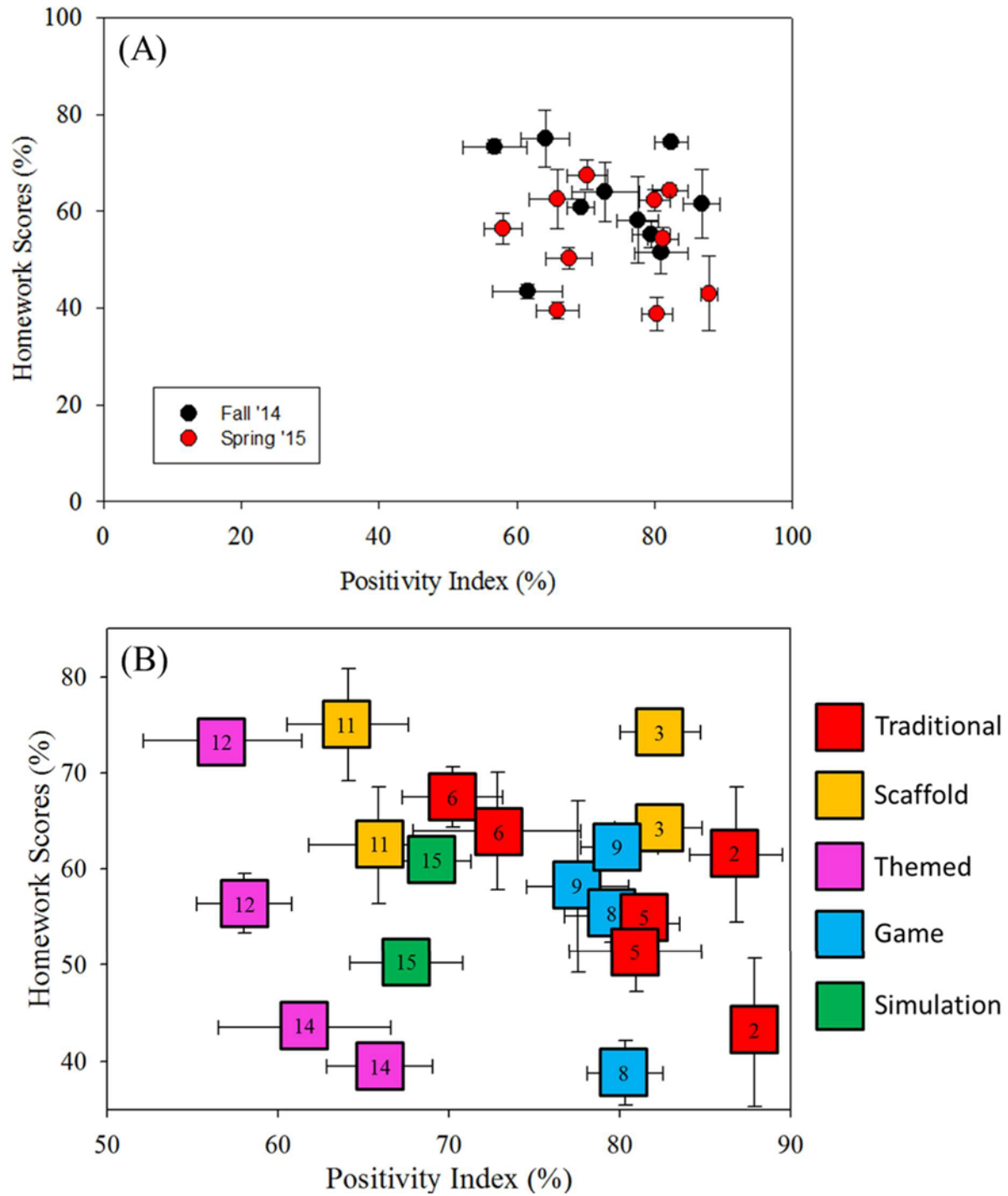


Figure 8.7 Homework scores as a function of PI for both semesters on (A) an absolute scale and (B) a truncated scale, color-coded by activity type and numbered by week.

chart for both semesters, in terms of both PI and homework performance. The games ranked closely together in terms of high positivity and average content scores, with one exception. Trends for traditional worksheets are perhaps difficult to judge, but the overall correlation for Weeks 5 and 6 are identical within error for both semesters. In addition, Week 2 yielded the highest overall PI in both semesters, although homework performance was varied. This higher positivity could, however, be attributed to this simply being the first activity of the semester. Indeed, we can potentially infer an impact of the progression of the semester, as there is a continuous decrease in PI from Week 2 to Week 6, before an increase upon implementation of the game activities. Starting at Weeks 8 and 9, the game activities, we again see a continuous decrease until Week 12, before another increase at the end of the semester. Additional possible inferences to be gleaned from these influences are discussed in more detail in Section 8.7.

### 8.7 Final Reflections from Students

During Week 16, finals week, the students were given one last survey that asked them to reflect upon their experiences in CHEM 111 and the recitation program in particular. Once again, these questions spanned both Likert-scale and free response, and covered topics such as “favorite/least favorite activity” and “most/least successful activity”. In addition, students were given questions virtually identical (modification was simply to verb tense to indicate past tense at the end of the semester) to A, B, and C from Section 8.5. Results from these questions, Fig. 8.8, provided comparative data for the students’ overall opinions from the beginning of the semester (Fig. 8.4) to the end (Fig. 8.8). This comparison reveals a significant increase in the number of negative responses from CHEM 111 students. Indeed, the average of positive responses for each question in the initial and final weeks for both semesters, the magnitude of this change in student perception can be determined. For Question A, in which students were asked about their interest

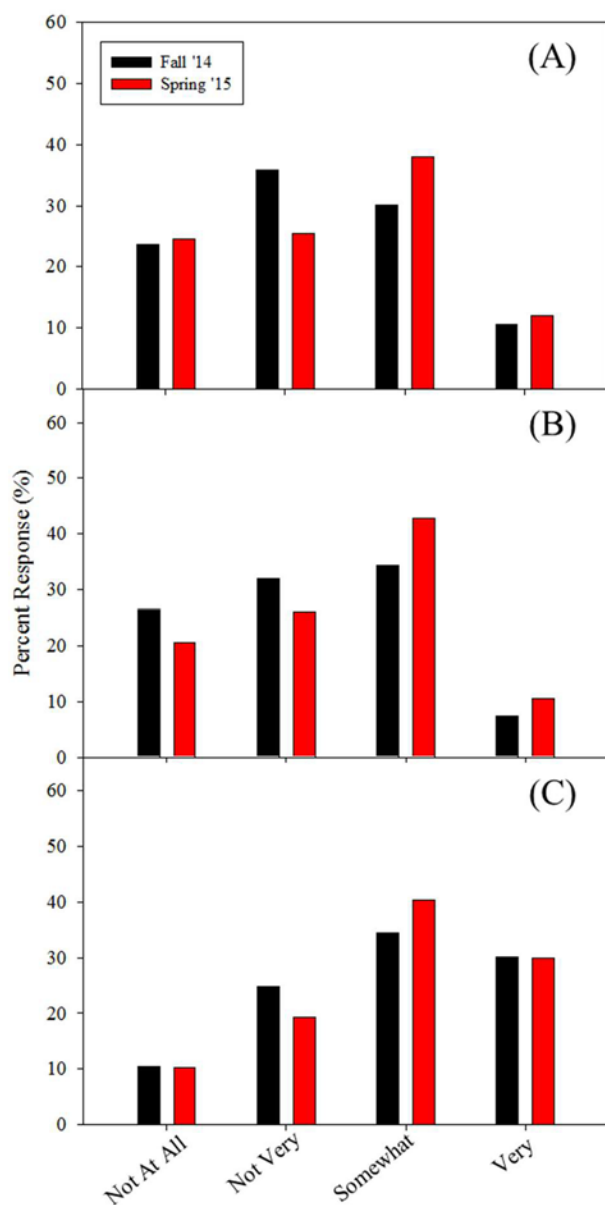


Figure 8.8 Percent of student responses to each of the four available answer categories for three different questions, when surveyed at the end of the semester. The questions posed in each of the two semesters studied were: (A) How interested are you in chemistry after completing the CHEM 111 course? (B) How important do you think recitation was to your understanding of the course material? (C) How important do you think CHEM 111 material will be to your desired career/major?

in the course material, the responses were  $81 \pm 5\%$  positive initially and  $45 \pm 7\%$  positive at the end. This means that nearly half of the students who reported an interest in chemistry at the beginning of the semester did not retain those feelings at the conclusion of the course. For Question C, which asked students to evaluate the importance of the coursework to their desired career, the initial positive responses were  $86 \pm 2\%$  and the final responses were  $67 \pm 4\%$  positive. This nearly 20% change suggests that a significant fraction of students who lost interest in chemistry, still recognized and valued the content as important to their academic and professional careers.

Perhaps the most relevant question to this research study arises from Question B. Here, students were asked to predict how important recitation was to their overall understanding of the course material at the beginning of the semester and then to evaluate its efficacy at the end of the semester. An average of  $95 \pm 2\%$  of students reported positively at the onset of the semester, but this number dropped to  $48 \pm 8\%$  during the final week. Thus, much like with the overall interest in chemistry, approximately half of the students felt as though the recitation component of the course did not meet their initial expectations. Although causal relationships for the shift in student attitude reported from the beginning of the semester to the end were not fully revealed, the data presented clearly illustrate a disconnect between student expectations and their perceptions of their experience in CHEM 111. Indeed, these data do not indicate that the recitation failed to help students, but it does suggest that although the majority expected recitation to be beneficial, in the end only half of them reported that it was. Note that within the CHEM 111 classroom, the vast majority of students reported an interest in chemistry and recitation in particular, and recognized the overall importance of the coursework to their desired

field of study. Regardless of the accuracy of these perceptions, students felt as though these expectations were not met and reported a loss of interest in chemistry as a whole.

These results must also be paired with the reported positivity from week-to-week, however, as the weekly PI of each activity was always greater than 50%. This means that the majority of students reported being interested and engaged by the activities they participated in on a week-to-week basis. In other words, they reported the overall success of the entire course lower than they reported the success of any individual activity within the course. Although the ability of the recitation activities to improve understanding is paramount to the students' opinions of the activities themselves, a low overall perception of recitation could negatively impact student participation and interest.

This is especially valuable data in light of literature evidence of the role that student expectations play in academic success. For example, Redish and coworkers report an observed degradation in student expectations over the length of an introductory college physics course.<sup>30</sup> This work also suggests that students at four-year liberal arts institutions report the highest classroom expectations, followed by those from large state universities, with those from two-year institutions falling below those. Additionally, work by Sander et al. highlights the importance of assessing student opinions within undergraduate courses and states: "Collecting and considering student expectations and preferences of teaching style could be an effective means of giving students a voice in course delivery and help focus course team discussion on teaching, learning and assessment."<sup>31</sup> In light of such evidence, it is imperative not only to acknowledge but also to address the data presented herein. Ultimately, if CSU students feel as though their expectations for the recitation component of general chemistry are not being met, this can significantly impact

not only their opinion of this specific course but also their opinion of chemistry, or more globally science, in general.

Apart from insight into student opinions and content performance, there are additional pieces of information that were collected from the final survey of the year. These data speak to student's ability to make predictions with respect to their experience in the course, which can provide context for some of their other responses. For example, students were asked in the initial and final surveys about the amount of time they expected to spend working on general chemistry outside of class each week and how much time they actually spent. Figure 8.9 highlights student response across both semesters, indicating that more students claimed they spent 0-3 hours/week on chemistry than those who originally predicted they would spend this amount of time. At the same time, fewer students reported spending 3 or more hours/week on chemistry than had originally predicted they would spend this amount of time. Ultimately, this shows that students over-predicted the amount of time they would spend on chemistry each week. Interestingly, the response of 3-6 hours/week was the most popular response at both the beginning and end of the semester across the entire academic year, with an average of 53% of students reporting to have invested that amount of time over the course of the semester. The largest shift from Week 1 to Week 16 for both semesters occurred within the 1-3 hours/week choice, which increased by 13% in the fall semester and 8% in the spring semester. This information is difficult to directly relate to academic success, but relationships exist between student performance and time spent on certain topics. For example, Tai and coworkers found that the amount of time spent on stoichiometry is positively correlated with student success in an introductory chemistry class.<sup>48</sup> Clearly, this is an area for further study. One possibility for future studies would be to ask students for the amount of time they spent on their chemistry course each week (i.e. more "in the

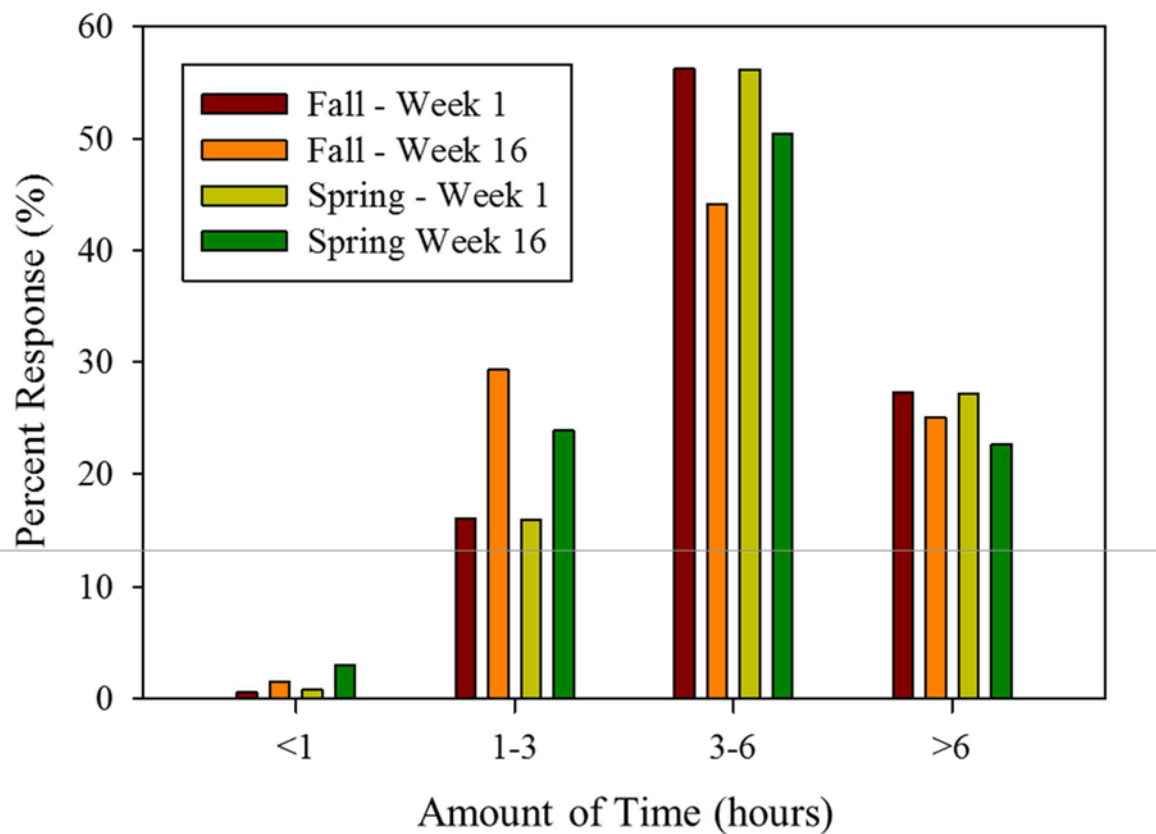


Figure 8.9 Student responses to the question “How many hours do you anticipate spending on chemistry outside of class each week?” (Week 1) and “How much time did you spend on chemistry outside of class each week?” (Week 16).

moment”) as well as asking how they spent that time (e.g. working problems, reading the text, etc.). These types of data could then potentially be correlated with performance on individual assignments and/or exams.

Another question asked of students at both the beginning and end of the semester required a prediction of their course letter grade. At the beginning of the semester, students clearly had no data from which to draw this prediction, whereas at the end of the semester, they had all of their grades from assignments and exams, with the exception of the final exam, upon which to base their prediction. Figure 8.10 shows a breakdown of percent responses for each letter grade during Weeks 1 and 16, as well as the actual grades that students received. In the first week of the semester, only 2 students total (both in Spring 2015) predicted earning a failing grade (D or F). This is perhaps to be expected, as we would at least hope that students do not enter the semester with an expectation of failing. Beyond simply receiving a passing grade, however, an average of 42.5% of students predicted earning an A and 49.1% predicted earning a B, with only 8.3% of students initially predicted earning a C for their final grade. This type of heavily weighted over-prediction is in keeping with results seen in other studies for general chemistry students at CSU.<sup>49</sup> In these studies, however, the focus was on a student’s ability to predict their exam grade immediately following completion of the exam itself. Still, the vast majority of students were found to over-predict their grades.

In the days before the final exam, students significantly alter their grade predictions, with only 12.9% predicting an A grade, 46.8% indicating they anticipated receiving a B grade and 35.6% predicting an overall grade of C (average across both semesters). This leaves 4.7% of students expecting to receive a D or F. Although this shift in grade predictions speaks to a reassessment of a likely outcome, presumably based on performance, these self-assessments are



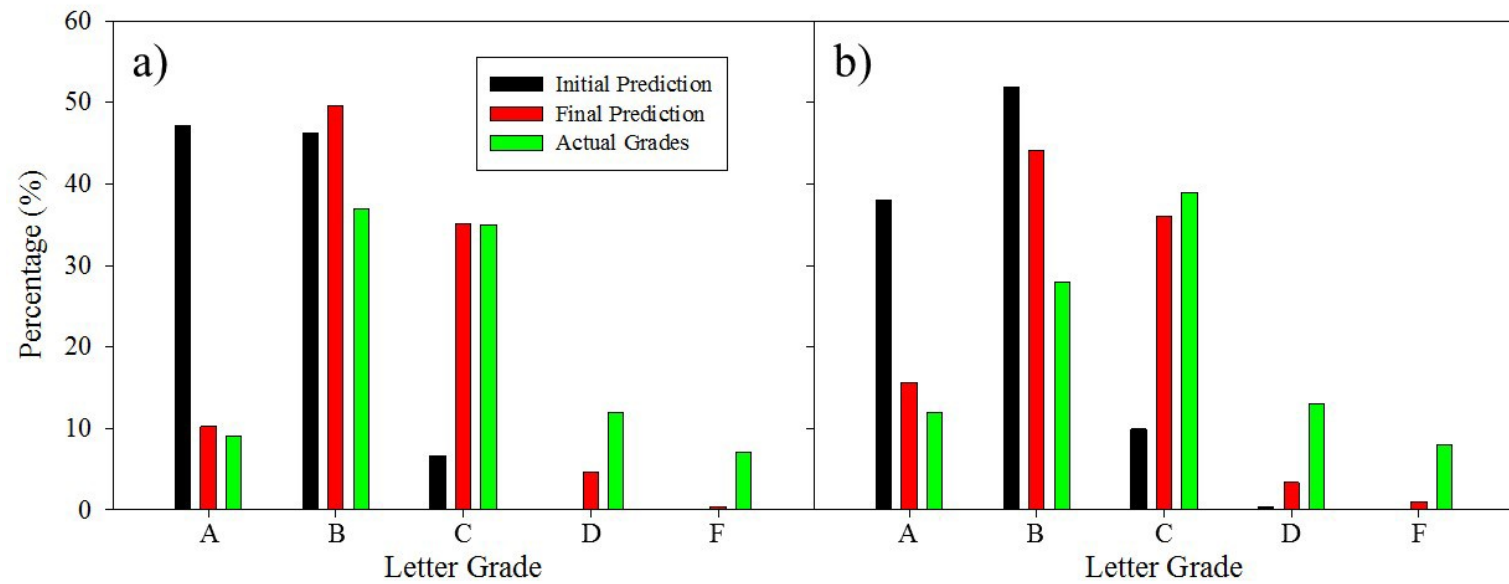


Figure 8.10 Student responses question “What grade do you expect to receive in this course?” when asked the first week of the course (black) and then again during finals week (red) for a) Fall 2015 and b) Spring 2015. The final column (green) represents the true grade breakdown after completion of the semester.

again somewhat over-confident. Indeed, the actual average grade breakdown across the academic year was: A – 10.5%; B – 32.5%; C – 37.0%; D – 12.5%; and F – 7.5%. Notably the final overall prediction for both A and C are within 2.5% of the actual grades assigned. There is, however, a chance that this statistic is purely coincidental as the final grade breakdown arises from ALL enrolled students, whether or not they consented to participate in this research study. Additionally, the students making predictions within the weekly homework surveys could easily change from Weeks 1-16, as participation is optional. Furthermore, these recorded responses are not linked to individual student names. Future work may attempt to refine these data so as to include only those data who consented and participated in both the initial and final surveys.

Nevertheless, this serves as an example of the shift in awareness of the CHEM 111 student body as the semester progresses. It is important, however, to acknowledge that this significant disconnect between initial expectations and final predictions, could play a role in the overall negative shift in student opinion. If they are becoming more aware of the likelihood that they will not achieve their initial goals, it is not unrealistic to assume that this has an overall negative impact on their impressions of the course.

Ultimately, this work serves as a starting point in the complete evaluation of the CHEM 111 recitation program at Colorado State University. It shows a strong positive attitude for students entering the classroom, while also demonstrating an overall positive experience for the students in both attitude and concept retention, Fig. 8.7(A). It also suggests that the type of activity in which students engage plays a role in both their attitude and classroom success, with scaffold activities providing higher average homework scores. An additional benefit to these scaffolded activities is that they provide more flexibility to course instructors, allowing them to tailor core assignments.

## 8.8 Preliminary Qualitative Analysis of Survey Data

To more adequately explore the nuances of this complex attitude/performance correlation, a number of steps could be taken with the data already collected as there is a multitude of insight that could be gleaned. For example, this work focused exclusively on the multiple choice questions recorded over two semesters. In addition to these data, an immense amount of short answer, qualitative data were also collected in the weekly surveys. Preliminary attempts were made to generate a coding system to numerically evaluate these free response answers. To do this, responses to a single short answer question (from a single week) were downloaded from SurveyMonkey® and assigned a numerical value corresponding to the order in which the answers were received. Using the random number generator found at [www.randomizer.org](http://www.randomizer.org), a set of 50 numbers was created and the corresponding responses were selected. Each of these 50 short answer responses was given 1-3 short code(s) intended to capture the most important aspects of the response. After this initial coding, another 50 numbers were randomly generated and the codes used in the previous set were used exclusively to code this second set of responses. Responses that could not be coded, because of either a lack of response or a self-reported absence on the day of the activity, were categorized as other. Once a final set of codes was generated, it was applied to the entire answer set, ensuring that all answers could be coded.

To test this methodology, we selected the survey question “What was your favorite aspect of this week’s activity?”, and a set of 10 codes were compiled. The codes were (1) activity, (2) group work, (3) practice, (4) learning, (5) enjoyment, (6) GTA involvement, (7) change in activity, (8) iClicker questions, (9) time commitment, and (10) other. Note that these are simplified codes, meaning that they attempt to capture a potentially complex response with just a

few key words. For example, the code activity was used when a student reported that their favorite aspect of the week's recitation was a particular component of the activity itself, whereas the code enjoyment was used when students reported that they had fun completing the activity. These codes were then applied to the responses for five different weeks in the Fall 2014 semester, with each style of activity represented. Figure 8.11 shows the frequency of three key codes across those five weeks. These particular codes were included as they address both attitude and efficacy, as reported earlier. In Week 3, a scaffold activity, the greatest number of students report that their favorite aspect of the activity was getting to do practice problems (or practicing a particular skill) and feeling as though they learned something while completing the activity. A much smaller number of students, however, reported enjoying the activity. By comparison, in Week 8, students participated in one of the game activities. Here we see a significant increase in the number of students who reported their favorite aspect being the enjoyment they received from the activity, and the codes learn and practice appear less often. Such efforts in coding present the potential for significantly increased understanding as well as improved efforts to correlate student opinions and outcomes. There are, however, many inherent challenges in this qualitative analysis as well. For example, coding should be independently verified by multiple coders to ensure a strong agreement between the attributions of a code to a particular response. This also reduces the chance of researcher bias in the coding process. Indeed, efforts were made to verify codes by two different researchers with the data presented in Fig. 8.11. These efforts resulted in a 94.6% correlation between the two researchers, indicating a high level of validity in the coding system.

One complicating factor in performing the coding work was the changes that appeared in both the content questions and activities between the two semesters. Indeed, slight modifications

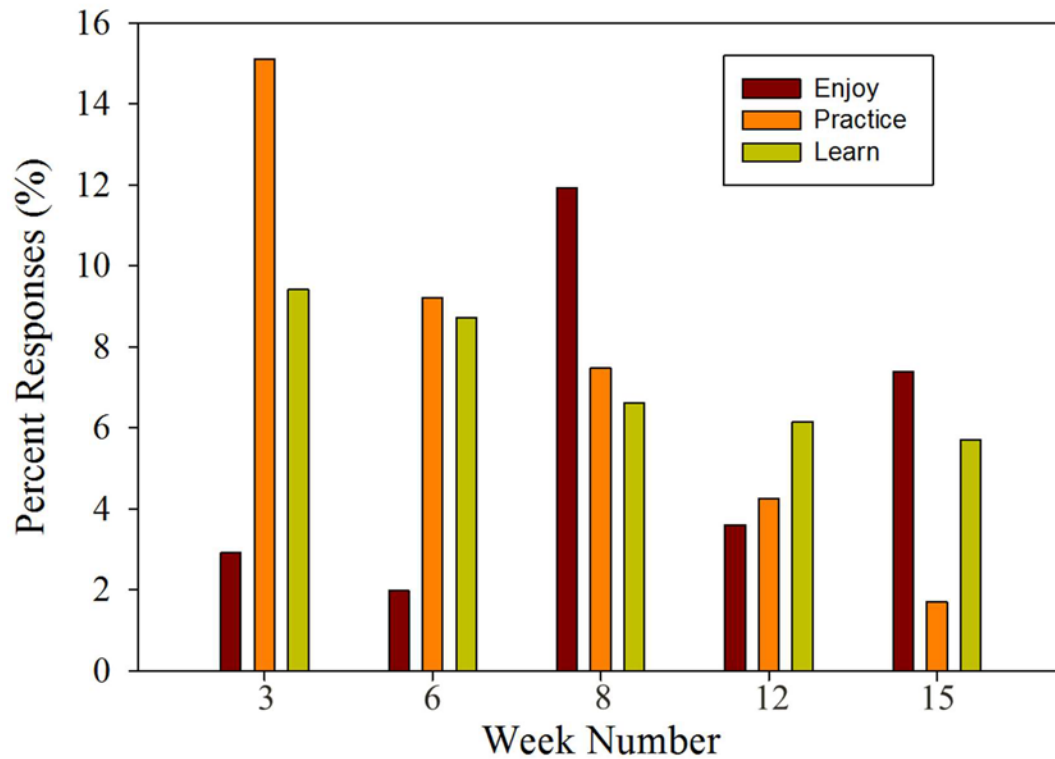


Figure 8.11 Preliminary results from the coding of a free response question (“What was your favorite aspect of this week’s activity?”) in the Fall 2014 semester. The weeks chosen represent one week of each activity style, and percent responses shown correspond to 3 of the 10 codes used to analyze responses.

were made in several areas between the two semesters, potentially skewing responses and our ability to interpret the qualitative data. Responses for each short answer question were collected during each week of the entire academic year and could be coded at a later date, if so desired. Such efforts may yield interesting trends in the favorite and least favorite activities of the students, as well as insight into their shifting opinions and attitudes. Attributing some causality in those trends may be difficult because of the changes present between the semesters. A decrease in the number of altered variables would potentially provide more meaningful analysis. Identical content questions, activities, and comparable student populations would be especially valuable. For example, the fall semester course contains a majority of first-semester freshman, whereas the spring semester course is populated with a greater number of upper classmen and students repeating the course; thus, maintaining some continuity (and/or being able to appropriately account for variations) with respect to student population could prove beneficial. In conclusion, although comparisons made using numerical positivity data can yield valuable insight, the individual components elucidated from free response questions may vary significantly as a result of the composition of the enrolled student populous.

## 8.9 Summary and Future Directions

The work presented in this chapter arose from an effort to evaluate the effectiveness of general chemistry recitation at Colorado State. With a significant amount of turnover in course instructors and recitation GTAs, the recitation program became an area for potential curricular development activities. In many ways, these initial efforts to focus on the recitation program evolved into a greater analysis of student attitudes. Indeed, the shifting attitude observed in this work were not the initial focus of this study, but instead opened an unexpected avenue of

investigation. That being said, there are many opportunities for continued study, both in evaluating the efficacy of recitation and in determining its role in student opinions.

Any efforts to expand further upon this work will require some concerted efforts, the paramount of which is arguably to maintain as much consistency from this study to the next as possible. For example, with identical content questions, activities, code submissions, and semester schedules there is the potential for even more interpretation than given here. Indeed, the placement of a particular week's activity relative to a holiday weekend could play a role in student success or interest, as could the age and college experience of the students participating in those activities. For instance, perhaps upper classmen are more interested and engaged in games than their younger counterparts or vice versa. Such questions could be the focus of continued work, allowing for significant expansion and extrapolation of the data and analysis shown here.

Additionally, there could be greater insight gained by presenting multiple recitation sections with different styles of activities. For example, to investigate the efficacy of games compared to scaffold worksheets, it may be beneficial to generate one activity of each style on a particular topic. This would allow results from individual sections in a given semester to be compared with one another. Such efforts, however, require multiple different activities to be generated each week. Moreover, some concepts are better suited to a particular activity style than others. Lastly, there is the issue of fairness and equity, as some students may view having to participate in one activity over another to be a hindrance or disadvantage to their learning. This could potentially be addressed by collecting data over an entire semester that is focused on one particular activity style and then a subsequent semester for another. From the qualitative analysis discussed above, some students reported that the change in the style of activity was their

favorite aspect of a particular week. Indeed, a decrease in student engagement may occur if the style of activity remains a constant over the entirety of a semester, as many researchers have investigated the link between academic boredom and poor student performance.<sup>50-54</sup> Another interesting approach could be to have exam responses included within the IRB protocol. By doing so, exam questions could be attributed to particular concepts and longer-term retention could be investigated, as opposed to the current method of only a few days.

Ultimately, the work presented herein shows a series of interesting trends and raises several additional questions to be explored regarding CHEM 111 recitation activities. Investigating any number of them may provide valuable insight into the interplay between student interest and positive learning outcomes within the CHEM 111 recitation program, as well as chemistry recitation programs in general. Such efforts, however, will require a strong buy-in from the course instructors or need to be performed by the instructors themselves because many of the suggested future studies would require significant control over the recitation program from semester to semester. Indeed, feedback gained through such research can present new opportunities and ideas for instruction as well as minor edits or approaches designed to improve the student experience. These subtle changes, however, may impact student responses and performance and would need to be minimized as much as possible, especially in longitudinal studies. The culmination of such work could lead to significantly tailored recitation activities and implementation styles, and by more adequately exploring the role recitation and the activities performed play in student learning, a program can be developed which will hopefully maximize student success and more effectively meet the initial expectations of the students themselves.



## REFERENCES

1. Hoetker, J.; Ahlbrand Jr, W. P., The Persistence of the Recitation. *American Educational Research Journal* 1969, 145-167.
2. Stodolsky, S. S.; Ferguson, T. L.; Wimpelberg, K., The Recitation Persists, but What Does it Look Like? *Journal of Curriculum Studies* 1981, 13 (2), 121-130.
3. Husband, R. W., A Statistical Comparison of the Efficacy of Large Lecture Versus Smaller Recitation Sections Upon Achievement in General Psychology. *The Journal of Psychology* 1951, 31 (2), 297-300.
4. Lodish, H. F.; Rodriguez, R. K., Points of View: Lectures: Can't Learn with Them, Can't Learn without Them: A Combination of Lectures, Problem Sets, and Recitation Sections Is an Excellent Way To Teach Undergraduate Cell Biology at a High Level. *Cell Biology Education* 2004, 3 (4), 202-204.
5. Lyle, K. S.; Robinson, W. R., A Statistical Evaluation: Peer-Led Team Learning in an Organic Chemistry Course. *Journal of Chemical Education* 2003, 80 (2), 132.
6. Mahalingam, M.; Schaefer, F.; Morlino, E., Promoting Student Learning through Group Problem Solving in General Chemistry Recitations. *Journal of Chemical Education* 2008, 85 (11), 1577.
7. Stock, W. A.; Ward, K.; Folsom, J.; Borrenpohl, T.; Mumford, S.; Pershin, Z.; Carriere, D.; Smart, H., Cheap and Effective: The Impact of Student-Led Recitation Classes on Learning Outcomes in Introductory Economics. *The Journal of Economic Education* 2013, 44 (1), 1-16.
8. Watt, J. X.; Feldhaus, C. R.; Sorge, B. H.; Fore, G. A.; Gavrin, A. D.; Marrs, K. A., The Effects of Implementing Recitation Activities on Success Rates in a College Calculus Course. *Journal of the Scholarship of Teaching and Learning* 2014, 14 (4), 1-17.
9. Gosser, D. K.; Roth, V., The Workshop Chemistry Project: Peer-Led Team-Learning. *Journal of Chemical Education* 1998, 75 (2), 185.
10. Hockings, S. C.; DeAngelis, K. J.; Frey, R. F., Peer-Led Team Learning in General Chemistry: Implementation and Evaluation. *Journal of Chemical Education* 2008, 85 (7), 990.
11. Huynh, K. P.; Jacho-Chávez, D. T.; Self, J. K., The Efficacy of Collaborative Learning Recitation Sessions on Student Outcomes. *American Economic Review* 2010, 100 (2).
12. Warfa, A.-R. M., Using Cooperative Learning to Teach Chemistry: A Meta-analytic Review. *Journal of Chemical Education* 2016, 93 (2), 248-255.
13. Gall, M. D.; Ward, B. A.; Berliner, D. C.; Cahen, L. S.; Winne, P. H.; Elashoff, J. D.; Stanton, G. C., Effects of Questioning Techniques and Recitation on Student Learning. *American Educational Research Journal* 1978, 15 (2), 175-199.
14. Nystrand, M.; Gamoran, A., Student Engagement: When Recitation Becomes Conversation. ERIC 1990.
15. Paulsen, M. B.; Smart, J. C., *Higher Education: Handbook of Theory and Research*. Springer: 2013.
16. Gall, M. D. In *Effects of Teaching by Recitation on Learning*, Annual Meeting of the American Psychological Association 1975.
17. McCormick, N. J.; Clark, L. M.; Raines, J. M., Engaging Students in Critical Thinking and Problem Solving: A Brief Review of the Literature. *Journal of Studies in Education* 2015, 5 (4), 100-113.

18. Webster, T. J.; Hooper, L., Supplemental Instruction for Introductory Chemistry Courses: A Preliminary Investigation. *Journal of Chemical Education* 1998, 75 (3), 328.
19. Johnson, D. W.; Johnson, R. T., *Learning Together and Alone: Cooperative, Competitive, and Individualistic Learning*. Prentice-Hall, Inc: 1987.
20. Johnson, D. W.; Johnson, R. T., *Cooperation and Competition: Theory and Research*. Interaction Book Company: 1989.
21. Johnson, D. W.; Johnson, R. T.; Smith, K. A., *Active Learning: Cooperation in the College Classroom*. ERIC: 1998.
22. Johnson, R. T.; Johnson, D. W., Cooperative Learning in the Science Classroom. *Science and Children* 1986, 24, 31-32.
23. Bowen, C. W., A Quantitative Literature Review of Cooperative Learning Effects on High School and College Chemistry Achievement. *Journal of Chemical Education* 2000, 77 (1), 116.
24. Totten, S., *Cooperative Learning: A Guide to Research*. Garland: New York, 1991.
25. Bergin, D. A., Influences on Classroom Interest. *Educational Psychologist* 1999, 34 (2), 87-98.
26. Berg, C.; R., A., Factors Related to Observed Attitude Change Toward Learning Chemistry Among University Students. *Chemistry Education Research and Practice* 2005, 6 (1), 1-18.
27. Dalgety, J.; Coll, R. K.; Jones, A., Development of Chemistry Attitudes and Experiences Questionnaire (CAEQ). *Journal of Research in Science Teaching* 2003, 40 (7), 649-668.
28. Dougherty, R. C.; Bowen, C. W.; Berger, T.; Rees, W.; Mellon, E. K.; Pulliam, E., Cooperative Learning and Enhanced Communication: Effects on Student Performance, Retention, and Attitudes in General Chemistry. *Journal of Chemical Education* 1995, 72 (9), 793.
29. Pintrich, P. R., A Motivational Science Perspective on the Role of Student Motivation in Learning and Teaching Contexts. *Journal of Educational Psychology* 2003, 95 (4), 667.
30. Redish, E. F.; Saul, J. M.; Steinberg, R. N., Student Expectations in Introductory Physics. *American Journal of Physics* 1998, 66 (3), 212-224.
31. Sander, P.; Stevenson, K.; King, M.; Coates, D., University Students' Expectations of Teaching. *Studies in Higher Education* 2000, 25 (3), 309-323.
32. Singh, K.; Granville, M.; Dika, S., Mathematics and Science Achievement: Effects of Motivation, Interest, and Academic Engagement. *Journal of Educational Research* 2002, 95 (6), 323-332.
33. Smith, K. A.; Sheppard, S. D.; Johnson, D. W.; Johnson, R. T., Pedagogies of Engagement: Classroom-Based Practices. *Journal of Engineering Education* 2005, 94 (1), 87-101.
34. Lent, R. W.; Brown, S. D.; Larkin, K. C., Relation of Self-Efficacy Expectations to Academic Achievement and Persistence. *Journal of Counseling Psychology* 1984, 31 (3), 356.
35. Ainley, M.; Hidi, S.; Berndorff, D., Interest, Learning, and the Psychological Processes that Mediate their Relationship. *Journal of Educational Psychology* 2002, 94 (3), 545-561.
36. Perkins, K.; Adams, W.; Dubson, M.; Finkelstein, N.; Reid, S.; Wieman, C.; LeMaster, R., PhET: Interactive Simulations for Teaching and Learning Physics. *The Physics Teacher* 2006, 44 (1), 18-23.
37. Adams, W. K., Student Engagement and Learning with PhET Interactive Simulations. *Il Nuovo Cimento C* 2010, 33 (3), 21-32.

38. Wieman, C. E.; Adams, W. K.; Perkins, K. K., PhET: Simulations that Enhance Learning. *Science* 2008, 322 (5902), 682-683.
39. De Jong, T., Scaffolds for Scientific Discovery Learning. *Handling Complexity in Learning Environments: Theory and Research* 2006, 107-128.
40. Ge, X.; Yamashiro, K. A.; Lee, J., Pre-Class Planning to Scaffold Students for Online Collaborative Learning Activities. *Educational Technology & Society* 2000, 3 (3), 159-168.
41. Hmelo-Silver, C. E.; Duncan, R. G.; Chinn, C. A., Scaffolding and Achievement in Problem-Based and Inquiry Learning: A Response to Kirschner, Sweller, and Clark. *Educational Psychologist* 2007, 42 (2), 99-107.
42. McNeill, K. L.; Lizotte, D. J.; Krajcik, J.; Marx, R. W., Supporting Students' Construction of Scientific Explanations by Fading Scaffolds in Instructional Materials. *The Journal of the Learning Sciences* 2006, 15 (2), 153-191.
43. Molenaar, I.; van Boxtel, C. A. M.; Slegers, P. J. C., Metacognitive Scaffolding in an Innovative Learning Arrangement. *Instructional Science* 2011, 39 (6), 785-803.
44. Pata, K.; Sarapuu, T., Framework for Scaffolding the Development of Problem Representations by Collaborative Design. In *Designing for Change in Networked Learning Environments*, Springer: 2003; pp 189-198.
45. Gabel, D.; Sherwood, R. D., Analyzing Difficulties with Mole-Concept Tasks by Using Familiar Analog Tasks. *Journal of Research in Science Teaching* 1984, 21 (8), 843-851.
46. Nurrenbern, S. C. *Problem Solving Behaviors of Concrete and Formal Operational High School Chemistry Students when Solving Chemistry Problems Requiring Piagetian Formal Reasoning Skills*. Purdue University, 1979.
47. Yalcinalp, S.; Geban, Ö.; Özkan, I., Effectiveness of Using Computer-Assisted Supplementary Instruction for Teaching the Mole Concept. *Journal of Research in Science Teaching* 1995, 32 (10), 1083-1095.
48. Tai, R. H.; Sadler, P. M.; Loehr, J. F., Factors Influencing Success in Introductory College Chemistry. *Journal of Research in Science Teaching* 2005, 42 (9), 987-1012.
49. Hawker, M. J.; Dysleski, L.; Rickey, D., Investigating General Chemistry Students' Metacognitive Monitoring of Their Exam Performance by Measuring Postdiction Accuracies Over Time. *Journal of Chemical Education* 2016, 93 (5), 832-840.
50. Acee, T. W.; Kim, H.; Kim, H. J.; Kim, J.-I.; Chu, H.-N. R.; Kim, M.; Cho, Y.; Wicker, F. W., Academic Boredom in Under- and Over-Challenging Situations. *Contemporary Educational Psychology* 2010, 35 (1), 17-27.
51. Schutz, P. A.; DeCuir, J. T., Inquiry on Emotions in Education. *Educational Psychologist* 2002, 37 (2), 125-134.
52. Eren, A.; Coskun, H., Students' Level of Boredom, Boredom Coping Strategies, Epistemic Curiosity, and Graded Performance. *The Journal of Educational Research* 2016, 109 (6), 574-588.
53. Fulmer, S. M.; D'Mello, S. K.; Strain, A.; Graesser, A. C., Interest-Based Text Preference Moderates the Effect of Text Difficulty on Engagement and Learning. *Contemporary Educational Psychology* 2015, 41, 98-110.
54. Obergruesser, S.; Stoeger, H., The Role of Emotions, Motivation, and Learning Behavior in Underachievement and Results of an Intervention. *High Ability Studies* 2015, 26 (1), 167-190.

## APPENDIX A

### INDEPENDENT RESEARCH PROPOSAL

This appendix contains the entirety of the independent research proposal, entitled Advanced Density Functional Theory Calculations for Improved Modeling of Plasma-Catalytic Waste Gas Remediation, prepared by Joshua M. Blechle in fulfillment of the doctoral requirements of the Department of Chemistry at Colorado State University. It provides discussion of the utilization of computational methods to improve our understanding of the mechanisms involved in plasma-assisted exhaust control. The proposed study serves as a melding of undergraduate and graduate research interests, with Figs. A.4 and A.5 representing work completed by the author in the laboratory of Dr. Eric V. Patterson at Truman State University.

#### A.1 Abstract

A fundamental understanding of energetic gas-surface reactions is integral to further exploring the utility of plasma processing for a variety of applications, one of which is the use of plasma-catalytic systems for waste gas remediation. Although these systems show promise for being more effective than traditional gas treatments, such as three-way catalytic converters, optimization and reproducibility have not been achieved. The primary reason for these difficulties is a lack of knowledge of the chemistry occurring at the catalytic surface, including mechanisms and thermodynamics. However, thanks to improvements in plasma diagnostics and computational methods, there is now the potential to use density functional theory (DFT) to effectively explore the gas-surface mechanisms that drive these systems. In this proposal, nitric

oxide molecules and platinum surfaces will serve as model systems for exploring gas conversion. Using a combination of time-dependent DFT methods, the gas and surface geometries will be determined independently. Then, using atom-centered density matrix propagation, the multi-dimensional potential energy surface will be simulated. This technique will allow for elucidation of all possible reactions (and associated probabilities) that are available within a range of experimentally-derived system energies. Such results would help correlate system energetics and successful gas conversion, ultimately allowing for improved optimization of plasma-catalytic systems. Achieving a fundamental understanding of gas-surface reactivity represents a major step forward in evaluating the potential effectiveness of these systems in an industrial remediation setting. environments.

## A.2 Background and Significance

For over two decades, scientists have been studying the environmental impact of using low-temperature plasmas (LTPs) for waste gas remediation.<sup>1-3</sup> There has been strong debate over both the viability and efficacy of LTPs in an applied setting, with one of the more promising methods being plasma catalysis.<sup>4-6</sup> This dual-technique system has been studied extensively, especially for nitrogen oxides ( $N_xO_y$ ) formed in combustion processes.<sup>7-9</sup> Indeed, plasma catalytic systems have been shown to be a highly effective remediation tool relative to current exhaust treatment methods, especially in successfully converting  $N_xO_y$  species to  $N_2$  and  $O_2$  products, Fig. A.1. This is commonly attributed to the plasma's ability to aid in precursor decomposition, essentially helping to drive the conversion reactions toward completion. However, due to the complex chemical nature of LTPs, a fundamental understanding of these systems is limited. In addition, not much is known about the gas-surface reactions occurring on

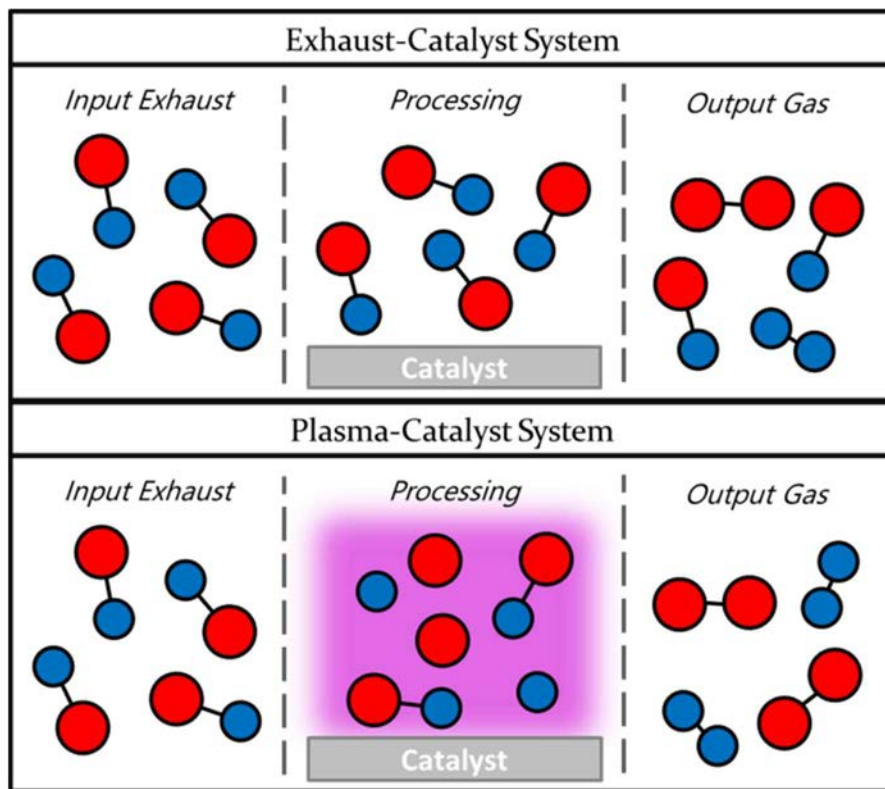


Figure A.1 Representation of current exhaust-catalysis systems (top) compared to plasma-catalysis systems (bottom) that show improved conversion.

the catalyst surface. As such, plasma-catalytic systems have not achieved a high degree of implementation. The unpredictability of exhaust gas composition, the variability in the energetics between different plasma systems, and the vast array of potential catalytic surfaces makes a comprehensive assessment of this technique difficult.

To address this expansive parameter space and the complexity of each component therein, efforts must be made to establish a fundamental understanding of the chemistry occurring within these systems. One way to approach this problem is through the use of plasma diagnostics, techniques designed to provide species identification and energetic information about the plasma itself.<sup>10-16</sup> Alternatively, theoretical simulations of the gas-surface interface can help establish mechanisms and reactivities.<sup>17-24</sup> Such work exists in multiple forms for plasma catalytic systems, but little is done to bridge the gap between these disparate approaches.<sup>25-27</sup>

### A.3 Specific Aims

The proposed work focuses on utilizing plasma modelling which can be further enhanced by the work of experimentally determined system energies to determine the gas-surface reactions present within LTP systems, Fig A.2. The specific aims of this work include:

- Aim A: Develop a calculation-based approach to modeling molecule-surface interactions in LTPs, specifically the interactions of NO with Pt surfaces,
- Aim B: Derive thermodynamic data for NO-Pt reactions, and
- Aim C: Extrapolate results from the NO-Pt system to other molecules and catalytic surfaces of interest to plasma-catalytic removal of atmospheric pollutants.

These aims will be achieved through the exploration of a series of calculations, utilizing the following specific objectives/tasks (which address the above specific aims as indicated):

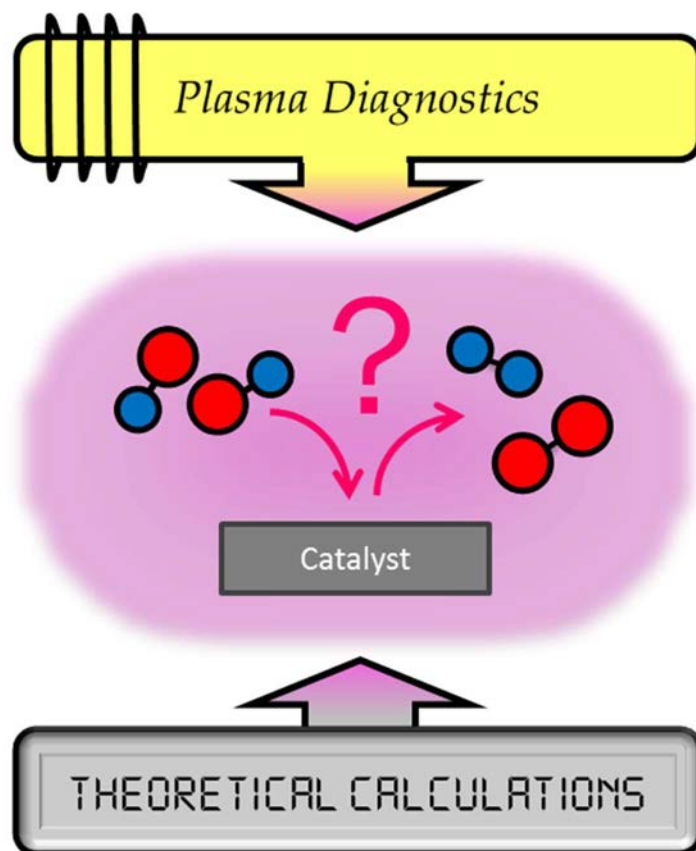


Figure A.2 Concept of proposed work. Utilizing theoretical calculations, enhanced with plasma diagnostics, to investigate the gas-surface interactions of NO.



1. Optimize both ground and excited state geometries of the NO molecule using multi-reference configuration interaction (MC-CI) and time-dependent density functional theory (TD-DFT) to properly capture valence orbital occupation (Aim A).
2. Optimize the platinum surface geometry using iterative DFT calculations (Aim A).
3. Apply energy correction models (based off experimental results) to the NO molecule to reproduce plasma conditions (Aims A and B).
4. Utilize DFT calculations to find the optimized gas-surface transition state for the reaction of NO with platinum (Aims A and B).
5. From the optimized, energy-corrected transition state, apply atom-centered density matrix propagation (ADMP) calculations to determine the multi-dimensional potential energy surface (MD-PES) for a range of kinetic trajectories of NO (Aims B and C).

Through this methodology, we can derive a host of possible NO-platinum reactions and the thermodynamic conditions required for each of them. Such work would provide unparalleled insight into the reactivity of NO within a plasma-catalytic system, and could serve as a template for proper tuning of LTP systems to achieve a more complete and reliable gas phase conversion of NO. Indeed, the proposed work is the necessary first step for adequately exploring and understanding more complex exhaust gas systems. Proper evaluation of the efficacy of plasma-catalytic systems for waste gas remediation cannot be achieved without a fundamental understanding of the possible surface-mediated mechanisms and the role of the plasma's diverse energetic environment on those reactions..

## A.4 Design and Methods

### (1) Optimize both ground and excited state geometries of the NO molecule

Here, calculations focus on the electronic structure of NO and its direct excitation profile. While LTP systems are dominated by neutral species, they can span a large range of electronic states. Indeed, excitation of NO is a primary reaction within NO plasma systems, and as such, it is important to adequately characterize these excited-state species as well. The proposed work will be completed in Gaussian 09, as the program comes with desired density functionals and basis sets<sup>28</sup>. To begin, the NO ground state can be optimized utilizing the aug-cc-pVTZ basis set and the APFD density functional. The aug- prefix corresponds to augmented (or diffuse) functions, whereas cc-pVTZ describes Dunning's correlation consistent triple-zeta functions that are designed to simulate the 3s, 2p, 1d, 4s, 3p, 2d, and 1f valence orbitals.<sup>29</sup> The APFD refers to the Austin-Peterson-Frisch function with dispersion forces, which has been shown to avoid generating inaccurate long-range interactive forces that exist within many DFT models. This feature of the calculations will become extremely important when the surface is added to the simulation.<sup>30</sup> This combination of functional and basis set has been shown to effectively model N and O systems to provide an accurate geometry that can be used for the transition state determination. Subsequent natural transition orbital determinations can also be performed using APFD/aug-cc-pVTZ. An example is shown in Fig. A.3, which depicts the different orbital geometries associated with an electron excited from the  $2\pi$  orbital in the NO ground state to a large 3s-like orbital in the  $2\Sigma$  state (lowest excited state). The  $2\Sigma$  state is best described as the CO triple bond electronic configuration of  $\text{NO}^+$  with the remaining electron in a 3s Rydberg orbital. The energy of the  $2\Sigma$  state (5.45 eV) and the relatively low ionization potential of NO (9.26 eV) suggests a nearly 4 eV energy range for valence excitations, easily covered within an LTP system. Proposed electronic structure calculations will explore the role of NO formation

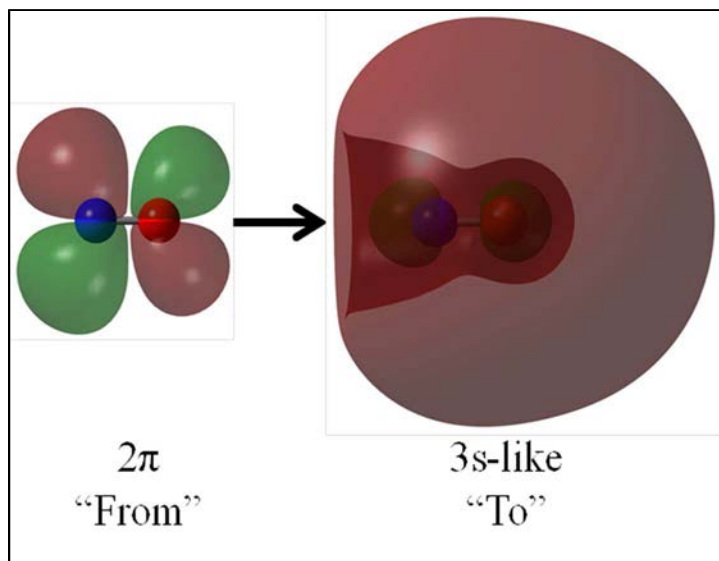


Figure A.3 TD-DFT representation of the natural transition orbitals for excitation of NO from the ground state  $2\pi$  orbital (“From”) to a large 3s-like orbital (“To”).

mechanisms within LTPs. Electronic structure theory (MR-CI and TD-DFT, aug-cc-pVTZ basis) calculations will be used to characterize the excitation profile for NO formed from NO plasma systems, and this work can be expanded to cover N<sub>2</sub>O, N<sub>2</sub>/O<sub>2</sub>, and more complex “exhaust-like” precursor systems (e.g. N<sub>2</sub>/O<sub>2</sub>/H<sub>2</sub>O/CH<sub>4</sub>).

## (2) Optimize the platinum surface geometry

Structure optimizations have been achieved with a variety of catalytic surfaces using DFT methods.<sup>23, 31-34</sup> The advantage of DFT over the more common molecular dynamics (MD) calculations is the computational efficiency and accuracy, but the drawback is that DFT systems are generally limited to systems of only ~100 atoms. Thus, it can be difficult to adequately express both bulk and surface properties. However, Santarossa and coworkers have shown that it is possible to address this issue by optimizing a 108-Pt atom surface and replicating this structure along the three Cartesian axes until a 864-Pt atom lattice is generated.<sup>35</sup> This work suggests that we will be able to successfully computationally optimize a platinum surface, thereby providing a platform from which we can further our NO studies. As such, a similar approach to that of Santarossa is proposed here using methods contained in the Gaussian 09 interface.

Initially, the LanL2DZ basis set will be used. This basis set builds on the Dunning’s correlation consistent functions (used in the NO optimizations) and includes the Los Alamos effective core potentials, which are intended for elements in the 6<sup>th</sup> period.<sup>36</sup> To improve computational efficiency, the 108-Pt atom surface can be optimized at lower levels of theory, such as B3LYP. The output from this file can then be used as the starting geometry for subsequent optimizations, until a geometry can be achieved at the APFD functional (to match the NO and NO\* structures). As a result, this combination of basis sets and theory will allow for consistency across individual calculations, while still accounting for the increased electron interactions found in the platinum atom. In addition, as the unit cell of the platinum structure

increases, it may be necessary to take into account the computational cost of the iterative optimizations, especially considering future calculations. To complete the entirety of this work, it may be necessary to limit the overall size of the unit cell significantly. It is also important to note that the optimizations described have been performed under similar levels of theory as discussed in the literature and can therefore be verified for consistency. The rest of the proposed work, however, will rely heavily on a combination of various approaches that have yet to be applied in the manner proposed herein and necessary to effectively achieve the overall aims of the project.

### (3) Apply energy correction models

Diagnostic efforts to explore the internal temperatures of plasma-catalytic systems are of increasing interest.<sup>10-16</sup> In particular, recent work has demonstrated the increase in vibrational excitation with LTP systems, especially relative to the quenching of rotational states (hence LTPs often being described as a non-equilibrium state). Efforts to characterize the energy partitioning of NO within LTPs are virtually non-existent in the literature, but comparisons can be made to other systems. First, van Gessel and coworkers studied energies of NO within atmospheric pressure plasmas (which are not generally considered LTPs), finding rotational and gas temperatures approaching ~10,000 K.<sup>37</sup> These temperatures dropped sharply as distance from the ignition site of the plasma increased, demonstrating a gradient effect to the energy. A similar trend (albeit with lower temperatures) has been seen in a variety of LTP systems, which are more directly applicable to the work proposed herein. One example, by Rahman et al. describes the spatial and temporal resolution of a hydrogen LTP system.<sup>38</sup> This work reports gas temperatures of the LTP ranging from 300-700 K as a function of distance from ignition region and time from ignition. Such work, as well as the efforts of Biloiu et al. using N<sub>2</sub> LTPs, provides a basis for energy corrections within the given simulations.<sup>39</sup> Although TD-DFT calculations

can provide insight into electrical properties of the system (and therefore electronic excitation), it is necessary for the calculations to take place at  $T = 0$  K. Thus, the use of ab initio methods must be employed to account for more realistic plasma temperatures.<sup>40</sup>

One of the complicating factors to this approach, however, is not only the elevated temperature but the change in state. Average ab initio calculations assume reactions occur in the gas phase, but the impact of state can be dramatic. As an example, Fig. A.4 shows the difference in energy for an identical reaction taking place in gas and aqueous phases. In this example, solvation is achieved through the use of the integral equation formalism of the polarizable continuum model (IEF-PCM). This formulation surrounds independent atoms with a sphere of dielectric charge equal to that of water, thus approximating solvation of each atom. Such processes have been shown to have a high degree of agreement with experimental results, suggesting that a similar approach would be ideal for our LTP system. Indeed, there are many different plasma continuum models available; however, none appear within the Gaussian program.<sup>41-45</sup> This is inconvenient because Gaussian is ideal for future ADMP calculations. Thus, the optimized NO and NO\* structures from the TD-DFT calculations must be moved to another computational package (such as COMSOL) for this step in the process. The goal will be to optimize structures using a magnetohydrodynamics (MHD) continuum model, in which the plasma is simulated by treating individual molecules as though they were an electrically-conducting liquid in the presence of magnetic fields.<sup>46-48</sup> This will generate a new optimized structure that reflects the increased energy and electrical properties of the LTP. Such a structure will improve upon the original gas-phase structures from Step 1, and allow for a more accurate reaction to be modeled in the tasks described below.

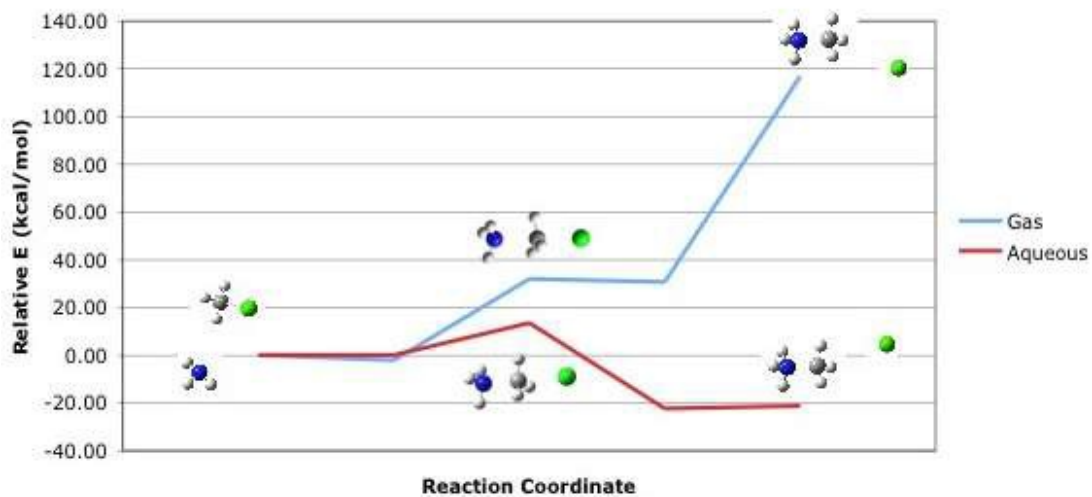


Figure A.4 Two PESs derived using ab initio calculations for the reaction of  $\text{NH}_3$  and  $\text{CH}_3\text{Cl}$ . This representative data demonstrates the impact of phase simulation in reaction energetics.

. The next step will be to consider that many waste gas remediation systems utilize post-plasma catalysis, which means that the surface is placed some distance downstream of the plasma ignition. This is important because at some distance from the ignition source there will be a transition between plasma and gas phases. Therefore, it is not an unreasonable assumption to think of the surface as interacting with plasma molecules within the gas phase. Thus, for the purposes of simplifying these calculations, the exact chemistry of the catalytic reactions can be investigated through plasma-state geometries and gas-phase calculations. Specifically, the output of the MHD plasma calculations can be returned to Gaussian09, and it is expected to adequately describe the plasma-state's electrical and temperature dependence. In the next step of this process, that geometry can be treated as a gas-phase geometry at temperatures ranging from 300-700 K, to match common gas temperatures found in LTPs.

#### (4) Find the optimized gas-surface transition state

LTP diagnostics have shown quenching of vibrational energy at a surface, leading to heating of the surface until it achieves a temperature similar to that of the gas. Thus, the transition state can be thought of a plasma-phase molecule quenching to achieve a high temperature gas-like energy profile, further support of the energy correction approach suggested above. This means that the transition state can be determined across a range of temperatures, using the plasma geometry. Because the geometry of the NO-Pt transition state is currently unknown, many transition-state DFT methods are not available, as they require the user to constrain the geometry based on previously determined structures. Thus, the transition states in this work must be determined using a chain-of-state method. Chain-of-state uses the independent reactant geometries and brings them together via simultaneous energy minimizations, ultimately creating a connected structure.<sup>49</sup> RPATH, or replica path, is a hybrid DFT/MD chain-of-state method that has been used to find transition states in macromolecule and



surface reactions.<sup>50</sup> Specifically, RPATH works by replicating the initial geometries over a series of iterations in which the distance between the structures is continually reduced. Energies are evaluated at each replication until a saddle point is determined. RPATH can also be constrained so that the individual reactant geometries maintain their independent structure, which is of interest because the NO geometries are specific to the plasma-state (due to the previous energy corrections).<sup>51</sup> It is also important to note that multiple transition states containing NO molecules will need to be determined, with various combinations of electronic states (i.e., NO/NO, NO/NO\*, NO\*/NO\*). These transition states will not only allow for mapping of the PES, but will also provide valuable information as to the bonding conditions and energetics of the transition state. This task will mark the completion of Specific Aim A, as it provides an optimized structure that corresponds to the interactions of plasma-state NO with solid-state NO.

#### (5) Apply ADMP calculations to determine the MD-PES

To begin, ADMP calculations will be completed under APFD/aug-cc-pVTZ conditions, to maintain consistency with the original geometries. The reason for utilizing ADMP is that it is a hybrid DFT-MD calculation that treats electrons quantum-mechanically but nuclei classically.<sup>52-55</sup> Thus, nuclear movement can be thought of as kinetic in nature, although there is a more explicit calculation of electron-mediated processes, like bond formation and excitation. Specifically, ADMP calculations take input transition state geometries and apply a range of kinetic trajectories to the nuclei within the system. Based on an input parameter called “step-size”, the calculation then allows the nuclei to shift some distance along that trajectory before optimizing the electron interactions at that point. This process is repeated along the same trajectory for a user-defined number of steps. The result is a series of geometries along a reaction coordinate. Provided a sufficient number of steps are included within the input file,

there will be a point at which the calculated energy of the system does not change and it can be assumed that the reaction has reached completion. By monitoring the energies of the individual step geometries, a PES surface (much like the ones shown in Fig. A.4) can be determined, and the complexity of the PES is therefore dictated by the step size. Thus, a single ADMP calculation can be thought of as one potential reaction from a given transition state, with one set of applied trajectories. It is important to note, however, that the trajectories are randomly applied based on the range of input temperatures and there can be a nearly infinite number of unique ADMP calculated reactions, even with a constant number of steps and step sizes.

Ultimately, numerous ADMP calculations are necessary to adequately evaluate the possible reactions of a single transition state. To ease the evaluation of ADMP results, similar final product geometries are often grouped and characterized together. For example collected results from 100 separate ADMP calculations on the reaction of a warfare agent simulant molecule and hydrogen peroxide are shown in Fig. A.5. From these 100 calculations, four different classes of reactions were observed, (1) phosphorus-sulfur bond cleavage (P-S), (2) formation of a hydroxide radical (OH), (3) formation of water (H<sub>2</sub>O), and (4) a geometry rearrangement to a trigonal bipyramidal structure (TBP). From these calculations, it can be inferred that water formation is the most likely result from this reaction, whereas hydroxide formation is the least likely. By averaging the energies from the calculations of a particular class, a single PES for that class can be derived. By repeating the process for each class, an MD-PES that corresponds to a single transition state is created.

Possible plasma-surface reactions include surface adsorption, precursor decomposition, desorption of NO, formation of N<sub>2</sub> and O<sub>2</sub>, as well as a host of others. By comparing the different transition states (depending on the electronic state of NO) and trajectories therein, we

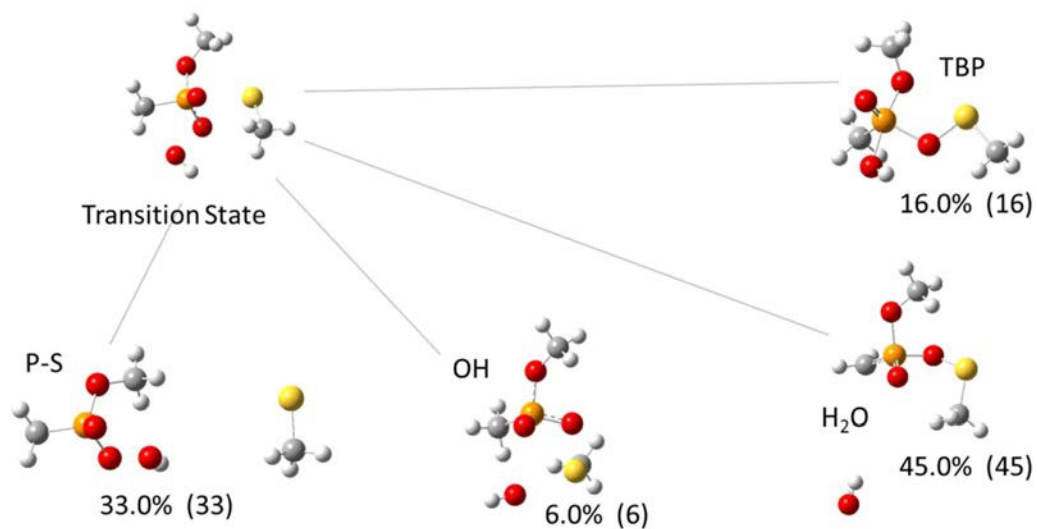


Figure A.5 Results from 100 separate ADMP calculations starting at the same transition state of the reaction of hydrogen peroxide with O,S-dimethyl methylphosphonothiolate, yielding four different final products depending on the initial nuclear velocities assigned to the transition state structure.

can elucidate information about the energy barriers and species dependence related to plasma-catalysis. Although ultimately a series of ADMP calculations will be necessary to determine the appropriate step sizes and number of steps to balance computational cost with reaction completion, successful conditions can be repeated for subsequent calculations. It is also important to acknowledge that because of the large range of gas temperature parameters associated with these systems, the number of possible random trajectories is dramatically increased. As a result, it may be necessary to complete hundreds of successful ADMP calculations to generate a sufficiently comprehensive MD-PES, especially considering the number of atoms that are independently optimized within the proposed system. This task will mark the completion of Specific Aim B, as it will provide unique energetic information related to the reaction of various NO species at platinum surfaces. These data can be used to address a range of possible NO-Pt reactions as well as the relative probabilities of the reactions within an LTP system. Ultimately, such results will offer tremendous opportunities for further experimentation and interpretation, with a unique thermodynamic perspective on NO remediation at catalytic surfaces. environments.

#### A.5 Summary

The proposed work aims to determine the species and energy dependence on plasma-catalyzed conversion of NO, and ultimately enhancing our ability to properly simulate similar gas-surface reactions. By utilizing advances in DFT calculations, it is possible to optimize structures for NO and NO\* that adequately reflect vibrational excitation and orbital configurations as well as appropriate platinum structures that capture bulk and surface characteristics. Using plasma continuum techniques, the NO structures can then be optimized to reflect appropriate plasma conditions which are derived from increased experimental diagnostic

efforts. Three different transition states can be determined based on the combination of NO species geometries used. The transition state geometries can subsequently be optimized for gas-phase temperatures, also based on experimental results using ab initio methods. Finally, using a range of possible kinetic trajectories, ADMP can be used to determine energy-dependent mechanisms for the reaction of NO at a platinum surface.

If successful, this work could play a significant role in the assessment and advancement of plasma-catalytic waste gas remediation applications. A fundamental understanding of the gas-surface reactions, including mechanism and energy dependence, would allow for experimental diagnostic efforts to focus on tuning LTP systems to the conditions that are shown to be optimal computationally for successful conversion. Indeed, successful and reproducible remediation is necessary before LTPs can be utilized in industrial applications. In addition, successful completion of this work would be applicable to a multiple  $N_xO_y$  species in more complex, exhaust-like environments by serving as a model system, in keeping with Specific Aim C. Indeed, the work proposed herein could also be expanded to include more complex systems and surface interactions. Such steps would allow for further advancement in abatement LTP systems, and assessment of the efficacy in a variety of applications.

## REFERENCES

1. Aerts, R.; Tu, X.; Van Gaens, W.; Whitehead, J. C.; Bogaerts, A., Gas Purification by Nonthermal Plasma: A Case Study of Ethylene. *Environmental Science & Technology* 2013, 47 (12), 6478-6485.
2. Penetrante, B. M.; Brusasco, R. M.; Merritt, B. T.; Vogtlin, G. E., Environmental Applications of Low-Temperature Plasmas. *Pure and Applied Chemistry* 1999, 71 (10), 1829-1835.
3. Vandebroucke, A. M.; Morent, R.; De Geyter, N.; Leys, C., Non-Thermal Plasmas for Non-Catalytic and Catalytic VOC Abatement. *Journal of Hazardous Materials* 2011, 195, 30-54.
4. Mizuno, A., Generation of Non-Thermal Plasma Combined with Catalysts and Their Application in Environmental Technology. *Catalysis Today* 2013, 211, 2-8.
5. Van Durme, J.; Dewulf, J.; Leys, C.; Van Langenhove, H., Combining Non-Thermal Plasma with Heterogeneous Catalysis in Waste Gas Treatment: A Review. *Applied Catalysis B: Environmental* 2008, 78 (3-4), 324-333.
6. Whitehead, J. C., Plasma Catalysis: A Solution for Environmental Problems. *Pure and Applied Chemistry* 2010, 82 (6), 1329-1336.
7. Broer, S.; Hammer, T., Selective Catalytic Reduction of Nitrogen Oxides by Combining a Non-Thermal Plasma and a V<sub>2</sub>O<sub>5</sub>-WO<sub>3</sub>/TiO<sub>2</sub> Catalyst. *Applied Catalysis B: Environmental* 2000, 28 (2), 101-111.
8. Dorai, R.; Hassouni, K.; Kushner, M. J., Interaction Between Soot Particles and NO<sub>x</sub> During Dielectric Barrier Discharge Plasma Remediation of Simulated Diesel Exhaust. *Journal of Applied Physics* 2000, 88 (10), 6060-6071.
9. Penetrante, B. M.; Hsiao, M. C.; Merritt, B. T.; Vogtlin, G. E.; Wallman, P. H., Techniques for Nonthermal Plasma Processing of NO in N<sub>2</sub>. *IEEE Transactions on Plasma Science* 1995, 23 (4), 679-687.
10. Aerts, R.; Martens, T.; Bogaerts, A., Influence of Vibrational States on CO<sub>2</sub> Splitting by Dielectric Barrier Discharges. *Journal of Physical Chemistry C* 2012, 116 (44), 23257-23273.
11. Demidyuk, V.; Whitehead, J. C., Influence of Temperature on Gas-Phase Toluene Decomposition in Plasma-Catalytic System. *Plasma Chemistry and Plasma Processing* 2007, 27 (1), 85-94.
12. Hu, X.; Li, H.; Wu, T., Approaching and Bond Breaking Energies in the C-H Activation and Their Application in Catalyst Design. *Journal of Physical Chemistry A* 2011, 115 (5), 904-910.
13. Li, S.; Zheng, W.; Tang, Z.; Gu, F., Plasma Heating and Temperature Difference Between Gas Pellets in Packed Bed With Dielectric Barrier Discharge Under Natural Convection Condition. *Heat Transfer Engineering* 2012, 33 (7), 609-617.
14. Nozaki, T.; Muto, N.; Kado, S.; Okazaki, K., Dissociation of Vibrationally Excited Methane on Ni Catalyst: Part 1. Application to Methane Steam Reforming. *Catalysis Today* 2004, 89 (1-2), 57-65.
15. Smith, R. R.; Killelea, D. R.; DelSesto, D. F.; Utz, A. L., Preference for Vibrational over Translational Energy in a Gas-Surface Reaction. *Science* 2004, 304 (5673), 992-995.

16. Tu, X.; Whitehead, J. C., Plasma-Catalytic Dry Reforming of Methane in an Atmospheric Dielectric Barrier Discharge: Understanding the Synergistic Effect at Low Temperature. *Applied Catalysis B: Environmental* 2012, 125, 439-448.
17. De Bie, C.; Martens, T.; van Dijk, J.; Paulussen, S.; Verheyde, B.; Corthals, S.; Bogaerts, A., Dielectric Barrier Discharges Used for the Conversion of Greenhouse Gases: Modeling the Plasma Chemistry by Fluid Simulations. *Plasma Sources Science & Technology* 2011, 20 (2).
18. El-Khoury, P. Z.; Bylaska, E. J.; Hess, W. P., Time Domain Simulations of Chemical Bonding Effects in Surface-Enhanced Spectroscopy. *Journal of Chemical Physics* 2013, 139 (17).
19. Frauenheim, T.; Seifert, G.; Elstner, M.; Niehaus, T.; Kohler, C.; Amkreutz, M.; Sternberg, M.; Hajnal, Z.; Di Carlo, A.; Suhai, S., Atomistic Simulations of Complex Materials: Ground-State and Excited-State Properties. *Journal of Physics: Condensed Matter* 2002, 14 (11), 3015-3047.
20. Rega, N.; Brancato, G.; Petrone, A.; Caruso, P.; Barone, V., Vibrational Analysis of X-Ray Absorption Fine Structure Thermal Factors by Ab Initio Molecular Dynamics: The Zn(II) Ion in Aqueous Solution as a Case Study. *Journal of Chemical Physics* 2011, 134 (7).
21. Somers, W.; Bogaerts, A.; van Duin, A. C. T.; Neyts, E. C., Plasma Species Interacting with Nickel Surfaces: Toward an Atomic Scale Understanding of Plasma-Catalysis. *Journal of Physical Chemistry C* 2012, 116 (39), 20958-20965.
22. Somers, W.; Bogaerts, A.; van Duin, A. C. T.; Neyts, E. C., Interactions of Plasma Species on Nickel Catalysts: A Reactive Molecular Dynamics Study on the Influence of Temperature and Surface Structure. *Applied Catalysis B: Environmental* 2014, 154, 1-8.
23. Wang, F.; Zhang, D.; Xu, X.; Ding, Y., Theoretical Study of the CO Oxidation Mediated by  $\text{Au}_3^+$ ,  $\text{Au}_3$ , and  $\text{Au}_3^-$ : Mechanism and Charge State Effect of Gold on Its Catalytic Activity. *Journal of Physical Chemistry C* 2009, 113 (42), 18032-18039.
24. Yang, Y., Direct Non-Oxidative Methane Conversion by Non-Thermal Plasma: Modeling Study. *Plasma Chemistry and Plasma Processing* 2003, 23 (2), 327-346.
25. Kraus, M.; Egli, W.; Haffner, K.; Eliasson, B.; Kogelschatz, U.; Wokaun, A., Investigation of Mechanistic Aspects of the Catalytic  $\text{CO}_2$  Reforming of Methane in a Dielectric-Barrier Discharge Using Optical Emission Spectroscopy and Kinetic Modeling. *Physical Chemistry Chemical Physics* 2002, 4 (4), 668-675.
26. Martin, A. R.; Shawcross, J. T.; Whitehead, J. C., The Oxidation of Carbon Soot in a Non-Thermal, Atmospheric Pressure Plasma: Experiment and Modelling. *Journal of Advanced Oxidation Technologies* 2005, 8 (2), 126-132.
27. Pietrzyk, P.; Gil, B.; Sojka, Z., Combining Computational and In Situ Spectroscopies Joint with Molecular Modeling for Determination of Reaction Intermediates of deNO(x) Process-CuZSM-5 Catalyst Case Study. *Catalysis Today* 2007, 126 (1-2), 103-111.
28. Frisch, M. J.; Trucks, G. W.; Schlegel, H. B.; Scuseria, G. E.; Robb, M. A.; Cheeseman, J. R.; Scalmani, G.; Barone, V.; Mennucci, B.; Petersson, G. A.; Nakatsuji, H.; Caricato, M.; Li, X.; Hratchian, H. P.; Izmaylov, A. F.; Bloino, J.; Zheng, G.; Sonnenberg, J. L.; Hada, M.; Ehara, M.; Toyota, K.; Fukuda, R.; Hasegawa, J.; Ishida, M.; Nakajima, T.; Honda, Y.; Kitao, O.; Nakai, H.; Vreven, T.; Montgomery Jr., J. A.; Peralta, J. E.; Ogliaro, F.; Bearpark, M. J.; Heyd, J.; Brothers, E. N.; Kudin, K. N.; Staroverov, V. N.; Kobayashi, R.; Normand, J.; Raghavachari, K.; Rendell, A. P.; Burant, J. C.; Iyengar, S. S.; Tomasi, J.; Cossi, M.; Rega, N.; Millam, N. J.; Klene, M.; Knox, J. E.; Cross, J. B.; Bakken, V.; Adamo, C.; Jaramillo, J.; Gomperts, R.; Stratmann, R. E.; Yazyev, O.; Austin, A. J.; Cammi, R.; Pomelli, C.; Ochterski, J. W.; Martin, R.

- L.; Morokuma, K.; Zakrzewski, V. G.; Voth, G. A.; Salvador, P.; Dannenberg, J. J.; Dapprich, S.; Daniels, A. D.; Farkas, Ö.; Foresman, J. B.; Ortiz, J. V.; Cioslowski, J.; Fox, D. J. Gaussian 09, Gaussian, Inc.: Wallingford, CT, USA, 2009.
29. Kendall, R. A.; Dunning, T. H.; Harrison, R. J., Electron Affinities of the First-Row Atoms Revisited: Systematic Basis Sets and Wave Functions. *Journal of Chemical Physics* 1992, 96 (9), 6796-6806.
  30. Austin, A.; Petersson, G. A.; Frisch, M. J.; Dobek, F. J.; Scalmani, G.; Throssell, K., A Density Functional with Spherical Atom Dispersion Terms. *Journal of Chemical Theory and Computation* 2012, 8 (12), 4989-5007.
  31. Qi, W. J.; Ran, J. Y.; Wang, R. R.; Du, X. S.; Shi, J.; Ran, M. C., Kinetic Mechanism of Effects of Hydrogen Addition on Methane Catalytic Combustion Over Pt(111) Surface: A DFT Study with Cluster Modeling. *Computational Materials Science* 2016, 111, 430-442.
  32. Lytvynenko, A. S.; Kolotilov, S. V.; Kiskin, M. A.; Eremenko, I. L.; Novotortsev, V. M., Modeling of Catalytically Active Metal Complex Species and Intermediates in Reactions of Organic Halides Electroreduction. *Physical Chemistry Chemical Physics* 2015, 17 (8), 5594-5605.
  33. Sun, S. J.; Li, C. Y.; Zhang, D. S.; Wang, Y. J., Density Functional Theory Study of the Adsorption and Dissociation of O<sub>2</sub> on CuO(111) Surface. *Applied Surface Science* 2015, 333, 229-234.
  34. Pinto, L. M. C.; Maia, G., Selected Properties of Pt(111) Modified Surfaces: A DFT Study. *Electrochemistry Communications* 2015, 60, 135-138.
  35. Santarossa, G.; Vargas, A.; Iannuzzi, M.; Pignedoli, C. A.; Passerone, D.; Baiker, A., Modeling Bulk and Surface Pt Using the “Gaussian and Plane Wave” Density Functional Theory Formalism: Validation and Comparison to k-Point Plane Wave Calculations. *The Journal of Chemical Physics* 2008, 129 (23), 234703.
  36. Hay, P. J.; Wadt, W. R., Ab Initio Effective Core Potentials for Molecular Calculations: Potentials for K to Au Including the Outermost Core Orbitals. *Journal of Chemical Physics* 1985, 82 (1), 299-310.
  37. van Gessel, A. F. H.; Hrycak, B.; Jasiński, M.; Mizeraczyk, J.; van der Mullen, J. J. A. M.; Bruggeman, P. J., Temperature and NO Density Measurements by LIF and OES on an Atmospheric Pressure Plasma Jet. *Journal of Physics D: Applied Physics* 2013, 46 (9), 095201.
  38. Abdel Rahman, M.; Gans, T.; Dobele, H. F.; Döbele, H. F., Space and Time Resolved Rotational State Populations and Gas Temperatures in an Inductively Coupled Hydrogen RF Discharge. *Plasma Sources Science & Technology* 2005, 14 (1), 51-60.
  39. Biloiu, C.; Sun, X.; Harvey, Z.; Scime, E., Determination of Rotational and Vibrational Temperatures of a Nitrogen Helicon Plasma. *Review of Scientific Instruments* 2006, 77 (10), 10F117.
  40. Hafner, J., Ab-Initio Simulations of Materials using VASP: Density-Functional Theory and Beyond. *Journal of Computational Chemistry* 2008, 29 (13), 2044-2078.
  41. Bose, D.; Govindan, T. R.; Meyyappan, M., A Continuum Model for the Inductively Coupled Plasma Reactor in Semiconductor Processing. *Journal of the Electrochemical Society* 1999, 146 (7), 2705-2711.
  42. Kushner, M. J.; Collison, W. Z.; Grapperhaus, M. J.; Holland, J. P.; Barnes, M. S., A Three-Dimensional Model for Inductively Coupled Plasma Etching Reactors: Azimuthal Symmetry, Coil Properties, and Comparison to Experiments. *Journal of Applied Physics* 1996, 80 (3), 1337-1344.



43. Lymberopoulos, D. P.; Economou, D. J., Two-Dimensional Simulation of Polysilicon Etching with Chlorine in a High Density Plasma Reactor. *IEEE Transactions on Plasma Science* 1995, 23 (4), 573-580.
44. Ventzek, P. L. G.; Hoekstra, R. J.; Kushner, M. J., Two-Dimensional Modeling of High Plasma Density Inductively Coupled Sources for Materials Processing. *Journal of Vacuum Science & Technology B* 1994, 12 (1), 461-477.
45. Wise, R. S.; Lymberopoulos, D. P.; Economou, D. J., Rapid Two-Dimensional Self-Consistent Simulation of Inductively Coupled Plasma and Comparison with Experimental Data. *Applied Physics Letters* 1996, 68 (18), 2499-2501.
46. Parent, B.; Macheret, S. O.; Shneider, M. N., Modeling Weakly-Ionized Plasmas in Magnetic Field: A New Computationally-Efficient Approach. *Journal of Computational Physics* 2015, 300, 779-799.
47. Ikhlef, N.; Hacib, T.; Leroy, O.; Mekiddeche, M. R., Nonlinear Compressible Magnetohydrodynamic Flows Modeling of a Process ICP Torch. *European Physical Journal: Applied Physics* 2012, 58 (1).
48. Ikhlef, N.; Leroy, O.; Mekideche, M. R., Computational Model of Thermal-Fluid Flow in a Radio-Frequency Plasma Torch. *Contributions to Plasma Physics* 2014, 54 (8), 735-745.
49. Tao, P.; Hodošček, M.; Larkin, J. D.; Shao, Y.; Brooks, B. R., Comparison of Three Chain-of-States Methods: Nudged Elastic Band and Replica Path with Restraints or Constraints. *Journal of Chemical Theory and Computation* 2012, 8 (12), 5035-5051.
50. Czerminski, R.; Elber, R., Reaction Path Study of Conformational Transitions in Flexible Systems: Applications to Peptides. *Journal of Chemical Physics* 1990, 92 (9), 5580.
51. Brokaw, J. B.; Haas, K. R.; Chu, J.-W., Reaction Path Optimization with Holonomic Constraints and Kinetic Energy Potentials. *Journal of Chemical Theory and Computation* 2009, 5 (8), 2050-2061.
52. Iyengar, S. S.; Schlegel, H. B.; Millam, J. M.; Voth, G. A.; Scuseria, G. E.; Frisch, M. J., Ab Initio Molecular Dynamics: Propagating the Density Matrix with Gaussian Orbitals II: Generalizations Based on Mass-Weighting, Idempotency, Energy Conservation and Choice of Initial Conditions. *Journal of Chemical Physics* 2001, 115 (22), 10291-10302.
53. Iyengar, S. S.; Schlegel, H. B.; Voth, G. A., Atom-Centered Density Matrix Propagation (ADMP): Generalizations Using Bohmian Mechanics. *Journal of Physical Chemistry A* 2003, 107 (37), 7269-7277.
54. Iyengar, S. S.; Schlegel, H. B.; Voth, G. A.; Millam, J. M.; Scuseria, G. E.; Frisch, M. J., Ab Initio Molecular Dynamics: Propagating the Density Matrix with Gaussian Orbitals IV: Formal Analysis of the Deviations from Born-Oppenheimer Dynamics. *Israel Journal of Chemistry* 2002, 42 (2-3), 191-202.
55. Jay, A. N.; Daniel, K. A.; Patterson, E. V., Atom-Centered Density Matrix Propagation Calculations on the Methyl Transfer from CH<sub>3</sub>Cl to NH<sub>3</sub>: Gas-Phase and Continuum-Solvated Trajectories. *Journal of Chemical Theory and Computation* 2007, 3 (2), 336-343.

## APPENDIX B

### SUPPLEMENTAL INFORMATION FOR RECITATION STUDIES

This appendix contains survey questions and final versions of the scaffold activities designed for use in the General Chemistry I (CHEM 111) recitation program, data for which can be found in Chapter 8. The survey questions shown are taken from Weeks 1, 3, and 16 of the Spring 2015 semester. Week 1 (B.1) contains the initial survey questions, Week 3 (B.2) shows an example weekly survey, and Week 16 (B.3) contains the final survey questions. All surveys have been reformatted for the purpose of clarity, as they were originally administered via SurveyMonkey®. The worksheets were presented by graduate teaching assistants and asked students to play the role of a chemist working for the fictional company, ChemLight. The first activity (B.4) is a fully scaffolded activity on the concepts of the mole and molecular mass (administered in Week 3). Each step is structured to guide students through the process and problem solving approach necessary to complete the worksheet. The second activity (B.5) is a partially scaffolded activity, in which pieces of the original version were removed by the instructors to provide less guidance to the students (administered in Week 11). Worksheets have also been reformatted for the purposes of this document, though the original structure remains intact. The concepts in this activity focus heavily on stoichiometry and unit conversions that are key to solving complex general chemistry problems. The skills presented in these worksheets are absolutely vital to success not only in CHEM 111, but also in the rest of the chemistry curricula, whether it be General Chemistry II, Organic Chemistry I and II, or beyond. Indeed, these concepts are deeply rooted in chemistry coursework, making further opportunities to engage with the material outside of lecture a valuable opportunity.

## B.1 Week 1 Survey

1. If you have discussed CHEM 111 with other students at CSU, what have you heard about the recitation format?
2. What types of activities do you expect to engage in during recitation?
3. Why do you think CSU uses a recitation format for CHEM 111? What do you think the benefits of this system are?
4. How important do you think the recitation format will be to your understanding of the course material?
  - a. Very Important
  - b. Somewhat Important
  - c. Not Very Important
  - d. Not At All Important
5. How interested are you in chemistry and the CHEM 111 course?
  - a. Very Interested
  - b. Somewhat Interested
  - c. Not Very Interested
  - d. Not At All Interested
6. How important do you think CHEM 111 material is to your desired career/major?
  - a. Very Important
  - b. Somewhat Important
  - c. Not Very Important
  - d. Not At All Important
7. Have you taken a chemistry course previously?
  - a. Yes – in high school
  - b. Yes – at CSU
  - c. Yes – at another university
  - d. No
8. How prepared do you feel for this CHEM 111 course?
  - a. Very Prepared
  - b. Somewhat Prepared
  - c. Not Very Prepared
  - d. Not At All Prepared
9. How much time do you expect to spend each week on CHEM 111 outside of the classroom?
  - a. Less than 1 hour
  - b. 1-3 hours
  - c. 3-6 hours
  - d. More than 6 hours
10. What grade do you anticipate receiving in CHEM 111 this semester?
  - a. A
  - b. B
  - c. C
  - d. D
11. What is your CSU ID number?

## B.2 Week 3 Survey

1. In what ways did this week's activity meet (or fail to meet) your expectations for recitation?
2. What was your favorite aspect of this week's activity?
3. What was your least favorite aspect of this week's activity?
4. How effective was this week's activity at engaging your interest in the material?
  - a. Very Effective
  - b. Somewhat Effective
  - c. Not Very Effective
  - d. Not At All Effective
5. How successful was this week's activity in improving your understanding of the material?
  - a. Very Successful
  - b. Somewhat Successful
  - c. Not Very Successful
  - d. Not At All Successful
6. How reliant were you on the help of your TA to complete this week's activity?
  - a. Very Reliant
  - b. Somewhat Reliant
  - c. Not Very Reliant
  - d. Not At All Reliant
7. Overall, how satisfied were you with this week's activity?
  - e. Very Satisfied
  - f. Somewhat Satisfied
  - g. Not Very Satisfied
  - h. Not At All Satisfied
8. How interested would you be in participating in a similarly structured activity in the future?
  - a. Very Interested
  - b. Somewhat Interested
  - c. Not Very Interested
  - d. Not At All Interested
9. Isotopes of a single element differ from one another in what way?
  - a. They have different numbers of protons in the nucleus
  - b. They have different numbers of neutrons in the nucleus
  - c. They have different numbers of electrons outside the nucleus
  - d. They have different numbers of protons and neutrons in the nucleus
10. An Avogadro's number of iron (Fe) atoms would weigh how much?
  - a. 55.9 g
  - b. 27.9 g
  - c.  $6.02 \times 10^{23}$  g
  - d.  $6.02 \times 10^{-23}$  g

11. Naturally occurring lithium (Li) consists of only two isotopes, Li-6 (6.02 amu) and Li-7 (7.02 amu). Using the periodic table, which of the isotopes have a greater abundance?
- Li-6
  - Li-7
  - Both are 50% abundant
  - Cannot Be Determined
12. What mass of arsenic (As) contains the same number of atoms as 61.85 g of argon (Ar)?
- 20.66 mg
  - 32.98 g
  - 116.0 g
  - 185.1 kg
13. Element Ft was found to have three isotopes. Samples of element Ft contain 29.70% of Ft-27, 8.70% of Ft-28, and 61.60% of Ft-30. The atomic masses of these isotopes are 27.1 amu, 28.0 amu, and 30.0 amu respectively. What is the relative atomic mass of Ft?
- 28.5 amu
  - 29.3 amu
  - 30.0 amu
  - 28.9 amu
14. What is your CSU ID number?

### B.3 Week 16 Survey

1. If another CSU student asked you about the CHEM 111 recitation format, what would you tell them and how would you describe it?
2. What was your overall impression of the recitation program?
3. Why do you think CSU uses a recitation format for CHEM 111? What do you think the benefits of this system are?
4. How important do you think the recitation format was to your understanding of the course material?
  - a. Very Important
  - b. Somewhat Important
  - c. Not Very Important
  - d. Not At All Important
5. How interested are you in chemistry after taking the CHEM 111 course?
  - a. Very Interested
  - b. Somewhat Interested
  - c. Not Very Interested
  - d. Not At All Interested
6. How important do you think CHEM 111 material was for your desired career/major?
  - a. Very Important
  - b. Somewhat Important
  - c. Not Very Important
  - d. Not At All Important
7. How much time did you spend each week on CHEM 111 outside of the classroom on average?
  - a. Less than 1 hour
  - b. 1-3 hours
  - c. 3-6 hours
  - d. More than 6 hours
8. What grade do you anticipate receiving in CHEM 111 this semester?
  - a. A
  - b. B
  - c. C
  - d. D
  - e. F
9. How beneficial to your learning was each of the following activities? (this question was asked of each activity between Week 1 to Week 15)
  - a. Very Beneficial
  - b. Beneficial
  - c. Neither Beneficial or Unbeneficial
  - d. Unbeneficial
  - e. Very Unbeneficial

10. How much did you enjoy each of the following activities? (this question was asked of each activity between Week 1 to Week 15)
- Very Enjoyable
  - Enjoyable
  - Neither Enjoyable or Unenjoyable
  - Unenjoyable
  - Very Unenjoyable
11. Other than the first week pre-test activity, what was your LEAST favorite recitation activity this semester?
- Week 2 – Dimensional Analysis Worksheet
  - Week 3 – The Mole Worksheet
  - Week 5 – Orbital/Electron Configuration Worksheet
  - Week 6 – Periodic Trends Worksheet
  - Week 8 – Molecular Shape and Polarity Game
  - Week 9 – Intermolecular Forces Game
  - Week 11 – Stoichiometry (Glow Stick) Worksheet
  - Week 12 – CSI Fort Collins Activity
  - Week 14 – Aluminum Recycling Activity
  - Week 15 – Gas Properties Simulations
12. Other than the first week pre-test activity, what was your MOST favorite recitation activity this semester?
- Week 2 – Dimensional Analysis Worksheet
  - Week 3 – The Mole Worksheet
  - Week 5 – Orbital/Electron Configuration Worksheet
  - Week 6 – Periodic Trends Worksheet
  - Week 8 – Molecular Shape and Polarity Game
  - Week 9 – Intermolecular Forces Game
  - Week 11 – Stoichiometry (Glow Stick) Worksheet
  - Week 12 – CSI Fort Collins Activity
  - Week 14 – Aluminum Recycling Activity
  - Week 15 – Gas Properties Simulations
13. What is your CSU ID number?

## B.4 The Mole Worksheet

Name: \_\_\_\_\_

Group Number: \_\_\_\_\_

Today, you are working as a chemist for a company in Las Vegas that specializes in making neon signs. Your boss enters your office and hands you a tube filled with argon gas. Argon gas helps to produce the purple colors seen in neon signs, but this tube is not working properly. He tells you that the tube is 4.5 feet long and 0.5 inches in diameter and filled with a pure sample of argon.



After inspecting the tube, you begin to wonder what you are to do with it. Your boss hands you a sheet of paper and asks you to provide him with some basic information on the argon gas. He believes that the tube may not be functioning properly due to the amount of gas in the tube. Your goal today will be to fill out the table of information requested by your boss, which will hopefully help with the design of a new argon tube.

	Mass of Argon (g)	Moles of Argon (mol)	
Number of $^{36}\text{Ar}$ Atoms	Number of $^{38}\text{Ar}$ Atoms	Number of $^{40}\text{Ar}$ Atoms	Total Number of Argon Atoms
Total Number of Protons	Total Number of Neutrons	Total Number of Electrons	Total Number of Particles

To begin, you look up information on argon and its isotopes. Unfortunately, you spill some coffee on your textbook which makes it impossible to read some of the argon data. Thus, you will need to complete this table as well.

18	39.948
<b>Ar</b>	
Argon	

Isotope	Mass (amu)	Abundance	# of Protons	# of Neutrons	# of Electrons
$^{36}\text{Ar}$	35.968				
$^{38}\text{Ar}$		0.0700%			
$^{40}\text{Ar}$	39.962	99.6000%	18	22	18



Next, you place an empty glass tube (of the same size) on your scale and compare the mass of the empty tube to that of the filled one given to you by your boss. This allows you to determine that there are 2.98 mg of argon in the glass tube. Convert this number to grams and add it to your table. Using only the previous information, you will be able to complete your boss' task.

1. Let's begin by completing the textbook table of information.

a. Remember that an atom's atomic number is the number of protons found in its nucleus. Therefore, the number of protons must remain constant for all isotopes in a pure sample of argon. We can also assume that these atoms do not have a charge since argon is a noble gas. As a result, the number of electrons should be equal to the number of protons. Finally, the mass number is the sum of protons and neutrons within the nucleus. The mass number is the value before the element symbol of an isotope. ( $^{40}\text{Ar}$  has a mass number of 40, so the number of protons and neutrons must sum to 40.) Using this information, fill in the number of proton, electrons, and neutrons in the second table.

b. Remember, the molar mass given on the periodic table is calculated via a weighted average. This means that each isotope contributes to the overall molar mass of an element based on its relative abundance in nature. For this reason, only stable (non-radioactive) isotopes are included in the calculation. Thus, molar mass is calculated from the following equation:

$$= [ \quad \quad \quad 1 * \quad \quad \quad 1 ] + [ \quad \quad \quad 2 * \quad \quad \quad 2 ] + \dots$$

We also know that the sum of all stable isotope abundances must equal 100%. If we subtract the abundance of  $^{40}\text{Ar}$  and  $^{38}\text{Ar}$  from 100, we can determine the abundance of  $^{36}\text{Ar}$ . Then, after adding that value to the previous equation, we can calculate the mass of the  $^{38}\text{Ar}$  isotope.

$$39.948 = 35.968 * \quad + \quad * 0.000700 + [ 39.962 * .996000 ]$$

Add the abundance of  $^{36}\text{Ar}$  and the mass of  $^{38}\text{Ar}$  to the second table.

2. Now, let's focus on the table given to you by your boss.

a. When talking about elements we must understand just how small they really are. For example, it takes an almost inconceivable amount of carbon atoms to produce a small diamond. And it will take a very large number of argon atoms to produce the 2.98mg of argon in our tube. Instead of using a quantity such as a million ( $1 \times 10^6$ ) or a billion ( $1 \times 10^9$ ) or even a quattuordecillion ( $1 \times 10^{45}$ ), chemists describe atoms in terms of a special quantity called the mole. A mole is  $6.022 \times 10^{23}$  (also called Avogadro's number). Thus, a mole is simply a number word, like "dozen" or "gross".

It is important to know that the mass reported on the periodic table is how much 1 mole of atoms weighs. This means that 1 mole of argon atoms weighs 39.948g. Thus, the mass value reported on the periodic table is often referred to as a molar mass, and can be reported with units of  $\frac{\text{g}}{\text{mol}}$

(this also means that  $1 \frac{\text{mol}}{\text{g}} = 1$  ).

b. To begin, we already know that we have  $2.98 \times 10^{23}$  g of argon in the tube. If we divide this number by the molar mass from the periodic table, we can calculate the number of moles of argon in the tube and add this value to our table.

$$2.98 \times 10^{23} \text{ g} * \frac{1 \text{ mol Ar}}{39.948 \text{ g}} = \underline{\hspace{2cm}} \text{ mol Ar}$$

c. We also know that there are  $6.022 \times 10^{23}$  atoms in a single mole. So, if we multiply our total number of moles by Avogadro's number, we will determine how many total atoms of argon we have.

$$\underline{\hspace{2cm}} \text{ mol Ar} * \frac{6.022 \times 10^{23} \text{ atoms}}{1 \text{ mol}} = \underline{\hspace{2cm}} \text{ atoms Ar}$$

d. If you take the total number of atoms and multiply it by the abundance of each isotope, you can determine how many atoms of each isotope are present in your sample.

$$\underline{\hspace{2cm}} \text{ atoms Ar} * \underline{\hspace{1cm}} = \underline{\hspace{2cm}} \text{ atoms } ^{36}\text{Ar}$$

$$\underline{\hspace{2cm}} \text{ atoms Ar} * 0.0007 = \underline{\hspace{2cm}} \text{ atoms } ^{38}\text{Ar}$$

$$\underline{\hspace{2cm}} \text{ atoms Ar} * 0.9960 = \underline{\hspace{2cm}} \text{ atoms } ^{40}\text{Ar}$$

e. The final step to complete our table is to determine the numbers of elementary particles. Let's start with protons. A pure sample of argon will contain the same number of protons in each atom, so we can determine the number of protons by multiplying the total number of atoms by the atomic number of argon.

$$\underline{\hspace{2cm}} \text{ atoms Ar} * \underline{\hspace{1cm}} = \underline{\hspace{2cm}} \text{ total protons}$$

f. As we have said before, (for a neutral atom) the number of protons is always equal to the number of electrons. Therefore, you can use the same value for electrons as you calculated for protons.

g. Now we must determine the total number of neutrons in our glass tube. However, since the number of neutrons differs between isotopes we will need to take that into account. Therefore, we must determine the number of neutrons for each isotope before we can find a total

number of neutrons. Complete the following equations.

$$\underline{\hspace{2cm}} \text{ atoms } ^{36}\text{Ar} * \frac{\underline{\hspace{1cm}}}{\underline{\hspace{1cm}} 11} = \underline{\hspace{2cm}} \text{ total neutrons from } ^{36}\text{Ar}$$

$$\underline{\hspace{2cm}} \text{ atoms } ^{38}\text{Ar} * \frac{\underline{\hspace{1cm}}}{\underline{\hspace{1cm}} 11} = \underline{\hspace{2cm}} \text{ total neutrons from } ^{38}\text{Ar}$$

$$\underline{\hspace{2cm}} \text{ atoms } ^{40}\text{Ar} * \frac{\underline{\hspace{1cm}}}{\underline{\hspace{1cm}} 11} = \underline{\hspace{2cm}} \text{ total neutrons from } ^{40}\text{Ar}$$

h. Adding up these three numbers will provide you with the total number of neutrons for the entire gas sample. Once this value is added to the table, the last step is to add up the total number of protons, neutrons, and electrons to determine the total number of particles.

$$\underline{\hspace{2cm}} \text{ protons} + \underline{\hspace{2cm}} \text{ electrons} + \underline{\hspace{2cm}} \text{ neutrons} = \underline{\hspace{2cm}} \text{ particles}$$

3. With this calculation, you can complete the table and finish up the rigorous task your boss has assigned. But first, let us look over our work. Since the design of a new argon tube for a sign on the Las Vegas strip will be dependent on the information you provide your boss, you'll want to make sure everything looks correct.

a. Consider the value you calculated for the total number of argon atoms. Explain why this value makes sense given what you know about the relationship between mass, moles, and atoms.

b. Now think about the values you calculated for the number of protons and the number of neutrons in the argon sample and compare them. Which of these values would you expect to be larger and why? Do your calculations match this prediction?

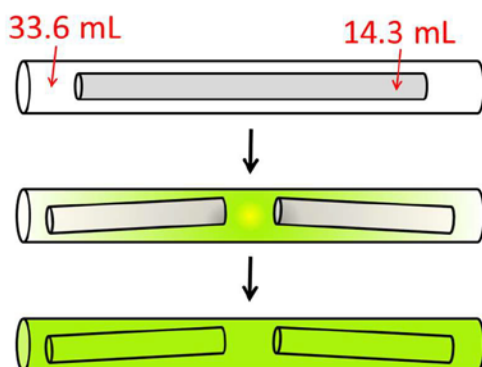
## B.5 Stoichiometry Worksheet

Name: \_\_\_\_\_

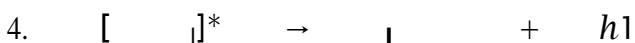
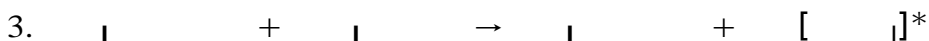
Group Number: \_\_\_\_\_

Today, you are back to working at ChemLight, the Las Vegas company that specializes in making neon signs. Work has been slow since you solved the problems with the argon gas tube, but this morning you have been called in for a special meeting with your boss. After sitting down in his office, he tells you that the company is considering moving in a new direction by manufacturing glow sticks.

He hands you some paperwork on glow sticks and tells you that he is interested in making a brighter green glow stick. It turns out that glow stick chemistry is fairly complicated and actually involves a series of reactions that occur as a sequence of several steps (described below). He asks you to create a prototype glow stick and determine the role that these connected reactions play in the emission of the glow stick. After some studying, you learn that glow sticks consist of two clear tubes, the outer made of plastic and the inner of glass. In the case of green glow sticks, the inner tube contains a mixture of two compounds: Cyalume ( $C_{14}H_{10}O_4$ ) and tetracene ( $C_{18}H_{12}$ ). The outer tube contains only aqueous hydrogen peroxide ( $H_2O_2$ ). When the inner tube is broken, a reaction takes place between hydrogen peroxide and Cyalume that excites the electrons in tetracene. When tetracene's electrons relax, they give off the photons (indicated by  $h\nu$  in a chemical reaction) that produce the characteristic glow. This process is called chemiluminescence. The more photons that are given off, the brighter the glow.



You sit down to write the equations that describe these processes. Unfortunately, Cyalume cannot be purchased and must be synthesized in the laboratory by reacting phenol ( $C_6H_5OH$ ) and oxalic acid ( $C_2H_2O_4$ ). This adds another reaction to the process. The entire set of reactions is shown on the next page. (NOTE: An asterisk [\*] is how chemists designate a molecule with electrons in excited states)



Now that you have all of the reactions in place, you can begin to investigate your boss's request. The first product you decide to investigate is carbon dioxide that is generated at the same time as excited state tetracene because generating too much carbon dioxide gas may cause the glow stick to explode.

1. In order to determine how much carbon dioxide will be produced, you will have work through reactions #1-3.
  - a. Start by balancing the four reactions above.
  - b. Specify where each reaction occurs (either in the lab or inside the glow stick)
  - c. Indicate whether each individual compound is present before and/or after the inner tube is broken.

2. The following table contains the formula and molecular mass of each compound present in the previous reactions. Complete the following table so that it can be used as a resource for the subsequent problems.

1 1.008 H Hydrogen	6 12.011 C Carbon	8 15.999 O Oxygen
-----------------------------	----------------------------	----------------------------

Name	Formula	Molecular Mass
phenol	C <sub>6</sub> H <sub>5</sub> OH	94.11 g/mol
oxalic acid	C <sub>2</sub> H <sub>2</sub> O <sub>4</sub>	
Cyalume	C <sub>14</sub> H <sub>10</sub> O <sub>4</sub>	
water	H <sub>2</sub> O	18.02 g/mol
hydrogen peroxide	H <sub>2</sub> O <sub>2</sub>	34.01 g/mol
peroxyacid ester	C <sub>2</sub> O <sub>4</sub>	88.02 g/mol
tetracene	C <sub>18</sub> H <sub>12</sub>	
carbon dioxide	CO <sub>2</sub>	44.01 g/mol

3. Now that you are familiar with the species and reactions, you are ready to begin to study how much carbon dioxide is produced. However, you must start by synthesizing Cyalume. You find only 2.55 mg of oxalic acid available in your lab which will limit your synthesis, and ultimately limit the production of carbon dioxide). Given this, you must determine how much phenol is needed to completely react with the oxalic acid to form Cyalume via reaction #1 (don't forget about significant figures).
- a. Now, to be able to convert between oxalic acid and phenol, you must find the number of moles of oxalic acid you have. Complete the following equation to determine the number of moles of oxalic acid.

$$2.55 \text{ mg} \times \frac{1 \text{ g}}{1000 \text{ mg}} \times \frac{1 \text{ mol}}{90.03 \text{ g}} = \text{_____ mol C}_2\text{H}_2\text{O}_4$$

- b. The next step is to use the balanced chemical equation to convert between moles of oxalic acid and moles of phenol. Complete the following equation to accomplish this.

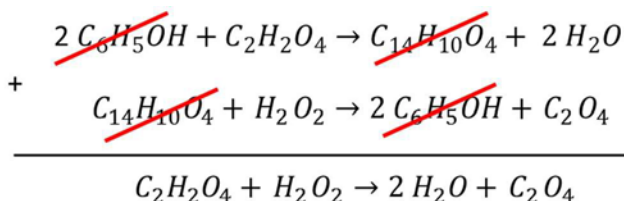
$$\underline{\hspace{2cm}} \text{ mol C}_2\text{H}_2\text{O}_4 * \frac{\underline{\hspace{2cm}}}{\underline{\hspace{2cm}}} = \underline{\hspace{2cm}} \text{ mol C}_6\text{H}_5\text{OH}$$

4. Now we can use a series of calculations to go from the moles of phenol to the moles of carbon dioxide. Do so below. (hint: use the same approach as above)
5. The Ideal Gas Law,  $PN = RT$  (in which P is pressure, V is volume, n is number of moles, T is temperature, and R is the gas constant), can be used to relate the moles of carbon dioxide to the pressure that the CO<sub>2</sub> gas molecules will exert on the outer tube. Luckily, one of your coworkers is an expert at using the Ideal Gas Law, and (after making a few assumptions about the temperature and volume) she estimates that number of CO<sub>2</sub> gas molecules produced by your reaction will generate a pressure of about 2.80 atmospheres within the glow stick. Atmospheres are a common unit of pressure and its units are abbreviated atm. Keeping in mind that more excited state molecules lead to a brighter glow stick, would there be any benefits of increasing the amount of CO<sub>2</sub> produced? If most glow sticks can only withstand a pressure of approximately 5.00 atm, is it safe to increase the amount of CO<sub>2</sub>? Why or why not?
6. Since you now know that the reaction is going to produce a safe amount of carbon dioxide, you can construct your glow stick prototype. Let's begin by looking at the inner tube, and how much tetracene to include in it. Calculate how many milligrams of tetracene you need to include in the inner tube to react completely.
7. Finally, you need to fill the outer tube with hydrogen peroxide. Since hydrogen peroxide is a liquid, you'll have to use the density (1.45 g/mL) to determine what volume to add. Convert to milliliters of hydrogen peroxide below. (hint: it may be easiest to start with moles of product calculated previously in an intermediate step, such as Cyalume)



8. With those measurements done, you assemble the prototype. However, before breaking the inner tube and testing the prototype, let's think about the reactions themselves. Sometimes, when you have a long series of reactions, it is beneficial to simplify those reactions into a single reaction equation. To do this, you sum the equations and remove species that occur in both the products and reactants.

- a. For example, the sum of equations 1 and 2 is done for you below. This creates a new equation that replaces and simplifies the original ones. (Note that the coefficients must also be taken into account when cancelling)



- b. Now, using the previous example as a template, sum all four of the balanced reactions on page 2, and write a single, simplified reaction below.

9. You'll notice that tetracene is not a part of the final simplified reaction. However, you've learned that tetracene is responsible for the color of the glow stick and is therefore a necessary component of the chemistry of glow sticks. How do you explain this?

10. Your boss requests that you build a second prototype that is identical to the first but with twice as much tetracene in the inner tube. He believes that this will increase the brightness significantly. Evaluate this approach below by discussing the relationship between excited tetracene and the other species present within these series of reactions (for example, think about the role that peroxyacid ester plays in this reaction). What other impacts might doubling the amount of tetracene have on the glow stick?